



Hydrochemistry, isotopes and groundwater modeling to characterize multi-layered aquifers flow system in the upper part of Awaj River - Damascus Basin (Syria)

Nazeer Asmael

► To cite this version:

Nazeer Asmael. Hydrochemistry, isotopes and groundwater modeling to characterize multi-layered aquifers flow system in the upper part of Awaj River - Damascus Basin (Syria). Earth Sciences. Université Michel de Montaigne - Bordeaux III, 2015. English. <NNT : 2015BOR30009>. <tel-01219132>

HAL Id: tel-01219132

<https://tel.archives-ouvertes.fr/tel-01219132>

Submitted on 22 Oct 2015

HAL is a multi-disciplinary open access archive for the deposit and dissemination of scientific research documents, whether they are published or not. The documents may come from teaching and research institutions in France or abroad, or from public or private research centers.

L'archive ouverte pluridisciplinaire **HAL**, est destinée au dépôt et à la diffusion de documents scientifiques de niveau recherche, publiés ou non, émanant des établissements d'enseignement et de recherche français ou étrangers, des laboratoires publics ou privés.



THÈSE

Présentée à L'Université Bordeaux Montaigne

Par Nazeer Asmael

École Doctorales des Université de Bordeaux Montaigne (ED 480)

Pour obtenir le grade de:

Docteur en Hydrogéologie

**Hydrochimie, isotopie et modélisation hydrodynamique pour la
caractérisation du système aquifère multicouche amont de la rivière
Awaj- Bassin de Damas (Syrie)**

Directeur de thèse: M. Alain Dupuy

Co-directeurs de thèse: M. Philippe Le Coustumer, M. Salim Hamid

Soutenue publiquement le 07 juillet 2015

Devant la commission d'examen

M. Frédéric HUNEAU, Professeur, Université de Corse	Président
M. Moumtaz RAZACK, Professeur, Université de Poitiers	Rapporteur
M. Mikael MOTELICA-HEINO, Professeur, Université d'Orléans	Rapporteur
M. Alain DUPUY, MCU HDR, Bordeaux INP	Examineur
M. Philippe LE COUSTUMER, MCU HDR, Université de Bordeaux	Examineur
M. Salim HAMAID, MCU HDR, Université de Damas	Examineur

ACKNOWLEDGEMENTS

After a little more than three years of starting this thesis, it is my pleasure to sit down in front of my computer to thank everyone who has participated directly or indirectly and contributed in one way or another in developing this work and writing this manuscript.

Before the acknowledgments, I would like to briefly mention how this doctorate research started. After obtaining my Master's degree in hydrology and water resources from IHE Institute (Delft, The Netherlands), the story that brought me to France to carry out this PhD thesis started when I came here as a visitor to accompany my wife Rim who was also doing her PhD at Université de Bordeaux 1. This allowed me to communicate with Professor "Frédéric Huneau" who helped and offered me this valuable opportunity to register and start my PhD under his supervision. So, thanks a lot due to both of you Rim and Prof. Huneau.

I would like to start by thanking my supervisors. I deeply express my deepest gratefulness to Prof **Frédéric Huneau**, who agreed to initiate this work and supervise it. Under his effective supervision and huge effort, we have published two articles during this research; hence working with Prof. HUNEAU has scientifically yielded prosperous result! Once again, thank you very much for your effort which I highly appreciate. I pursued my work under the supervision of Mr. **Alain Dupuy** and Mr. **Philippe Le Coustumer**. Sincere thanks go to Mr. **Dupuy** for his valuable time. He has offered patiently to develop and discuss the groundwater model which has, in my opinion, given me a good background in this field. I also would like to thank him for his help, sympathy, and open-mindedness which were extremely important for achieving my research objectives and overcome other related difficulties. Many thanks to Mr. **Le Coustumer**! His unlimited support and thoughtful guidance have aided me to overcome several problems and continue this work in the best possible way. Indeed, the support given by all of them made me feel home among my parents, whom I have not seen in the last four years, and really strengthen me to carry on this research.

My special thanks go to the other members of the jury, the two rapporteurs Prof. **Moumtaz Razack** and Prof. **Mikael Motelica-Heino**, who accepted to review and to evaluate this thesis and provided me with valuable comments.

I'm grateful to my co-director of thesis from Damascus University Dr. **Salim Hamid** for his unlimited and constant support and guidance in providing necessary information and needed data. Huge thanks are due to him for his support in easing and overcoming all relevant administrative procedures.

Sincere thanks and appreciation go to Dr. **Jan Willem Foppen** from UNESCO IHE Institute, Delft - The Netherlands, who has supervised me during my master project and developed the spreadsheet which has been extensively used in this research.

I owe special thanks to my sponsor "**Campus France**" and the **Foreign Affairs Ministry of France**, for their financial support (MAE grant n° 779091L and n° 839300A). Without their gratefully appreciated aid, I would not be able to do this research.

I would like to thank my colleagues with whom I have shared the same office, **Jessy Jaunat**, **Yohana Stupar** and **Morgan Le Lous**. I can say that I'm so happy to have and continue preserve their friendship. Special thanks to **Yohana** for her kindness and help in linguistic editing and enhancing the published articles. Thanks to **Morgan** for his help, friendship and productive discussions.

This study has been done at **ENSEGID** (Ecole Nationale Supérieure en Environnement Géoressources et Ingénierie du Développement Durable) so, I would like to express my appreciation to my fellow doctoral students and to all the ENSEGID's members, professors, for their contributions during this work. I specially would like to thank some teachers who helped me in answering some questions related to my research, Mr. **Michel Franceschi** and Mr. **Francois Larroque**. Special thank goes to Prof. **Adrian Cerepi** for his support and guidance.

I also would like to express my gratitude to the **University of Bordeaux 3** (Université Bordeaux Montaigne) which nominated me a member of **Bordeaux Alumni** program! Thanks to you Mr. **Rigollet** who helped in that. I must acknowledge the kindness of my sponsor in this program Mr. **Alain Cougrand** and the program coordinator Ms. **Caroline Pedezert**.

I would like to express my gratitude to my employer, **Damascus University**, Faculty of Sciences, Department of Geology for giving me this opportunity to come to France for doing my research.

My gratitude is also due to my colleagues in Damascus, Mr. **Abdallah Al-Kattea** and Dr. **Kasem Salih** from the General Directorate of Barada and Awaj Basin (GDBAB)-Syria, and Ms. **Taghreed Alsaleh** from Arab Center for the Studies of Arid Zones and Dry Lands (ACSAD) - Damascus for their assistance in providing required data and information for setting the groundwater model. Very special thanks go to Mrs. **Basma Al-Ali** for her aid in editing the final version of this thesis

I'm really very grateful to our friends here in France who were very close to my family especially **Eliane Gonthier** and **Odile Playoult**. Thanks a lot to both of you for your warm hospitality and care.

Finally I warmly would like to thank my “small family”, thanks to my wife **Rim** for her patience and sharing, to some extent, all of suffering, disappointment, worry, and success. For my lovely son (**Yamen!!**), who cannot realize that I'm motivated by him and that he is my reason to live! He really gives me all power and love that I need! My gratitude is to my “large family” in **Syria**, my **parents**, who always supported me even in unimagined or unseen manner! **My sisters** and **my brothers**, all of them illuminate my life.

At the end, this work is dedicated to all of my Syrian fellow countrymen who shed their precious blood for Syria... We pray for all of those who work honestly for the reconciliation and peace in Syria!

My apologies go to those whom I have failed to mention.

Abstract

In developing countries, such as Syria, the limited budgets as well as the lack of hydrological data affects the groundwater resources' assessment. The Barada and Awaj basin (Damascus Basin) is the most important and extensively utilized water basin in Syria. The upper part of Awaj River catchment occupies the southwestern part of this basin. In this arid region, groundwater is considered to be a main source of water supply for both drinking and irrigation purposes. In order to assess the main features characterizing the hydrogeological system in this area and estimate its groundwater resources potential, a multi approach methodology using hydrochemistry, environmental stable isotopes and groundwater modeling were used as integrated tools. The water budget of the upper aquifer horizon, where the most anthropogenic activities are concentrated, was developed.

The geological formations outcropping in the study area range from the Jurassic to the Quaternary. The Jurassic carbonate rocks are occupied the western region, while the plain region is characterized by the exposure of Neogene conglomerates, Quaternary alluvial proluvial deposits and the basalt of Quaternary and Miocene. The Small exposure of Cretaceous and Paleogene are found in the south-western part of the study area.

The detailed description of hydrogeochemical conditions, including major ions, physico-chemical and *in situ* field parameters, has underlined the very complex variability of the stratigraphic sequences and hence the numerous hydrogeological units within the study area. The hydrogeochemical evolution of groundwater reveals the domination of dissolution/precipitation mechanisms in this complex sequences, not only in the mountainous part of the area but also in the plain region. This was evidenced by the saturation indices of calcite and dolomite. However, and to less extent, the silicate hydrolysis and reverse ion exchange, involving clay minerals, were recognized in playing a considerable role in groundwater chemical composition. The dissolution of gypsum is recognized in some places, mainly in the Jurassic aquifer.

It was found that the groundwater's geochemistry at the upper part of the Awaj River is more controlled by the geogenic processes rather than the effect of anthropogenic activities. The hydrochemical facies of groundwater show that about 70% of water samples tend to have Ca-HCO₃ water type. This confirms the effect of carbonate rocks and the recent recharge of groundwater from atmospheric precipitation. The similarity in water type tends

to express the existence of a unique hydrochemical system where the individualised groundwater flow paths are difficult to delineate within the different hydro-stratigraphic units. However, a remarkable anthropogenic influence on the groundwater quality was observed through the infiltration of irrigation water and the effect of intensive use of mineral and organic fertilizers on nitrate level as well as the contamination by sewage water and animal waste disposal.

Consequently, hydrochemical patterns did not give enough evidences for expecting huge feeding flow from Jurassic aquifers towards the other aquifers. The hydrochemical processes are highly irregular in space, especially in the Jurassic aquifer, suggesting active dissolution/precipitation phenomena. The results indicate that this area is much more featured by recharge rather than discharge mechanisms. Thus, this area could be considered as a part of a major intermediate or regional flow system rather than a local one.

The isotope compositions of precipitation were used to construct a local meteoric water line in the study area as well as interpret the relationship between stable isotope depletion and altitude. Comparing the isotope composition of groundwater and precipitation implies an important rapid infiltration of atmospheric precipitation before significant evaporation takes place prior to or during the infiltration. This data also shows that the infiltrated precipitation provides the main source of recharge to the aquifers system all over the study area but the main recharge occurs over the mountainous parts through the karst landscape and fractured rocks. To a lesser extent, it also contributes to recharge the Neogene conglomerate and Quaternary alluvial aquifer in the plain region where the mixing of groundwater flow paths has been recognized. All the groundwater samples are situated to the left of the GMWL suggesting input of local rainfall that derives from weather front originating from the Mediterranean Sea.

Nevertheless and based on the hydrochemical and isotopic characteristics of groundwater, the study area is divided into two main sub-regions A and B. In the sub-region A which constitutes the western, south-western and north-western parts of the area, mainly the Jurassic aquifer where karstic features are well developed facilitated by cracks and fissures. These features increase the permeability coefficient and enhance the infiltration mechanism; hence this part is characterized by groundwater vulnerability to pollution. This was evidenced by high rates of nitrates resulting from sewage water infiltration. The hydrochemical processes are highly irregular in this part which suggests active dissolution

phenomena and deep vertical groundwater flow. The sub-region B occupies the south, central and eastern part of the area, mainly Neogene conglomerates and Quaternary alluvial aquifers. It is characterized by a shallow horizontal flow component associated with active interaction between groundwater and hosting rocks, evidenced by water chemistry evolution. The upward leakage of groundwater from deep aquifers seems to be an important component to maintain the Neogene/ Quaternary aquifer in this sub-region where the discharge occurs mainly through the major springs and groundwater withdrawal. The springs which are located in this sub-region, mainly in the recent basalt, yield significantly high discharge and cannot be classified under the perched springs but most likely are draining the deeper regional aquifers.

Developing numerical model simulating the groundwater flow performance in the study area was a useful alternative tool to evaluate the groundwater resources and understand its flow patterns in this region. The model's result indicates that the elevated Jurassic and Cretaceous aquifers became confined as they extend to the east toward the plain region and are overlain by younger formations. The hydraulic gradient of these aquifers was high enough to permit hydraulic connections between them and the overlying upper aquifer horizon through the upward leakage of groundwater. In the upper aquifer horizon, the groundwater dynamics is affected by different mechanisms in terms of recharge and discharge. The recharge is originating from different sources such as direct meteoric infiltration, lateral groundwater recharge along the contacts between Jurassic aquifer and the conglomerate escarpment of Neogene aquifer. The upward leakages of deep artesian water as well as the indirect recharge from the irrigation return flow play also a considerable role in recharging this aquifer. The discharge of this aquifer occurs mainly through the lateral outflow at the eastern boundary and groundwater withdrawal. The highland Jurassic aquifer is solely recharged by the infiltration of intensive rainfall and snowmelt.

Consequently, the simulation result is in good agreement with the result of interpretation of the hydrochemical and isotopic characteristics of the groundwater in dividing the study area into two different but linked flow systems. The first one is shallow and is developed in the unconsolidated or semi-consolidated Neogene/Quaternary aquifer, while the second one is deep and developed in the Cretaceous and Jurassic carbonate aquifers where the preferential flow component contributes potentially to the groundwater flow behaviour. Groundwater flow in the first system seems to be controlled by bedding and

lithostratigraphic units with a minor downward component. While in the second system, groundwater flow pathways constitute two main components. The first one is controlled by local conduits and active fault zones and discharges either as a preferential flow throughout a several karstic springs or recharges the upper aquifer horizon through the cavernous limestone as a lateral groundwater flow. The second one is recognized to be regional and controlled by the geological structures as deep vertical groundwater flow. The hydraulic connection between the two systems was observed. Accordingly, the local flow and deep circulation of groundwater seem to be controlling the flow system in the entire study area.

The most important components of the water budget of the upper aquifer horizon have been determined. The result indicated that the lateral discharge from the Jurassic karstic aquifer as well as the meteoric infiltration is the most important recharging component of this budget. The upward leakage of groundwater from deeper aquifers also plays an important role in recharging this aquifer. However, the lateral discharge from the eastern boundary of the model's domain is the largest discharge component which indicates that the study area can be considered as a main recharge region of the western side of the Barada and Awaj Basin. The simulated result as well as the hydrochemical characteristics of groundwater in the study area suggests the extension of the orographic basin boundary toward the west direction.

Keywords:

Aquifer, hydrochemistry, stable isotopes, FEFLOW, groundwater modeling, water budget, water resources management, Mt. Hermon, Syria

Résumé

Dans les pays en développement, tels que la Syrie, des ressources en eaux limitées associées au manque de données hydrologiques, se pose le problème de l'évaluation des ressources en eaux souterraines. Le bassin Barada et Awaj (région de Damas) est le plus important bassin hydrologique en Syrie et aussi le plus utilisé. La partie amont du bassin versant de la rivière Awaj occupe la partie sud-ouest du bassin Barada & Awaj, dans laquelle se développe un système aquifère multicouche. Dans cette région aride, l'eau souterraine est considérée comme la principale source d'approvisionnement en eau pour des usages principalement agricoles (irrigation) et alimentation en eau potable (consommation humaine). En vue d'évaluer les principales caractéristiques hydrogéologique et quantifier les ressources potentielles en eau souterraine de ce système aquifère, une approche méthodologique multicritères basée sur l'hydrochimie, les isotopes stables ($\delta^{18}\text{O}$ & $\delta^2\text{H}$) et une modélisation hydrodynamique ont été utilisés dans un outil intégré. Le bilan hydrogéologique de la nappe la plus superficielle de l'aquifère, où les activités anthropiques et les prélèvements sont concentrés, a été déterminé par une approche numérique quantitative.

L'analyse détaillée des paramètres hydrogéochimiques et physico-chimiques (ions majeurs et mineurs, conductivité, température, pH etc..) obtenus sur le terrain, a mis en évidence la très forte interrelation entre l'hétérogénéité des séquences stratigraphiques et l'hydrogéochimie des eaux, et donc des différentes unités hydrogéologiques de la zone d'étude. L'évolution hydrogéochimique des eaux souterraines révèle que les mécanismes de dissolution / précipitation dominant tant dans la zone montagneuse que dans la région de plaine. Cette tendance a été démontrée par les indices de saturation de calcite et la dolomite. Dans une moindre mesure, l'hydrolyse des silicates induit, notamment au contact des minéraux argileux, une composition chimique des eaux souterraines contrastée avec également des échanges ioniques importants. La dissolution des formations riches en gypse a été identifiée dans certains endroits, principalement dans les formations formant la nappe du Jurassique.

Il a également été constaté que la géochimie de l'eau souterraine dans la partie amont du bassin de la rivière Awaj est contrôlée par des processus géogéniques plutôt qu'anthropiques. Du point de vue des faciès hydrochimiques, les eaux souterraines du bassin versant de la rivière Awaj sont de type carbonaté (Ca-HCO_3) comme l'indiquent

près de 70% des échantillons d'eau analysés. Cela confirme l'interaction avec des roches carbonatées et la recharge des eaux souterraines par des précipitations atmosphériques récentes. Ce faciès des eaux tend à démontrer l'existence d'un système hydrochimique unique, où les trajets d'écoulement singuliers des eaux souterraines sont difficiles à délimiter à l'intérieur des différentes unités hydro-stratigraphiques. A noter, il existe une influence anthropique remarquable sur la qualité chimique des eaux souterraines via l'infiltration des eaux d'irrigation, qui sous l'effet de l'utilisation intensive d'engrais minéraux (nitrates et phosphates) et organiques, conduisent à une contamination en nitrates ainsi que par les eaux usées (déchets animaux et humains).

Les processus hydrochimiques observés sont irréguliers du point de vue spatial, en particulier dans l'aquifère du Jurassique, suggérant un phénomène de dissolution / précipitation assez actif. En général, le résultat de l'évolution hydrochimique indique que cette zone est beaucoup plus concernée par l'impact des recharges plutôt que par les exhaures. Les modèles hydrochimiques suggèrent que la zone amont pourrait être considérée comme dépendant d'un système d'écoulement intermédiaire ou régional plutôt que local. Ils n'apportent pas d'éléments vis-à-vis des flux nécessaires à l'alimentation des aquifères Jurassique vers les autres aquifères

Les compositions isotopiques des précipitations ont permis de construire la droite météorique locale de la zone d'étude. Elles permettent de proposer une interprétation entre l'appauvrissement des isotopes stables en fonction de l'altitude. En comparant la composition isotopique des eaux souterraines avec celles des précipitations, il apparaît que l'infiltration rapide des précipitations atmosphériques se produit avant l'évaporation de ces dernières.

Ces données montrent également que les eaux de précipitation infiltrées constituent la principale source de la recharge de l'aquifère et ce dans toute la zone d'étude. Cependant la recharge principale se produit dans les régions montagneuses carbonatées karstiques et les formations basaltiques composées de roches fracturées. A noter également, mais dans une moindre mesure, la contribution à la recharge de l'aquifère alluvial de la zone de plaine, par des eaux infiltrées au travers des formations conglomératiques du Néogène et du Quaternaire. Toutes les analyses isotopiques réalisées sur les échantillons d'eau souterraine sont situés à la gauche de la GMWL suggérant l'entrée de précipitations locales venant du climat maritime et donc l'influence de la mer Méditerranée. En fonction des

caractéristiques hydrochimiques et isotopiques observées pour les eaux souterraines, la zone d'étude est divisée en deux principales sous-régions A et B.

La sous-région A, constitue la partie occidentale du bassin. Elle est principalement formée de l'aquifère du Jurassique où les mécanismes karstiques de dissolution des formations carbonatées et gypseuses sont bien développés et grandement facilités par le réseau de fissures et de crevasses. Il favorise la perméabilité des couches et améliore l'infiltration. Il est possible de conclure que cette sous-région A se caractérise par une vulnérabilité des eaux souterraines aux intrants de surfaces possiblement contaminés et donc une fragilité à ce type de pollution de surface. Ceci est attesté par les taux élevés de nitrates résultant de l'infiltration des eaux usées et d'irrigation. Les processus hydrochimiques sont très irréguliers dans cette zone suggérant que les mécanismes de dissolution (interaction eaux – roches) sont actifs. En profondeur des flux verticaux d'eaux souterraines existent pour maintenir la charge des aquifères supérieurs du Néogène et du Quaternaire. Ces derniers sont affectés par des flux sortants liés aux nombreuses émergences (sources) et pompages (forages et puits). Les sources de cette région localisées dans les formations basaltiques, avec des débits importants ne sont pas classées comme sources perchées mais directement alimentées par les flux ascendants des aquifères profonds (drainance ascendante).

La sous-région B au sud, occupe la partie centrale et orientale du bassin versant. Elle est essentiellement géologiquement caractérisée par des conglomérats du Néogène et du Quaternaire qui forment les aquifères alluviaux. Ils sont caractérisés par des écoulements horizontaux, peu profonds, et fortement marqués par l'interaction dynamique entre les eaux souterraines et les roches encaissantes, comme en témoigne l'évolution de la chimie de ces eaux. Les flux ascendants des aquifères profonds semblent être une composante importante au maintien de l'équilibre de l'aquifère du Néogène / Quaternaire ;

Nous avons développé un modèle numérique pouvant évaluer les différents écoulements des eaux souterraines dans la zone d'étude, afin de quantifier les ressources en eaux souterraines, de préciser les quantités mises en jeu dans les différents aquifères propres à cette région.

Le résultat du modèle développé, indique que les aquifères du Jurassique et du Crétacé supérieur sont confinés lors de l'extension vers l'est en direction de la zone de plaine et sont recouverts par les formations plus récentes. Le gradient hydraulique de ces différents aquifères est suffisamment élevé pour permettre les connexions hydrauliques entre

aquifères. Le modèle confirme l'alimentation de la première nappe libre par une drainance verticale ascendante. Dans cette nappe, les circulations souterraines sont affectées par différents mécanismes de réalimentation et de décharge. La recharge est essentiellement marquée par une dynamique d'infiltration directe et rapide des eaux météoritiques, mais aussi latéralement le long des contacts entre l'aquifère du Jurassique et ceux des escarpements conglomératiques du Néogène. Les flux sortants affectant l'aquifère du Neogene sont principalement dus aux sorties latérales aux limites est du bassin, ainsi que par les prélèvements directs dans les eaux souterraines. L'aquifère du Jurassique supérieur est quant à lui uniquement alimenté par l'infiltration des précipitations et lors de la fonte des neiges.

En conséquence, les résultats obtenus par simulation numériques sont en bon accord avec les données hydrochimiques et isotopiques des eaux souterraines. Le modèle conforte ainsi l'hypothèse d'un diviser la zone d'étude en deux systèmes d'écoulement différents, le premier système de surface (faible profondeur) et se développant dans les formations géologiques poreuses (basaltes et conglomérats non cimentés) du Néogène et l'aquifère Quaternaire. Un second système se trouve en profondeur et se développe dans les carbonates du Jurassique et du Crétacé. Les liaisons hydrauliques entre les deux systèmes ont été mises en évidence. La balance des eaux souterraines dans le premier système semble être contrôlée par la lithologie des unités stratigraphiques. En revanche, dans le second système, les écoulements des eaux souterraines semblent avoir deux composantes principales. La première est contrôlée par des émergences locales situées dans les zones faillées (actives). Les débits d'exhaure permettent de recharger la première nappe à travers les calcaires par écoulement latérale. La seconde composante est régionale et contrôlée par les structures géologiques permettant une composante verticale des eaux souterraines profondes.

En conséquence et d'une manière générale, les flux mis en jeu dans la nappe profonde semblent être gérés par un système d'écoulement complexe (descendant pour la partie amont et la recharge, et ascendant pour la partie aval et la drainance) affectant l'ensemble de la zone d'étude.

Les plus importantes composantes, pour la gestion des ressources en eau, du premier horizon de l'aquifère Jurassique de type karstique ont été déterminées. Elles indiquent que:

Le flux d'exhaure latéral dans la zone karstique est intense et largement compensé par une infiltration rapide des eaux pluviales.

La drainance verticale ascendante d'eaux souterraines provenant de l'aquifère profond joue également un rôle important dans la recharge de la nappe de surface.

La recharge principale s'effectue du côté ouest du bassin versant de Barada et de la rivière Awaj.

Le résultat simulé de la balance des eaux du bassin hydrogéologique étudié, associé aux caractéristiques hydrochimiques des eaux souterraines suggère une extension aux limites du bassin orographiques en direction de l'ouest.

Mots-clés:

aquifère, hydrochimie, isotopes stables, FEFLOW; modélisation des eaux souterraines; budget de l'eau, la gestion des ressources en eau, Mt. Hermon, la Syrie.

المخلص

تؤثر محدودية الموارد المائية والمالية سلباً في إدارة هذه الموارد في دولٍ كثيرةٍ تقع في المناطق الجافة وشبه الجافة، ولاسيما النامية منها مثل سورية.

يعد حوض بردى والأعوج واحداً من الأحواض المائية المهمة في سورية لجهة حجم الاستهلاك المائي فيه من أجل تغطية الاحتياجات المتزايدة من المياه في قطاعي الشرب والزراعة، والتي تعتمد بشكلٍ أساسي على المياه الجوفية.

تشغل منطقة الدراسة التي تناولها هذا البحث القسم الأعلى من حوض نهر الأعوج، والذي يحتل الجزء الجنوبي الغربي من هذا الحوض.

أُتبع في البحث منهجية اعتمدت على التكامل ما بين الطرائق الهيدروكيميائية، وطريقة النظائر، إضافة للنمذجة الرياضية، وذلك بهدف تقييم الخصائص الهيدروجيولوجية النازمة لحركة المياه الجوفية في منطقة الدراسة، ودراسة العلاقة الهيدروديناميكية بين مختلف الطبقات الحاملة للمياه الجوفية، وبناءً عليه فُدرت الموازنة المائية للطبقة المائية العليا، والتي يعتمد عليها معظم النشاطات البشرية المستهلكة للمياه.

دُرست الخصائص الهيدروكيميائية للمياه الجوفية من خلال تتبع تغيرات الأيونات الرئيسية فيها، ونسبها الأيونية، إضافة لخصائصها الفيزيوكيميائية المتمثلة بقياس البارامترات الحقلية، وقد عكست قيم هذه الخصائص درجة التعقيد العالية لمنطقة الدراسة من الناحية الجيولوجية، والتكتونية، وبالتالي من الناحية الهيدروجيولوجية، وقد تبين من خلال تتبع تغيرات الصفات الهيدروكيميائية للمياه الجوفية الدور الكبير الذي يلعبه كلٌّ من انحلال وترسيب الصخور الكربوناتيّة في المياه الجوفية ضمن كافة أنحاء منطقة الدراسة، والذي استُدل عليه من خلال قيم معامل التشبع لهذه الصخور، أما بالنسبة لانحلال السيليكات، وخاصة التبادل الأيوني العكسي، فقد تبين أنهما يأتیان في المرتبة الثانية من ناحية التأثير في هذا التركيب، وقد لوحظ أيضاً تأثير انحلال الجص على تراكيب بعض العينات، ولاسيما المأخوذة من الطبقة العائدة للعصر الجوراسي.

يتحكم المنشأ الجيولوجي للطبقات الحاملة للمياه في الخصائص الكيميائية لهذه المياه، بينما يكون تأثير النشاطات البشرية ضعيفاً على هذه الخصائص، وقد أظهرت هذه الخصائص أن أكثر من 70% من العينات المدروسة يغلب عليها الصفة الكربوناتيّة الكلسية، والتي تؤكد بدورها على التأثير الكبير للصخور الكربوناتيّة من جهة، وعلى التغذية الحديثة للحوامل المائية من الهطولات المطرية من جهة أخرى.

يشير التشابه في الصفات الكيميائية للمياه الجوفية إلى احتمالية سيطرة نظام هيدروكيميائي متماثل الخواص، بحيث يصعب تتبع مسار حركة المياه الجوفية من خلال تتبع تطور هذه الصفات، وقد لوحظ دور واضح لتأثير النشاطات البشرية على خصائص المياه الجوفية في بعض أجزاء المنطقة المدروسة، وذلك من خلال الاستخدام المكثف للأسمدة العضوية والكيميائية في الزراعة، وتأثير الصرف الصحي، الأمر الذي أدى إلى رفع مستوى النترات في المياه الجوفية بمنطقة الدراسة.

إن تتبع التغيرات الكيميائية المترافقة مع حركة المياه الجوفية، والتي تتميز بعدم انتظامها لم يعطِ دلالة واضحة، وكافية عن التغذية الكبيرة المتوقعة من الطبقة الجوراسية الكارستية المتكشفة في القسم الجبلي باتجاه الطبقة النيوجينية الرباعية في القسم السهلي من منطقة الدراسة، وهو ما يشير إلى سيطرة خاصية التغذية مقارنة مع التصريف، وبالتالي يمكن اعتبار منطقة الدراسة جزءاً من منطقة تغذية رئيسية تشمل مناطق أوسع انتشاراً.

استُخدمت الخصائص النظائرية للأمطار من أجل إنشاء خط الأمطار المحلي بالاعتماد على البيانات المتوفرة في 12 محطة مناخية يقع معظمها في/ أو بجوار المنطقة المدروسة، كما استُخدمت هذه الخصائص وتغيراتها مع الارتفاع عن سطح البحر لتحديد التدرج النظائري (درجة النضوب) لكلٍ من الأكسجين -18، والديوتيريوم.

إن مقارنة الخصائص النظائرية لكلٍ من مياه الأمطار والمياه الجوفية في منطقة الدراسة تشير إلى إمكانية التغذية المباشرة للمياه الجوفية من الهطولات المطرية، والتلجبية، وذلك قبل حدوث تبخّر مهم لمياه الهطولات، سواء كان ذلك

قبل أو أثناء عملية الرش، من جهة أخرى أشارت دراسة هذه الخصائص أيضاً إلى الدور الكبير الذي تلعبه هذه الهطولات في تغذية الحوامل المائية الجوفية، ولاسيما في القسم الجبلي ذي الطبيعة الكارستية المتشققة، ومن المفيد الإشارة هنا كذلك إلى أن جميع عينات المياه الجوفية تقع إلى الشمال من خط المياه العالمي، مما يؤشر إلى إمكانية تغذية الطبقات الحاملة لهذه المياه بشكل مباشر من الأمطار الناتجة عن الجبهة الهوائية المتولدة من تأثير البحر الأبيض المتوسط.

بناءً على نتائج دراسة الخصائص الكيميائية والنظائرية للمياه الجوفية يمكن تقسيم منطقة الدراسة إلى قسمين أساسيين هما القسم الجبلي الذي يشمل الأجزاء الغربية، والجنوبية الغربية، والشمالية الغربية، حيث تسود التكتشفات الجوراسية الكارستية، والقسم السهلي الذي يشمل بشكل رئيس الأجزاء الجنوبية، والشرقية والمتوسطة، حيث تسيطر تكتشفات الكونغلوميرا النيوجينية، واللحقيات الرباعية.

يمتاز القسم الأول الجبلي بقابلية عالية للتلوث، وبخاصية الجريانات الرأسية فيه، وذلك بسبب طبيعته الكارستية، وبنيته الفالقية، أما في القسم الثاني السهلي، فغالباً ما تكون الجريانات تحت السطحية أفقية، وتترافق مع تفاعل نشط بين المياه الجوفية والصخور الحاملة، كما يبدو أن التبادل المائي الراسي بين الطبقات العميقة، والطبقة المائية العليا المتمثلة بشكل رئيس بطبقة الكونغلوميرا النيوجينية يلعب دوراً بارزاً في تغذية هذه الطبقة، ويمكن الاستدلال على ذلك من خلال التصاريح العالية نسبياً للينابيع الواقعة في القسم السهلي، وطبيعة التركيب النظائري لمياه هذه الينابيع.

تضمن البحث أيضاً تطوير نموذج رياضي يحاكي الجريانات الجوفية في مختلف الطبقات الحاملة لمنطقة الدراسة، وذلك بالاستناد على البيانات المتوفرة، وقد دلت نتائج هذا النموذج على أن الطبقتين الجوراسية والكريتاسية المتكشفتين في القسم الجبلي تتحولان إلى طبقات مضغوطة عندما تمتدان باتجاه الشرق، وتغطيها التوضعات الجيولوجية الأحدث، كما بينت هذه النتائج أن التدرج الهيدروليكي لهذه الطبقات يكون كبيراً لدرجة تسمح بالتبادل المائي مع الطبقة المائية العليا عبر التسرب الصاعد للمياه الجوفية، وبناءً عليه فإن عملية تغذية الطبقة المائية العليا تتم من تغذية مباشرة تأتي من مياه الأمطار الراشحة نحو باطن الأرض، ومن تغذية جانبية من خلال الطبقة الجوراسية عند توضع طبقة النيوجين الكونغلوميرية على تماس مباشر مع هذه الطبقة، ومن تغذية رأسية صاعدة تأتي من الطبقات العميقة، وأخيراً من تغذية غير مباشرة عبر رواجه مياه الري، وفواقد نقل المياه من أجل الاستخدامات الزراعية والمنزلية، ومياه الصرف الصحي، أما فيما يتعلق بالطبقة الجوراسية، فهي تتغذي، وبشكل حصري من مياه الأمطار، والمياه الناتجة عن ذوبان الثلوج.

دلت الدراسة المتكاملة لكل من الخصائص الهيدروكيميائية والنظائرية والهيدروديناميكية للمياه الجوفية في المنطقة المدروسة على احتمال وجود نظامين هيدروجيولوجيين مختلفين فيها، ولكنهما يتصلان هيدروليكيًا ببعضهما البعض، وعلى أن النظام الأول يتميز بأنه ضحل نسبياً، ويتشكل ضمن الصخور النيوجينية والرباعية ضعيفة التماسك مما يسهل حركة المياه الجوفية فيه، بينما يتميز النظام الثاني المتشكل في الصخور الكريتاسية والجوراسية العميقة، بأنه عميق وتطغى عليه البنية الكارستية المتشققة ونظام القنوات والفوالق، وهو ما يساعد على حركة وتصريف المياه الجوفية فيه من خلال خاصية الجريان المفضل.

حددت مركبات الموازنة المائية في الطبقة المائية العليا من منطقة الدراسة بالاعتماد على كل من النمذجة الرياضية، والبيانات التي توافرت حول كميات الهطول المطري، وتصاريح الينابيع، وكميات الضخ، وغيرها من العوامل الأخرى المؤثرة في هذه الطبقة، ومن خلال ذلك تبين أن الجريان الجانبي والعمودي من طبقة الجوراسي يشكل المركبة الأهم في تغذية هذه الطبقة، يأتي بعدها التغذية الرشحية من الهطولات المطرية، أما من ناحية التصريف، فإن الجريان الجانبي من هذه الطبقة باتجاه الشرق خارج منطقة النموذج يشكل المركبة الأكبر للتصريف، مما يؤكد أن منطقة الدراسة تشكل منطقة تغذية رئيسية في الجزء الغربي من حوض بردى والأعوج.

إن توسيع حدود الحوض المذكور باتجاه الغرب قد يبرر النتائج التي تم التوصل إليها سواء لجهة المركبة الكبيرة نسبياً للتغذية المائية القادمة من طبقة الجوراسي للطبقة المائية العليا، أو لجهة التصاريح العالية نسبياً للينابيع المتدفقة من القسم السهلي لمنطقة الدراسة.

بالاستناد على كل ما سبق، يمكن تلخيص أهم النتائج التي تم التوصل إليها في هذا البحث بالنقاط الأساسية الآتية:

- تأكيد تأثير الاستخدام المكثف للأسمدة الكيميائية في القسم السهلي حيث تتركز معظم الأنشطة الزراعية وكذلك تأثير مياه الصرف الصحي ولاسيما في القسم الجبلي (قلعة جندل، بقعسم... الخ) الذي يمتاز بقابلية تلوث عالية بسبب طبيعته الكارستية، على زيادة مستوى النترات في المياه الجوفية.
- وجود تغذية رأسية صاعدة من الطبقات العميقة المضغوطة باتجاه الحامل الأول، وقد بينت ذلك نتائج الدراسة الكيميائية والنظائرية، وأكدت عليها نتائج النموذج الرياضي، مع الإشارة هنا إلى أن معظم الدراسات السابقة افترضت وجود هذه التغذية.
- تحديد أنماط الجريان السائدة في منطقة الدراسة، حيث يسود الجريان تحت السطحي الأفقي في القسم السهلي بينما يسيطر الجريان الجوفي شبه العمودي في القسم الجبلي.
- يمكن اعتبار منطقة الدراسة منطقة تغذية رئيسية أكثر مما هي منطقة تصريف، وذلك اعتماداً على التغير في خصائص التراكيب الكيميائية والنظائرية للمياه الجوفية، ويمكن بالتالي اعتبار هذه المنطقة جزءاً من منطقة تغذية تشغل حدودها مناطق أوسع انتشاراً.
- ظهرت درجة التعقيد الجيولوجي والليتولوجي في منطقة الدراسة بشكل واضح من خلال الصفات الهيدروكيميائية في هذه المنطقة، وتغير التراكيب الكيميائية، ونسبها الأيونية، ومؤشرات التشبع بالمياه الجوفية فيها، والتي لم تسمح بالتنوع الدقيق لمسارات حركة المياه الجوفية ضمنها.
- تُعد النتائج التي تم التوصل إليها بالنمذجة الرياضية مثيرة للاهتمام، لأنها تعطي إشارة واضحة لوجود اتصال هيدوليكي بين الحوامل المائية العميقة والسطحية، والتي لم تكن مؤكدة مسبقاً، كما أن تقدير الموازنة المائية للطبقة المائية العليا، التي تُمثل المصدر الرئيس للتزود بالمياه من أجل الاستخدام الزراعي يُعتبر أيضاً من النتائج الهامة لهذا البحث.
- أثبتت نتائج النمذجة الرياضية، بأن الظروف الطبيعية، والبنية الجيولوجية والتكتونية تلعب الدور الرئيس في نظام المياه الجوفية السائد في منطقة الدراسة بغض النظر عن تزايد النشاطات المستهلكة للمياه في هذه المنطقة.
- يجب الإشارة بناءً على النتائج التي تم التوصل إليها ولاسيما الحجم الكبير نسبياً لمركبة الجريان الجوفي سواء الجانبي أو الرأسي من الطبقات العميقة باتجاه الطبقة المائية العليا إلى إمكانية عدم التوافق بين نقاط الفصل المائي السطحي والجوفي في القسم الجبلي من المنطقة المدروسة وبالتالي إمكانية انزياح حدود الحوض في تلك المنطقة باتجاه الغرب.

الكلمات المفتاحية:

حامل مائي، الهيدروكيمياء، النظائر البيئية، FEFLOW، النمذجة الرياضية، الموازنة المائية، إدارة الموارد المائية، جبل الحرمون، سورية

Table of Contents

ACKNOWLEDGEMENTS	3
Abstract	6
Résumé	10
المخلص	15
Table of Contents	18
List of Figures	21
List of Tables	25
Introduction	26
Chapter 1. General setting of the Study area	31
1.1. General Characteristics of the Study Area	31
1.2. Geology	34
1.2.1. Stratigraphy	34
1.2.1.1. Jurassic	34
1.2.1.2. Cretaceous	35
1.2.1.3. Paleogene	35
1.2.1.4. Neogene formations	36
1.2.1.5. Quaternary deposits	37
1.2.1.6. Basaltic rocks	37
1.2.2. Structures	42
1.3. Hydro-climatology	46
1.4. Hydrology.....	48
1.4.1. Awaj River.....	49
1.4.2. Major springs	53
1.4.2.1. Mambej spring	55
1.4.2.2. Talmasiat spring.....	56
1.4.2.3. Tabibieh spring	58
1.4.2.4. High Beit Jinn spring	58
1.4.2.5. Beit Jinn spring	60
1.5. Aquifer systems (Hydrogeology)	63
1.5.1. Jurassic Unit	66
1.5.2. Cretaceous Unit	67
1.5.3. The sedimentary Miocene–Quaternary aquifer	67

1.5.4. The Middle Miocene volcanic aquifer.....	67
Chapter 2. Methodology	73
2.1. Sampling, analysis and database preparation	73
2.2. Constructing of groundwater model.....	79
Chapter 3. Hydrochemistry to delineate groundwater flow pattern in the study area	82
<i>Introduction</i>.....	82
3.1. Results and discussion.....	83
3.1.1. Calcite, Dolomite and Gypsum Dissolution	83
3.1.2. Dedolomitization Process	90
3.1.3. Silicate hydrolysis.....	94
3.1.4. Redox processes	100
3.1.5. Stuyfzand classification	101
3.1.6. Correlation between groundwater flow pattern and hydrochemical behaviour	103
Chapter 4. Hydrochemical facies and isotopes to characterize the origin and recharge mechanisms of the groundwater in the study area	105
<i>Introduction</i>.....	105
4.1. Result and discussion	106
4.1.1. Water- Rock interaction and salts dissolution	106
4.1.2. Hydrochemical facies	109
4.1.3. Pollution Index (PI) and fecal contamination.....	113
4.1.4. Stable isotope composition of atmospheric precipitation and groundwater.....	116
4.1.4.1. Origin of air masses	116
4.1.4.2. Local meteoric water line.....	117
4.1.4.3. Altitude effect and tritium unit changes.....	121
4.1.4.4. Groundwater response to input precipitation.....	123
4.1.5. Equipotential contour lines and hydrogeological subdivision of the study area	125
Chapter 5. Groundwater modeling approach to estimate the water budget of the upper aquifer horizon in the model domain and assess the hydraulic relationship between multilayered aquifers.....	128
<i>Introduction</i>.....	128
5.1. Conceptual model.....	129
5.2. Boundary conditions	131
5.3. Input data.....	134

5.3.1. Recharge	134
5.3.2. Net Pumping	135
5.3.3. Spatial distribution of hydraulic conductivity	137
5.4. Steady-state calibration	138
5.4.1. The result of simulated hydraulic head in the different aquifers	139
5.4.2. Integrated water budget for the upper aquifer horizon	142
Chapter 6. General conclusion and Prospective	146
6.1. General conclusion	146
6.2. Prospective	150
6.3. Conclusion générale	151
6.4. Perspectives	156
References	159
Supplemental data tables	173
Appendices.....	184
<i>Appendix A Published Article</i>	<i>184</i>
<i>Appendices B Published Article</i>	<i>206</i>
<i>Appendices C Published Article</i>	<i>229</i>

List of Figures

Fig. 1-1 The location site of the study area and map of Syria divided into 7 hydrogeological basins.	31
Fig. 1- 2 Elevation contour lines of the study area as well as the 3D view of this area.	33
Fig. 1- 3 Range of the Paleogene thickness in the study area.....	36
Fig. 1- 4 Range of Neogene thickness in the study area.....	37
Fig. 1- 5 Shows the soils that derived from the weathering of the basalt of the Neogene age in the study area.	38
Fig. 1- 6 Geological map of the study area modified from Selkhozpromexport 1986, as well as three geological cross sections and one geophysical profile.....	39
Fig. 1- 7 Graphical logs of the stratigraphy in the Barada and Awaj Basin (Kattan 2006) ..	41
Fig. 1- 8 Bedding and folding phenomena in the carbonate rocks of Jurassic (Arneh valley).	43
Fig. 1- 9 Majors fault in the study area (updating from Selkhozpromexport 1986).....	44
Fig. 1- 10 Three cross sections: A-B, C-D, and E-F (Fig. 1-6), demonstrate the subsurface lithology as well as the major structures within the study area. (Modified from RDWSSA 2006)	45
Fig. 1-11 Geophysical profile G-H (Fig. 1-6), demonstrates the subsurface structures (Modified from RDWSSA 2006)	45
Fig. 1-12 Precipitation isopleths map based on the amount of precipitation measured at the six meteorological stations located in the study area during the hydrological year 2009-2010.	48
Fig. 1- 13 The Arneh Valley where the Sebarani tributary of Awaj River is generated and flowing.....	50
Fig. 1- 14 Kneseh and Rashasheh springs emerge from the upper part of Arneh valley (Jurassic aquifer).....	50
Fig. 1- 15 Schematic layout correspond to Sebarani tributary from Arneh toward the plain area throughout several geological formations.....	51
Fig. 1-16 Hydrograph shows the monthly average discharge of Awaj River from the hydrological years 1930-1931 until 2009-2010 after the recharge of Tabibieh spring.	52
Fig. 1- 17 Annual discharge of Awaj River from the hydrological years 1930-1931 until 2009-2010 after the recharge of Tabibieh spring	52
Fig. 1- 18 Location sites of major springs in the study area	54
Fig. 1- 19 Mambej spring and its probable schematic framework	55
Fig. 1- 20 The variations of the monthly discharge of Mambej spring and the annual amount of precipitation measured at Arneh station.....	56
Fig. 1- 21 Talmasiat spring which emerges from the Quaternary basalt.	57
Fig. 1- 22 The variations of the monthly discharge of Talmasiat spring and the annual amount of precipitation measured at Arneh station.....	57
Fig. 1- 23 The variations of the monthly discharge of Tabibieh spring and the yearly amount of precipitation measured at Arneh station.....	58
Fig. 1- 24 High Beit Jinn spring which emerges at the limit between the Jurassic and Cretaceous formations.	59

Fig. 1-25 The relationship between high Beit Jinn spring and the annual amount of precipitation measured at Arneh station.	60
Fig. 1- 26 Beit Jinn spring which emerges from the exposure of Paleogene southwest of the study area.	61
Fig. 1- 27 The relationship between Beit Jinn spring and the annual amount of precipitation measured at Arneh station.	61
Fig. 1- 28 The mean annual discharge of 5 major springs in the study area.	63
Fig. 1- 29 The hydraulic zones in the karstified aquifer in Syria, after Burdon and Safadi, 1964.	65
Fig. 1- 30 Jurassic limestone demonstrates the karstification and rillenkarren along the fractures.	66
Fig. 1- 31 The hydrogeological map of the study area.	68
Fig. 1- 32 Different aquifers and aquitards discriminated in the study area. 1, 3 and 5 are aquifers, 2 and 4 are aquitards.	69
Fig 2 - 1 Location map of sampling sites in the study area.	78
Fig 2 - 2 Framework of super-mesh of the model domain as well as three dimensional (3D) representation of the 6 layers and 7 slices consisting of this model domain.	81
Fig. 3 - 1 Opened and closed systems dissolution of carbonate rocks determined with PHREEQC and pH as a function of $p\text{CO}_2$ (atm) calculated values in the water samples.	84
Fig. 3 - 2 Calcium, magnesium and alkalinity concentration in mmol l^{-1} as a function of $p\text{CO}_2$ (atm) calculated values; solid lines are the alkalinity, calcium and magnesium determined with PHREEQC for pure calcite and dolomite dissolution.	85
Fig. 3 - 3 Scatter plot of the saturation indices (SI) of calcite and dolomite determined in the water samples.	87
Fig. 3 - 4 Classification and spatial distribution of saturation index of calcite in the water samples with chart showing the SI of calcite as a function of $p\text{CO}_2$ (atm) calculated values.	88
Fig. 3 - 5 The $\text{Mg}^{2+}/\text{Ca}^{2+}$ molar ratio as a function of $p\text{CO}_2$ (atm) calculated values.	89
Fig. 3 - 6 Scatter charts of Ca^{2+} , Mg^{2+} (mmol.l^{-1}) and pH as a function of SO_4^{2-} (mmol.l^{-1}).	91
Fig. 3 - 7 Saturation indices of calcite, dolomite and gypsum as a function of SO_4^{2-} (mmol l^{-1}).	92
Fig. 3 - 8 Classification and spatial distribution of saturation index of dolomite in the water samples.	94
Fig. 3 - 9 Classification and spatial distribution of SiO_2 (mg l^{-1}) concentration in water samples.	96
Fig. 3 - 10 Stability diagram of both Ca-Plagioclase (anorthite) and Na-Plagioclase (albite) and their possible weathering products.	98
Fig. 3 - 11 $\text{Na}^+/\text{Ca}^{2+}$ versus $\text{Mg}^{2+}/\text{Ca}^{2+}$ molar ratios in the water samples, (after Han and Liu, 2004).	99

Fig. 3 - 12 Scattered plots of $(Ca^{2+} + mg^{2+})$ vs $(HCO_3^- + SO_4^{2-})$ showing the effect of carbonate rock dissolution and silicate hydrolysis on groundwater composition.	100
Fig. 3 - 13 Stability diagram of redox conditions range based on the relationship between pH and PE and the distribution of water samples.	101
Fig. 3 - 14 Water types based on Stuyfzand classification.	102
Fig. 3 - 15 Schematic groundwater flow patterns based on major springs discharge and hydrochemical tracers and the associated hydrogeological subarea based on these patterns.	104
Fig. 4 - 1 Contribution of processes, other than evaporation, to the groundwater composition (cations effect).	108
Fig. 4 - 2 Contribution of processes, other than evaporation, to the groundwater composition (anions effect).	108
Fig. 4 - 3 Scatters plots of Na^+/Cl^- vs $Ca^{2+}/(HCO_3^- + SO_4^{2-})$ and $(Ca^{2+} + mg^{2+})$ vs $(HCO_3^- + SO_4^{2-})$	109
Fig. 4 - 4 a) Modified piper diagram depicting hydrochemical facies of groundwater in the study area (b) spatial distribution and classification of these facies.	111
Fig. 4 - 5 Representative stiff diagrams of selected samples for visual observation of spatial variation in their water chemistry. The spatial visualization of electrical conductivity (EC) is also shown in this figure.	113
Fig. 4 - 6 Spatial visualization of the pollution index (PI) (a). The total coliform and fecal coliform (<i>Escherichia coli</i>) measured in 3 spring water samples during March-April 2006 are also shown (b).	115
Fig. 4 - 7 Scatter plot shows the relationship between NO_3^- ($mmolL^{-1}$) vs Cl^- ($mmolL^{-1}$)	116
Fig. 4 - 8 The locations map of sampling sites of atmospheric precipitation in Barada and Awaj Basin and other basins in Syria.	118
Fig. 4 - 9 The locations of groundwater sampling points for environmental isotopes investigations.	119
Fig. 4 - 10 The relationship between $\delta^{18}O$ and δ^2H in the atmospheric precipitation (Weighted Mean) and in the groundwater samples.	121
Fig. 4 - 11 The relationship between the both $\delta^{18}O$ and δ^2H and altitude for precipitation and groundwater samples.	122
Fig. 4 - 12 The relationship between tritium unit and the distance from the Syrian shoreline.	123
Fig. 4 - 13 Change of $\delta^{18}O$ in the Beit Jinn spring during the year of 1994.	124
Fig. 4 - 14 Equipotential contours map based on groundwater level measured in 31 monitoring wells during October 2006. The associated hydrogeological sub-regions (A and B) as well as cross section C-D are depicted.	126
Fig. 4 - 15 The fluctuations of monthly groundwater level of the well 46RK from 2004 until 2011.	127
Fig. 5- 1 Schematic hydrogeological cross section C-D (Fig. 4-14) demonstrates conceptual hydrogeological model.	130

Fig. 5 - 2 Two dimensional (2D) FEFLOW mesh for the groundwater model and the spatial distribution of boundary conditions, springs and observation wells as well as the equipotential contours of measured initial hydraulic head for September 2010.	132
Fig. 5 - 3 Variogram associated with the performance of kriging interpolation method....	133
Fig. 5 - 4 Irrigation field location sites and spatial distribution of abstraction wells.	136
Fig. 5 - 5 The irrigations method applied in the study area (plain region).	137
Fig. 5 - 6 Spatial distribution of the hydraulic conductivity in the model domain (upper aquifer horizon).	138
Fig. 5 - 7 The comparison between measured and simulated initial hydraulic head in the upper aquifer horizon, September 2010.	139
Fig. 5 - 8 Scatter plot of measured and simulated initial hydraulic head for September 2010.	140
Fig. 5 - 9 Simulated equipotential contours lines in the Cretaceous aquifer, September 2010.	142
Fig. 5 - 10 Simulated equipotential contours lines in the Jurassic aquifer, September 2010.	142
Fig. 5 - 11 Three dimensional (3D) numerical model showing computed water budget in the upper aquifer horizon applied for steady-state simulation during September 2010. The positive inflow and negative outflow values are expressed in Mm ³ y ⁻¹	145

List of Tables

Table1-1 Average discharge of major springs in the study area during several hydrological years.....	53
Table 2 - 1 Site locations of the samples collected during the first fieldwork campaign (2006) as well as other samples from Selkhozpromexport (1986).....	74
Table 2 - 2 Site locations of the samples collected during the second fieldwork campaign (2012).....	77
Table 3 - 1 List of sampling sites and chemical composition of water samples collected during November and December 2006 and the historical data based on Selkhozpromexport study performed on 1986.	173
Table 4 - 1 Major ions concentration in the precipitation samples collected from three stations located in the study area.	107
table 4 - 2 List of sampling sites and chemical composition of water samples collected during August 2012.	179
table 4 - 3 Environmental stable isotopic composition measured in groundwater samples collected from 18 sites in the study area during August 2012 as addition to 3 samples from Selkhozpromexport 1986.	180
table 4 - 4 Environmental stable isotopic composition and amount of precipitation measured in different meteorological stations in Syria. 1989-1990 data from Kattan (1997a), 1983-1984 data from Selkhozpromexport (1986) and Arneh data from Kattan (2006).....	181
Table 5 - 1 Possible amounts of water entering and leaving a groundwater system of the upper aquifer horizon and the primary information used to calculate different components of the groundwater budget in this horizon. Units are in $Mm^3.y^{-1}$	144

Introduction

Syria occupies the eastern coast of the Mediterranean Sea. It is a largely arid country with a land area of about 185,000 km² of which around one third is arable land or forests and the remaining is desert and rocky mountain area (Higano and Melhem 2002). Water has always been an important resource in the Middle East and has had strategic implications. This area is considered one part of the world where water scarcity is severe and precarious (Berkoff 1994, Brielmann 2008). It is a common and often-expressed assumption that "the next war in the Middle East will be about water" contended, for instance, by former UN general secretary Boutros Boutros-Ghali (Fröhlich 2012). The struggle for fresh water in this area was a primer cause of the 1967 Arab-Israeli war and has contributed to other military quarrels in the region.

Over the last few decades, the rapid growth and socio-economic development in most of the sectors especially agricultural and light industry as well as the effect of climate changes have severely affected water resources in the whole country and lead to water quality and quantity degradation. The sufficient availability of water resources are considered to be the key for prosper economic development in agricultural countries such as Syria. The agricultural sector consumes more than 80% of total water resources of the country (Kaisi *et al.* 2006). The dry continental climate is prevailing in the eastern Mediterranean Basin, leading to substantial decrease in average precipitation (Al-Charideh 2007). Issar (2008) has concluded that the future increase in global temperature will cause the dryness and desertification over the Mediterranean regions. The combination of climate change effects with the increase in population density in these regions will undoubtedly produce starvation and exacerbate poverty there. The recent drought which began in 2007 in the Middle East has further strained the limited water resources in the region which is quite alarming. This requires immediate reaction to achieve water resources sustainability (U.S. Department of Agriculture –USDA 2008, Integrated Regional Information Networks 2010, Voss *et al.* 2013). Fröhlich (2012) has mentioned that so many Syrian farmers have lost their livelihood due to an on-going drought which has reduced the amount of arable land through desertification and put enormous pressure on the previously scarce natural water resources. According to Abou Zakhem and Hafez (2010) the average decrease of rainfall in Syria was about 18% over the last 10 years.

Syria is characterized by low rainfall with annual and seasonal variations. In Barada and Awaj Basin (Damascus Basin), the percentage of actual rainfall to average rainfall during 2000 was 59% while a year earlier it was just 16% (Elhadj 2004). In the Hermon region and according to joint climate-hydrology simulations result, the decrease in annual precipitation amount will be about 25% in the coming years (Suppan *et al.* 2008). Since streams flow and groundwater renewability are essentially generated by precipitation, in simple words, one cannot imagine a region scarce in precipitation, will ever enjoy abundance of surface and groundwater resources. However, the impact of climate changes on groundwater resources depends upon the change in the volume and distribution of groundwater recharge (Kumar 2012), but this impact is difficult to assess (Seiler and Gat 2007, Brielmann 2008). Nevertheless, it is well recognized that regional depletion of groundwater resources is a global-scale problem (Konikow and Kendy 2005, Kløve *et al.* 2013).

According to Mourad and Berndtsson (2012), the annual available water per capita in Syria will decrease from 2684 m³ in 1970 to 620 m³ in 2025. The Syrian government's development policy has encouraged the expansion of the irrigation area in order to reach food self-sufficiency, but no consideration was given to the sustainability of groundwater resources. Groundwater abstraction in Syria exceeds by far its recharge in almost all regions, and all tapped aquifers are overexploited (Stadler *et al.* 2012). Hence water scarcity and its sustainable use in all sectors is becoming a matter of social, economic and political concern. The challenges of water scarcity are heightened by the increasing costs of developing new water resources, land degradation in irrigated areas, groundwater depletion, water pollution, and ecosystem degradation (Rosegrant and Cline 2003, Aw-Hassan *et al.* 2014). Syria suffers from both water scarcity and misdistribution of its water resources. Its surface water is typically scarce by nature, and the situation is even made worse by the fact that most of them are trans-boundary. The rapid growth of population which is considered to be amongst the highest in the world, 2.9% in 2003 and 2.5% in 2010, (CBS 2010, Aw-Hassan *et al.* 2014) leads to redoubling the Syria's population every 22-25 year (Abed Rabboh 2007). The heterogeneous distribution of water resources over water basins as well as the unbalanced distribution of population over these basins causes greater pressure on water resources.

The use of groundwater in Syria dates back to centuries ago. Currently, groundwater provides the necessary supplies for drinking and domestic purposes as well as for agricultural and industrial purposes. Syria's local agricultural policy of subsidized inputs and supported prices for the expansion of cotton, wheat, maize and beetroot areas, is leading to more demand for groundwater irrigation. Groundwater is estimated to constitute more than 50% of the total amount of irrigation water in the country. (JICA 1997, Jumaa *et al.* 1999, Zhou *et al.* 2010). In Barada and Awaj basin, the total withdrawal from groundwater and surface water resources for irrigation purposes amounts to $786 \text{ Mm}^3\text{y}^{-1}$ while the withdrawal of 269 and $76 \text{ Mm}^3\text{y}^{-1}$ are for the domestic and industrial purposes respectively (Kaisi *et al.* 2006). Moreover, Damascus is located in this basin, it characterized by uncontrolled rural-urban migration and mushrooming illegal settlement. To overcome the water demand increasing across the city, the policy makers are started looking to other possibilities in order to adjust the pressure on water demand. More areas in the basin are being investigated for additional water supply and the study area is one of the most promised areas.

Sustainable, management and careful use of the scarce groundwater resources is the most prominent challenge for the country, this requires more knowledge about groundwater systems, which became a key issue. Such knowledge is especially critical in arid and semi-arid regions, where natural recharge and discharge rates are often low and groundwater pumping can rapidly dominate the behavior of the system. Springs are probably the most widely available means for providing groundwater mainly in the karstic carbonate rocks. For instance, the Fegih spring, the main source of potable water supply in the capital city of Damascus, is considered to be the third largest karstic spring in the world (La-moreaux 1989). Groundwater is over-exploited in most of the basins due to the fact that water extraction rates overcome by far available water recharge rates. This causes water deficiency in most regions of Syria and declining in spring' discharges.

The Barada and Awaj Basin is considered to be one of the most important seven basins constituting Syria (Fig.1-1). In spite of the fact that this basin has no significant water resources, it constitutes an important water supply for the capital city, Damascus. From historical point of view; the two main rivers in this basin (Barada and Aawaj), after which the basin is named, are considered to be a vital socioeconomic supply, sustaining the agricultural activities in this basin (INECO 2009).

The carbonate aquifers system of Cenomanian-Turonian of Upper Cretaceous and Jurassic, which dominates in the study area, represent the most important water-bearing systems in the Barada and Awaj Basin and even in Syria and the major Mediterranean countries (Al Charideh 2011). The reasons behind that are their great interannual recharge (storage capacity) and the easy restoration of their groundwater either naturally by huge discharge of issuing springs or artificially with remarkable potential of groundwater abstraction (JICA 2001). These water bearings are the main exploitable resources for domestic water supply in large cities such as; Damascus, Latakia, Beirut and the West Bank. However, and in most cases, these aquifers are not exploited in an appropriate way. This partly caused by the lack of knowledge about their hydrogeological characteristics. For instance, Ras El Ain spring, the main spring of the Khabour River, the main left bank tributary of the Euphrates River (Al Khabour basin, Fig.1-1), is dry some months of the year in the present, while it was one of the largest karst springs in the world with a mean annual discharge of about $38 \text{ m}^3\text{S}^{-1}$ in the 40s and 50s (Burdon and Safadi 1963 and 1964, El-Hakim and Bakalowicz 2007).

The importance of the Hermon area in addition to its strategic location, comes from the fact that its snowcap and precipitation feed every stream, spring and river in that area. The evaluation and assessment of water resources in the upper part of Aawaj River catchment are based on the identification of origin and recharge/discharge mechanisms controlling groundwater flow by using hydrochemical and environmental isotope technique (^{18}O , ^2H). Moreover, groundwater modeling will contribute in understanding the relationship between the complex multi-layered aquifers in this area. It is likely that the obtained will remain part of the strategy aimed at sustainable water resources management in Barada and Awaj basin.

Such a combination has been proved to be a valuable tool for understanding many hydrogeological problems. Further significance of applying of these methods came from the fact that they can easily and successfully be used to detect the groundwater resources and its recharge and discharge mechanisms. Application of such techniques was recently introduced to the country through several investigations in different basins of Syria (Kattan 1997a, 1997b, 2006 and 2008, Kattan *et al.* 2010, Saad *et al.* 2005, Al-Charideh 2007, 2011, 2012^a and 2012^b, Al Charideh and Abou Zakhem 2010^a and 2010^b, Luijendijk and Bruggeman 2008, Stadler *et al.* 2012, Al Charideh and Hasan 2013).

In the natural circumstances, water availability is a function of recharge effort and extraction rate. The decreasing water resources in the study area as a result of climate variability and increasing of water demand is one of the major challenges facing the habitants over there. The population in the whole study area is about 40,000 who are distributed in 14 villages and two Palestinian refugees' camps and is strongly depending on agricultural resources (fruits, olives, beans and vegetables).

This research aims at: (I) Determining the groundwater origin and its geochemical evaluation based on rock-water interactions within the framework of its complex geology and morphology. (II) Identifying the major hydro-geochemical processes controlling the groundwater quality and the dominating water types based on their chemical compositions and ionic ratios. (III) Interpret the groundwater flow behaviour and assess the recharge and discharge mechanisms in the study area. (IV) Give a quantitative estimation for groundwater budget of the upper aquifer horizon, where the majority of habitants and the agricultural activities are well developed, under steady-state conditions.

Chapter 1. General setting of the Study area

1.1. General Characteristics of the Study Area

The Barada and Awaj basin forms the northern part of Mt. Al-Arab graben of southwestern Syria and lies between $32^{\circ} 43'$ and $33^{\circ} 55'$ of latitude N and $35^{\circ} 48'$ and $37^{\circ} 05'$ of longitude E (Fig. 1-1). It covers an area of about 8,692 km². As a result of a series of tectonic, volcanic and weathering events, which has started in the late Mesozoic period (Dubertret 1932, Ponikarov 1967, Selkhozpromexport 1986 La-Moreaux *et al.* 1989, Kattan 2006), several fold structures are appeared, such as Mt. Anti-Lebanon (up to 2,466 ma.s.l), Mt. Hermon (2,814 ma.s.l), Palmyrides (1,308 ma.s.l) and Mt. Arab (1,790 ma.s.l).

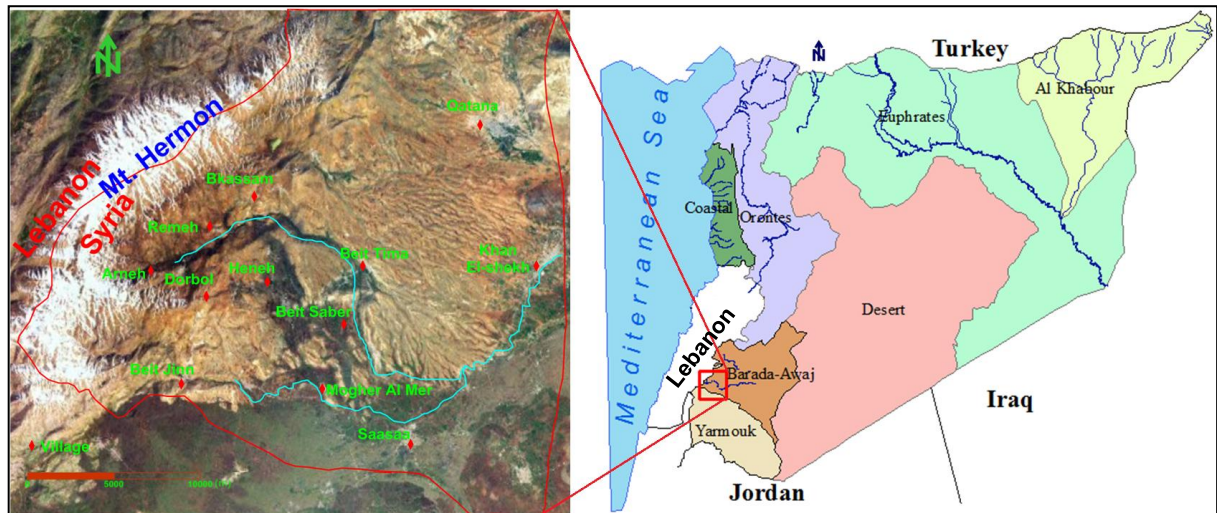


Fig.1-1 The location site of the study area and map of Syria divided into 7 hydrogeological basins.

From a hydrological point of view and as aforementioned, Syria is divided into 7 hydrogeological basins (Fig.1-1), and the study area is shared between Syria, Lebanon and occupied territories. Hydro-politically, the problems over water in this area still the main obstacle for reaching peace between Syria and occupied territories. This area is considered as a part of vital regional area in terms of future water security of these countries. The Israel's occupation since 1967 of the Golan Heights has given it not just vantage points of considerable military strategic but also the effective upstream positions over water resources at this area.

The study area (Fig. 1-1) covers an area of approximately 600 km² and is considered to be a major recharge area of the Aawaj River which is a main water course in that area and mostly characterized by a seasonal flow regime. The total long of this river is 91 km and its supply catchment area estimated to be 1120 km² (MOI 2005). This stream is formed by the junction of two main tributaries (Jenani and Sebarani), which are fed from a large number of karstic springs that are distributed along the slope of Mt. Hermon in the Arneh and Beit Jinn valleys. The annual average discharge of Aawaj River in the normal circumstances is 4.7 m³S⁻¹ between the years 1982-2004 (MOI 2005) which has decreased to approximately 2.2 m³S⁻¹ with a total dry out period during summer in recent years (2004-2014) [(Melhem and Higano 2001). In dry year such as the hydrological year 2000-2001, its average discharge was 0.5m³.S⁻¹ during winter while it dries out during summer (Elhadj 2004). This river loses most or all of its resources as it flows towards Damascus depression by the intensive exploitation along its course for irrigation purposes. In the former days, the river was terminated in Hijaneh Lake as a final natural drainage system. This lake is located at the central part of Barada and Awaj basin and is dried out nowadays.

The average discharge of the springs located in the study area ranges between 0 and 0.3 m³S⁻¹ during summer and between 0.025 and 2.7 m³S⁻¹ during winter (RDWSSA 2006).

From the geomorphological point of view, the area can be considered as a result of Jurassic to recent deposition, tectonic, and volcanic. Sporadic uplift along with comprehensive folding and faulting at shallow depth has resulted in a variety of surface forms and geologic structures. This area can be divided into three parts, mountain ridges, volcanic district and plain area. The mountains occupy the western part with anticlines or hogbacks shapes which are resulted from the Neogene and Quaternary tectonic structure (folding and/or faulting). The major sharp deep valleys in-between follow synclinal structures, occur as strike valleys parallel to hogbacks or are the result of Pleistocene erosion along normal faults of significant displacement. The karst features are well-developed in this part at surface and even in deeper parts. The volcanic formations occupy the southern part as an outcome of effusive rocks during the Neogene and Quaternary periods. The plain region occupies more than 1/3 of the whole study area in the central and eastern parts where the exposure of Neogene and Quaternary formations are dominating. The elevation in the study area varies between 800 and 2800 ma.s.l (Fig. 1-2).

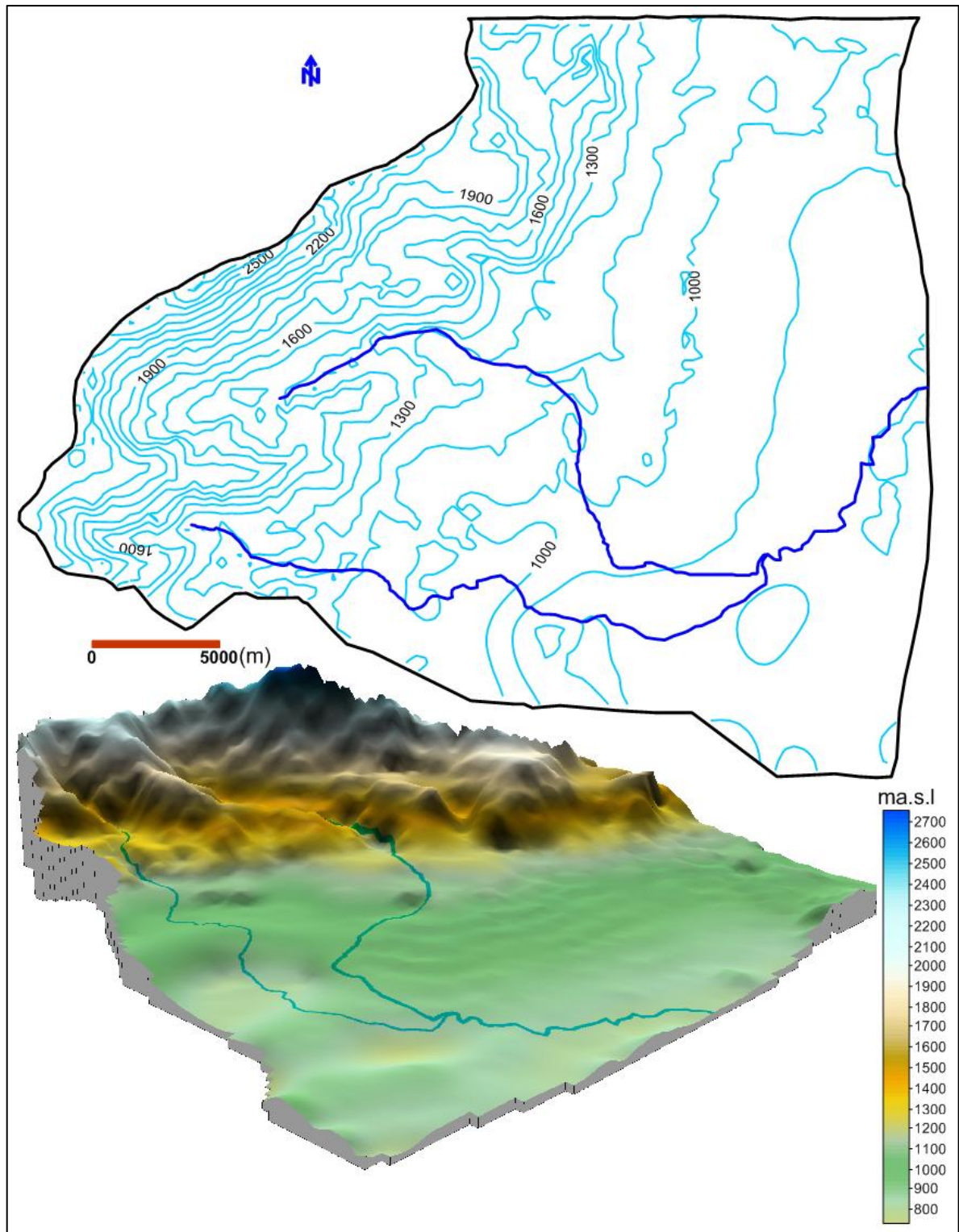


Fig. 1- 2 Elevation contour lines of the study area as well as the 3D view of this area.

1.2. Geology

From geological point of view, the Barada and Awaj basin is situated at the junction between two major structures: the Mt. Arab depression in the south; and the Palmyrides-fold system, which includes also the Mt. Anti- Lebanon, in the northwestern side.

The detailed stratigraphy and tectonic is an important issue in order to understand the hydrogeological setting of the study area. In Barada and Awaj Basin, pre-Jurassic deposits are not known (Wolfart 1964). However, the main formations outcropping in the study area date back to Jurassic up to Quaternary period. The complex of thick karstified strata of Jurassic limestone which interbeds with dolomite, dolomitic limestone gypsiferous limestone and marl is outcropped in the western portion of the study area in the Mt. Hermon. The plain areas are characterized by the exposures of Neogene and Quaternary deposits. The small exposure of Paleogene and Cretaceous are found locally in the southwestern part of the study area.

1.2.1. Stratigraphy

During the Middle and Upper Jurassic followed by the Upper Cretaceous era, thick carbonate deposits have been formed in the Mediterranean region. They are separated by complexes, impermeable series of sandstone, marls, and marly limestone of the Aptian-Alpian age. The different formations in the study area are described below from bottom to top.

1.2.1.1. Jurassic

The Jurassic rock sequences extend from the Middle to Upper Jurassic. The Middle Jurassic formations are illustrated by both Bajocian and Bathonian Formations, the Bajocian formations are partially exposed in the western portion of the study area in Mt. Hermon, and extend westward beyond the Lebanese border. The thickness of this rock sequence ranges between 200-750 m. These strata are mainly composed of dolomitic limestone and organic limestone. The Bathonian formation is exposed in the vicinity of Arneh village. It is mainly composed of rusty brownish limestone and marly limestone. The approximate thickness of this formation can reach 110 m. The Upper Jurassic strata are composed of the Callovian and Kimmeridgian formations. The Callovian rock sequence is exposed in wide areas of the eastern part of Mt. Hermon. This rock is mostly composed of

gray limestone overlain by dolomitic limestone and gray dolomite. The approximate thickness of this rock varies between 350-700 m. The Kimmeridgian formation is composed of white organic limestone and its thickness ranges between 50 and 70 m. In the Barada and Awaj Basin, most of the uplifted blocks are composed of Jurassic formations.

1.2.1.2. Cretaceous

Some minor outcrops of the Cretaceous rock sequence are found in the southwestern part of the study area. The Cretaceous sequence ranges from Aptian to Senonian. The Aptian layers composed of sandstones cemented with calcite, marls, and iron oxides. The lower part of Aptian is characterized by the intercalations of basaltic and brown marly. The total thickness of Aptian may range between 70 and 100 m. The Albian layers are mostly composed of organic limestone containing marls and clays of an approximate thickness of 120-250 m.

The Cenomanian-Turonian rock strata are conformably lying over the Albian layers. These strata are composed mainly of limestone and dolomitic limestone layers which had affected by intensive tectonic movement accompanied by caves and high fractured zones during the Alpine orogenesis. The total thickness of these layers formations can reach a value of 600 m (Ponikarov 1967). The Senonian layers are composed of dolomitic limestone and marly limestone containing phosphate, chert nodules and clay. The average thickness of this formation may vary between 200-300 m in the study area. The Beit Jinn valley penetrates these formations where the Beit Jinn and high Beit Jinn springs emerge to form the Jenani tributary of Awaj River.

1.2.1.3. Paleogene

The Paleogene rock sequence and as aforementioned are exposed in a small part in the south-west of the study area. These formations consist of Paleocene, Lower, Middle and Upper Eocene Formations. The Paleocene rock sequence is made of intercalation of marly layers and clayey limestone. The Lower-Middle Eocene formations composed of marly limestone with chert nodules, which lie conformably over the Senonian rock sequence. The Upper Eocene rock sequence consists of limestone characterized by nummulites. Fig. 1-3 shows the range of Paleogene thickness in the study area which implies that this thickness reaches a highest value in the central part of the study area.

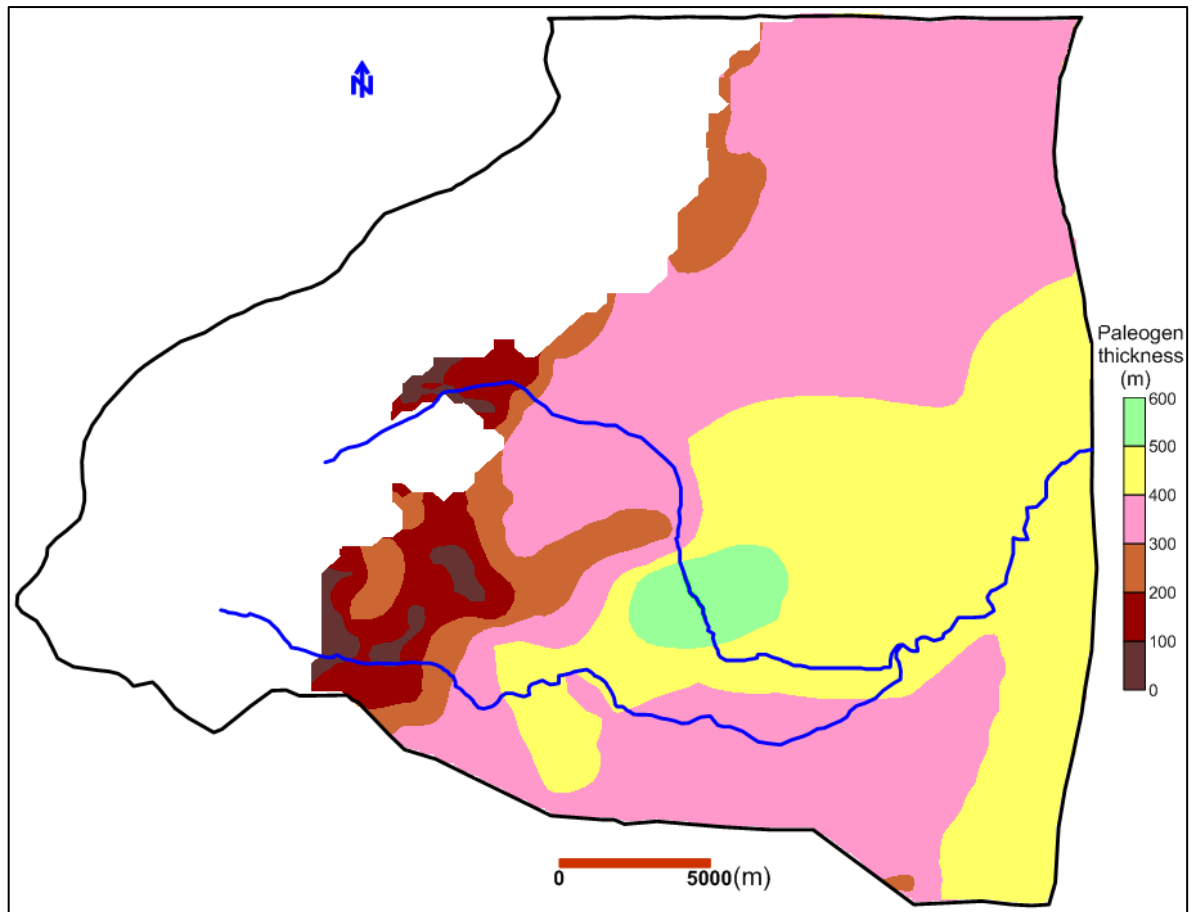


Fig. 1- 3 Range of the Paleogene thickness in the study area.

1.2.1.4. Neogene formations

The Neogene rock sequence is usually situated unconformity on the oldest rock sequence varying in age from the Jurassic to Paleogene. This rock sequence occupies the central and eastern part of the study area. It consists of the Pliocene and Miocene rock sequence. The Pliocene rock sequence is made mainly of conglomerates. The Miocene rock sequence consists of limestone and marly limestone. Dark colored basalts mainly of Miocene age which result from the uplift and block faulting, characterized by fractures filled with calcite, are found locally beneath the conglomerates of Pliocene age. It covers the sedimentary layers of Oligocene, Upper Eocene and post Paleogene continental deposits. The thickness of Neogene rock sequence increases toward the east and southeast. Fig. 1-4 shows the thickness of Neogene rock sequence in the study area.

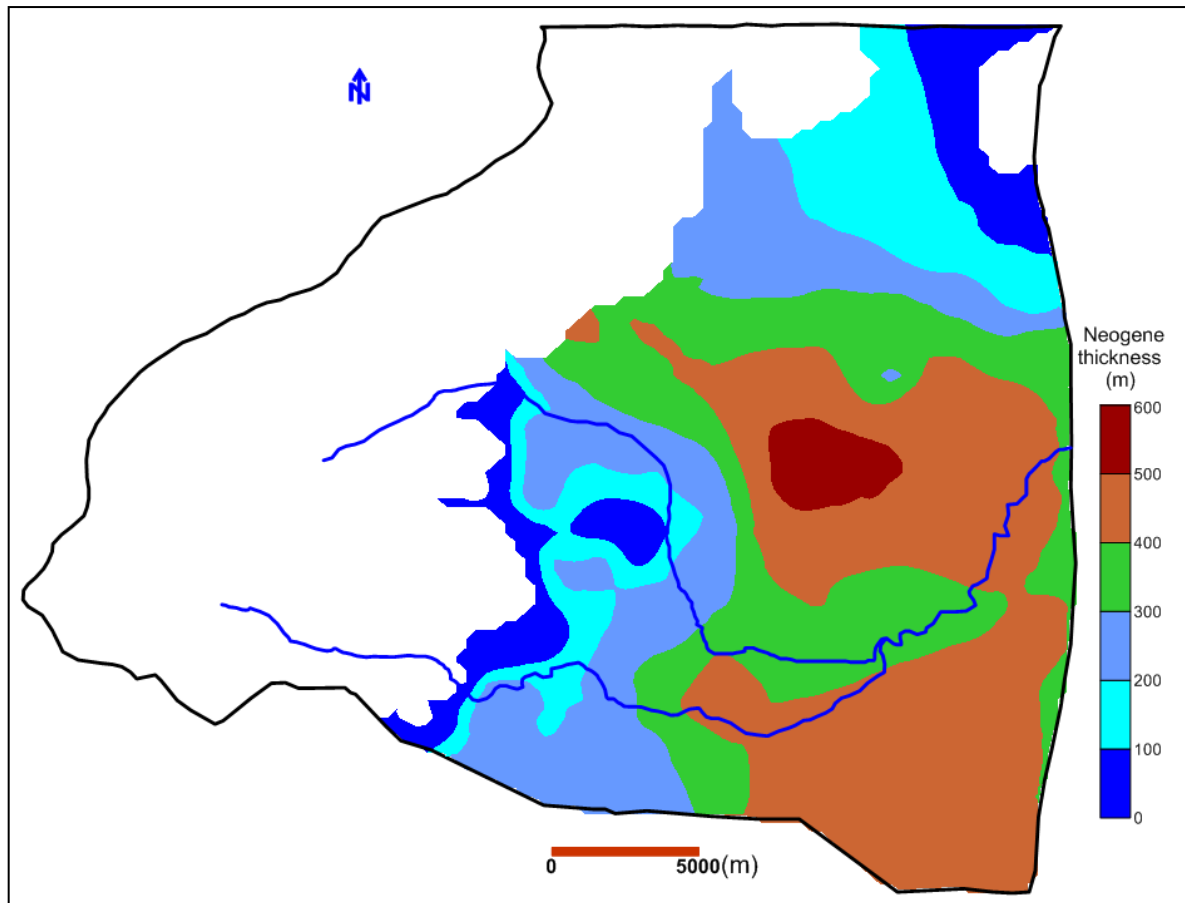


Fig. 1- 4 Range of Neogene thickness in the study area

1.2.1.5. Quaternary deposits

Quaternary deposits are mainly found in the plain area around the junction point of the Sebarani and Jinani tributaries. They consist of alluvial and alluvial-proluvial accumulated deposits such as gravel, loose sands, unconsolidated conglomerates, soil and clays. Their thickness varies between 2 and 15 m and may reach a thickness of 70 m or even more in some places in Barada and Awaj Basin.

1.2.1.6. Basaltic rocks

The basaltic rocks in the study area is considered to be as a part of extensive volcanic field which developed during the Cenozoic in the northwestern part of the Arabian plate and culminated in the extrusion of plateau basalt. (Mor 1993). This undulating plateau extends beyond the Syrian borders into Jordan and Saudi Arabia (United Nations 1982). The majority of those basalt rocks were outpoured after the Oligocene and the extrusion has continued intermittently until the start of the historical times. The Quaternary basalts

resulting from lava overflow from volcanic vents (Dubertret 1955) are located in the southern portion of the study area. These deposits are considered as the last extrusion occurred in historical time (Mouty *et al.* 1992). According to Asfahani and Abdul Ghani (2012), four kinds of basalt can be distinguished in the study area: hard massive basalt, hard basalt, pyroclastic basalt and the alteration basalt products and clay. The basalts of Miocene are weathered in places into basaltic soil (Fig. 1- 5). The geological map of the study area is shown in Fig. 1- 6.



Fig. 1- 5 Shows the soils that derived from the weathering of the basalt of the Neogene age in the study area.

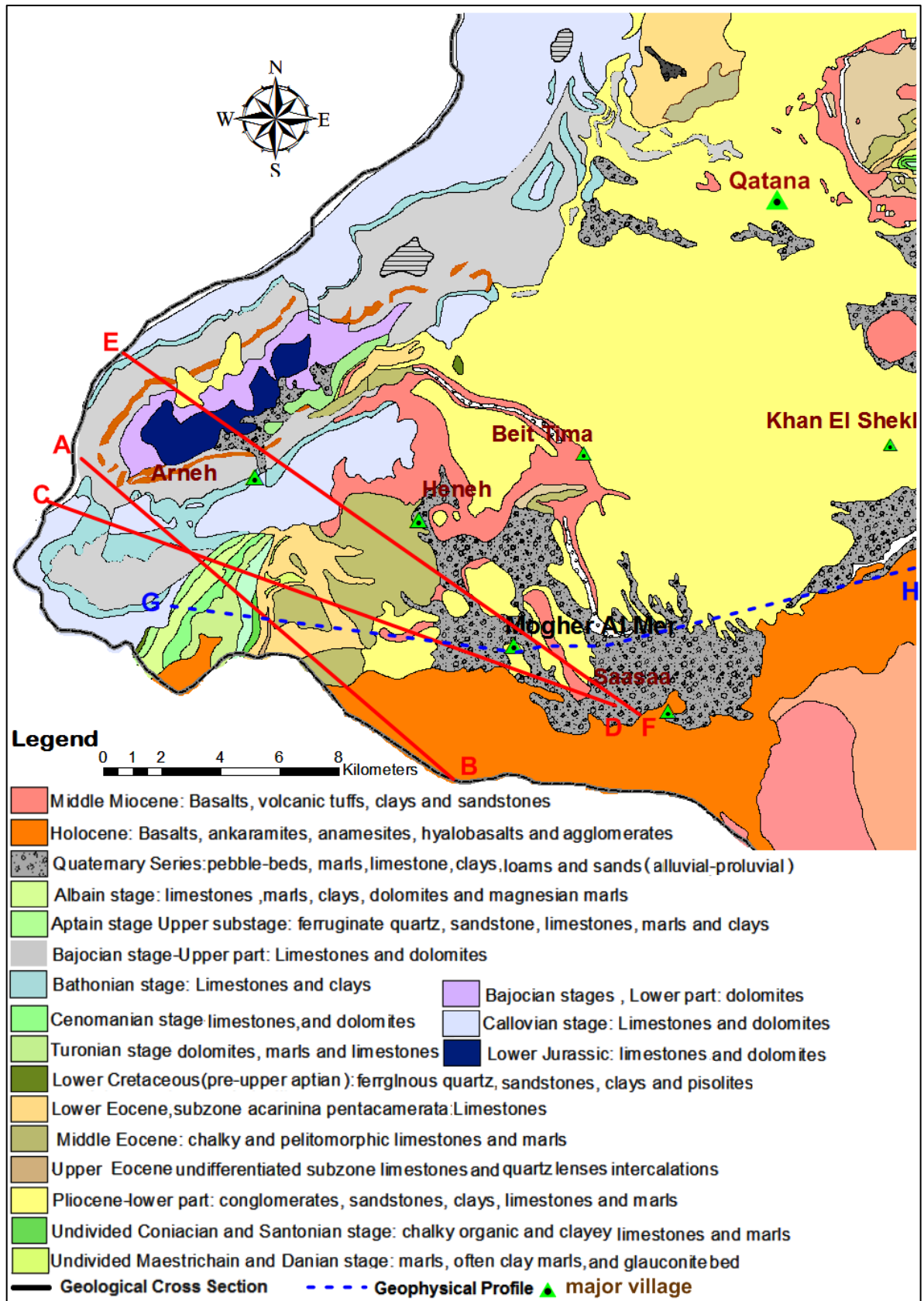


Fig. 1- 6 Geological map of the study area modified from Selkhozpromexport 1986, as well as three geological cross sections and one geophysical profile.

The rock sequences of different geological age play major role in terms of the aquifer's characteristics such as aquifer type, storage capacities and hydrodynamic properties. The graphic logs of that record the stratigraphy of the Barada and Awaj Basin is shown in Fig. 1-7




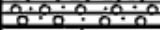
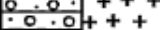
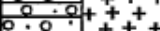








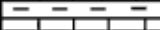

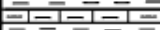
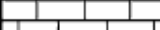
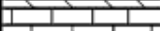
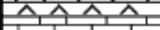
GEOLOGICAL AGE		FORMATION	MAX. THICKNESS IN METERS	LITHOLOGY	
QUATERNARY	QUATERNARY	RECENT	V V V V V V V V V	VARIABLE	 LIMESTONE
		QUATERNARY	V V V V V V V V V	250	 DOLOMITE
TERTIARY	NEOGENE	PLIOCENE	 	550	MARL OOLITIC LIMESTONE
		MIOCENE	 	650	LACUSTRINE CARBONATE CLAYEY LIMESTONE
					100
	PALEOGENE	EOCENE	 	850	CLAY SANDSTONE
		PALEOCENE			100
		MESOZOIC	CRETACEOUS	SENONIAN	
TURONIAN				120	ANHYDRITE & GYPSUM
CENOMANIAN				570	CHERT
					NEOGENE BASALTS
ALBIAN				270	QUATERNARY BASALTS
JURASSIC	APTIAN			60	
	UPPER JURASSIC			400	
	MIDDLE JURASSIC		 	1700	
LOWER JURASSIC		150			

Fig. 1- 7 Graphical logs of the stratigraphy in the Barada and Awaj Basin (Kattan 2006)

The soils in Mt. Hermon are thin and even absent in the higher altitude; it decreases in thickness with increasing altitude and slope while it can reach a thick of 2-3 m in the plain region which enhances the development of agricultural activities.

1.2.2. Structures

The geological history of Syria from the Triassic age to the present day records numerous tectonic upheavals which have interrupted, changed or modified the sedimentation, and altered the rocks which existed before each tectonic episode (Burdon and Safadi 1964). The major branches of Red Sea-Dead Sea Rift Valley transform faults system forms the boundary that links the Arabian plate convergence in southern Turkey with the active seafloor spreading in the Red Sea. This system is cutting the study area which makes it very complicated from the tectonic point of view (Quennell 1959, Freund 1965, Bartov 1974, Bartov *et al.* 1980, Garfunkel 1981 and 1989, Mor 1993). The faults of this system are characterized by irregular shape, direction, terrain structure and land folds (Malkawi *et al.* 1995). Important folding structures seem to be predominated as a result of the tectonic movement during Oligocene/Pleistocene. In the central part of the rift, it produces a horst-graben structure which elevated the Mt. Hermon as large fold and lowered the Bekka in Lebanon and the Ghab in Syria as a large depression (Burdon and Safadi, 1964).

The Mt. Hermon, Jabal El Sheikh in Arabic, (Fig. 1-1), is 55 km long and 25 km wide. This mountain comprises an area of about 1250 km² and is formed the western part of the Barada and Awaj Basin (Rimmer and Salingar 2006). It is an open isolated major trending anticline that lies along the south-western margin of the Early Mesozoic Palmyride rift system (Wilson *et al.* 2000). It is long and continuous with hinge axis trending in NE-SW direction parallel to the Syrian - Lebanese boundary. It has had a complex, episodic, tectonic history involving phases of extensional and compressional deformation throughout the Mesozoic/Cenozoic period (Shimron 1998, Wilson *et al.* 2000).

The intensive tectonic stresses (compressing, folding and vertical movement), have induced dense jointing, faulting and fracturing of the Mt. Hermon ridge which played a basic role in terms of infiltration coefficient, the storage capacity of the rocks and the location and rate of water discharge. Generally, most strata from Jurassic to Cretaceous age are dipping in a southeast direction. Minor bedding disturbance can be found depending on

local structural disturbance. Fig. 1-8 shows the bedding and folding phenomena depicted in the field visit in the Arneh Valley.



Fig. 1- 8 Bedding and folding phenomena in the carbonate rocks of Jurassic (Arneh valley).

Several phases of faulting combined with tectonic rotation gave rise to chaotic look like fault sets. In general, two major fault directions can be recognized; the first one tending in northeast-southwest parallel to the hinge axis of Mt. Hermon, and the second one oriented to northwest-southeast. The second type of faults is extensively observed in the study area mainly in the central part. Fig. 1-9 shows the major faults depicted in the study area which play a significant hydrogeological role.

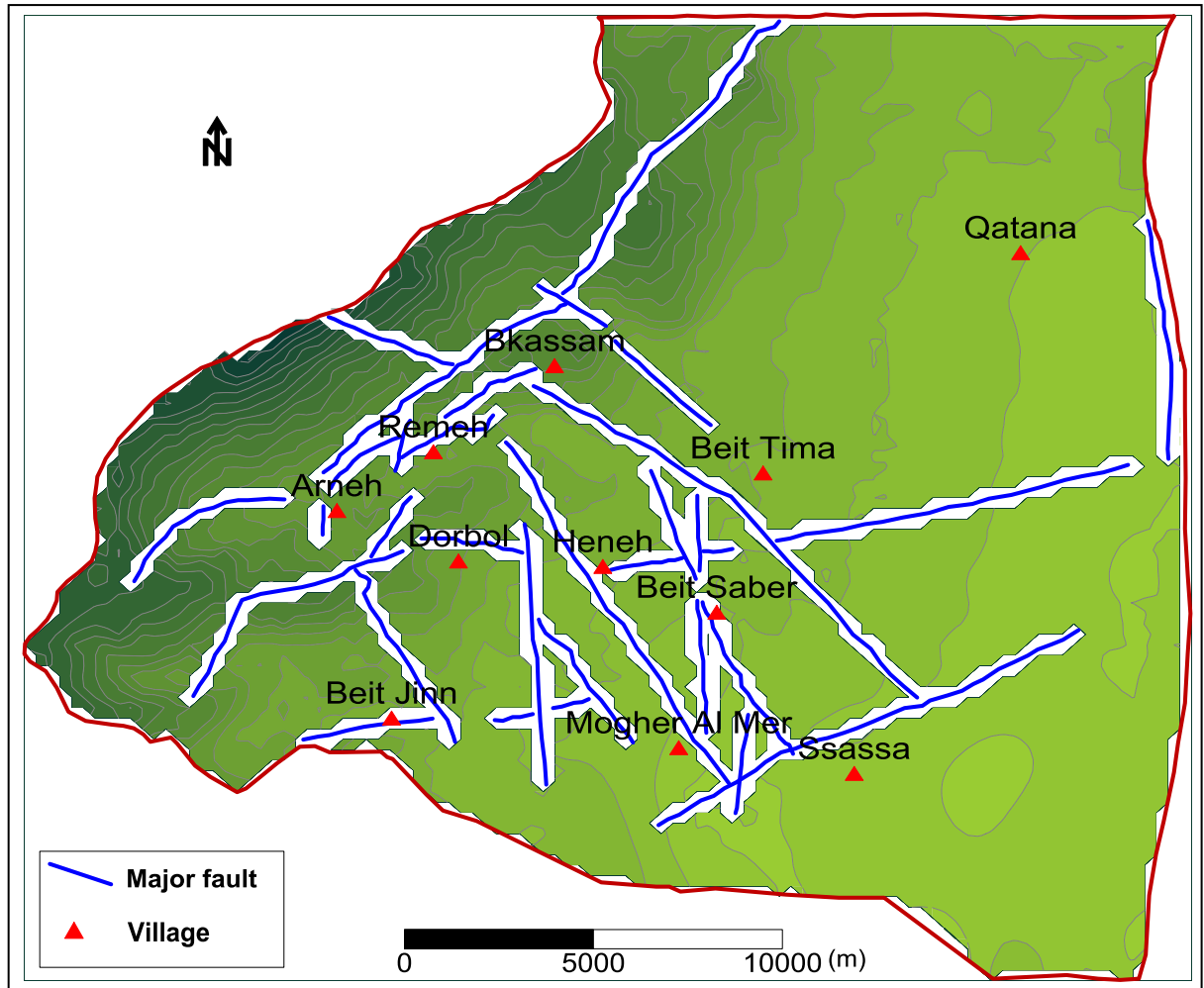


Fig. 1- 9 Majors fault in the study area (updating from Selkhozpromexport 1986)

The three geological cross sections, geophysical profile showing the subsurface lithology and the major structures within the study area are provided in Fig. 1-10 and Fig. 1-11 respectively.

Based on the cross section that runs along the geophysical profile, it appears that faults F1, F3, and F4 have lowered the Neogene-Paleogene-Cretaceous sequences with respect to the older strata of Jurassic age.

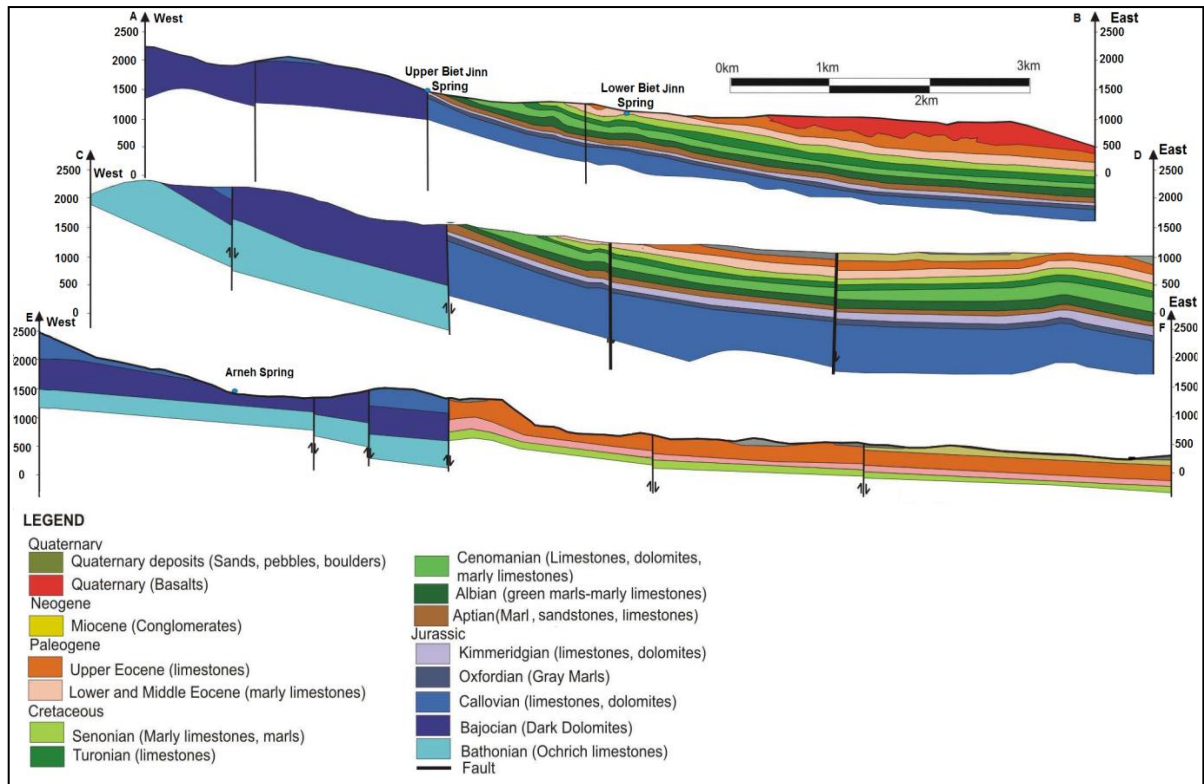


Fig. 1- 10 Three cross sections: A-B, C-D, and E-F (Fig. 1-6), demonstrate the subsurface lithology as well as the major structures within the study area. (Modified from RDWSSA 2006)

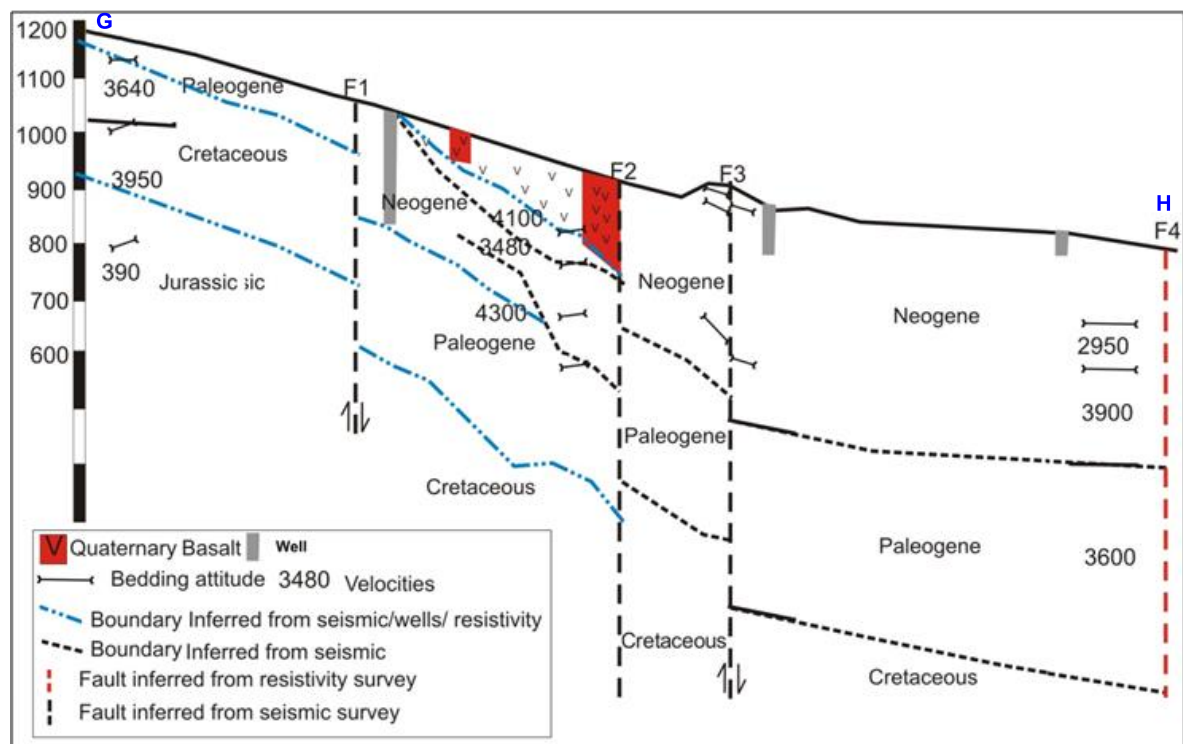


Fig. 1-11 Geophysical profile G-H (Fig. 1-6), demonstrates the subsurface structures (Modified from RDWSSA 2006)

The majority of the aquifers in the study area are weakly permeable outside of the tectonic zones and karstic process. Mt. Hermon displays a multiphase of karstic system. The most important factors controlling karst development are geological features, altitude defining the climatic belts, the local slope gradient and the paleohydrological evolutionary history of the mountain (Frumkin *et al.* 1998). The well-developed karstic features enhance large preferential groundwater flow and relatively little surface runoff (Rimmer and Salingar 2006).

1.3. Hydro-climatology

The climate of the study area is generally considered as modified Mediterranean type with continental influence (warm dry summer and cool rainy winter, with two transitional periods in spring and autumn). Its climate is determined by dynamic factors that are related to the circulation of the atmospheric air masses inside and outside the area. In winter times, the semi-permanent system of the cold Siberian high pressure is dominating, while in summer times, the Indian Monsoon low pressure is prevailing. Thus, the climate conditions of this area are often subject to high variability due to the influence of different air mass circulation and the local effect of two main geographical features, the Mediterranean Sea and the Anti-Lebanon Mountains.

The principal meteorological factors which produce precipitation are cyclonic disturbances formed over the Mediterranean Sea, or the Atlantic Ocean. In summer the subtropical region of the Azores anticyclone, establishes itself over the coastal area of the Mediterranean, thereby preventing the penetration of the cyclones from the sea into the eastern Mediterranean region. In spring a low pressure area is formed as a result of the movement of the Khamasin wind system into Syria and adjacent areas. As a result of recent climate changes, including a decrease in winter temperatures and total precipitation amount as well as an increase in summer temperatures, lead to prevailing of dry continental climate over this region (IPCC 2001, Alpert *et al.* 2008).

In Syria there is only 2-3 months annually in which rainfall exceeds evapotranspiration to permit groundwater recharge (Bijay-Singh *et al.* 1995). More than 60% of the country receives less than 250 mm y^{-1} , which makes its water scarce (Mourad and Berndtsson 2011). Annual precipitation in Barada and Awaj Basin varies between 86 and 1000 mm y^{-1} , which made this basin classified into four zones, hot desert, arid, semiarid and moderate zone

(RDWSSA 2006). In the study area, the climate conditions varies from semi-humid (moderate) in the western portion in Mt. Hermon, to semi-arid in the plain region which is located in the central and eastern portions. Between December and March the higher region of Mt. Hermon (> 1500 ma.s.l), usually receives the precipitation in the form of snow which may persist until June.

In the study area, the amount of precipitation decreases eastwards, and varies from more than 1000 mm^{-1} in the Mt. Hermon to less than 300 mm^{-1} in the eastern part of this area. The wide range of the amount of precipitation in this relatively small area is related to the existence of mountains which constitute a barrier preventing wet depression from the Mediterranean Sea to reach the eastern region. Fig. 1-12 shows the spatial distribution of the amount of precipitation measured at six meteorological stations located in the study area during the hydrological year 2009-2010.

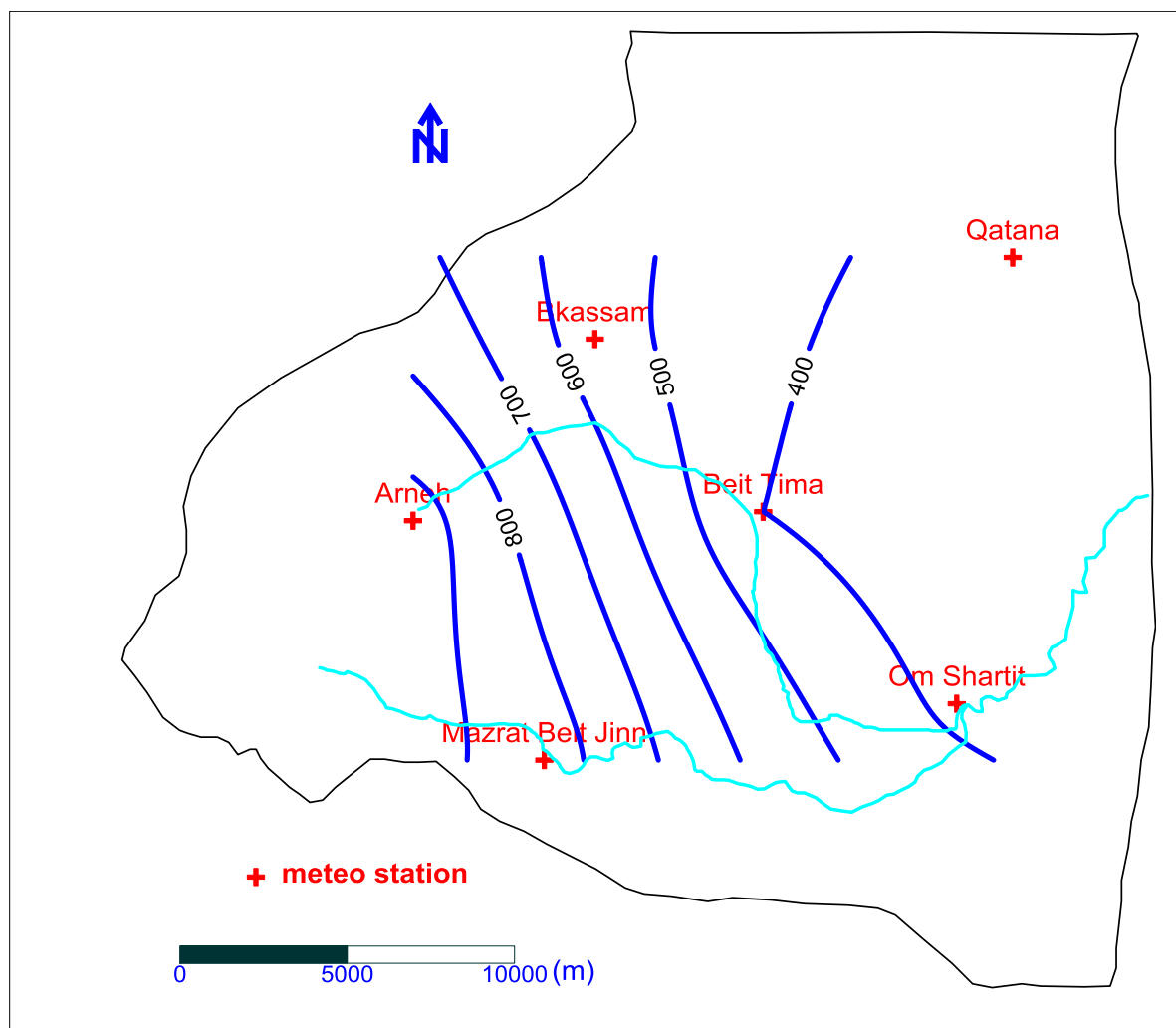


Fig. 1-12 Precipitation isopleths map based on the amount of precipitation measured at the six meteorological stations located in the study area during the hydrological year 2009-2010.

The monthly average of air temperature ranges between 25° and 27°C in summer within the plain region, while this value is about 19° C in the mountains at elevation above 2000 ms.s.l during the same period. In winter, the monthly average of air temperature ranges from 10° to 15°C within the plain area and decreases to less than 0 °C above 1500 ma.s.l. According to Alpert *et al.* (2008), the average temperature over the Eastern Mediterranean area has increased by 1.5-4 °C in the last 100 years

The relative humidity values are essentially related to temperature oscillation (JICA, 2001), thus low monthly values are usually about 24-50% during summer (July and August) and may reach up to 60–70% during winter (January and February). The humidity values generally decrease eastward across the recharge area for any given elevation. The reason behind that is due to increasing distance from the principal source of water vapor, the Mediterranean Sea, and the increasing effectiveness of a rain-shadow as the moisture is carried eastward across the Anti-Lebanon by winter storms. The annual potential evaporation varies between 1,500 mmy^{-1} in the flatlands to 1,100 mmy^{-1} in the mountainous parts. the lowest values of potential evaporation estimated to be 500 mmy^{-1} for the altitude more 2600 ma.s.l. Evapotranspiration in the mountainous area varies between 300-400 mmy^{-1} while it is about 100 mmy^{-1} in the flatland area (Selkhozpromexport 1986; Kattan 1997b).

1.4. Hydrology

The drainage network of the study area is influenced by climatic, topographic, geomorphic, geologic, ecological and anthropogenic conditions prevailing in that area. From the satellite photo (Fig. 1-1), it is clear that the ancient drainage network plays an important role in the formation of Neogene conglomerate which occupies the plain region. In this area, three alluvial fans can be determined of which one is relatively large compared to the others.

1.4.1. Awaj River

The denser drainage network is found along the slopes of the Mt. Hermon ridge at the altitude of more than 1000 ma.s.l where the two tributaries of Awaj River (Sebarani and Jenani) are generated. This river is considered as a main form of surface water in the study area. During summer, it used for irrigation purposes through more than 20 canals branching out into the plain region. The major factors affecting streams discharge in this area are precipitation and snowmelt. The amount of snowfall at the altitude between 2200m and 2400m is estimated to be between 1100 and 1700 mm. The snowmelt contributes to about 80% of the total precipitation for the altitude more than 2400 m, and about 60% for the altitude between 2000 and 2400 m, while this value is about 30% at the altitude of 1500 m (MOI 1994). Surprisingly, it was observed that snowfall on Mt. Hermon and Anti-Lebanon had twice the water content as the same volume of snow falling at the same altitude on the Alps (Aouad-Rizk *et al.* 2005, Brielmann 2008).

According to Scanlon *et al.* (2006) and Brielmann (2008), the preferential flow through fractures rocks in the valleys of semi-arid region is a common phenomenon. The main tributary of Awaj River (Sebarani) starts beneath the central peak from the exposure of Jurassic formations in the western side of the study area near Arneh village (Arneh Valley, Fig. 1-13).



Fig. 1- 13 The Arneh Valley where the Sebarani tributary of Awaj River is generated and flowing

The discharge of karstified Jurassic carbonate rocks as a preferential (quick) flow through small but numerous karstic springs, which emerge mainly at the interfaces of main faults or impermeable formations, forms the main recharge source of this tributary. These springs are Daboura, Almashraa, Bardeh₁, Bardeh₂, Salt, Saba, Kneiseh, Rashasheh, Arneh and others seasonal one. Fig. 1-14 shows Kneiseh and Rashasheh springs as an example of these springs.



Fig. 1- 14 Kneiseh and Rashasheh springs emerge from the upper part of Arneh valley (Jurassic aquifer).

The average discharge of these springs from the hydrological years 1974-1975 until 2008-2009 is calculated to be $25 \text{ Mm}^3 \cdot \text{y}^{-1}$. This tributary flows from the west near Arneh village towards the east until the south of Bkassam village. After that it flows towards south-west in the deep valley until Beit Tima village where it flows southward until Beit saber village. After Beit Saber village this tributary flows in the plain area towards east and joins the Jenani tributary to form the Awaj River which is recharged by Tabibieh spring after about 1.5 km of the junction point (Fig. 1-1). The Beit Tima gauging station is located about 14 km after Arneh station with an average discharge of about $29 \text{ Mm}^3 \cdot \text{y}^{-1}$ calculated from the hydrological years 1950-1951 until 2008-2009. The following measurement station is located in Beit Saber village after about 7 km, and the average discharge measured in this station is about $21 \text{ Mm}^3 \cdot \text{y}^{-1}$ from the hydrological years 1991-1992 until

2006-2007. The average discharge in Abo Qaouq gauging station, located about 7 km after Beit Saber station before the junction point is calculated to be $17.3 \text{ Mm}^3\text{y}^{-1}$. The gradient of this tributary decreases from 0.4 in Arneh region to 0.014 near Saasaa village.

Fig. 1-15 shows the flow path of Sebarani tributary in the different geological formations from Arneh village to the plain region and the change of its discharge at the different gauging stations.

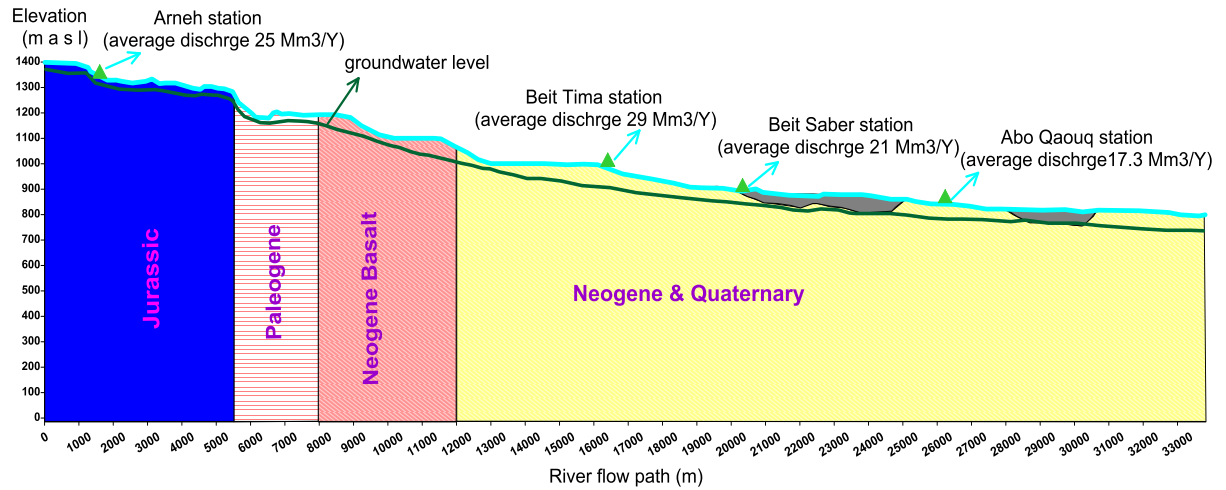


Fig. 1- 15 Schematic layout correspond to Sebarani tributary from Arneh toward the plain area throughout several geological formations

The Jenani tributary is formed few kilometers to the south of Sebarani tributary where the high Beit jinn spring is emerged at the contact of Jurassic and Cretaceous formations. This tributary flows in the concrete canal from west to east in the Cretaceous and Paleogene formations for about 7 km where it is recharged by Beit Jinn spring. After that it reaches the plain area of Quaternary, Neogene and basalt formation and recharges by the major springs of Mambej, Talmasit and Tell Assyouf. According to the available data between the years 1991 and 2010, the discharge of this tributary changes between 0 and $4 \text{ m}^3\text{S}^{-1}$ during summer and spring respectively.

Fig. 1-16 shows the monthly average discharge of Awaj River for a long period of measurement between the hydrological years 1930-1931 and 2009-2010 at the gauging station after the recharge point of Tabibieh spring. This discharge changes according to the discharge of Jenani and Sebarani tributaries as well as the discharge of Tabibieh spring. The hydrograph shows that the river has started to become dry during the summer period

from the hydrological year 1998-1999 as a result of drought effect as well as the increasing of water exploitation.

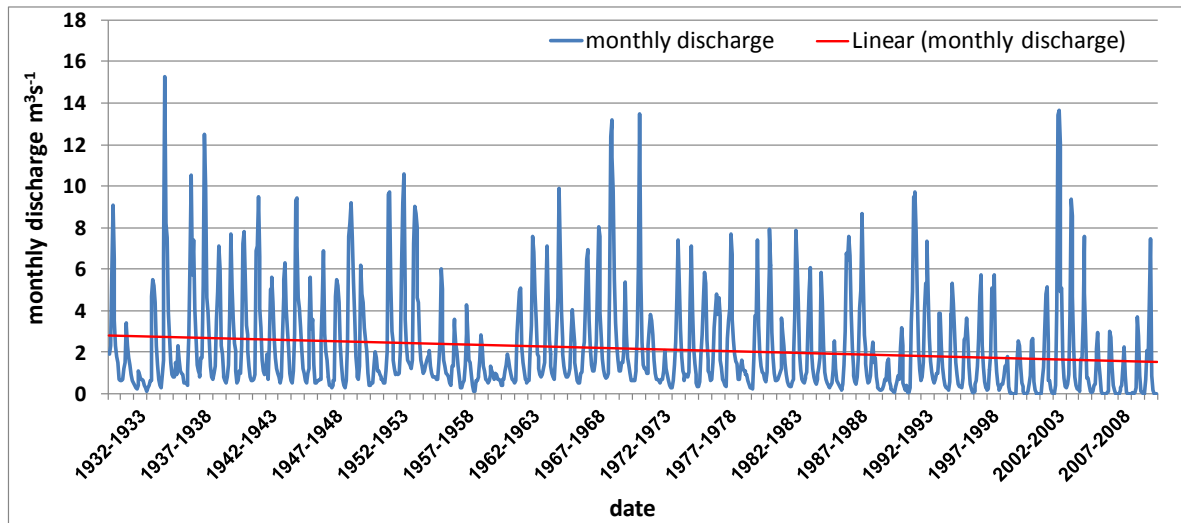


Fig. 1-16 Hydrograph shows the monthly average discharge of Awaj River from the hydrological years 1930-1931 until 2009-2010 after the recharge of Tabibieh spring.

The total annual average discharge of this river during the same period is shown on Fig. 1-17. The minimum value was measured during the hydrological year 2007-2008 ($14 \text{ M m}^3\cdot\text{y}^{-1}$) while the maximum value was measured during the hydrological year 1968-1969 ($177 \text{ M m}^3\cdot\text{y}^{-1}$). From these last two figures, we see that the trend shows a decrease in the river discharge with time.

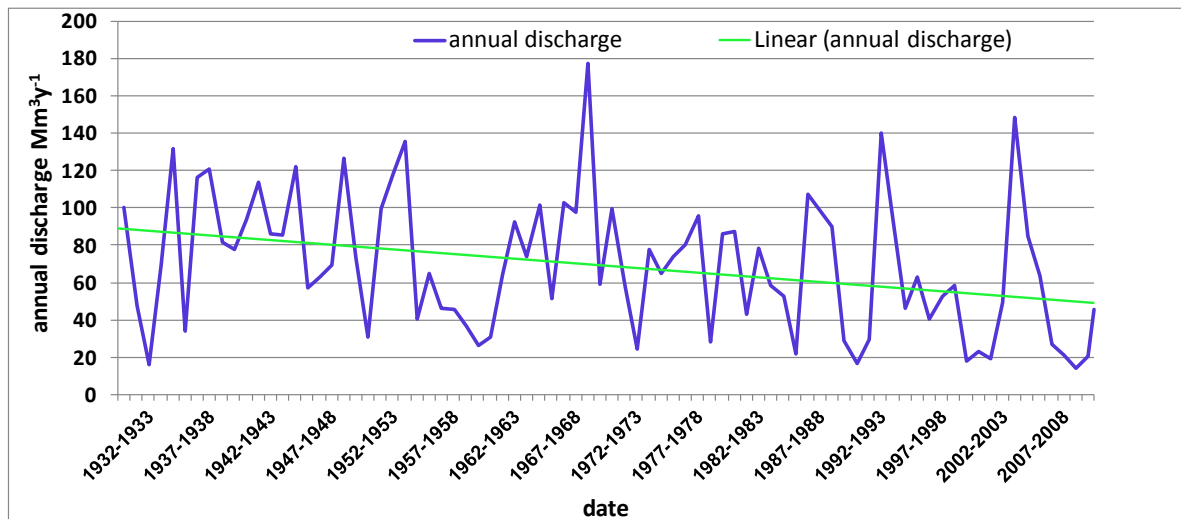


Fig. 1- 17 Annual discharge of Awaj River from the hydrological years 1930-1931 until 2009-2010 after the recharge of Tabibieh spring

1.4.2. Major springs

The complexity of the karstic features plays a key role in the flow regime of the springs located in the study area. Bakalowicz *et al.* (2008) have concluded that the karst around the Mediterranean region is probably the most complex one in the world because of the superimposition of several consecutive karst phases corresponding to very different base levels.

In the study area there are about 30 springs in addition to a large number of seasonal ones. From the potential discharge point of view, the major springs are classified into three groups as shown in the table 1-1. The spatial distribution of these springs in the study area is shown in Fig. 1-18.

Table1-1 Average discharge of major springs in the study area during several hydrological years.

Group	Spring name	Observation period	Average discharge $Q_m^3S^{-1}$	Average discharge $Q_M m^3y^{-1}$
Group1	Beit Jinn	1974-2005	0.793	25
	Talmasiat	1974-2005	0.683	21.5
	Tabibieh	1974-2005	0.655	20.7
	Mambej	1974-2005	0.617	19.5
	High Beit Jinn	1992-2005	0.445	14
Group2	Almashraa	1996-2005	0.217	6.8
	Ras alin	1984-2005	0.198	6.2
	Daboura	1996-2005	0.227	7.2
	Bardeh2	1974-2005	0.148	4.7
	Salt	1961-1974	0.127	4
	Saba	1974-2005	0.108	3.4
	Albardeh-Remeh	1974-2005	0.102	3.2
	Tall Assyouf	2005-2011	0.097	3.1
	Bardeh1	2002-2005	0.086	2.7
	Group3	Kneiseh	1992-2005	0.051
Hasibi		1974-2005	0.049	1.5
Ras alwadi		1985-2005	0.042	1.3
Rashasheh		1974-2005	0.041	1.3
Jandal		1975-2010	0.04	1.3
Mbaya		1985-2005	0.029	0.9
Dorbol		1974-2005	0.028	0.9
Arneh		1974-2005	0.026	0.8
Njaim		1996-2005	0.024	0.8
Rejmeh		1974-2005	0.022	0.7

Shabaanet Remeh	1992-2005	0.021	0.7
Ain Radoan	1969-2005	0.021	0.7
Husenieh	1984-2005	0.016	0.5

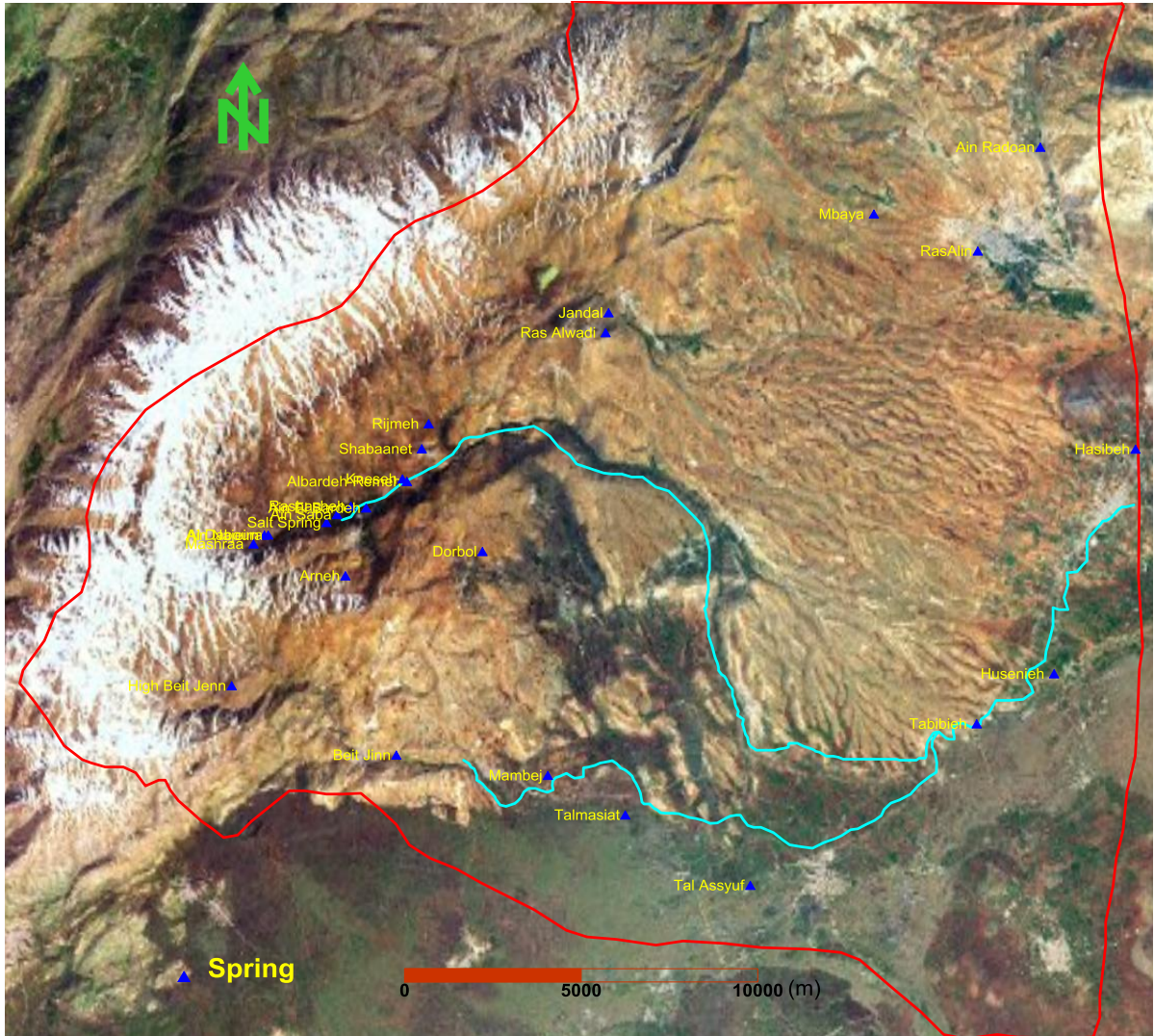


Fig. 1- 18 Location sites of major springs in the study area

The average annual discharge of these springs changes between 0.5 and 25 Mm^3y^{-1} and it ranges between 0-0.15 and 0.02-2.7 m^3s^{-1} for the summer and winter respectively except for the Mambej spring which could reach a value of about 5.3 m^3s^{-1} during the flood period.

From the comparison of the average amounts of precipitation which recharges the groundwater at the exposed part of Jurassic aquifer to the total discharge of the karstic springs located in this part, it is likely be concluded that this discharge is rather small compared to this recharge. This indicates that the major component of groundwater recharge is flows as a deep flow facilitated by bedding, conduits and major faults.

Because of the importance of the major springs which are located in the southern part of the study area (group 1, table 1-1) in terms of irrigation and domestic purposes, the hydrological system of these springs will be briefly explained.

1.4.2.1. Mambej spring

The Mambej spring (Fig. 1-19) is characterized by high discharge during storm events and drought during most of the year. However, the high discharge of this spring after the storm events is a result of quick and large response to such events. The flow regime of this spring could be developed in an intricate system of dissolution-enlarged fissures within the epikarst which becomes saturated and in connect to the main drainage system during storm events or generated from a cave-like structure and flowed in the underground canals system.

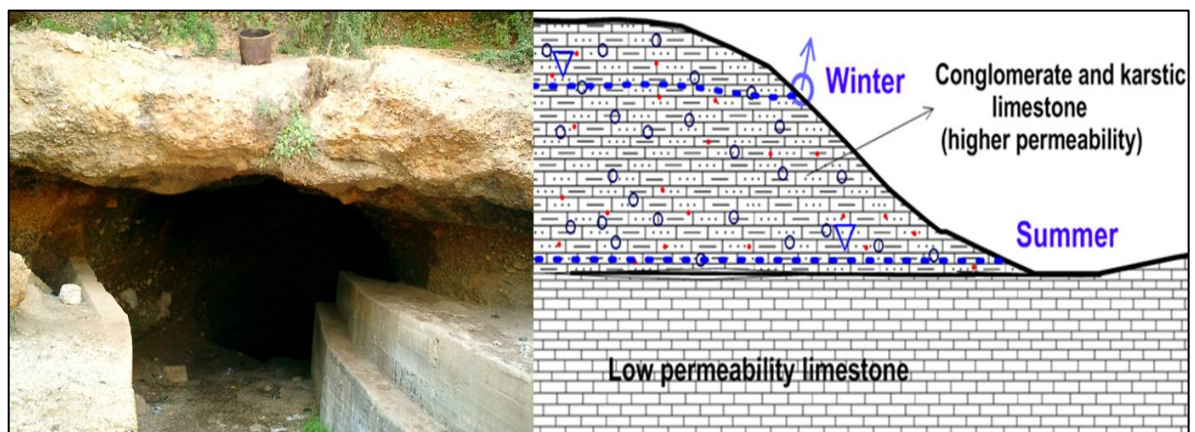


Fig. 1- 19 Mambej spring and its probable schematic framework

The variation of Mambej spring discharge during the period 1974-2012 together with the annual amount of atmospheric precipitation measured in the Arneh station during the period 1974-2006 are shown on the Fig. 1-20

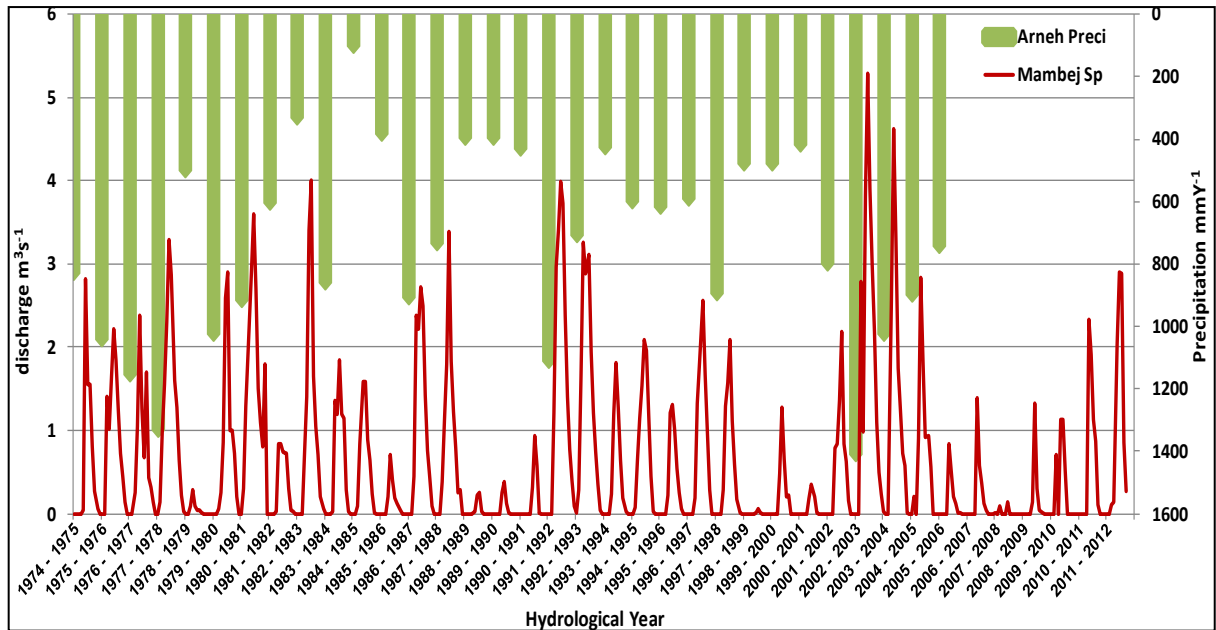


Fig. 1- 20 The variations of the monthly discharge of Mambej spring and the annual amount of precipitation measured at Arneh station.

The quick response of this spring to intense rainfall events is denoted by the typical peaks in the spring hydrograph.

1.4.2.2. Talmasiat spring

The Talmasiat spring (Fig. 1-21) is characterized by significant amount of discharge and demonstrates a strong relationship with the amount of atmospheric precipitation (Fig. 1-22). This spring does not dry out during summer and is characterized by base flow which does not goes under $0.15 \text{ m}^3\text{s}^{-1}$ as well as a less variation in its hydrograph ranges during the observation period. This indicates that the recharge area of this spring extending outside of the exposure of the recent basalts where the spring emerges from. The upward leakage of groundwater from the deeper aquifers might maintain the discharge of this spring. The decrease trend in this spring discharge as a result of drought effect during the last ten years is observed in its hydrograph (Fig. 1-22).



Fig. 1- 21 Talmasiat spring which emerges from the Quaternary basalt.

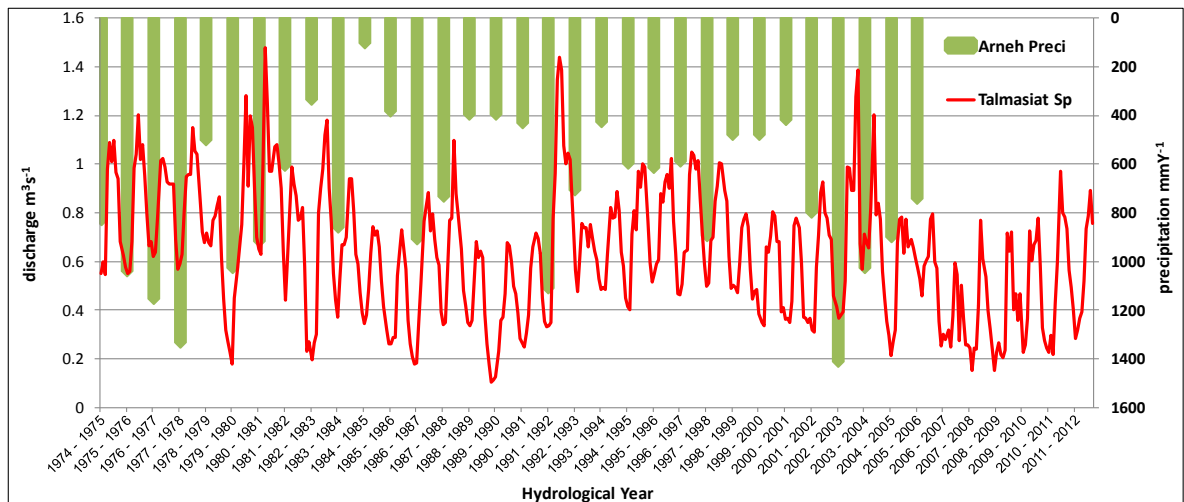


Fig. 1- 22 The variations of the monthly discharge of Talmasiat spring and the annual amount of precipitation measured at Arneh station.

1.4.2.3. Tabibieh spring

The Tabibieh spring is located in the eastern part of the study area where the groundwater recharge by the atmospheric precipitation is insignificant. According to the isotope compositions and geological structures, the regional groundwater flow seems to be converted from the mountain part to discharge by this spring. The relationship between the discharge of this spring and the amount of precipitation measured in Arneh station (Fig. 1-23) shows a clear correlation between two variables. This spring is started to dry out during the summer from the year of 1999 as a result of drilling three groundwater wells close to this spring for domestic purposes.

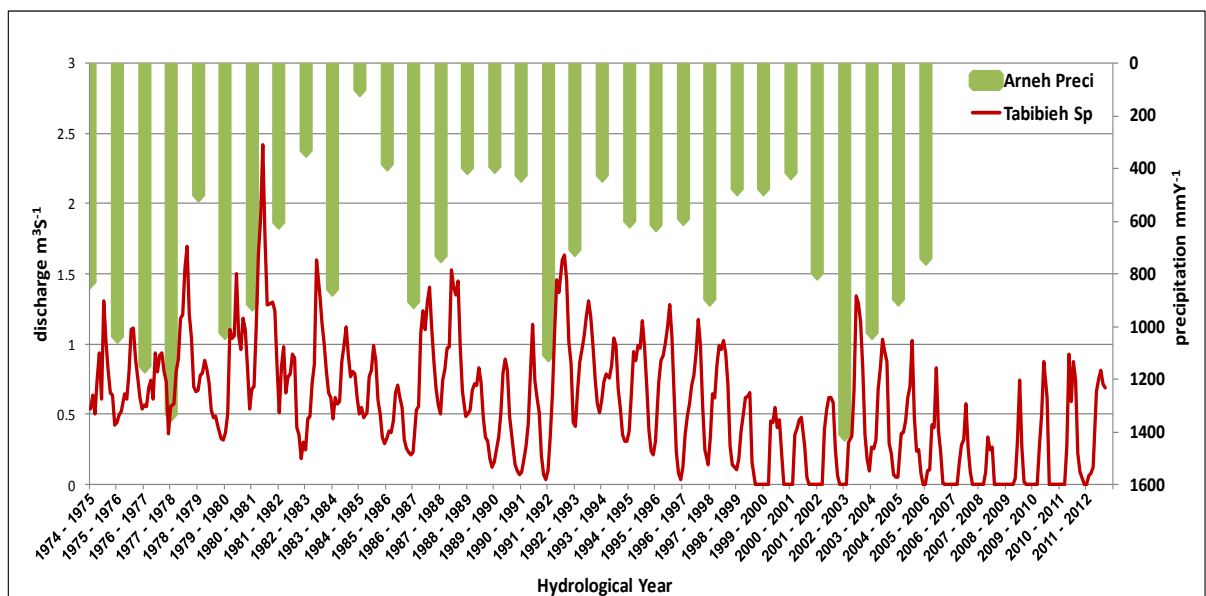


Fig. 1- 23 The variations of the monthly discharge of Tabibieh spring and the yearly amount of precipitation measured at Arneh station.

1.4.2.4. High Beit Jinn spring

The High Beit Jinn spring (Fig. 1-24) emerges at the structural contact between Cretaceous and Jurassic strata in the south-east flank of Mt. Hermon.



Fig. 1- 24 High Beit Jinn spring which emerges at the limit between the Jurassic and Cretaceous formations.

The discharge monthly variation of this spring, which dries out during summer, as well as the amount of precipitation measured at Arneh station (Fig. 1-25), indicates a significant relationship between these two variables. The quick response to the precipitation event indicates the domination of karstic features in the supply catchment of this spring in the elevated Jurassic formations. Its discharge increases significantly in spring time as a result of snowmelt on Mt. Hermon.

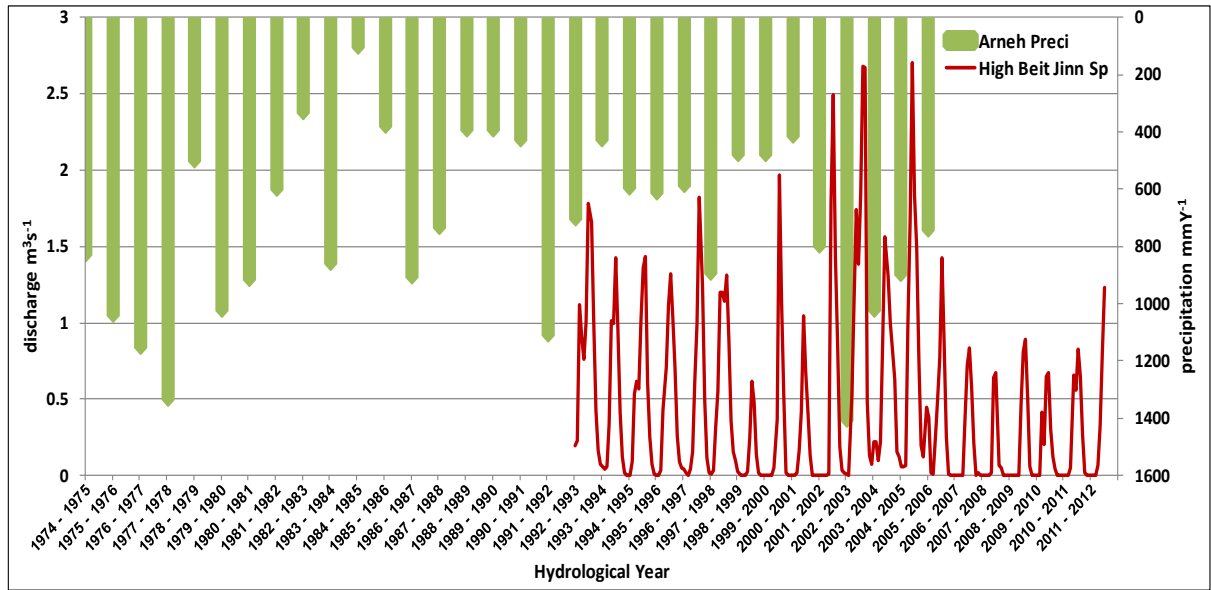


Fig. 1-25 The relationship between high Beit Jinn spring and the annual amount of precipitation measured at Arneh station.

1.4.2.5. Beit Jinn spring

Beit Jinn spring (Fig. 1-26), emerges from the karstic limestone of the Paleogene. This spring demonstrates slightly a different regime. Its hydrograph (Fig. 1-27) shows more variability during the measured period. The existence of marl and clayey limestone in the Paleogene formation might reduce the rapid infiltration into the karst system and contributes to the flow regime and discharge mechanism of this spring.



Fig. 1- 26 Beit Jinn spring which emerges from the exposure of Paleogene southwest of the study area.

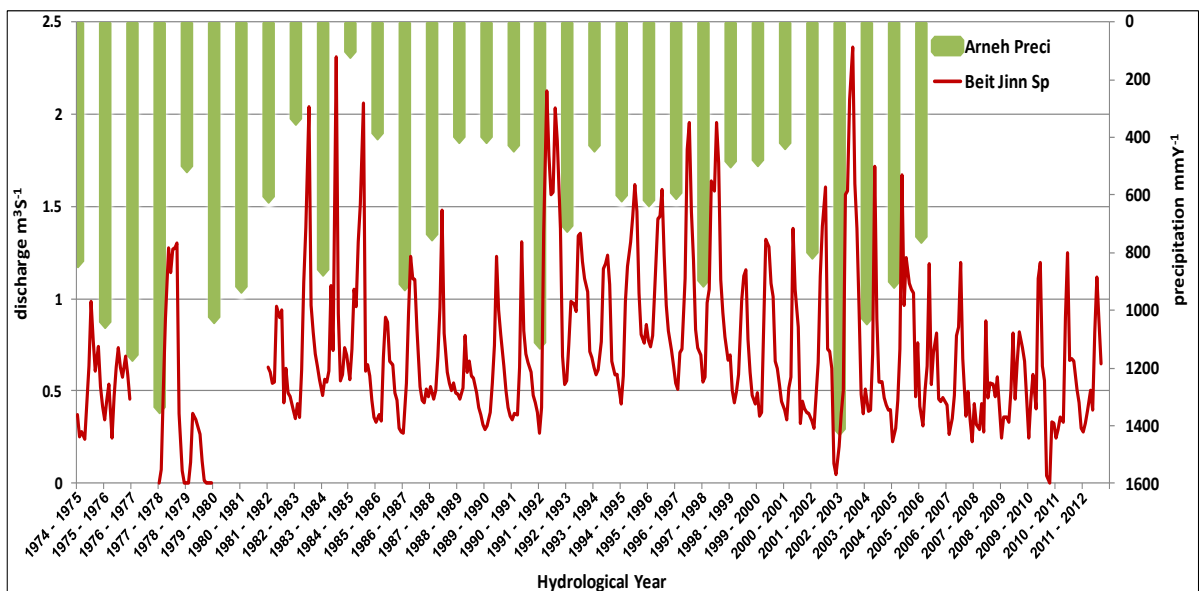


Fig. 1- 27 The relationship between Beit Jinn spring and the annual amount of precipitation measured at Arneh station.

From the five figures, which demonstrate the hydrograph variations of these five springs with the amount of precipitation measured at Arneh station, it can be seen that these springs response in remarkable similarity. The difference in these springs discharge between summer and winter and the significant existence of quick flow component indicate that the main source of spring recharge is the atmospheric precipitation as well as the effects of the karst, faults and conduits on their regime. The peak discharges of these springs are almost associated with the peaks of precipitation amounts with respective time lags can be explained by the effect of snowmelt. The isotope compositions of these springs water, as discussed later, indicate that atmospheric precipitation over the Jurassic formation is the main source of these springs recharge in addition to the direct infiltration in the local area.

The distinguished differences between the behaviors of these springs are mainly dependent on the different geological formations where the springs emerge from, the dominant meteorological conditions and the distance from the recharge area as well as the thickness of the saturated zone. For instance, the high Beit Jinn spring outlet lies close to the recharge area and it emerges from the karstic limestone. The quick and high volume of groundwater discharge characterizes this spring regime. On the other hand, Talmasiat spring which emerges far away from the recharge area is characterized by much larger size of the catchment feeding this spring thus; the changes of this spring hydrograph is bit different comparing with the Hight Beit Jinn spring. The location of this spring in the Quaternary basalt might control its regime during the entire period of the year.

However, in spite of these differences, the flow regime of these springs can be divided into two components, the first one is fast (conduit flow) through the conduits which characterizes the spring discharge after storm events, while the second is slow (diffusive matrix flow) which occurs during base flow conditions as a result of draining fissures system. The biggest amount of discharge during winter period (storm event), and the wide variations in the hydrograph throughout the hydrological years was measured mainly in Mambej spring. The shape of this spring hydrograph implies the significant effect of karst system on its regime. The highly likely existence of sinkholes system which drains the rainfall rapidly, results in quick recharge flow paths and substantially affects the flow regime of this spring. The snow cover residing on Mt. Hermon during winter acts as an external reservoir which plays an important role on feeding these springs especially during

the spring period. Based on the available data, Fig. 1-28 shows the mean annual discharge of these five springs measured in Mm^3y^{-1} .

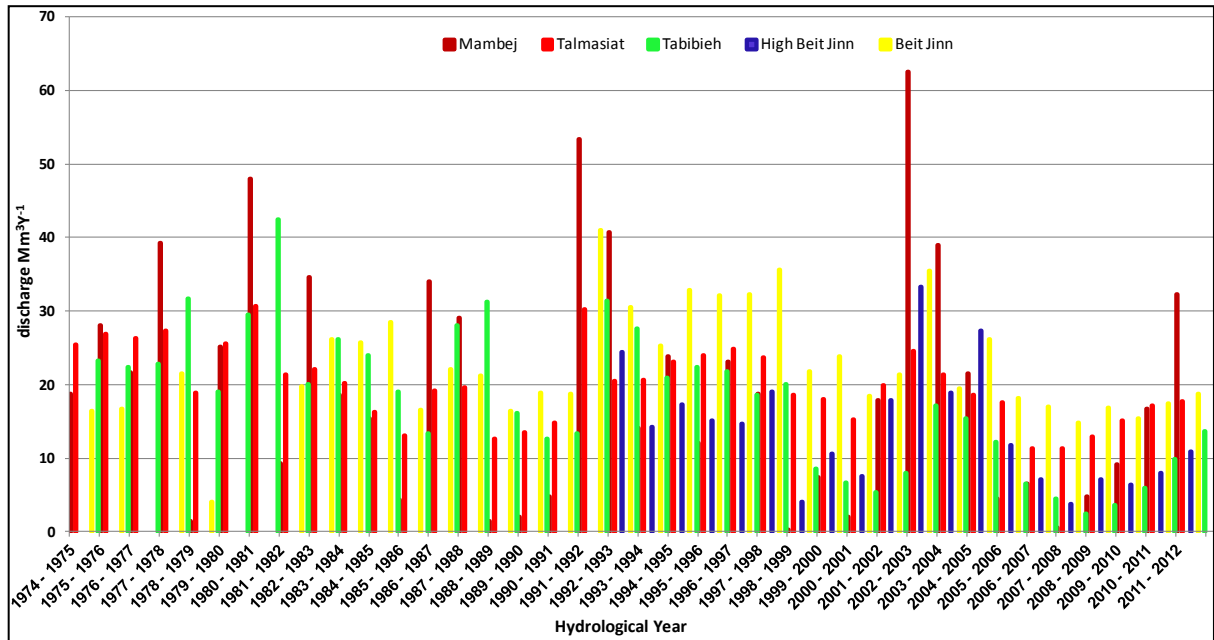


Fig. 1- 28 The mean annual discharge of 5 major springs in the study area.

The amount of all springs' discharge in the study area calculated to be $155 \text{ Mm}^3\text{.Y}^{-1}$ based on the mentioned period of observations in the table 1-1.

1.5. Aquifer systems (Hydrogeology)

The majority of water flow in the study area is subsurface flow. The aquifers in this area can be classified into karstic and porous aquifers. The karstic aquifers consist of fractured soluble rock such as limestones, dolomites and gypsum, which upon dissolution along faults and prime fractures create a secondary porosity. Such aquifers belong to Jurassic, Cenomanian-Turonian, and Upper Eocene units (Al-Charideh 2012^a). Porous aquifer consists of unconsolidated or semi-consolidated sediments, such as Pliocene conglomerate units and Quaternary aquifer. Groundwater flow in karstic aquifers is controlled by three types of porosities, intergranular matrix porosity, which develops directly with the genesis of the carbonates, fracture/fissure porosity which develops later on and conduit porosity which results from the second one (White 1988, Brielmann 2008). In the karstified limestone aquifers, three zones can be recognized (Fig. 1-29): The upper carapace zone which forms the upper portion of the limestone formation. This zone has

either been rendered impermeable by the plugging and resealing of the openings or has remained unkarstified. The central open karst zone, in which the karst openings are filled with groundwater in active circulation zones, so that openings enlarge in horizontal and downward directions. The third one is the lower un-karstified carbonate zone, in which the joints and openings are filled with groundwater that is saturated with bicarbonate and no longer aggressive, so that the karsification proceeds slowly.

Highly karstified, tectonically broken rocks and the step-like pattern of the slope create favorable infiltration conditions for precipitation in the elevated Jurassic aquifers. The majority of groundwater transport in this system takes place in the conduits and faults, while the majority of storage occurs in the fissure and rock matrix porosities. Therefore, the major springs in Syria are found to arise predominantly along fault traces, fault junctions, and fracture zones developed in the karst aquifer (La-Moreaux *et al.* 1989). The exposure of the karstified aquifers in the mountain area shows unfavorable conditions for exploitation by drilling, however, when they underlie at a reasonable depth in the plain area, they form a favorable aquifer.

The presence of karstic landscapes such as dolines (sinkholes) and lapiaz renders the recharge area more than pervious, consequently that makes it characterized by heterogeneous hydraulic regime. Fig. 1-30 shows the rillenkarren and karsification processes along the fractures in the Jurassic aquifer of the study area.

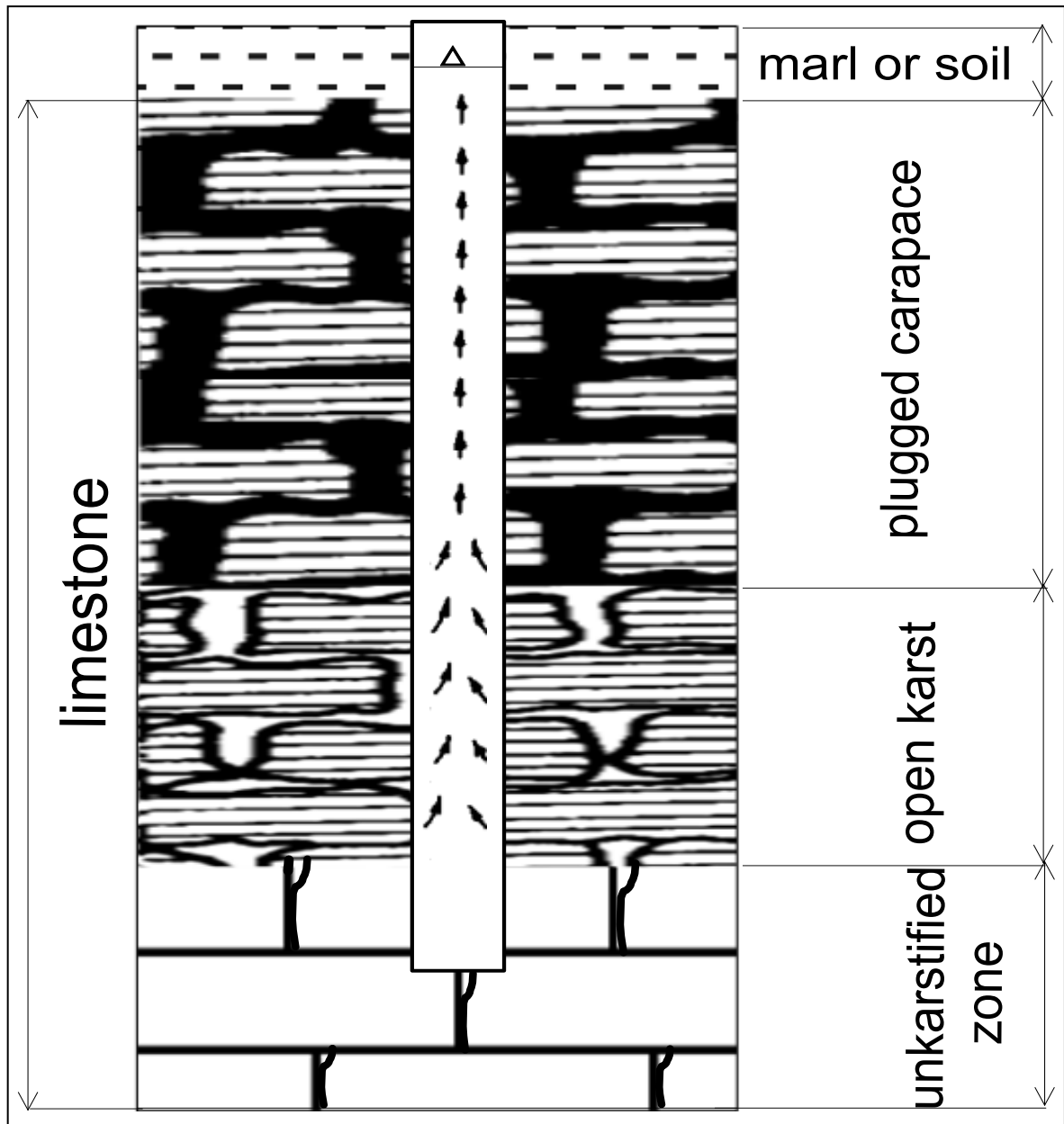


Fig. 1- 29 The hydraulic zones in the karstified aquifer in Syria, after Burdon and Safadi, 1964.

The aquicludes, generally consist of impervious layers, such as marly unit, which do not have ability to transmit groundwater. The basalts, if not intensely fractured can also be considered to a certain extent as an aquiclude (Kattan 1997^b, 2006).



Fig. 1- 30 Jurassic limestone demonstrates the karstification and rillenkarren along the fractures.

The major hydrogeological units in the study area are described as bellow.

1.5.1. Jurassic Unit

The rocks of this unit are primarily encountered on Mt. Hermon. They form thick layers of limestone interbedded with dolomite and dolomitic limestone and to less extent with marl and gypsiferous layers. They are broken by bedding, jointing, and fissures which have been enlarged as a result of karst processes. This Jurassic massifs form extensive storage reservoirs for infiltrated water, and are considered as one of the most resourceful formations. They are generally enclosed by less permeable or impermeable rocks of lower Cretaceous. Its hydraulic conductivity value changes between 2 and 99.3 md^{-1} , and thus the transmissivity could attain a value of about 3,085 m^2d^{-1} .

The recharge of this aquifer is made from direct infiltration of precipitation during the short rainy season dominated by continuous snow melting at the elevations varying between 1300 and 2800 ma.s.l in the eastern flank of Mt. Hermon. The Jurassic aquifer generally discharges in the upper or middle parts of the main river valleys.

1.5.2. Cretaceous Unit

The Cretaceous unit is illustrated by Cenomanian–Turonian system which consists of the aquiferous member of this unit. Its thickness ranges between 400 and 1000 m. The rocks formations of this unit consist of massive stratum of limestone, dolomitic limestone and crystalline dolomite with interbeds of argillaceous limestone, marl and sandstone. The hydraulic conductivity of this unit can reach a value up to 80 m d^{-1} and its transmissivity ranges from 12 to $7,435 \text{ m}^2\text{d}^{-1}$. The existence of high rates of fissures and large karst caves in this aquifer system renders it very important from the hydrogeological point of view (La-Moreaux *et al.* 1989).

The recharge of this aquifer results from direct infiltration of rainfall. Additional recharge might occur by the hydraulic exchange where the Cretaceous strata are in contact with the Jurassic aquifers throughout the fault zones.

1.5.3. The sedimentary Miocene–Quaternary aquifer

The rocks of this complex (thickness 65–630 m) are widespread on the foothill of Mt. Hermon and in the plain area. These rocks consist of gravels and conglomerates which are associated with interbeds of clay, sandstone and limestone. As clay content increases and/or aquifer thickness decreases, the transmissivity value can drop down from 756 to $0.05 \text{ m}^2\text{d}^{-1}$. (Kattan 2006)

1.5.4. The Middle Miocene volcanic aquifer

This aquifer consists of fissured basalts which are extensively cracked and associated with thin beds and lens of sand and sandstone and is overlaid by the conglomerates aquifer of Pliocene. When these formations underlaid by impermeable beds such as marl which acts as a hydraulic barrier, the amount of rainfall is quite high (about 300 mmy^{-1}), and the topography is favorable for infiltration, this basalt rocks can form an aquifer. Groundwater flow in these rocks is most likely to be controlled by rock matrix and fractures porosity. The transmissivity of this aquifer is about $30\text{-}150 \text{ m}^2\text{d}^{-1}$. However, the springs, which emerge from the Quaternary basalts, might originate from deeper aquifer, such as the Neogene conglomerates or other related deeper aquifers. Fig. 1-31 shows the hydrogeological map of the study area which displays the different aquifers and water bearing rocks in this area.

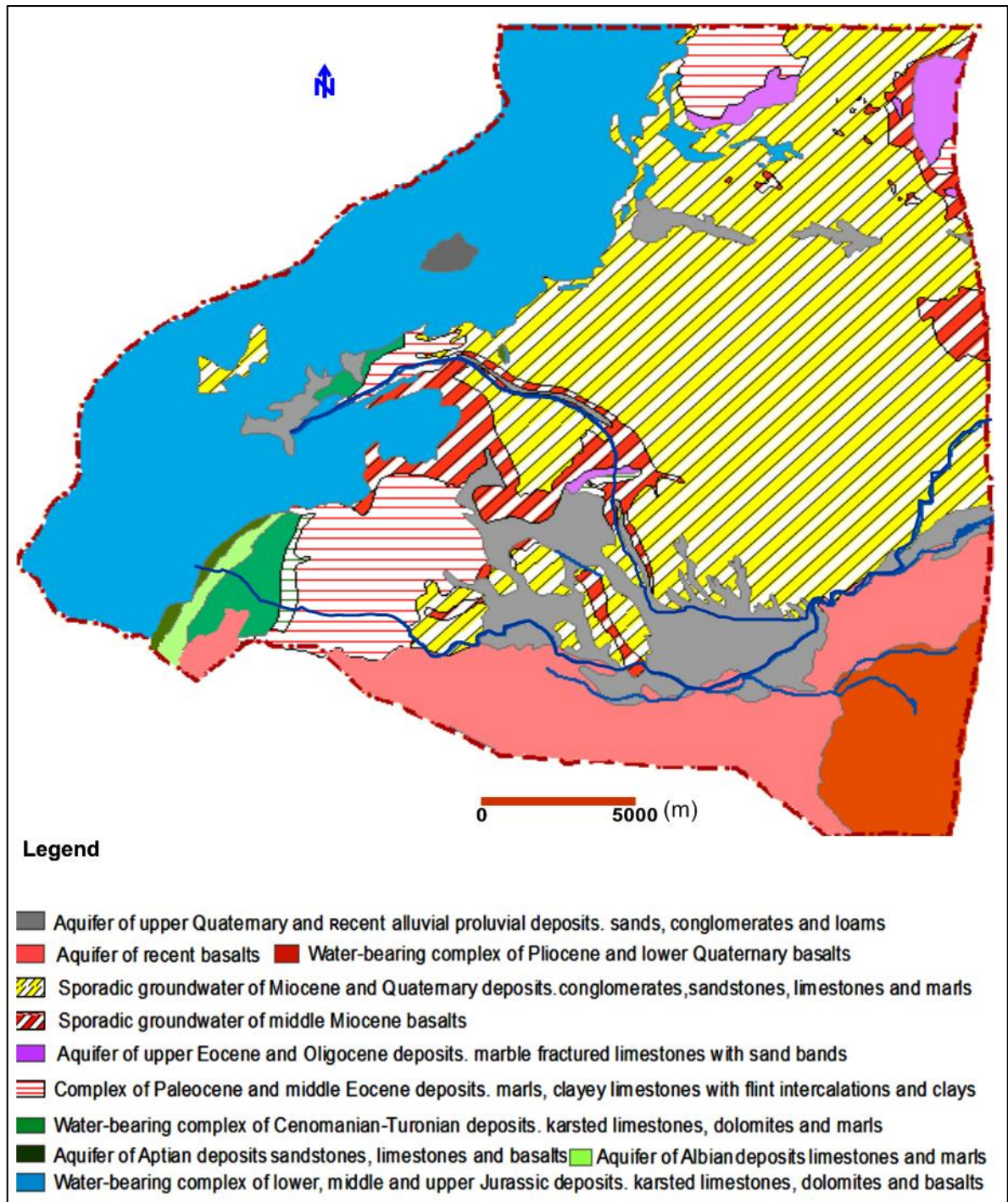


Fig. 1- 31 The hydrogeological map of the study area.

According to Selkhozpromexport (1986), the discrimination between different aquifers and aquitards in the study area has been made, as shown in Fig. 1-32 and described below:

System		Lithostratigraphy		
Quaternary	Recent	Basalt	alluvial	1
	Upper		proluvial deposits	
	Lower	Basalt	Conglomerate and marly limestone	
Neogene	Pliocene	Basalt		
	Miocene	Basalt		
Paleogene	Oligocene	crystline and argillaceous limestone and marle		2
	Eocene			
	Paleocen	Chalk, Marl and Clayey Limestone		
Cretaceous	Upper	Mastrichtian		3
		Coniacian		
		Turonian	Dolomitic Limestone	
	Lower	Cenomanian	Limestone	4
		Albian	Argillaceous limestone, sandstone, marl and clay	
		Aptian		
Jurassic	Upper	Limestone, Dolomite and Marls		5
	Lower			

Fig. 1- 32 Different aquifers and aquitards discriminated in the study area. 1, 3 and 5 are aquifers, 2 and 4 are aquitards.

1- Aquifer of the Recent basalt

This aquifer is located in the southern and south-eastern parts of the study area. Generally, it is an unconfined aquifer; the clay bands which separate the lava sheets play the role of creating local confined bed. Because of low amount of precipitation over these deposits, they are generally dried. The thickness of these deposits ranges between 20 m and

45 m. they are lying on Pliocene-Lower Quaternary basalt and Pliocene conglomerate. The transmissivity of this aquifer is estimated to be about $42.6 \text{ m}^2\text{d}^{-1}$ and its hydraulic conductivity varies with wide limits within an average value of about 1 md^{-1} . The Talmasiat spring emerges from this aquifer.

2- Unconfined aquifer of Upper and Recent Quaternary alluvial-proluvial deposits

The thickness of this aquifer ranges from 3 m to 15 m in the study area. It lies mainly on Pliocene conglomerates and the basalt of Miocene. Its hydraulic conductivity changes between $3.7\text{-}13 \text{ md}^{-1}$ while its transmissivity ranges between 200 and $900 \text{ m}^2\text{d}^{-1}$. This aquifer is recharged mainly by irrigation return flow and numerous canals that distribute the surface water of Awaj River for the irrigation purpose. The recharge by the atmospheric precipitation plays a minor role for this aquifer. The easy exploitation by tapping wells especially for agricultural purposes has resulted in depletion of this aquifer as a result of overexploitation.

3- Aquifer of lower Quaternary and Pliocene basalt

It outcrops in a small part at the south-easternmost part of the study area. This formation is overlaid by the recent basalt and lies either on Middle Miocene basalt or on Paleocene chalk-like and clayey limestone or marl. The thickness of this aquifer ranges between 40 m and 85 m and is considered as fissured unconfined aquifer. It contains interbedded clay layers separating the individual lava and sheets. The fissures of this aquifer are usually filled-in with clay or calcite. Its hydraulic conductivity ranges between 0.13 and 2 md^{-1} while its transmissivity changes between 50 and $70 \text{ m}^2\text{d}^{-1}$.

4- Sporadic groundwater in the Neogene/Quaternary deposits

Generally these deposits are outcropping along the foothill of Mt. Hermon; they occupy the major part of the study area. They are overlaid by the recent basalt, the alluvial deposits of Quaternary and the basalt of Pliocene-Lower Quaternary, while they are usually lying on the Middle Miocene basalt and Upper Eocene limestone in the inter mountain depression. The thickness of these deposits ranges between 300 m and 550 m. These deposits consist in pebble and conglomerates interbedded with clay, limestone and sandstones. They contain sporadic groundwater in the form of individual lenses and inter-layers in the zones of increasing fractures and/or karstification. The permeability of this water bearing changes

between 0.1 and 9.5 md^{-1} while its transmissivity varies between 15-400 m^2d^{-1} which increases significantly in the fractured and dislocated zones to about 1300 m^2d^{-1} . The recharge amount of this aquifer from the meteoric precipitation decreases eastwards and the majority of groundwater abstraction wells are located in this aquifer.

5- Sporadic groundwater distribution in the Middle Miocene basalt

The deposits of Middle Miocene basalt crop out along the Sebrani tributary and in the region of Heneh village. These deposits are overlaid by Pliocene-Quaternary rocks and lie over the Upper and Middle Eocene carbonates rocks within a thickness changes between 80 m and 200 m. The hydraulic conductivity of this aquifer ranges between 0.3 and 1.4 md^{-1} and its transmissivity varies between 25 and 140 m^2d^{-1} .

6- Aquifer in the Upper Eocene-Oligocene Deposits

This deposit is overlaid by Miocene basalt and Neogene sediments; it lies over Middle Eocene chalk-like, argillaceous limestones and marl. Its thickness ranges between 40-95m. This aquifer is largely fractured and locally made of karstified limestone with interbedded lenses of quartz and fine grained sands in the upper part. The hydraulic conductivity of this aquifer varies between 0.2 and 2.4 md^{-1} and its transmissivity ranges between 15 and 700 m^2d^{-1} . According to reasonable similarity in the hydrogeological characteristics of the above six layers and for a modeling purpose, we will consider them as one aquifer horizon.

7- Impermeable complex of Coniacian-Mastrichtian and Paleocene- Middle Eocene strata

The thickness of these formations ranges between 200 and 600 m in the study area, it is lying on Cenomanian-Turonian strata. Due to the high degree of blockage of fissures by argillaceous material, these thick strata in general display low permeability and are assigned to be impermeable bed (aquitard).

8- Water bearing complex of Cenomania-Turonian strata

The average thickness of this complex ranges between 400 and 1000 m. When it crops out, the dominated water types are of fissure-karstic, fissure-vein and more rarely strata fissured unconfined aquifer. While, when it is plunging under the younger strata at a considerable depth, it becomes a confined aquifer. The infiltration coefficient of the exposed part of these formations estimates to be 70% in the mountain range.

The karstification process might affect the entire thickness of this complex. It is recharged by the infiltration of precipitation in the zone of its exposure as well as by probable upward leakage of groundwater from the Jurassic strata.

9- Aquifer of the Aptian-Albian stages

This aquifer developed in the limbs of the anticlinal structure. It is overlaid by Cenomanian-Turonain complex and it lies over Jurassic aquifers. Its thickness varies between 180-470 m. The hydraulic conductivity of this aquifer is about 0.15 md^{-1} while its transmissivity varies between 3 and $75 \text{ m}^2\text{d}^{-1}$ and it can be considered as an aquitard.

10- Water bearing complex of Lower-Upper Jurassic strata

The rocks of this complex outcrop in the western part of the study area. They are intensively karstified at the surface and under surface for several hundred of meters (Selkhozpromexport 1986). The existence of karst at significant depth promotes the formation of thick zone of free water exchange in the lower-upper Jurassic complex. The thickness of this aquifer varies between 1000 m and 2000 m. The water of this unit is of fracture and fracture karstic type. Its hydraulic conductivity ranges between 2 and 100 and in average is about 25 md^{-1} . Its transmissivity varies between 700-3090 m^2d^{-1} . The recharge of this aquifer is made from the atmospheric precipitation. The infiltration coefficient of this complex is estimated to be 60-80 %.

However, there are no reliable regionally continuous impermeable beds as a result of intensive dislocations that are dominated in the study area. It is quite evident that the zones of tectonic dislocation, when it transecting all of the aquifers of the sequence, it unites them into a single hydraulic system. According to Wolfart (1964), there is no hydraulic isolation between the aquifers in the Barada and Awaj basin because there are no beds between these aquifers can act as real aquicludes. Moreover, the relatively high discharge of some springs, as has been recognized, indicates that these springs could not be recharged either from a local infiltration or from the resources of single aquifer where they are emerging from.

Chapter 2. Methodology

2.1. Sampling, analysis and database preparation

For major ions and field parameters investigation, a total of 177 water samples from springs and the irrigation wells were used (Fig. 2-1). A total of 122 water samples were collected during two fieldwork campaigns. The first one took place in November and December during 2006 in which 107 samples were collected (table 2-1). While in the second one, the result of 15 samples collected during August 2012 were used (table 2-2). In addition, the database was completed with other available related analyzed samples from Selkhozpromexport (1986) (table 2-1). For groundwater isotopic composition, the results of 18 samples collected during the second field campaign (August 2012), and 3 samples from Selkhozpromexport (1986) were used (table 4-3). Prior to all groundwater samples collection, the non-operating pumping wells were pumped for about three to five minutes to ensure collection of representative samples. The exact wells depths are not available but in general and according to Ministry of Irrigation in Syria (MOI) and farmers, these depths range between 35 and 160 m. All the samples were collected in polyethylene bottles, which were rinsed twice with sample water. Two bottles of each water point were collected; one bottle was filtered (0.45 μm) and acidified with two drops of nitric acid, (HNO_3) for cations determination. Acidification stops most bacterial growth, inhibits oxidation reactions and precipitation of cations. The historical data available of the atmospheric precipitation isotopic content from 12 stations (Kattan 1997a, Selkhozpromexport 1986, Kattan 2006) were used to determine the local meteoric water line interpret the relationship between rainfall and groundwater in the study area

Field parameters such as electrical conductivity (EC), pH and alkalinity (HCO_3^-) were measured onsite. Within 30 days of sampling, all samples were analysed in the UNESCO-IHE Institute laboratory in The Netherlands. Cation concentrations were measured using an Absorption Spectrophotometer (AAS), whereas the anions were measured with Dionex Ion Chromatograph (DIOEX ICC-1000). Silica (as SiO_2) was measured by using HACH colorimeter. The samples of the second fieldwork campaign were analysed at the Hydrogeology Department of the University of Corsica (UMR 6134 CNRS) for both major ions and environmental isotopes of the water molecule ($\delta^{18}\text{O}$ and $\delta^2\text{H}$). In terms of major ions, ionic chromatography in liquid phase (DIONEX ICS- 1100) technique has been used,

while for isotopes determination, liquid water isotope laser spectrometer (LGR) technique was used.

Using PHREEQC (Parkhurst and Appelo 1999), different calculations were performed to determine chemical analysis error, water type according to Stuyfzand classification (Stuyfzand 1989), the saturation indices of a selection of minerals and the partial pressure of carbon dioxide as shown in tables 3-1 and . The major ions and field parameters are also shown in this table.

Table 2 - 1 Site locations of the samples collected during the first fieldwork campaign (2006) as well as other samples from Selkhozpromexport (1986)

Name	Location	Date	Type	X- coord	Y- coord
Artesian well	Arneh	Dec-06	W	328100	3692800
Drink well	Harfa	Nov-06	W	332200	3681500
Artesian well	Harfa	Nov-06	W	332200	3681520
well6	Heneh	Nov-06	W	335400	3691800
well1	Heneh	Nov-06	W	333300	3692800
well5	Heneh	Nov-06	W	336100	3691300
MJAlshekh	Heneh	Nov-06	W	334700	3690400
well1	Kleaa	Dec-06	W	343800	3685000
well2	Kleaa	Dec-06	W	344800	3685000
well3	Kleaa	Dec-06	W	345900	3684500
well1	Remeh	Dec-06	W	330400	3696400
well1	Dorbol	Nov-06	W	331900	3693200
well2	Dorbol	Nov-06	W	330800	3690700
well1	Drosha	Dec-06	W	350400	3698200
well2	Heneh	Nov-06	W	335400	3692350
well1	Knaker	Dec-06	W	348300	3683200
well2	Knaker	Dec-06	W	349400	3683300
well3	Knaker	Dec-06	W	349800	3684200
well4	Knaker	Dec-06	W	350000	3685200
well1	Saasaa	Nov-06	W	343000	3686900
well2	Saasaa	Dec-06	W	343250	3687100
well3	Saasaa	Dec-06	W	343150	3687100
well4	Saasaa	Dec-06	W	342900	3686300
well5	saasaa	Dec-06	W	343300	3686200
well6	Saasaa	Dec-06	W	343100	3686300
well7	Saasaa	Dec-06	W	343600	3684900
well8	Saasaa	Dec-06	W	343800	3686000
well9	Saasaa	Dec-06	W	343700	3686000
well10	Saasaa	Dec-06	W	343700	3685900
well12	Saasaa	Dec-06	W	345200	3684400

well14	Saasaa	Dec-06	W	341000	3684600
well15	Saasaa	Dec-06	W	343500	3684800
well16	Saasaa	Dec-06	W	342000	3684700
well17	saasaa	Dec-06	W	341900	3685000
well18	Saasaa	Dec-06	W	342200	3684850
well19	Saasaa	Dec-06	W	342200	3685350
well21	Saasaa	Dec-06	W	343300	3686700
well22	Saasaa	Dec-06	W	344800	3686100
well23	Saasaa	Dec-06	W	344700	3686900
well3	Dorbol	Nov-06	W	331800	3693000
well2	Abo Kaook	Dec-06	W	345050	3688100
well3	Abo Kaook	Dec-06	W	345700	3688200
well6	Beit Saber	Nov-06	W	342500	3688100
well2	Beit Tima	Nov-06	W	339300	3694200
well3	Beit Tima	Nov-06	W	339200	3694000
well1	Hosenieh	Dec-06	W	349100	3690800
well2	Hosenieh	Dec-06	W	348700	3691200
well3	Hosenieh	Dec-06	W	351300	3691000
well1	Tabibieh	Nov-06	W	344000	3688200
well1	Ainashara	Nov-06	W	333900	3693400
well4	Beit Saber	Nov-06	W	342300	3688000
well5	Beit Saber	Nov-06	W	340200	3689100
well7	Beit Saber	Dec-06	W	339000	3687000
well9	Beit Saber	Dec-06	W	337800	3690100
well1	Kafer Hour	Nov-06	W	338200	3693100
well2	Kafer Hour	Nov-06	W	338400	3693300
well3	Kafer Hour	Nov-06	W	338300	3693600
well1	Khazrajeh	Dec-06	W	340000	3685200
well3	Mogher Al Mer	Nov-06	W	334800	3689000
well2	Tabibieh	Dec-06	W	345700	3688900
well1	Talmasiat	Nov-06	W	335600	3686300
well2	Talmasiat	Nov-06	W	335600	3687000
well1	Khan Elshek	Dec-06	W	348300	3692900
well2	Khan Elshek	Dec-06	W	347200	3690300
well4	Khan Elshek	Dec-06	W	348050	3691300
well7	Khan Elshek	Dec-06	W	348300	3691600
well8	Khan Elshek	Dec-06	W	350000	3692100
well1	Mazrat Nafor	Dec-06	W	351500	3686800
well1	Mogher-Hene	Nov-06	W	335700	3690000
well2	Mogher-Hene	Nov-06	W	335700	3690600
well3	Mogher-Hene	Nov-06	W	335700	3691450
well4	Mogher Al Mer	Nov-06	W	336800	3688500
well5	Mogher Al Mer	Nov-06	W	336000	3688100
well6	Mogher Al Mer	Dec-06	W	337500	3689000
well7	Mogher Al Mer	Dec-06	W	337400	3689700
MambejWell	Mogher Al Mer	Nov-06	W	334150	3687700

8k	Arneh	Jun-82	W	328570	3692560
43k	Om Sharatet	Oct-84	W	346333	3688997
46k	Abo Kaook	Sep-83	W	346200	3688872
48K	Arneh	Oct-84	W	328237	3694288
49k	Arneh	Oct-83	W	328387	3694320
52K	Beit Tima	Jul-83	W	338520	3694060
53K	Beit Tima	Oct-84	W	338520	3694030
55K	Beit Jinn	May-83	W	329450	3687940
57K	Beit Jinn	May-84	W	329439	3687875
133K	Khan Elshek	Oct-83	W	350910	3695750
150k	Jdedet Artoz	Aug-83	W	352500	3704100
154k	Jdedet Aartoz	Oct-84	W	356530	3699340
165k	Dorbol	Apr-85	W	332941	3691911
181	Artouz	Oct-82	W	355470	3700050
184K	Beit Saber	Aug-85	W	338462	3691324
179	Artouz	Oct-82	W	353590	3700020
186	Khan Elshek	Apr-83	W	351190	3695430
265k	Kafer Quaq	Dec-84	W	341600	3708650
275k	arneh	Oct-85	W	328151	3694439
300	Khan Elshek	Oct-84	W	348380	3691460
720	Khan Elshek	Mar-85	W	350400	3697300
721	Qatana	Apr-85	W	346170	3703030
721a	Qatana	Apr-85	W	346000	3703240
740	Khan Elshek	Aug-85	W	347653	3694120
744	Khan Elshek	Aug-85	W	346889	3694144
3032	Kafer Qouq	May-84	W	342540	3706250
3036	Qatana	Oct-84	W	349260	3700460
3050	saasaa	Jun-82	W	342450	3686380
3055	Kleaa	May-84	W	348120	3684230
3072	Heneh	May-84	W	334750	3689980
Bet Jinn Sp	Beit Jinn	Nov-06	S	330030	3687890
Salt Spring	Arneh	Nov-06	S	328110	3694300
Arneh Spring	Arneh	Nov-06	S	328630	3692830
Albardeh Sp	Arneh	Nov-06	S	329200	3694700
Almshraa Sp	Arneh	Nov-06	S	326100	3693710
First Sp	Dorbol	Nov-06	S	331240	3692240
Fourth Sp	Dorbol	Nov-06	S	330950	3692840
Third Sp	Dorbol	Nov-06	S	331240	3692240
Ras Alin Sp	Qatana	Nov-06	S	346030	3701780
Hamana Sp	Beit Tima	Nov-06	S	338670	3693140
Spring 1	Beit Saber	Nov-06	S	338710	3690280
Spring 2	Beit Saber	Nov-06	S	339000	3690000
Upper Spring	Ainashara	Nov-06	S	333300	3695270
Spring 1	Kafer Hour	Nov-06	S	338000	3694490
Talmasiat Sp	Mogher Al Mer	Nov-06	S	336330	3686240
Ganat Spring	Hasebe	Dec-06	S	350370	3696320

Ain Aljoz	Kalaet Jandal	Nov-06	S	334780	3700300
Jandal Spring	Kalaet Jandal	Nov-06	S	335870	3700080
Mambej Spring	Mogher Al Mer	Nov-06	S	334200	3687330
First Spring	Bkassam	Nov-06	S	333730	3698280
High Spring	Beit Jinn	Nov-06	S	324900	3689800
Morkos Sprin	Arneh	Dec-06	S	325800	3694600
Kneseh Spring	Remeh	Dec-06	S	330200	3695500
Tamer Spring	Remeh	Dec-06	S	331000	3697200
Second Spring	Dorbol	Nov-06	S	332400	3693500
Saasaa Sp1	saasaa	Nov-06	S	341200	3685300
third Spring	Bkassam	Nov-06	S	333800	3699500
Ain Bala Sp	Qkatana	Nov-06	S	340300	3699300
Second Spring	Bkassam	Nov-06	S	334200	3697600
Down Spring	Ainashara	Nov-06	S	333300	3695150
Spring 1	Khrbt Souda	Nov-06	S	332200	3695600
33	Tal Assyuf	Jun-83	S	339770	3684300
41	Ain Saba	Dec-77	S	328400	3694520
43	Rashasheh	Sep-77	S	328780	3694750
44	Rijmeh	May-83	S	330920	3697020
45	Ras Alwadi	Jul-78	S	335790	3699530
46	Tabibieh	Aug-82	S	346000	3688750
47	Husenieh	Oct-83	S	348130	3690130
49	Mbaya	Oct-83	S	343170	3702800
51	Artouz Qanat	Aug-84	S	350280	3700070
10276	Mt. Hermon	Oct-84	S	324660	3693320
10285	Shabaanet	Oct-84	S	330730	3696330
10291	Mt. Hermon	Oct-84	S	324500	3693480
10292	Ain Najeem	Oct-84	S	326400	3693950
10297	Daboura	Oct-84	S	328000	3692450
10308	Beit Tima1	Oct-84	S	338680	3694020
10309	Beit Tima2	Oct-84	S	338240	3694410
10310	Mt. Hermon	Oct-84	S	331600	3698820
10311	Mt. Hermon	Oct-84	S	330090	3698820
10322	Mt. Hermon	Dec-84	S	328600	3695650
10325	Mt. Hermon	Dec-84	S	328210	3698350
10326	Mt. Hermon)	Dec-84	S	327540	3698790
10327	Albardeh	Dec-84	S	330320	3695430
10333	Ain Badran	Dec-84	S	332320	3696110

W: Well, S: Spring. The coordinates system is special for Syrian Arab Republic

Table 2 - 2 Site locations of the samples collected during the second fieldwork campaign (2012)

Name	Locations	Date	Type	X coord	Y coord
Beit Jinn	Beit Jinn	16/08/2012	S	330030	3687890
Arneh	Arneh	20/08/2012	S	328630	3692830
Almashraa	Arneh	20/08/2012	S	326100	3693710
Talmasiat	Mogher Al Mer	16/08/2012	S	336330	3686240
Jandal	Kalet Jandal	17/08/2012	S	335870	3700080
Mambej	Mogher Al Mer	16/08/2012	S	334200	3687330
Bkassam1	Bkassam	17/08/2012	S	333730	3698280
Kneseh	Remeh	20/08/2012	S	330200	3695500
Tamer	Remeh	20/08/2012	S	331000	3697200
Tal Assyuf	Mogher Al Mer	16/08/2012	S	339770	3684300
Rashasheh	Arneh	20/08/2012	S	328780	3694750
Alrjmeh	Remeh	20/08/2012	S	330920	3697020
Ras Alwadi	Kalet Jandal	17/08/2012	S	335790	3699530
Njaim Spring	Arneh	20/08/2012	S	326400	3693950
Jandal Drink Well	Kalet Jandal	17/08/2012	W	335180	3700980

W: Well, S: Spring. The coordinates system is special for Syrian Arab Republic

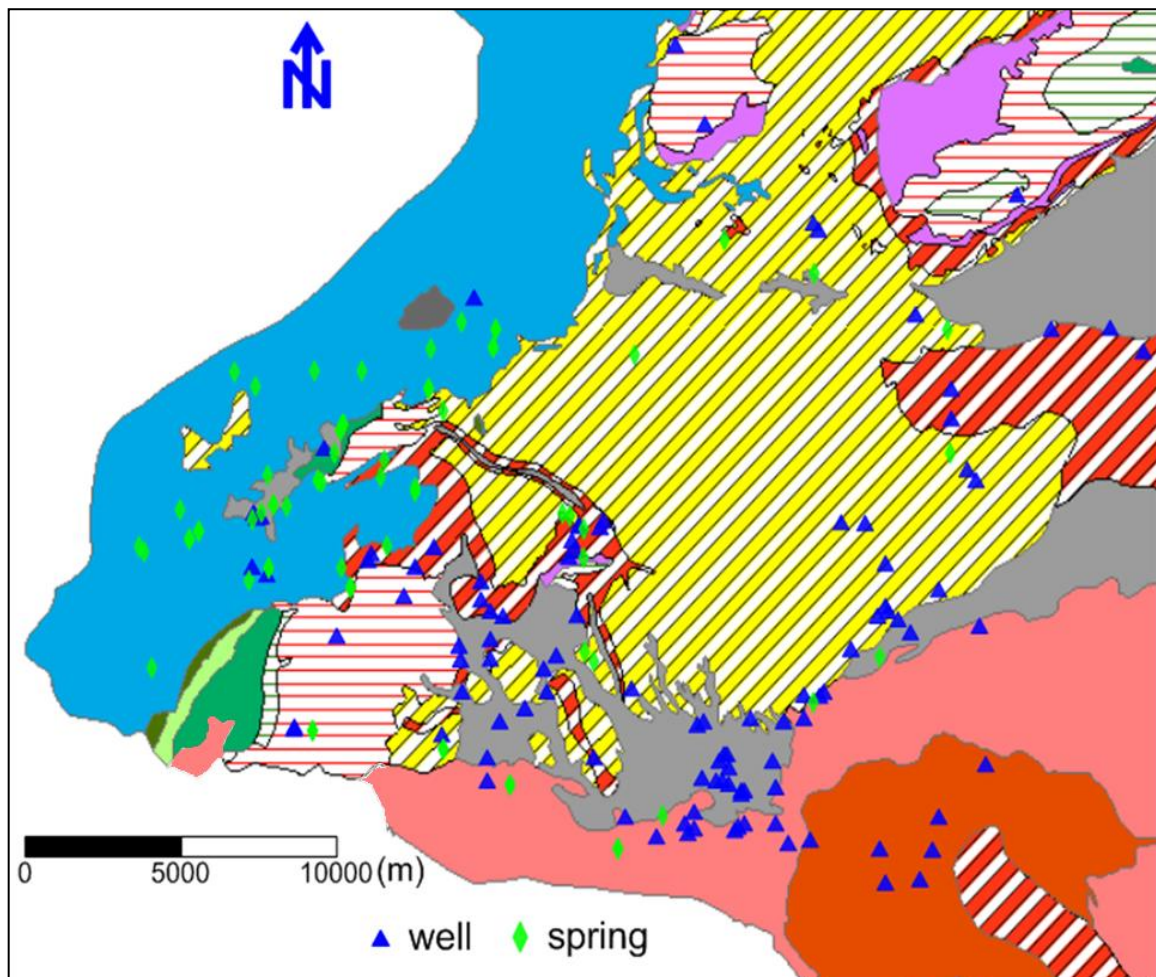


Fig 2 - 1 Location map of sampling sites in the study area.

2.2. Constructing of groundwater model

The model contains three aquifers and two aquitards. The first aquifer (upper aquifer) extends in the central, eastern and southeastern parts of the model domain within an area of about 380 km². It is consisted in the sedimentary rocks of Neogene/Quaternary, volcanic rocks of Middle Miocene and Upper Paleogene limestone. The thickness of these rocks complex changes between 65 and 630 m and this thickness increases toward the east. The top of this aquifer, which is considered unconfined, is based on a digital elevation model of the ground surface excluding a thin Quaternary basaltic layer (less than 100 m). This layer forms the southern boundary of the model and has been considered relatively as a thin aquitard. The second aquifer (Cenomanian-Turonian) extends over an area of about 440 km², while the third aquifer (Jurassic) extends over the whole model area. The average thicknesses of the second and the third aquifers have taken to be 450 and 900 m respectively. The groundwater system in the second and third aquifers is typically unconfined at higher altitude and become confined at the deeper part where they are overlaid by the marl of Paleogene, conglomerate of Neogene and basalt rocks.

In terms of aquitards, there are two aquitards in the study area. The first is occupied an area of about 420 km² while the second is extended over an area of 450 km². The reason behind the different area of the model layers is because these layers do not extend to the western site where the Jurassic layer is exposed. Where the aquifer or aquitard is absent, its thickness has taken to be 1 m and has given the characteristics of the lower existing layer. The first aquitard consists an alternation of chalk, marl and clayey limestone with chert of Coniacian-Mastrichtian, Paleocene and Middle Eocene which constitute one thick impermeable hydrogeological unit. The thickness of this unit changes between 200 and 600 m. The strata of Aptian-Alpian which consist of clayey sandstone, marly limestone, argillaceous limestone and marl, form the second aquitard in the model domain. The average thickness of these strata has been taken to be 200 m.

By using FEFLOW version 6 packages (DHI-WASY, FEFLOW User's manual 2010), the framework of super elements has been defined and then the 2D horizontal mesh of finite-element is generated using the automatic triangle option (Fig. 2-2). After that, 3D slices elevations (Fig. 2-2), layers properties and boundary conditions were defined. The advanced subsurface flow system was investigated under the steady-state condition. The 3D model grid consists of 6 layers, which correspond to aforementioned hydrogeological

units, and 7 slices. The total number of two dimensional triangular prismatic mesh elements is 48,702 with 29,162 nodes which have been generated based on all the basic geometrical information. The finite element method is characterized by its flexibility in generating the mesh and its capacity to simulate complex geometric forms and to refine the nodal grid around points and/or single lines. The finite element grid was generated automatically with reasonable refinement around the points in both plain area and Arneh region. These points illustrate the abstraction wells which are placed in the grid as fixed nodes at their exact positions as shown later. The spatial data were prepared by using Arc GIS (10) which can be totally interfaced with FEFLOW.

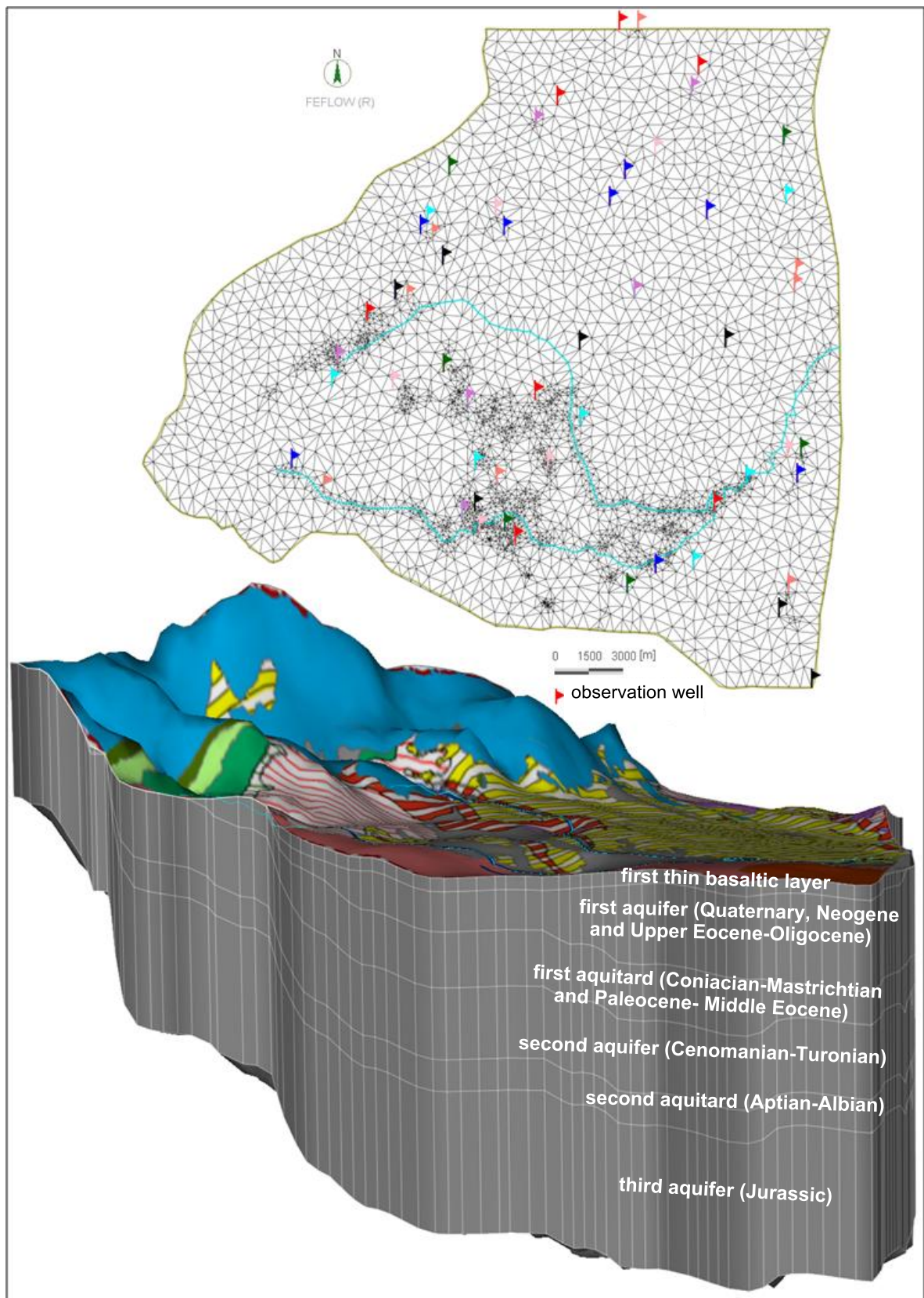


Fig 2 - 2 Framework of super-mesh of the model domain as well as three dimensional (3D) representation of the 6 layers and 7 slices consisting of this model domain.

Chapter 3. Hydrochemistry to delineate groundwater flow pattern in the study area

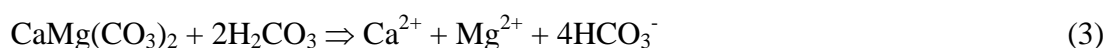
Introduction

The hydrogeochemical processes of the groundwater system help to obtain an insight into the contributions of water-rock interaction and anthropogenic influences on groundwater (Matthess 1982, Kumar *et al.* 2006, Varol and Davraz 2014). Using of major-ions as natural tracers has become a significant tool to delineate flow paths and interpret the spatial variations in water chemistry in the aquifers. However, the majority of these ions in the groundwater are subject to different processes such as dissolution of calcite and dolomite, cation exchange with the clay-humus complex and precipitation of calcite with CO₂ degassing at the small spring (Ribolzi *et al.* 2000). In order to predict any change in groundwater environments, it is necessary to understand the hydrochemical characteristics of the groundwater and its evolution under natural water circulation processes (Lawrence *et al.* 2000; Edmunds *et al.* 2002 and 2006; Guendouz *et al.* 2003; Wen *et al.* 2005; Ma *et al.* 2005; Ma and Edmunds 2006; Jianhua *et al.* 2009). The motion of groundwater along its flow paths increases the concentration of the chemical species. This depends on the geological formation, geological structure and determined by the interaction processes between the water and hosting rock (Domenico and Schwartz 1990; Freeze and Cherry 1979; Kortatsi 2007; Aghazadeh and Mogaddam 2011). Additional controls on groundwater characteristics are influenced by anthropogenic activities such as the pumping and pollution of groundwater. In many areas, particularly in the arid and semi-arid zones, groundwater quality degradation limits the supply of potable fresh water (Rakhmatullaev *et al.* 2012). Generally, groundwater is often a mixture of waters from different flow-paths; this is particularly true in heterogeneous systems such as well-developed karst and fractured rocks. This chapter has been developed based on the interpretation of dataset in table 3-1.

3.1. Results and discussion

3.1.1. Calcite, Dolomite and Gypsum Dissolution

The dissolution of limestones and dolomites is a dominant mineralization process which determines of groundwater chemical composition of carbonate systems. In many cases, the dissolution of gypsum has also a very important role (Flakova 1998). The solubility of carbonate minerals depends on many factors, such as water temperature, pressure, the presence of carbon dioxide, chemical composition of water, development of complexes, structure and texture of carbonates, size of crystals, contact time and biological activity (Flakova 1998). The most important factor determining solubility of minerals is the abundance of carbon dioxide in the system as shown in the following equations.



The process of calcite and dolomite dissolutions, takes place under conditions of open or closed systems, depending on the CO₂ pressure. Fig. 3-1 shows the pure calcite and dolomite dissolution under both open and close system dissolution as a function of CO₂ supply determined by PHREEQC (Parkhurst and Appelo 1999). The relationship between measured pH and calculated pCO₂ in the water samples is also shown on this figure. In the closed system, CO₂ decreases along the groundwater flow path. On the other hand, it remains constant in the open system case (Appelo and Postma 2005). The closed system is characterized by higher pH values, lower HCO₃⁻ content and decreasing CO₂ content along the flow path (CO₂ is consumed by the dissolution of carbonate rocks). In contrast, the open systems have a lower pH, higher HCO₃⁻ content and constant CO₂ content along the groundwater flow paths since there is a constant supply of CO₂ (Appelo and Postma 2005). The source of carbon dioxide in groundwater can be atmospheric, biological (degradation of organic matter) or volcanic origin. According to the Fig. 3-1, the ranges of calculated pCO₂ as a function of pH in the water samples comparing with those values of open and close systems dissolution determined by PHREEQC, indicated that the open system dissolution is prevailing in the study area.

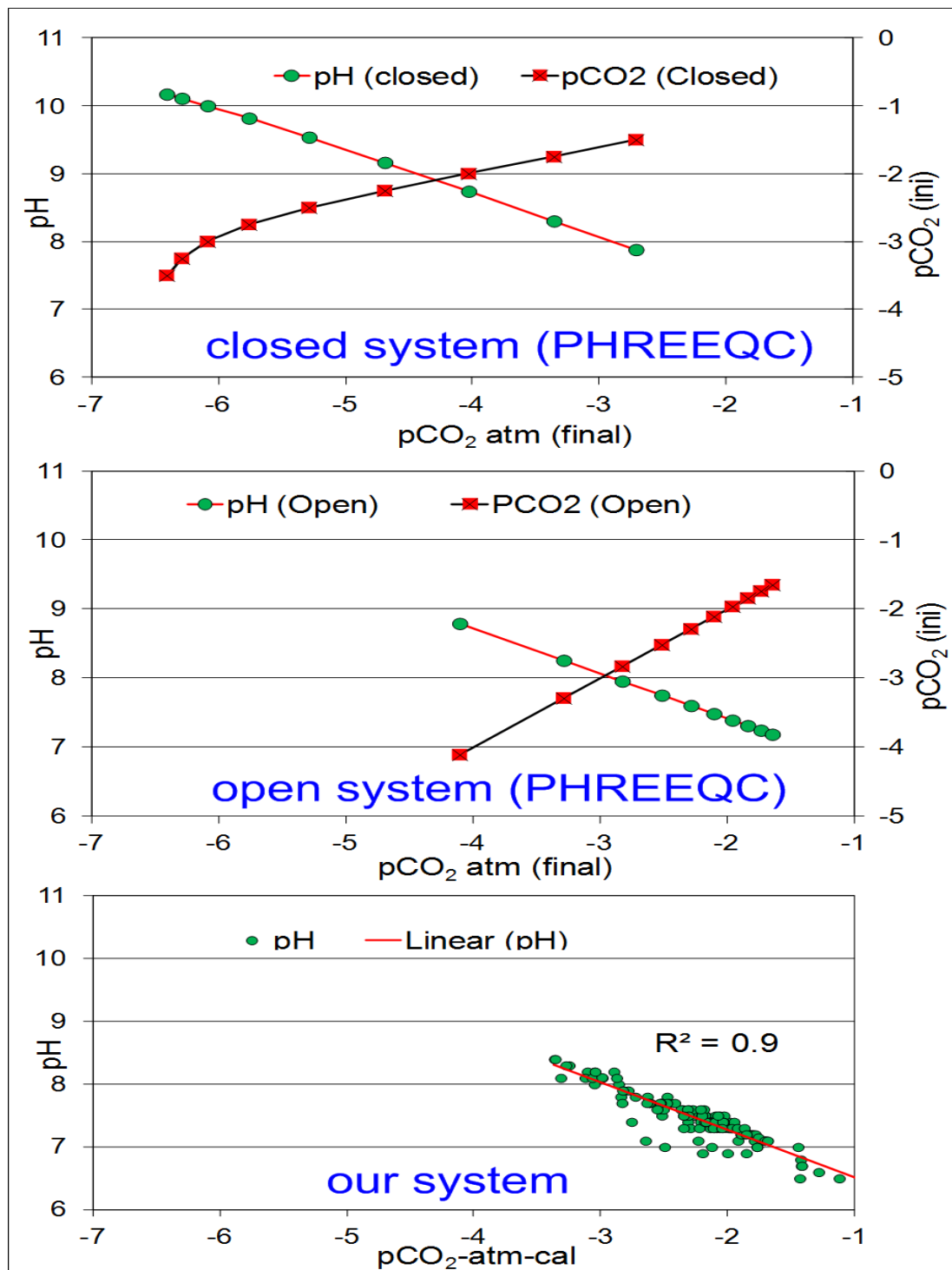


Fig. 3 - 1 Opened and closed systems dissolution of carbonate rocks determined with PHREEQC and pH as a function of pCO₂ (atm) calculated values in the water samples.

Meteoric water has a great influence on groundwater composition in the active groundwater circulation zone. During infiltration, it saturates with CO₂ as a result of organic matter degradation and becomes aggressive to calcite. Throughout the contacts between infiltrating water and limestone, dolomites and gypsum, congruent or incongruent

dissolution of carbonate minerals can occur. Mineral equilibrium calculations for groundwater are useful in predicting the presence of reactive minerals in the groundwater system and estimating mineral reactivity (Deutsch 1997; Jianhua *et al.* 2009).

Since open system dissolution of carbonates is suspected, bicarbonate, calcium and magnesium concentrations have been plotted as a function of calculated $p\text{CO}_2$ together with the pure calcite and dolomite dissolution determined with PHREEQC (Fig. 3-2). The PHREEQC lines and the scatter plot determine the dissolution state of the carbonate system. Distinctly, this graph shows different sources of calcium in water samples such as calcite, dolomite and gypsum dissolution because the majority of the samples are plotted above the PHREEQC line as a result of combined effect of dissolution of these minerals. In contrast, Bicarbonate and magnesium for most samples are situated lower of PHREEQC lines.

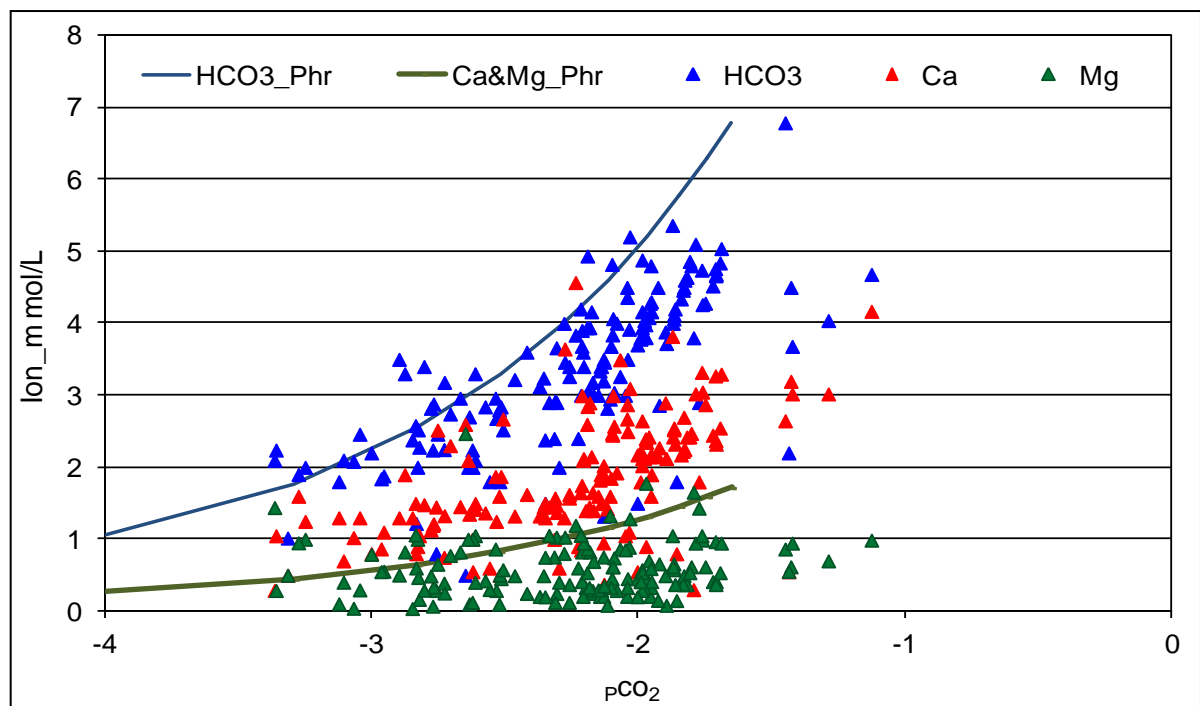


Fig. 3 - 2 Calcium, magnesium and alkalinity concentration in mmol^{-1} as a function of $p\text{CO}_2$ (atm) calculated values; solid lines are the alkalinity, calcium and magnesium determined with PHREEQC for pure calcite and dolomite dissolution.

The hydrochemical equilibrium conditions of groundwater and mineral phases of the hosting rocks can be evaluated by using saturation indices (SI). The saturation indices of particular mineral can be defined as the (logarithmic) ratio using the following formula (Stumm and Morgan 1981)

$$SI = \log_{10} \left[\frac{IAP}{K_{sp}(T)} \right] \quad (4)$$

Whereas IAP is the ion activity product of the mineral-water reaction (solution), $K_{sp}(T)$ is the thermodynamic equilibrium constant adjusted to the temperature of the given samples. When a mineral is in equilibrium with respect to a solution, the saturation index is zero. Under-saturation is indicated by a negative SI and super-saturation by a positive SI.

The scatter plot of saturation indices of calcite and dolomite are shown on Fig. 3-3. In this diagram, a central band of 0.4 units wide along each axis, represents essential equilibrium with respect to either mineral able to account for the possible errors that may occur in the measurement of pH, Mg^{2+} and Ca^{2+} . The four quadrants of the plotting field (I–IV) outside the equilibrium area represent different kinds of equilibrium conditions with respect to calcite and dolomite. The figure shows that some of the water samples are distributed in quadrant I and III, and most of them are situated in the central band of equilibrium. The samples in quadrant I represent supersaturating with respect to both carbonates and hence the domination of carbonate rocks. However, supersaturation can also be produced by other factors such as incongruent dissolution, rapid increase in temperature and CO_2 exsolution (Appelo and Postma 1996; Langmuir 1997; Aghazadeh and Mogaddam 2011). Water undergoing incongruent dissolution of dolomite or precipitation of calcite would plot in the quadrant II. The samples situated in quadrant III represent under-saturation with respect to major carbonate species, these samples correspond to water either coming from an environment where carbonates are impoverished, or to the water that has a short residence time in the hosting carbonates rocks which is not so sufficient for the mineral phases to react to equilibrium (Langmuir 1971; Kortatsi 2007). The samples located in the equilibrium central band, represent saturation with respect to either calcite or dolomite or both minerals.

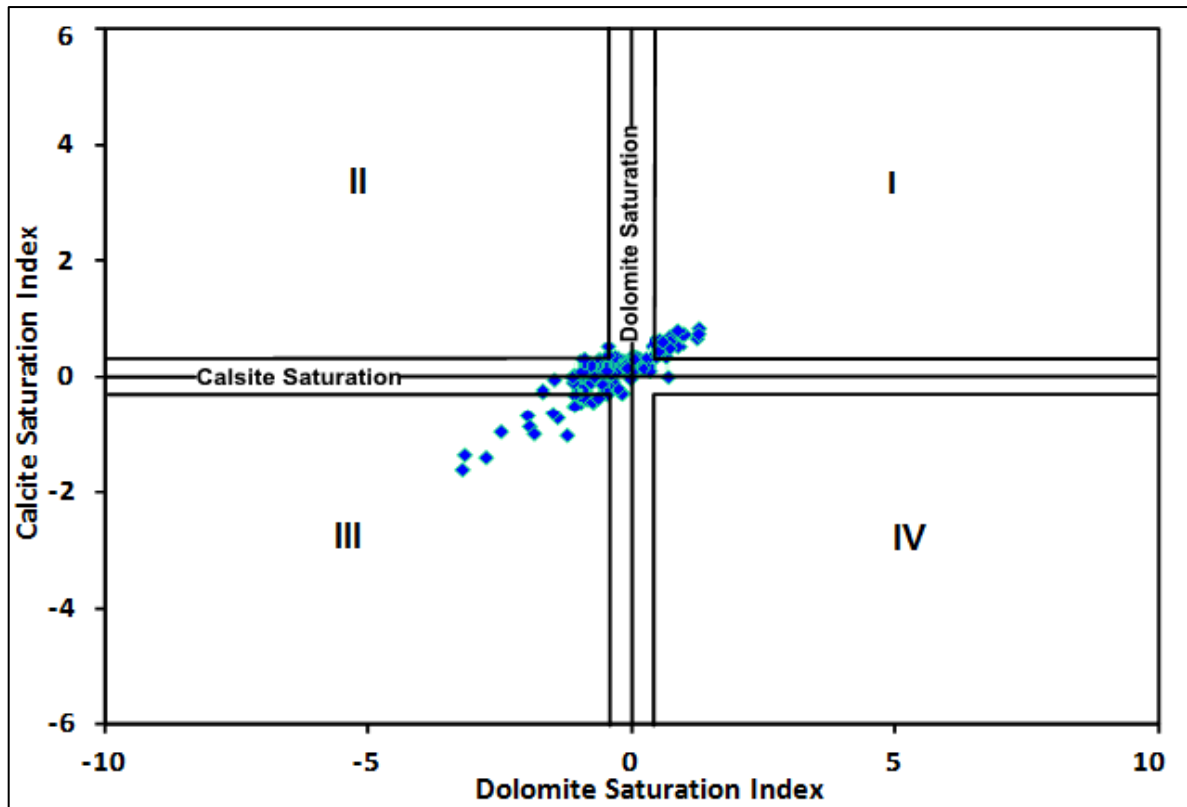


Fig. 3 - 3 Scatter plot of the saturation indices (SI) of calcite and dolomite determined in the water samples.

The SI of calcite as a function of calculated $p\text{CO}_2$ are shown on Fig. 3-4 (chart), and are close to or exceed zero for most samples. The classification and spatial distribution of this factor are shown on the same figure (map). The highest part of the Jurassic aquifer is characterized by low SI of calcite whereas relatively high values were measured in the lower parts levels near Arneh village. This is mostly due to short residence time and less amount of CO_2 as a result of vegetation absence in the higher parts characterized by limited soils development. The low SI of calcite near Arneh village might indicate a quick groundwater circulation from the north higher part towards the south lower part through the channels and conduits developed along faults and fractures as a preferential groundwater flow. The high values encountered in the alluvial and basalt aquifers might indicate a deep groundwater flow from Jurassic aquifers toward these aquifers controlled by sub-regional geological structures.

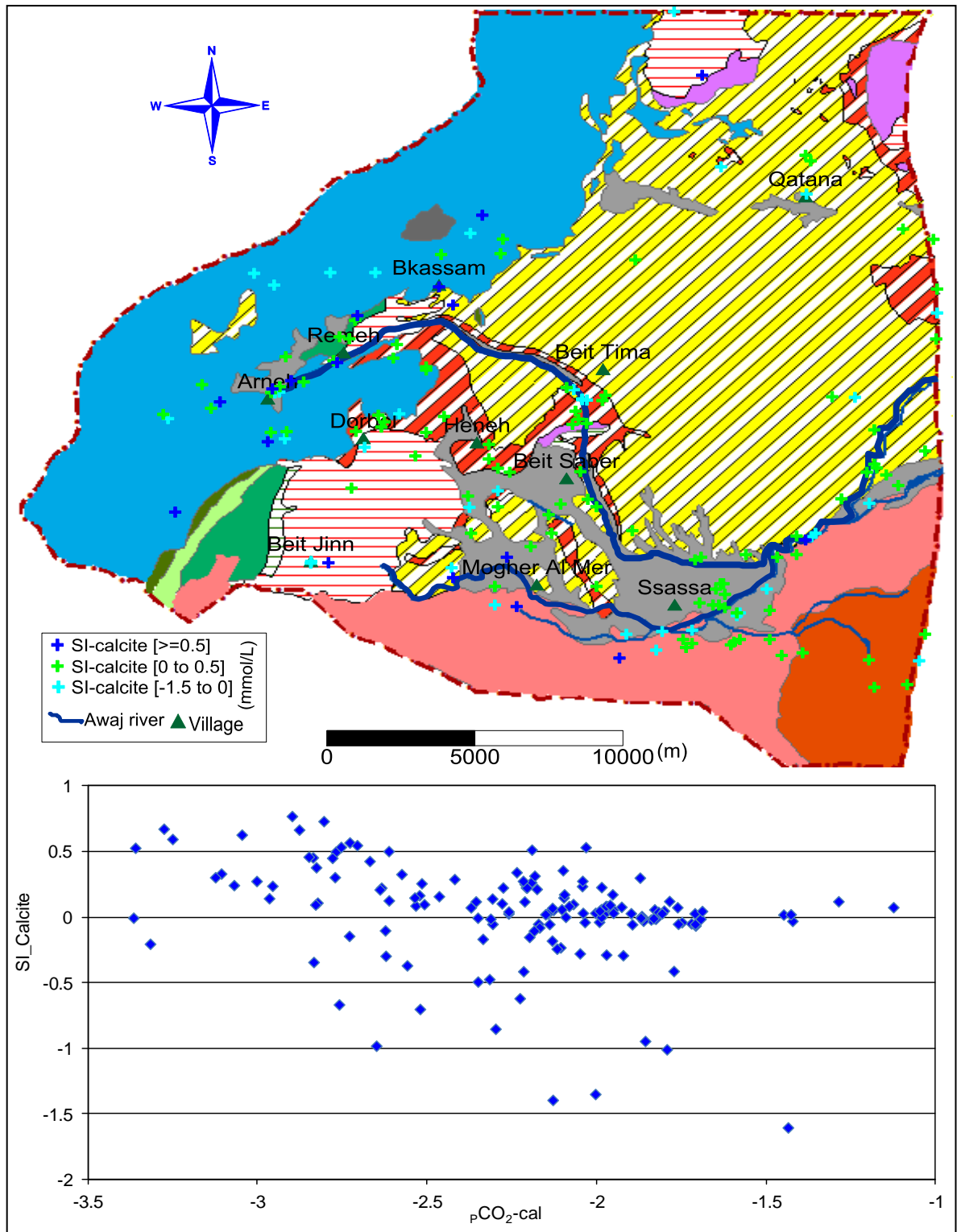


Fig. 3 - 4 Classification and spatial distribution of saturation index of calcite in the water samples with chart showing the SI of calcite as a function of pCO_2 (atm) calculated values.

The alternation of limestone and dolomite along the flow path is characterized by the Mg^{2+}/Ca^{2+} ratio. Mg^{2+}/Ca^{2+} ratios between 0.5 and 0.9 are typical for carbonate aquifers

(Hsu 1963; Stadler *et al.* 2012). For groundwater genetically bound to pure limestones, the Mg^{2+}/Ca^{2+} ratio is smaller than 0.1. On the other hand, water from pure dolomite is characterized by Mg^{2+}/Ca^{2+} ratios higher than 0.7 (Flakova 1998). However, even a very pure limestone can give rise to relatively high Mg^{2+}/Ca^{2+} ratios in water with a long residence time (Moral *et al.* 2008; McMahon *et al.* 2004; Batiot *et al.* 2003; López-Chicano *et al.* 2001; Edmunds and Smedley 2000; Fairchild *et al.* 2000; Plummer *et al.* 1978; Plummer 1977; Bicalho *et al.* 2012). Groundwater from the dolomitic limestone, or from mixed circuits, characterized by Mg^{2+}/Ca^{2+} ratio ranging from 0.1 to 0.7, depends on the degree of dolomitization of the limestone, or on the limestone/dolomite ratio along the flow path. In fresh water, Mg^{2+}/Ca^{2+} ratio values greater than 1 can be the result of water interacting with Mg-rich silicate rocks such as volcanic ones, with Mg^{2+} being derived from olivine (Schoeller 1956; Hem 1985; Vengosh 1994).

Fig. 3-5 shows that most of the samples indicate Mg^{2+}/Ca^{2+} ratios less than one and many of them less than 0.5. These values imply that the contact time between the infiltration water and hosting rocks was rather short and the dominance of calcite over dolomite dissolution. Few samples demonstrate values superior to 1 indicate the effect of basaltic rocks weathering or precipitation of gypsum resulting from an impoverishment in Ca ions, or sulphate reduction process facilitated by anaerobic conditions.

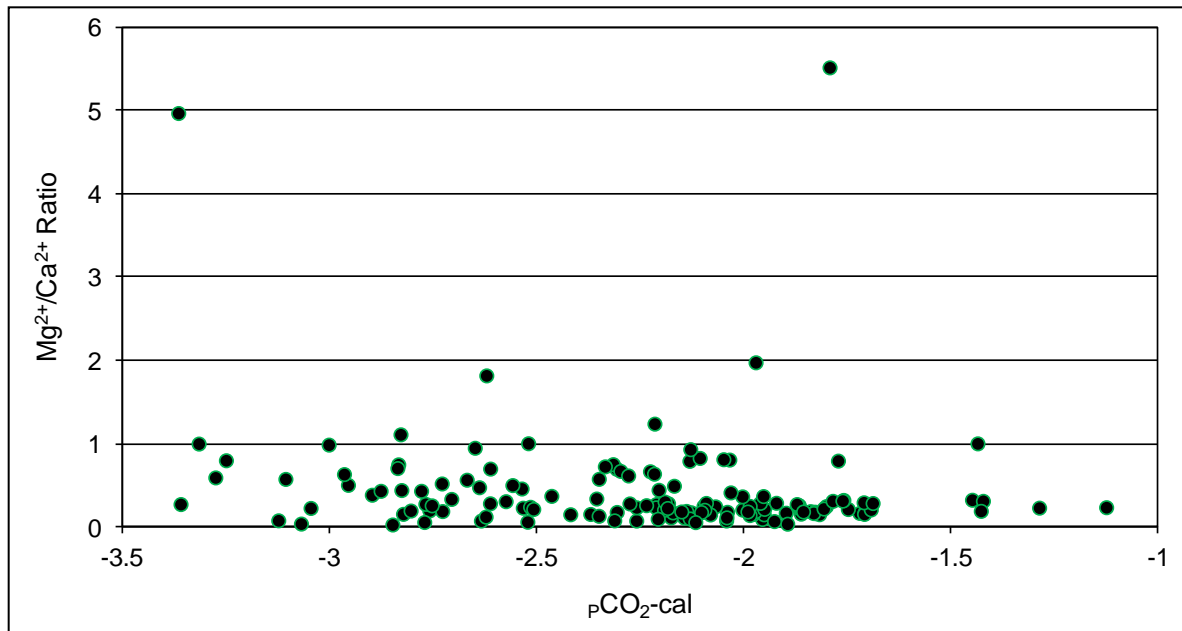


Fig. 3 - 5 The Mg^{2+}/Ca^{2+} molar ratio as a function of pCO_2 (atm) calculated values.

The dissolution of gypsum leads to increasing sulphate concentration in groundwater and to enhanced solubility of dolomite; consequently it lowers the solubility of calcite. SI of gypsum as a function of SO_4^{2-} concentration is plotted on Fig. 3-7. The relationship between two variables shows that the dissolution of gypsum is the main source of sulphate in these waters and a positive correlation was also found between them (correlation coefficient $r = 0.68$). This is associated with an increase in calcium concentration as shown on Fig. 3-6. This figure shows that there is no correlation between calcium and sulphate in most samples, only when sulphate concentration becomes greater than 0.5 mmolL^{-1} , the trend indicates a positive relationship between the two variables due to gypsum dissolution.

3.1.2. Dedolomitization Process

The contemporary occurrence of Mesozoic limestone and dolomites associated with gypsiferous layers of evaporitic origin, gives rise to Ca-sulphate- rich water which induces dissolution-precipitation processes in the dolomite-calcite mineral assemblage (Capaccioni *et al.* 2001). Dedolomitization process means, that the calcite precipitation (eq. 6) and dolomite dissolution (eq. 7) are driven by anhydrite (gypsum) dissolution (eq. 5) (Plummer *et al.* 1990). The dedolomitization is controlled by the three following reactions:



The increasing concentration of Ca^{2+} during the dissolution of gypsum leads to the precipitation of calcite. The loss of Ca^{2+} and HCO_3^- subsaturates the water with dolomite which dissolves and increases the Mg^{2+} concentrations in water (Fig. 3-6). The increase of Mg^{2+} concentrations causes an increase of Ca^{2+} concentration (Fig. 3-6), until the equilibrium is reached between water and both minerals. Thus, the gypsum dissolution brings about a substitution of dolomite by calcite.

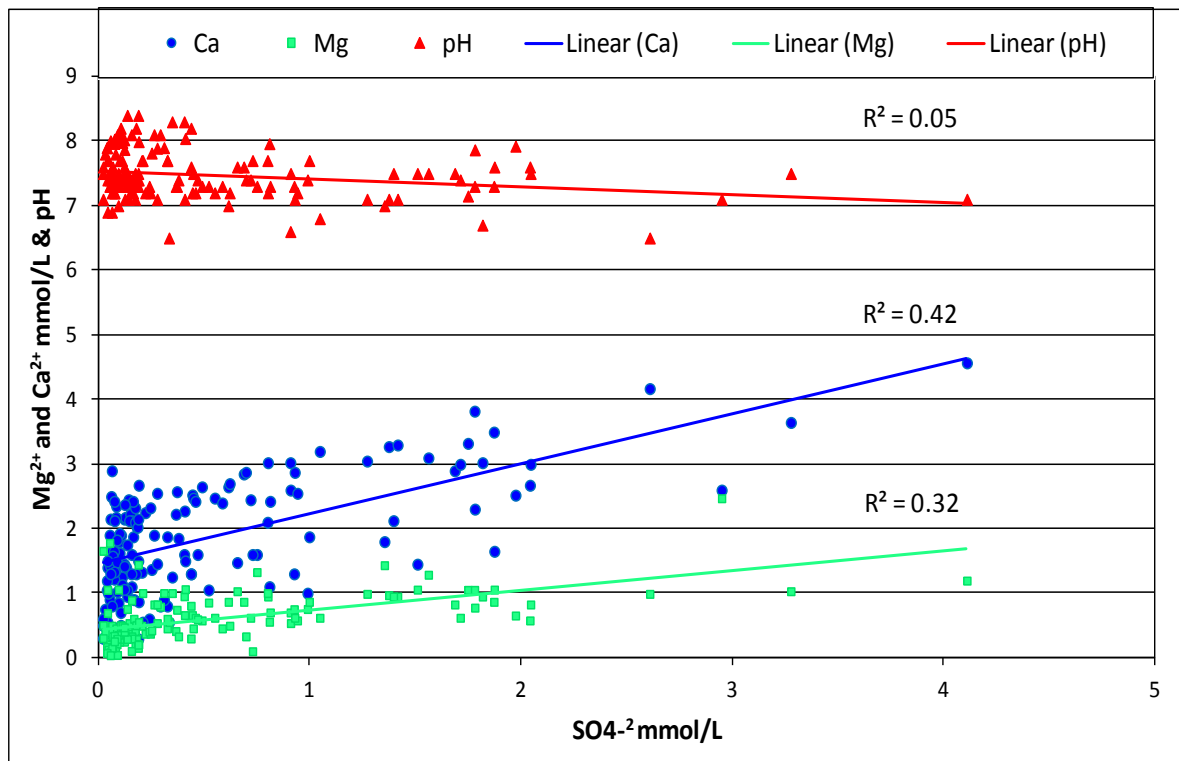


Fig. 3 - 6 Scatter charts of Ca^{2+} , Mg^{2+} (mmol.l^{-1}) and pH as a function of SO_4^{2-} (mmol.l^{-1}).

In the thermodynamic calculation, it is likely that gypsum dissolution is irreversible in most of the system, can occur irrespective of depth and will cease only when the water becomes saturated. However, the water remains at or near saturation with respect to calcite and dolomite. It is appropriate then to choose the dissolved sulphate as a reaction progress variable in examining the trend in the water quality data (Plummer *et al.* 1990) (Fig. 3-7).

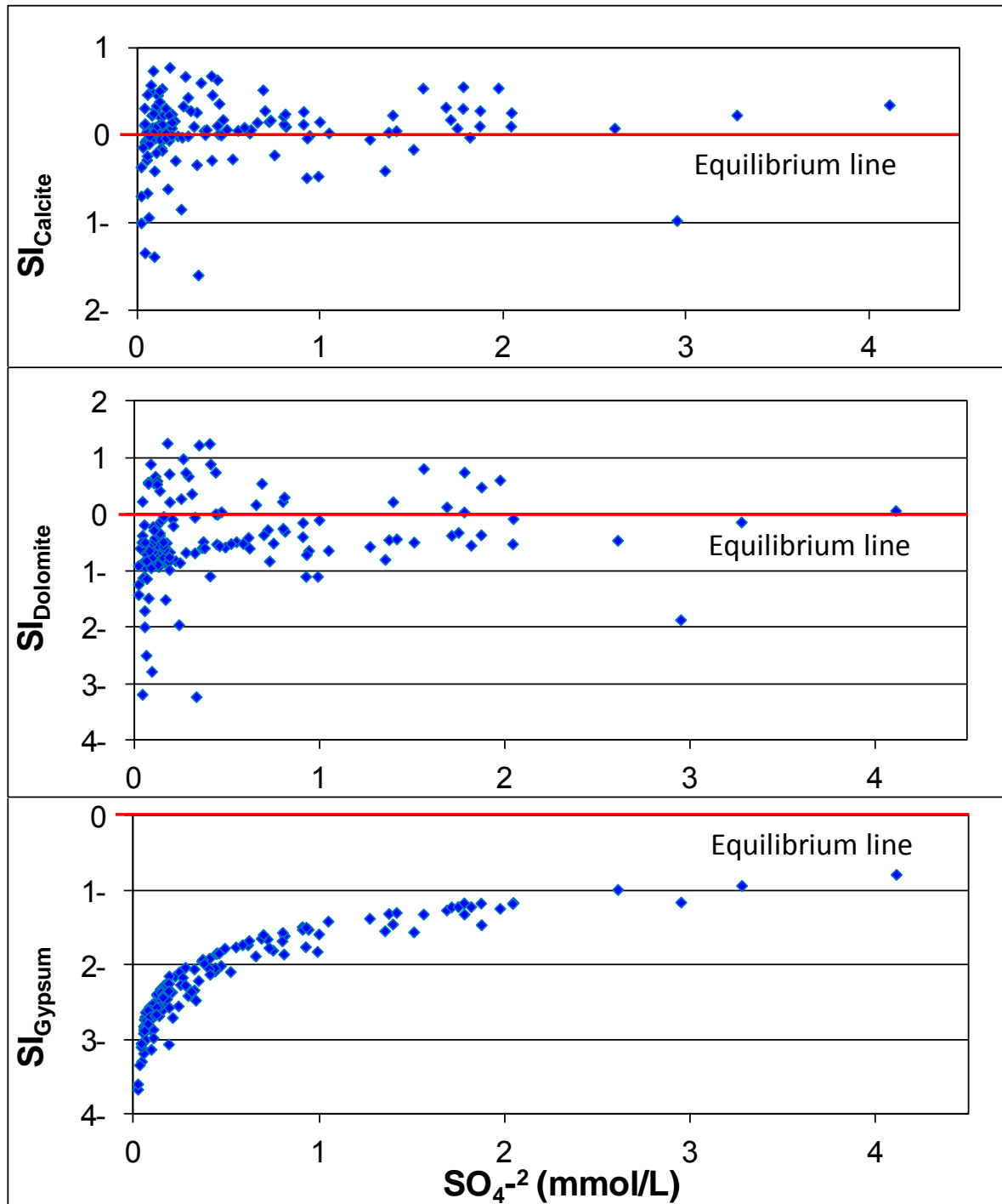


Fig. 3 - 7 Saturation indices of calcite, dolomite and gypsum as a function of SO_4^{-2} (mmol L^{-1}).

In general, the saturation index of calcite is positive for most of samples whereas it remains negative for most samples in terms of dolomite. Meaning that, on the one hand, precipitation of calcite occurs and on the other hand, saturation with dolomite continues. The samples that are characterized by low saturation indices of calcite and by low concentration of sulphate ($< 0.5 \text{ mmol/L}$), indicate that little or no gypsum dissolution

affected the chemical compositions of these water samples. Some samples that show over saturation of dolomite even with less content of the sulphate indicated that the dolomite dissolution was not driven by gypsum dissolution. When the sulphate concentration increases for some samples, they become near saturation with respect to dolomite if we accept an uncertainty of about ± 0.5 for saturation indexes determination. The majority of these samples are located in the Jurassic aquifer. SI of gypsum as a function of sulphate concentration evolves from under-saturated to quasi-saturated. The scarcity of gypsum in the aquifers system might be behind the low values of SI of gypsum. However, sulphate concentration increases with the development of gypsum dissolution. Fig. 3-8 shows that the high values of sulphate (more than 1 mmol/L) which are associated with over saturation with respect to dolomite were measured mainly near Arneh village. It indicates that an approach to dedolomitization process occurs there. This phenomenon was observed near Beit Tima and to the south of Arneh village which might be an indicator of groundwater flow pattern. Other high concentrations of sulphate which are not associated with over saturation of dolomite indicate additional sources of sulphate such as anthropogenic influences.

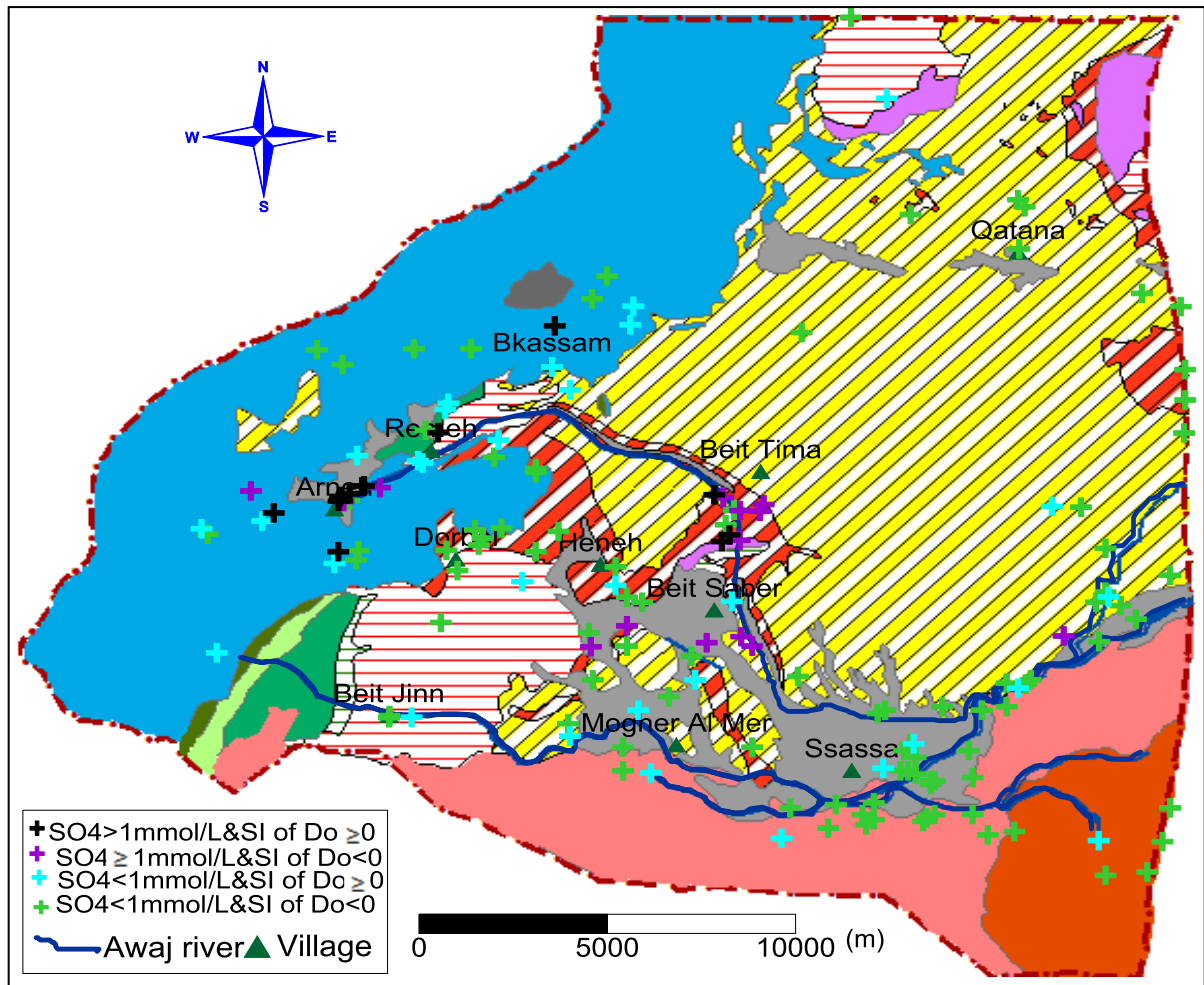


Fig. 3 - 8 Classification and spatial distribution of saturation index of dolomite in the water samples.

As a consequence of dedolomitization reactions, the calcite precipitation in the system causes a decrease of pH values due to H^+ released from HCO_3^- during the incorporation of CO_3 to calcite. In our case, the pH values are hardly going down as shown on Fig. 3-6 According to Figs. 3-6, 3-7 and 3-8 it is likely that an approach to dedolomitization processes occurs only in isolated places where the water came into contact with evaporites interbedded layers.

3.1.3. Silicate hydrolysis

The dissolved silica derives primarily from the weathering and subsequent dissolution of silicates and aluminosilicates in bedrocks and soils (Drever 1997, Brielmann, 2008). The weathering rates of silicate minerals depend on pH, temperature, lithology, vegetation and concentration of metal species. The effect of silicate hydrolysis on the water chemistry is

primarily the addition of cation and silica, given that high silica in the water samples indicates active degradation of silicate minerals. The silicate can be used as a conservative tracer based on the fact that it dissolves very quickly (Kennedy 1971, Brielmann, 2008)

The carbonate rocks have in general low contents of silicate minerals when compared to basaltic rocks. The silica values in the samples collected in 2006 are shown on Fig. 3-9. Clearly, a sharp boundary between three groups is observed. The first one is characterized by low silica concentration ($3.5\text{-}8.5\text{ mgL}^{-1}$) and located in the Jurassic aquifers. The second one is located in the Neogene and Quaternary aquifers and characterized by higher silica ($9\text{-}14\text{ mgL}^{-1}$). The highest concentration in silica, (third group, $15\text{-}31.5\text{ mgL}^{-1}$), was observed in the basaltic Miocene aquifer. This aquifer is more weathering compared with the Quaternary basalt enhancing the dissolution process of abundance aluminosilicate minerals in the shallow and weathering zone. High silicate content observed in the Neogene/Quaternary aquifers might indicate a flow patterns from the Miocene basaltic aquifer to the southeast direction toward these aquifers.

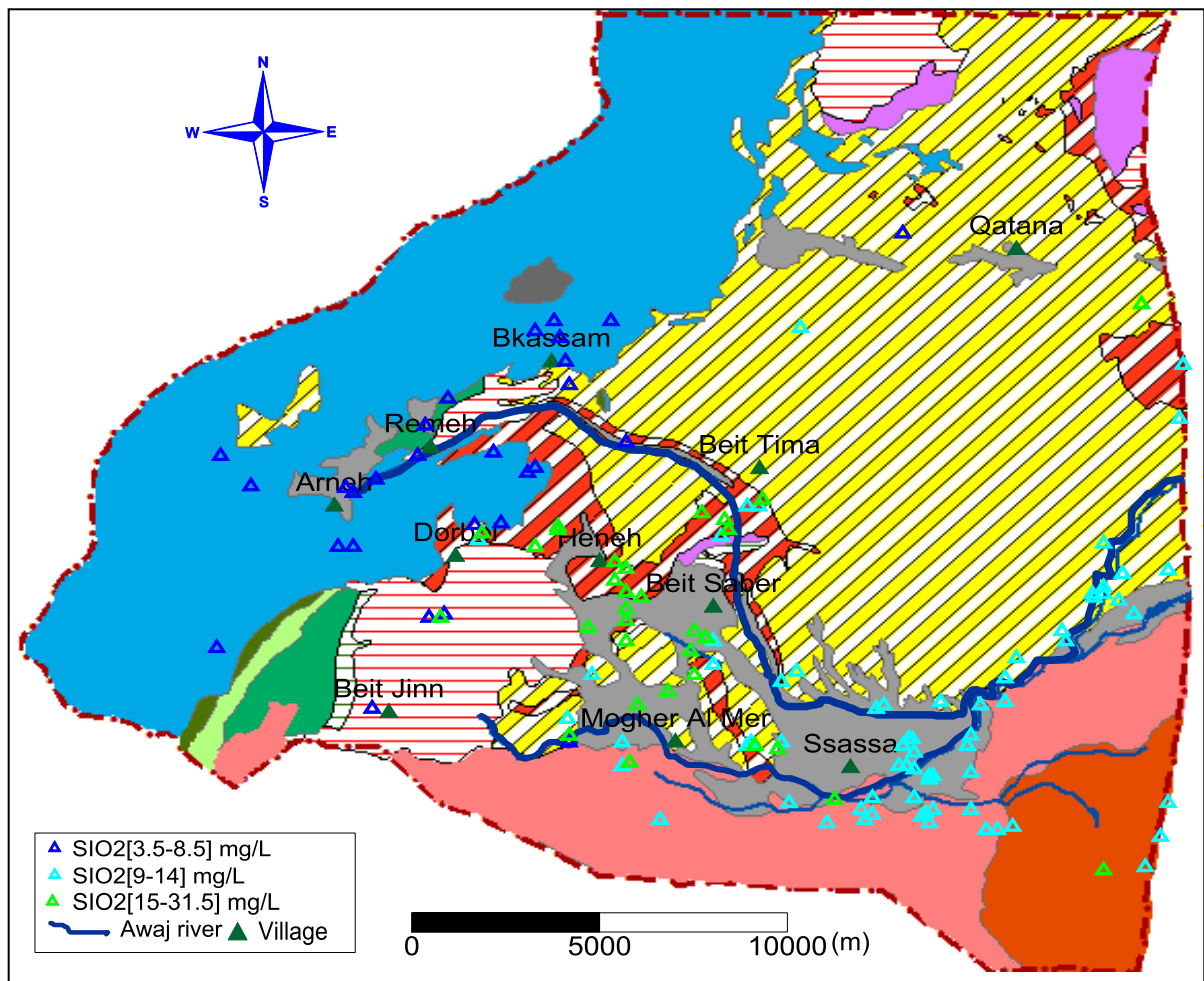


Fig. 3 - 9 Classification and spatial distribution of SiO_2 (mg l^{-1}) concentration in water samples.

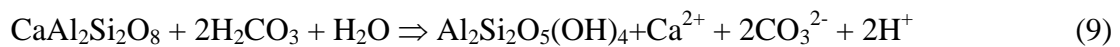
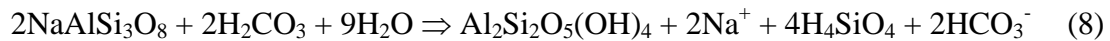
The solubility of different SiO_2 phases decreases with increasing crystallinity of the solid SiO_2 phase. The kinetics of precipitation decrease in the same order and are generally low compared with carbonate reactions. Therefore dissolved silica contents in the groundwater are normally highest in the weathering zone.

The mineral stability diagram is another approach to test the proposed hydrochemical evolution of silicate minerals and their stability (Drever 1988, Guler and Thyne 2004b). The stability fields for the Ca-Plagioclase (anorthite) and its possible weathering products, gibbsite, kaolinite, and Ca-montmorillonite as a function of $\log ([\text{Ca}^{2+}] / [\text{H}^+]^2)$ and $\log [\text{H}_4\text{SiO}_4]$ is shown on Fig. 3-10. In this case the kaolinite is more likely to be stable than, for example gibbsite, as a result of anorthite weathering products. This may be due to removing the Ca^{+2} from the system by the precipitation of Ca-salts. Some samples which

are located at or close to the stability field of montmorillonite, indicated that the typical aquifer of these water samples is most likely a basic rock (like basalts) (Appelo and Postma 2005).

Fig. 3-10 also shows the stability fields for the Na-Plagioclase (albite) and its potential weathering products, paragonite, gibbsite, kaolinite, and pyrophyllite as a function of $\log ([\text{Na}^+]/[\text{H}^+])$ and $\log [\text{H}_4\text{SiO}_4]$. It shows that the main reaction is the conversion of albite to kaolinite. Meaning that the primary silicate minerals such as plagioclase and clinopyroxene, can be dissolved and weathered to kaolinite which is more likely to be in equilibrium in the system. While noting some samples extending into the albite stability field suggesting that the equilibrium between clay and primary mineral is not likely to be the main process controlling the water chemistry (Guler and Thyne 2004b).

The two diagrams show that most of the groundwater samples are not in equilibrium neither with anorthite nor with albite, and they will decompose if they are present in the aquifers system as shown in the equations 8 and 9.



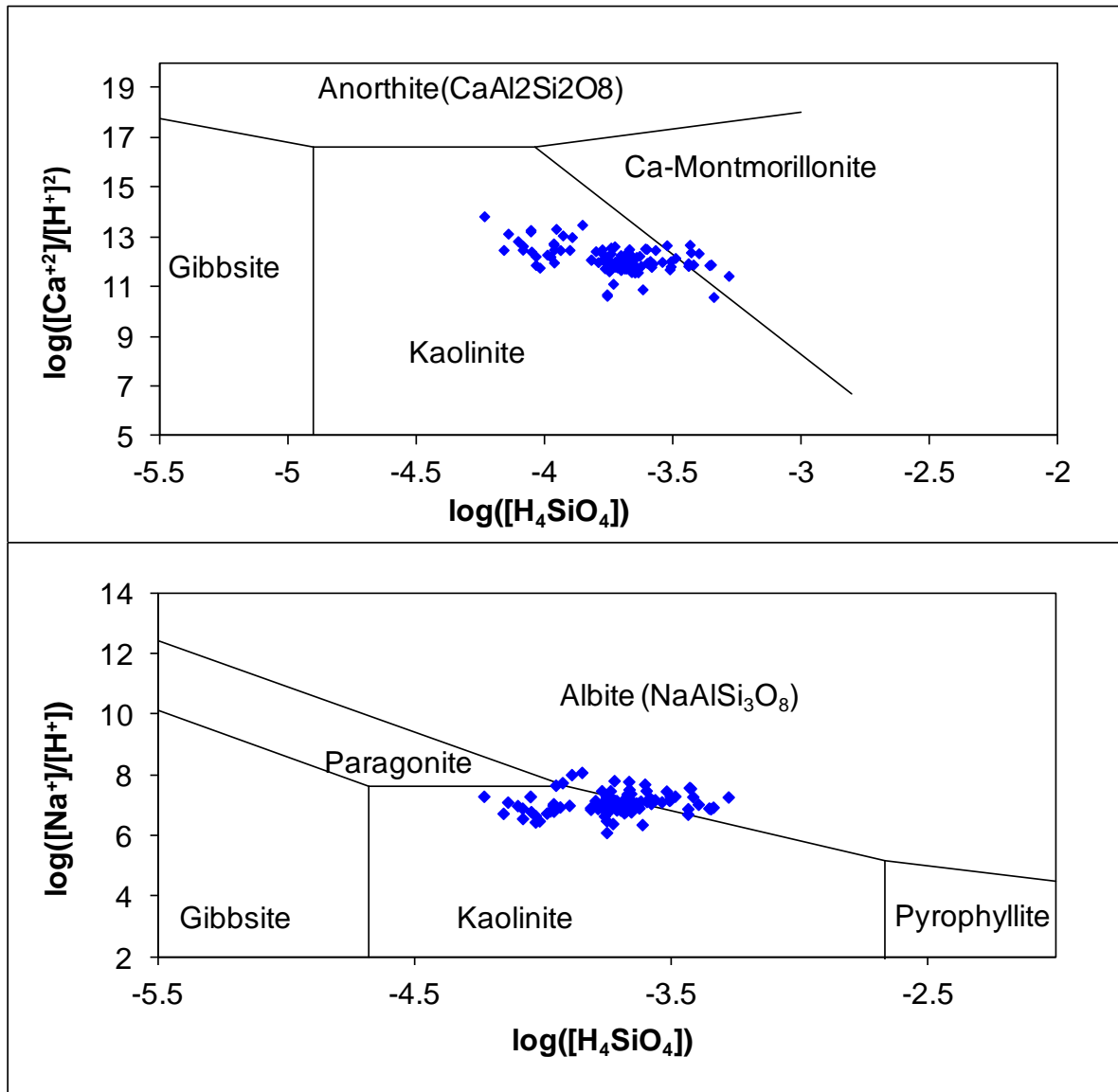


Fig. 3 - 10 Stability diagram of both Ca-Plagioclase (anorthite) and Na-Plagioclase (albite) and their possible weathering products.

According to Han and Liu (2004), the variation in the composition of water (Mg^{2+}/Ca^{2+} and Na^+/Ca^{2+}) can be used to distinguish limestone, dolomite and silicate rock sources of ions. Fig. 3-11 displays the covariation between the two molar ratios. These two ratios are almost equivalent because both of them vary over three orders of magnitude. Water samples composition seems to be affected by the mixing trend of three types of rock; most likely the carbonate rocks have a higher effect. It is noticeable that the Mg^{2+}/Ca^{2+} ratios of most samples are bellowing the $Mg^{2+}/Ca^{2+}=0.8$ line. This is probably due to non-equilibration of the waters simultaneously with calcite and dolomite as the contact time between them was rather short. The water equilibrated together with calcite and dolomite

gives an ideal molar $\text{Mg}^{2+}/\text{Ca}^{2+}$ ratio of about 0.8 (Appelo and Postma 1993, Han and Liu 2004).

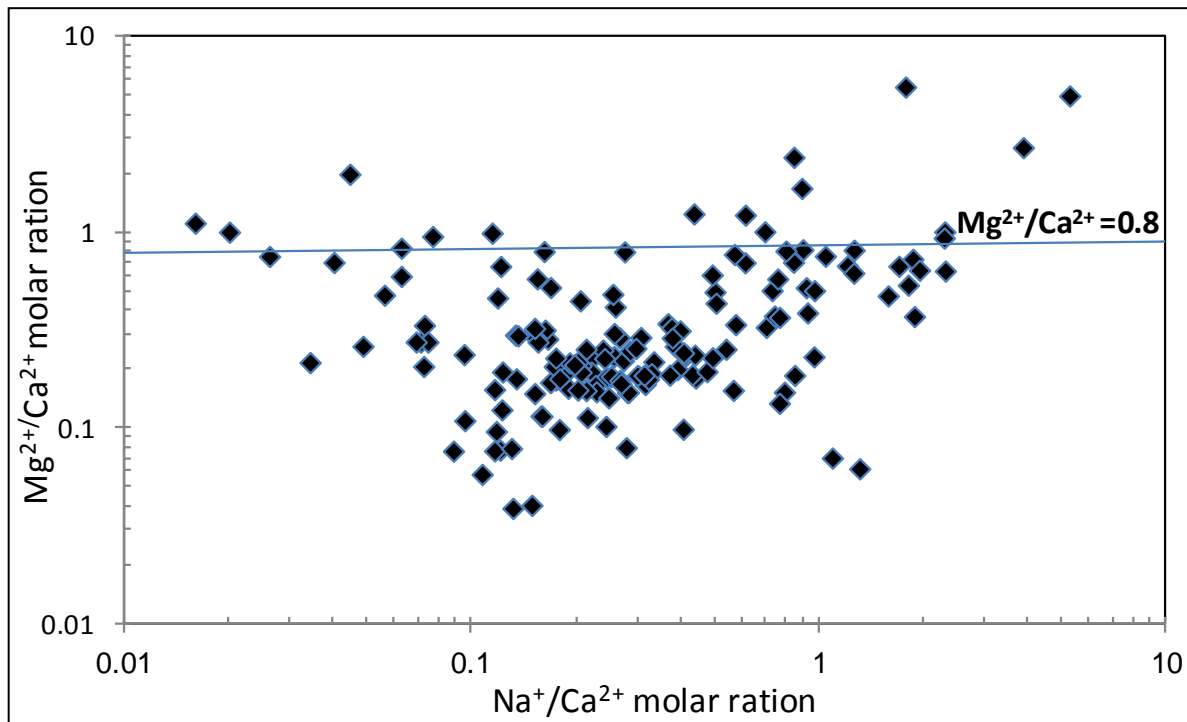


Fig. 3 - 11 $\text{Na}^{+}/\text{Ca}^{2+}$ versus $\text{Mg}^{2+}/\text{Ca}^{2+}$ molar ratios in the water samples, (after Han and Liu, 2004).

The role of carbonate dissolution and silicate hydrolysis on the groundwater composition has been studied by Datta and Tyagi (1996), who explained the effect of these rocks through the scattered plots of $(\text{Ca}^{2+} + \text{mg}^{2+})$ versus $(\text{HCO}_3^- + \text{SO}_4^{2-})$ as shown in Fig. 3-12.

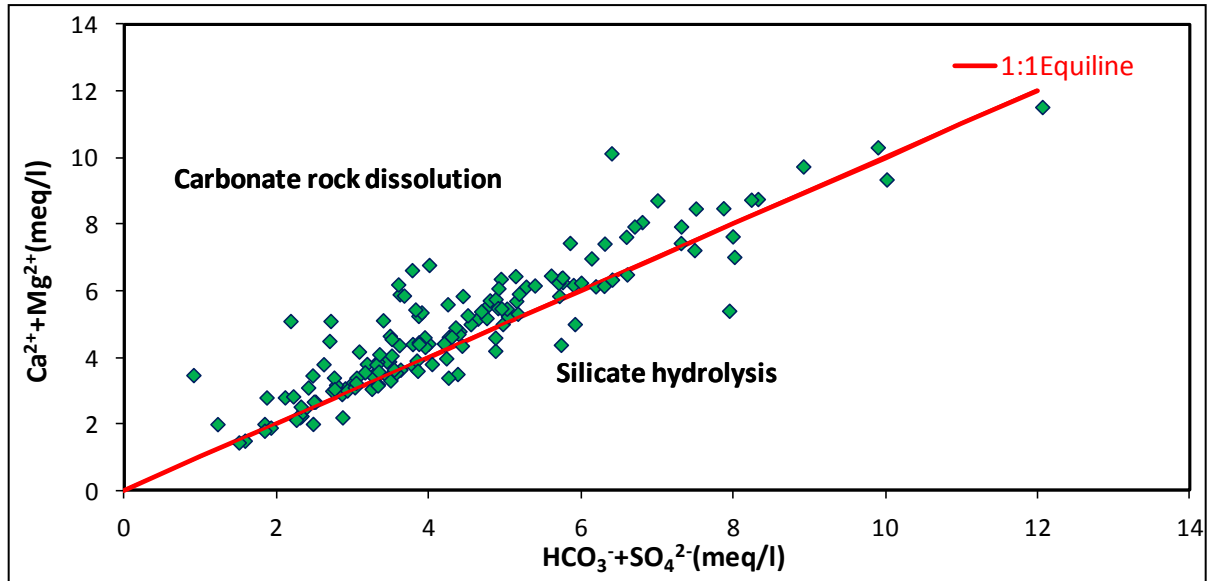


Fig. 3 - 12 Scattered plots of $(Ca^{2+} + mg^{2+})$ vs. $(HCO_3^- + SO_4^{2-})$ showing the effect of carbonate rock dissolution and silicate hydrolysis on groundwater composition.

The majority of water samples are located close to and above equiline in the $Ca^{2+} + Mg^{2+}$ side which indicates that, on the one hand, the dissolution of carbonate rocks is the major hydrochemical process in the system and on the other hand, the excess calcium and magnesium might be derived from other processes such as reverse ion exchange reactions. The locations of few samples below the equiline confirm the role of silicate hydrolysis as a major mechanism controlling the water chemistry of these samples.

3.1.4. Redox processes

The redox is a measurement of the relative difference in energy between the oxidants and the reductants present in the environment. The equilibrium composition of a redox system involving H^+ depends on both the pH and the pE. The interplay in the relationship between these two factors is conveniently illustrated by constructing a phase diagram in which the various lines represent states of (pE, pH) at which equilibrium occur. The redox conditions are first divided into oxic and anoxic environments depending upon the presence or absence of measurable amounts of dissolved oxygen. Based on the relationship between pH and pE, the Fig. 3-13 shows the stability diagram of redox conditions range within the aquifers. It can be stated that the redox conditions in the aquifers vary from aerobics to suboxics conditions, because no redox couple is clearly present in this case.

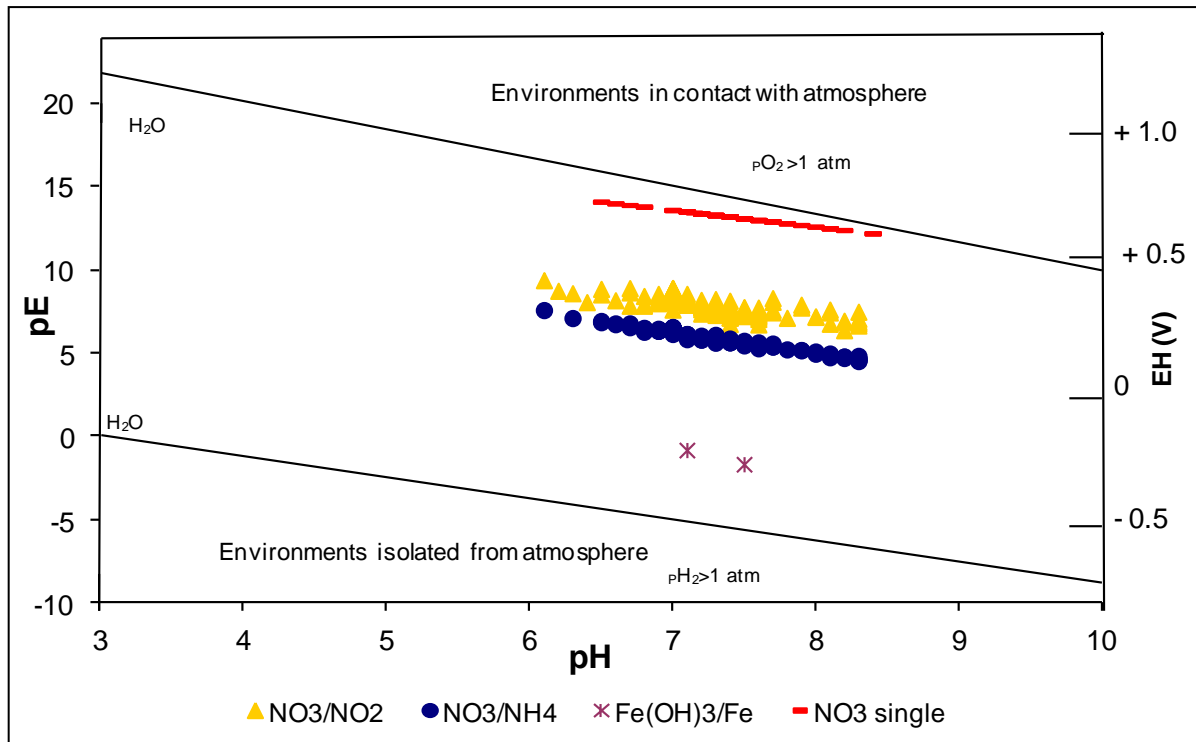


Fig. 3 - 13 Stability diagram of redox conditions range based on the relationship between pH and PE and the distribution of water samples.

3.1.5. Stuyfzand classification

In hydrochemical studies, classification serves the purpose of isolating a group of representative clusters (water groups). Stuyfzand (1989) had determined water type on the basis of chloride, alkalinity and the most important ions. According to that, the main type, type and subtype can be determined for each water sample (tables 3-1 and 4-2). The schematic of selected water samples are shown in Fig. 3-14. By using this method, groundwater can be classified as very oligohaline, oligohaline and fresh ($\text{Cl}^- < 150 \text{ mg l}^{-1}$ for all sample then the code changes between G, g and F). The factor F is mainly dominant in the central and southeastern parts of the area (plain part) as a result of intensive irrigation activities associated with high evaporation rates and return flow as well as the effect of topographic factor. The upward leakage from deeper aquifers, where the evaporites are present, can be another source of chloride. In terms of alkalinity values, the groundwater is classified as moderately low, moderate and moderately high (alkalinity varying between 1-8 meq l^{-1} and then the code changes between 1, 2 and 3). In general, HCO_3^- concentration increases with the general direction of the flow pattern which indicates the effects of

carbonate rocks dissolution by infiltrating CO₂-rich meteoric water, and dissolution of volcanic rocks.

The local appearance of Ca-NO₃ water types in the southwest of the plain area is a result of agricultural pollution. In the western part, mainly in the Jurassic aquifer, the calcium mix water type is present. The "Mix" anions water type refers to the water in which no anion family makes up more than 50% of the sum of anions. The existence of this water type, Indicates that more salt dissolution might take place (Coetsiers and Walraevens 2006).

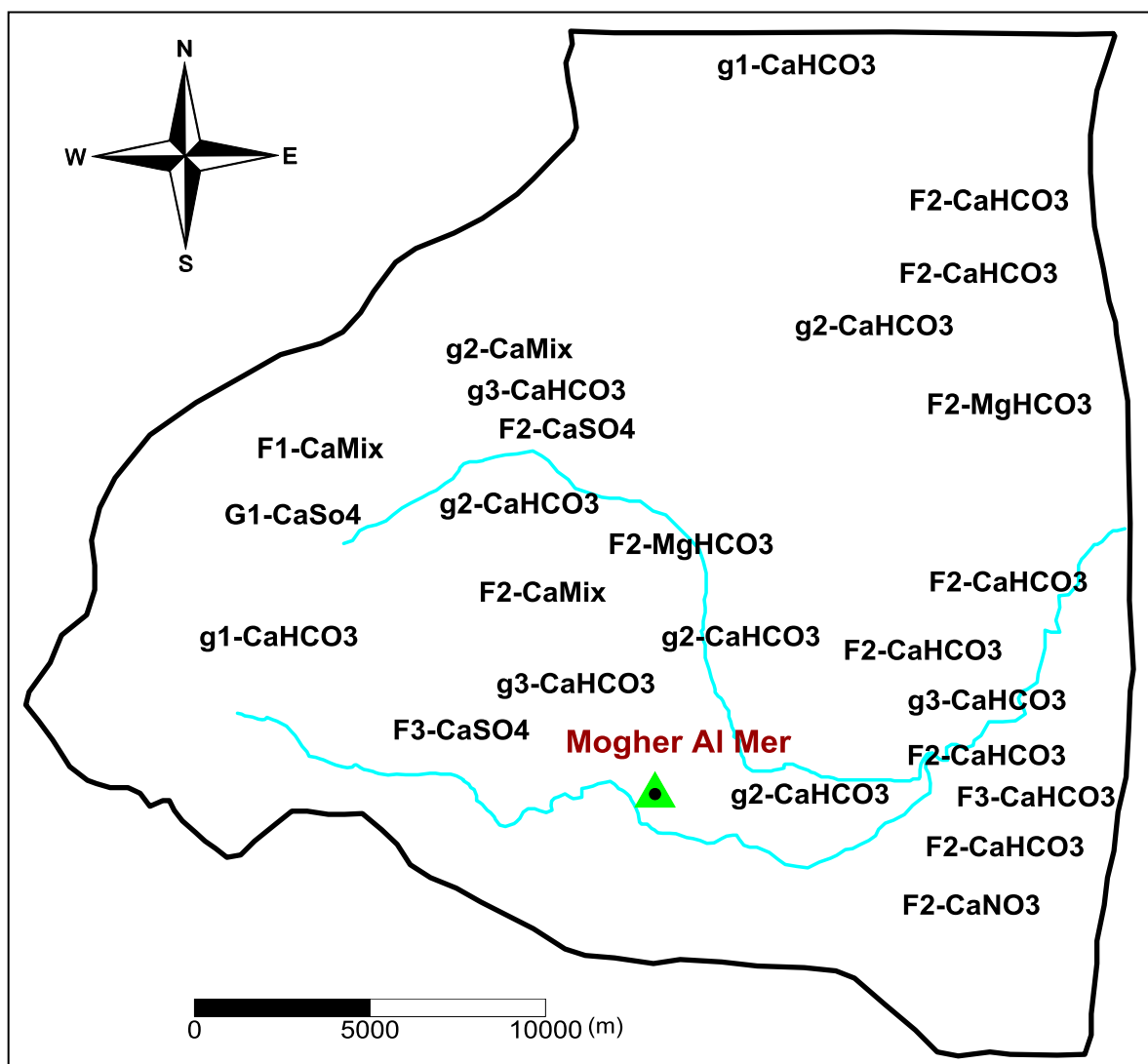


Fig. 3 - 14 Water types based on Stuyfzand classification.

3.1.6. Correlation between groundwater flow pattern and hydrochemical behaviour

According to hydrochemical characteristics of groundwater, groundwater discharge (mainly major springs), and geological and structural control, the study area has been divided into four subareas S_1 , S_2 , S_3 and S_4 (Fig. 3-15).

The groundwater flows in S_1 from the north in Mt. Hermon towards the south through the karstic channels and conduits. Groundwater in this subarea discharges in many springs located in the valley around the Arneh village; together these springs form one of two tributaries of the Awaj River (Sebarani). In S_2 , groundwater also flows in karstic channels in the Jurassic aquifer towards the south and the southeast to be discharged in the High Beit Jinn spring. In this area, another tributary of the Awaj River (Jenani) is generated. The average annual discharge of upper Beit Jinn spring is very close to the volume of the annual rainfall amount estimated over S_2 (RDWSSA 2006). And since the infiltration coefficient is estimated in 84 % for this area (RDWSSA 2006), the recharge area might not be correlated with the size of the geographic surface water catchment and therefore the basin boundaries could be extended towards the west (Fig. 3-15). In S_3 , groundwater flows towards Beit Jinn spring and it is also controlled by faulting and structural blocks. S_4 is the biggest subarea which includes the zones with higher groundwater withdrawals for intensive irrigation purposes. The Neogene and Jurassic outcropping formations are the main sources of water recharge in S_4 but it also receives the input of the upper Paleogene, Quaternary and Miocene basalt aquifers. In this area, water discharges through the major springs, Mambej, Talmasiat, Tell assyouf, and Tabibieh located from west to east. Numerous wells also exist in the Neogene conglomerate aquifer which is recharged from both the direct infiltration and the possible hydraulic exchange with the deeper Jurassic and Cretaceous aquifers. At the level of a major northwest-southeast fault cutting through the Neogene Plain, water is thought to converge to Tabibieh Spring. This spring originates in the east-west fault along the Awaj River.

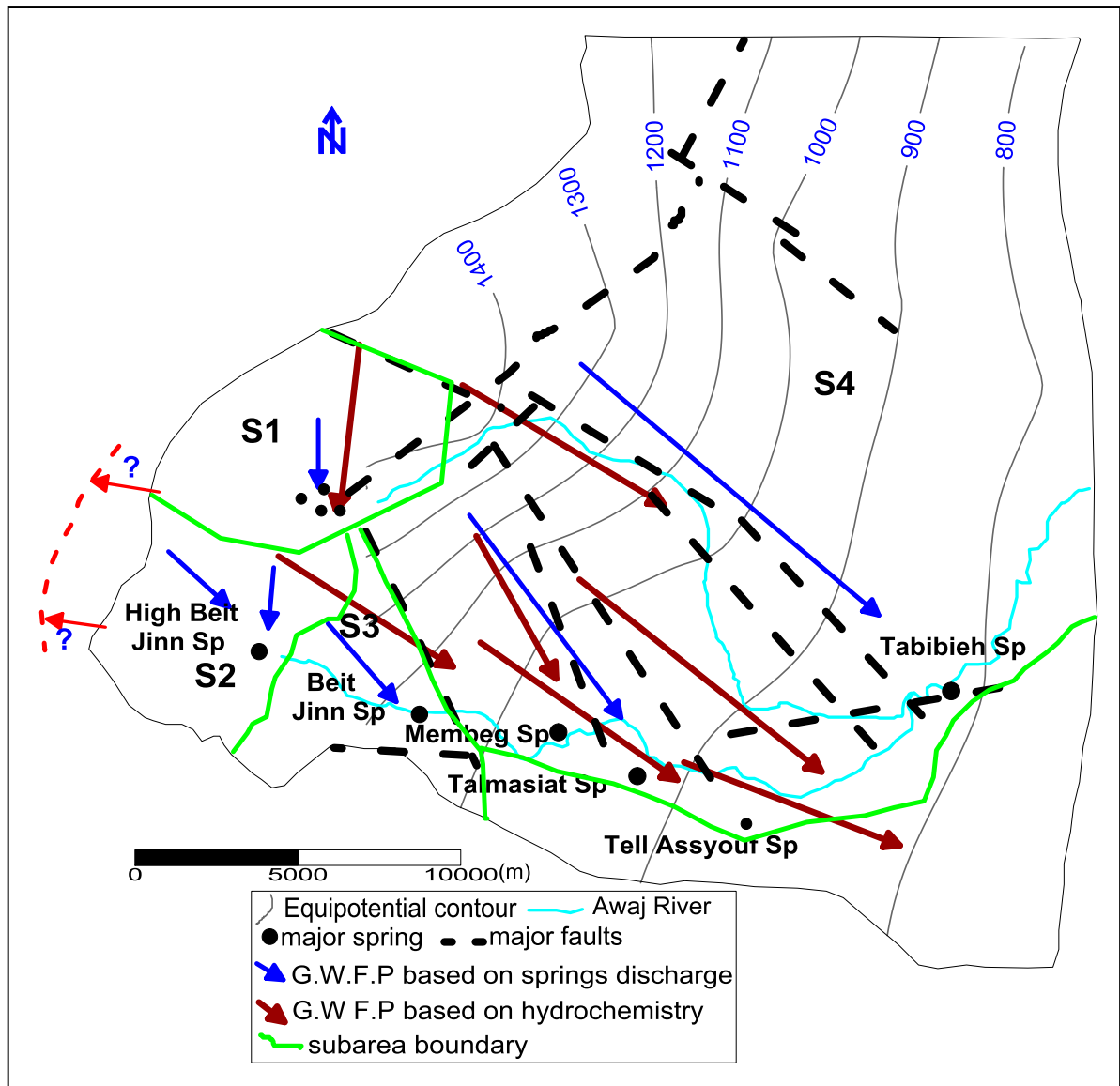


Fig. 3 - 15 Schematic groundwater flow patterns based on major springs discharge and hydrochemical tracers and the associated hydrogeological subarea based on these patterns.

A published paper stemmed from this chapter is appended (Appendix A)

Chapter 4. Hydrochemical facies and isotopes to characterize the origin and recharge mechanisms of the groundwater in the study area

Introduction

The data, which has been used in this chapter, is based on the historical data (Selkhozpromexport 1986, Asmael *et al.* 2014) as well as the obtained result from the samples analysis in the year of 2012.

Hydrochemical facies is another method used to classify groundwater into groups of samples whose assigned names indicate the most concentrated cations and anions in the water samples. This can be correlated with location and geology (Suk and Lee 1999, Barbieri *et al.* 2001, Guler *et al.* 2002, Guler and Thyne 2004^a). The vertical and horizontal groundwater flow patterns control the distribution of these facies. Abundance values are based on equivalents or milliequivalents (meq) rather than mg l^{-1} or molar concentrations.

Isotopes are atoms of the same element, in which the nuclei of the atoms have the same number of protons but different numbers of neutrons. The stable and naturally occurring isotopes of ^{18}O and $\delta^2\text{H}$ are components of the water molecule and thus they are ideal tracers to answer several hydrological problems. They have conservative properties and depend only on atmospheric conditions during recharge; consequently, they provide information on the recharge processes of groundwater (Bajjali 2008; Bajjali 2006, Fritz *et al.* 1981, Gat 1971). As a result, ^{18}O and $\delta^2\text{H}$ composition of precipitation throughout the world is linearly correlated and plots along a line known as the meteoric water line (Craig 1961). Differences in the isotopic composition of precipitation occur along this line if water vapour originated from evaporation of cooler or warmer seawater. This composition is also controlled by the isotope fractionation which occurs during transition processes such as evaporation, condensation and mixing. As the moist air masses move across continent, the heavier isotopes are preferentially removed by precipitation. However, the isotope compositions can change between storm events and even during the course of a single event (Heathcote and Lloyd 1986, Nativ and Mazor 1987, Rindsberger *et al.* 1990, Adar *et al.* 1998, Kubota and Tsuboyama 2003, Celle-Jeanton *et al.* 2004, Brielmann 2008).

4.1. Result and discussion

4.1.1. Water- Rock interaction and salts dissolution

Groundwater chemical characteristics change along its flow paths. These changes may reflect processes such as mixing of groundwater types, mineral dissolution and precipitation, ion exchange and redox reaction (Dehnavi *et al.* 2011, Varol and Davraz 2014). Using of binary diagram together with spatial distribution maps of analyzed results and ionic ratios, may aid in interpretation of the evolution trends.

Hydrochemical indices are commonly used to ascertain the possible chemical reactions of groundwater along a flow path and to identify groundwater evolution and recharge mechanisms in the aquifer (Zhu *et al.* 2007, Jianhua *et al.* 2009, Litaor *et al.* 2010). Evaluation of the groundwater potential to dissolve or precipitate minerals involves mainly the solubility indices (SI) of minerals under measured conditions of ionic concentrations, pH, and temperature.

The evaporation process represents the total amount or rate of transfer of liquid or solid water into atmospheric water vapour at the concerned watershed surface. Since the chloride is assumed to originate exclusively from precipitation, it is considered as one of the most conservative parameters once it is in the aqueous phase (Edmunds *et al.* 1985). The reason behind this is that it does not interact with constituents in the rock matrix/soil and it is not taken up by vegetation or removed from the system by evaporation. (Hem 1985, Luijendijk and Bruggeman 2008). The available average concentration of the major ions in the rainwater samples collected from three stations, Arneh, Remeh and Qatana (Table 4-1), as well as the major ions measured in the groundwater samples (tables 3-1,4-2) were used to determine the effect of evaporation on the groundwater composition by determination of the evaporation factor (EF) by using the following equation:

$$EF = \frac{Cl_s}{Cl_r} \quad (10)$$

Where Cl_s is the chloride concentration in the groundwater sample and Cl_r is the chloride concentration in the rain sample.

This factor and the major ions in the groundwater samples and rainwater samples have been used to determine the process that control the ion concentration in the groundwater samples excluding the evaporation effect by using the following equation:

$$P = I_s - (EF * I_r) \quad (11)$$

Whereas P is the processes that control the ion concentration in the groundwater samples other than evaporation, I_s is the specific ion concentration of groundwater sample, EF is the evaporation factor and I_r is the same ion concentration measured in the rainwater sample.

Table 4 - 1 Major ions concentration in the precipitation samples collected from three stations located in the study area.

Precipitation station	Date	Na ⁺	K ⁺	Mg ²⁺	Ca ²⁺	Cl ⁻	HCO ₃ ⁻	SO ₄ ²⁻
Remeh	Feb-85	0.11	0	0.2	0.3	0.5	2.4	0.08
Remeh	Mar-83	0.16	0	0.1	0.2	0.25	0.5	0
Remeh	Dec-84	0.07	0	0.35	0.9	1.2	1	0.12
Remeh	Jan-85	0.06	0	0.3	1	0.7	1.5	0.1
Qatana	Apr-84	0.14	0	0.3	0.9	0.2	2.6	0.03
Remeh	Feb-84	0.58	0	0.25	0.35	0.3	1	0.01
Arneh	1989-1993	0.11	0.01	0.15	0.16	0.24	0.35	0.03
Average		0.18	0	0.23	0.54	0.49	1.34	0.05

The spatial distribution of groundwater samples as shown in Fig. 4-1 and Fig. 4-2 and their deviation from the zero axis indicate that the major processes controlling groundwater composition in terms of the most major ions, are the mechanisms of other than evaporation such as water-rock interaction, while the evaporation process has a slight effect. This detection is in good agreement, as discussed later, with the interpretation of the groundwater isotopic composition.

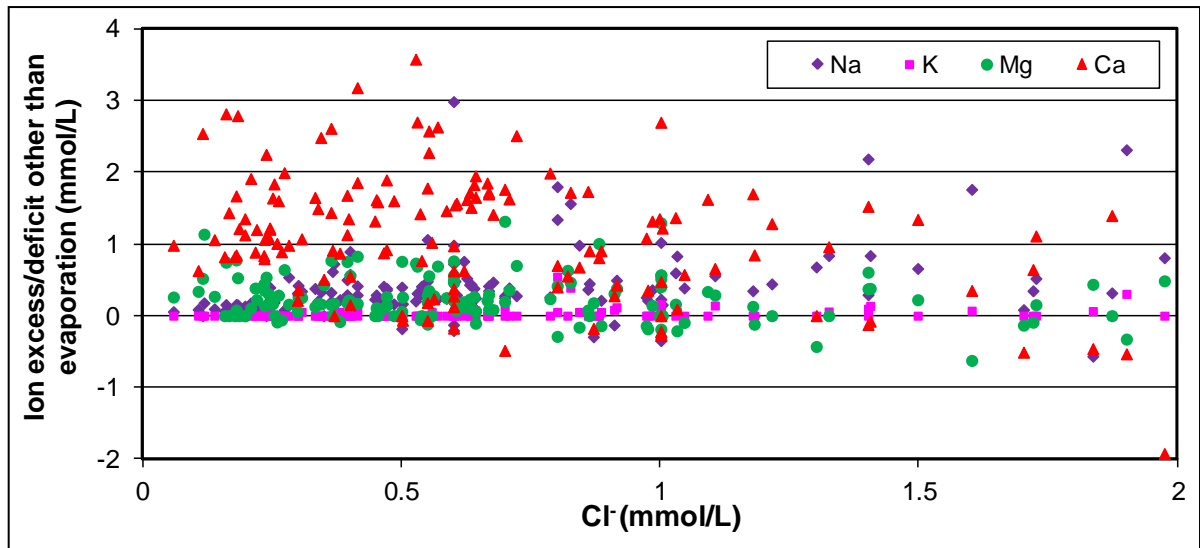


Fig. 4- 1 Contribution of processes, other than evaporation, to the groundwater composition (cations effect).

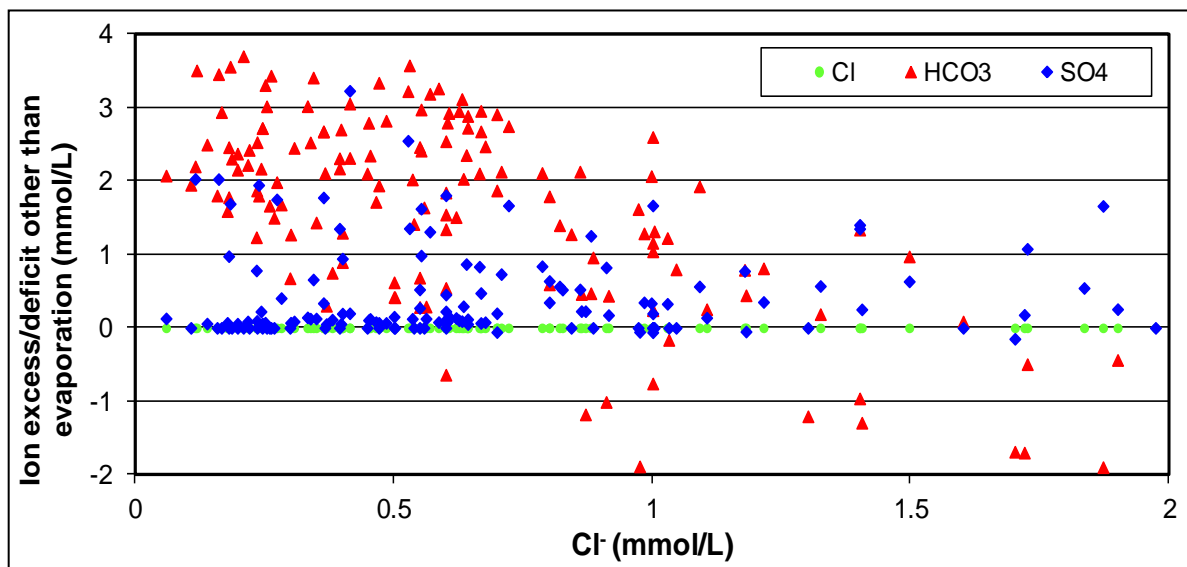


Fig. 4- 2 Contribution of processes, other than evaporation, to the groundwater composition (anions effect)

Based on this detection, the concentration of major ions in the groundwater, their ionic ratios and spatial distributions and binary relationships have been used in order to determine their sources and their relation to rocks composition and weathering process.

Fig. 4-3 shows the relationship between Na^+/Cl^- versus $Ca^{2+}/(HCO_3^-+SO_4^{2-})$. The distribution of groundwater samples indicates that the natural salt dissolution such as carbonates rock and silicate as well as the effect of reverse cation exchange, enhanced by

the existence of clay minerals, are the main processes controlling groundwater composition in the study area. Some samples indicate the effect of cation exchange which plotted in the field demonstrated a deficit in Na^+ and an excess in Ca^{2+} .

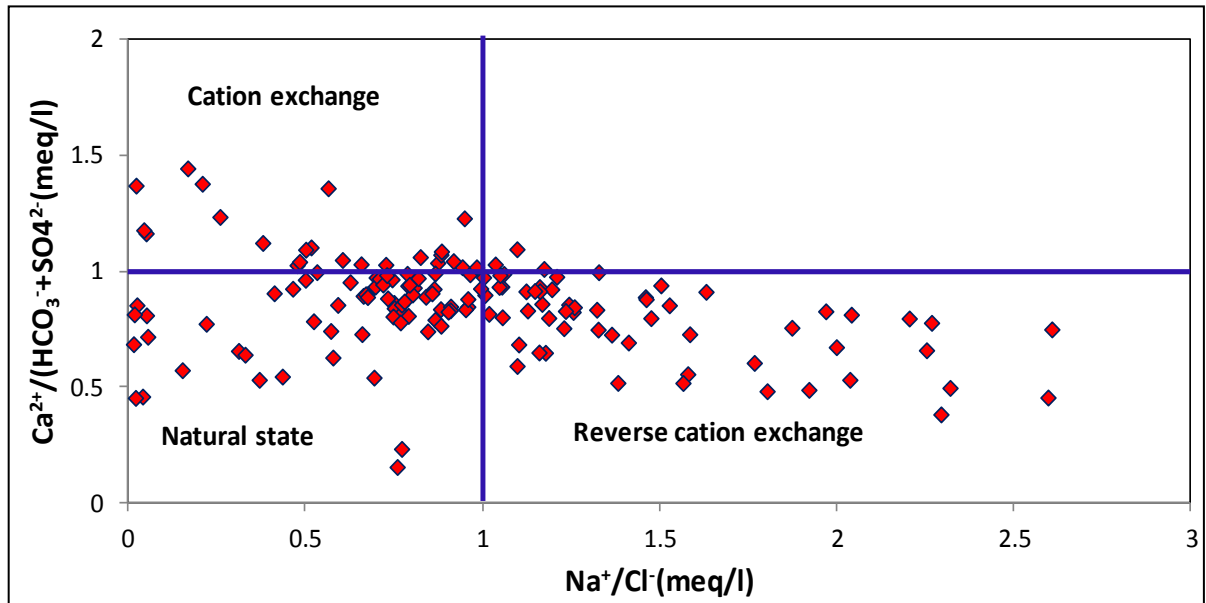


Fig. 4 - 3 Scatters plots of Na^+/Cl^- vs $\text{Ca}^{2+}/(\text{HCO}_3^- + \text{SO}_4^{2-})$ and $(\text{Ca}^{2+} + \text{mg}^{2+})$ vs $(\text{HCO}_3^- + \text{SO}_4^{2-})$

4.1.2. Hydrochemical facies

Piper diagram (Piper 1944) can be used to demonstrate the hydrochemical facies of analysed water samples. This diagram provides a convenient method to display, classify and compare water types based on the ionic composition of different water samples (Hem 1985). This diagram shows the relative contribution of major cations and anions, on a charge-equivalent basis, to the total ionic content of the water. Cation and anion concentrations for each water samples are converted to total meq l^{-1} and plotted as percentages of their respective totals in two base triangles. The cation and anion relative percentages in each triangle are then projected into a diamond-shaped grid, showing clustering of samples that have similar chemical compositions (hydrochemical facies). The diagram can be used to depict the evolution of groundwater chemistry as water flows along flow paths. Thus, the piper diagram represents water samples by their chemical composition and their source.

The hydrochemical facies according to the Piper diagram and the spatial distribution of these facies are shown in Fig. 4-4. From this figure it has been seen that all the water samples demonstrate an excess in alkaline earth (Ca^{2+} , Mg^{2+}) compared to the alkalis metal (Na^+ , K^+). The weak acidic anion (HCO_3^-) of the majority of these samples exceeded the strong acidic anions (Cl^- , SO_4^{2-}). About 70% of water samples tend to have anion chemistry dominated by HCO_3^- and cation composition dominated by Ca^{2+} (Ca- HCO_3 water type). This indicates the short duration of water-rock interaction and the effect of dissolution/precipitation of carbonate rocks as well as recently recharge of groundwater from atmospheric precipitation. The similarity in water type tends to express the existence of a unique hydrochemical system notwithstanding the very complex tectonic setting and stratigraphic sequences. Hence, the waters had the same or similar origins and flow paths, where individualised groundwater flow paths are difficult to delineate within the different hydro-stratigraphic unit. The Ca- SO_4 , Ca- SO_4 - HCO_3 , Ca-mixed SO_4 - HCO_3 , Ca-mixed HCO_3 - SO_4 and Ca- HCO_3 - SO_4 water types characterize some springs near Arneh and Beit Tima villages (11% of all water samples). The local presence of this water type suggests the dissolution of evaporite minerals. Kattan (2006) had concluded that the water type of major tributary of Awaj River (Sebarani), which is feed by several karstic springs located in the uppermost of Arneh valley, is calcium-sulfate type. Few samples (6% of all samples), demonstrate a water type of Ca-Cl- HCO_3 , Ca-mixed Cl- HCO_3 and Ca-Mixed HCO_3 -Cl. The dissolution of evaporite minerals and possible pollution from wastewater, animal manure and chemical fertilizer may have contributed to the chemical composition of these samples. A mixed cation-mixed anion water types characterized about of 10% of the water samples. This water type, and as aforementioned, indicates that more salts dissolution takes place. The reverse cation exchange as well as the dissolution of silicate mineral might play a role in this water type. The remaining samples (about 3%) demonstrate a water type of Mg- HCO_3 and Mg-Ca- HCO_3 .

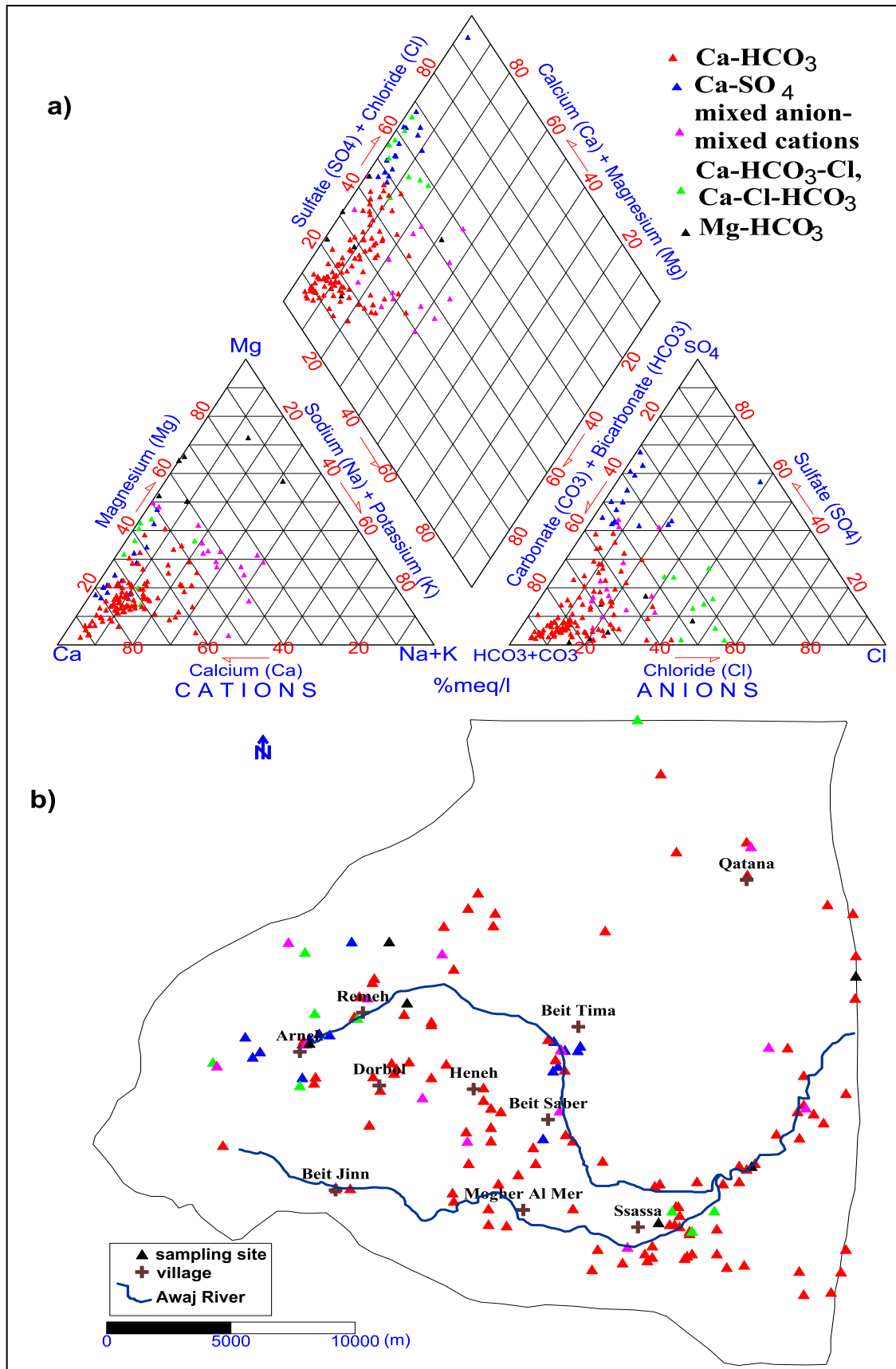


Fig. 4 - 4 a) Modified piper diagram depicting hydrochemical facies of groundwater in the study area (b) spatial distribution and classification of these facies.

Stiff diagram map (Stiff 1951) is used to compare the ionic composition of water samples between different locations. The stiff diagram is a polygon created from three horizontal axes extended on both sides of a vertical axis. Cations are plotted on the left side of the axis and anions are plotted on the right side, both in meqL^{-1} . A greater distance from the vertical axis represents a larger ionic concentration. The shape allows a quick interpretation of the type for each water sample and gives an approximate indication about the dissolved solid concentration according to shape size. This can serve as a baseline to monitor changes in groundwater composition. The unique differences and correlation in mineral composition of groundwater can help provide a better understanding of extend of the aquifer systems.

Fig. 4-5 shows the spatial distribution of stiff diagrams constructed for chosen groundwater samples based on their geographical distribution in the study area. The electrical conductivity (EC) is usually an indication that solutes are being mixed into the groundwater. It is highly correlated with type and concentrations of ions in solution especially with Ca^{+2} , HCO_3^- , thus it can be used to infer the total dissolved solids content in natural water (Hartmann, 2008). The spatial distribution of this parameter together with stiffs diagram is shown in the same figure.

As discussed earlier, the form of groundwater samples' stiff diagram has reinforced the similarity in the hydrochemical behavior of aquifer system based on the correlation in the mineral composition of these samples. In general, stiff diagrams constructed for wells samples demonstrate largest shapes compared to the ones of spring samples. The reason behind this might be that the majority of springs are located in the karstic aquifers and well flushed zones of active circulation and hence short residence time, so that all the soluble salts have been washed away and discharged through the spring. In contrast, water' wells is from zones of less active circulation and hence long residence time. The majority of the wells are located in the plain area where the evaporation and topographic factors as well as groundwater flow direction increase the salt water concentration. Groundwater is predominantly fresh (electrical conductivity (EC) $<1000 \mu\text{S}/\text{Cm}$). The high EC measured near Arneh village in the mountain area is the result of high sulfate concentration.

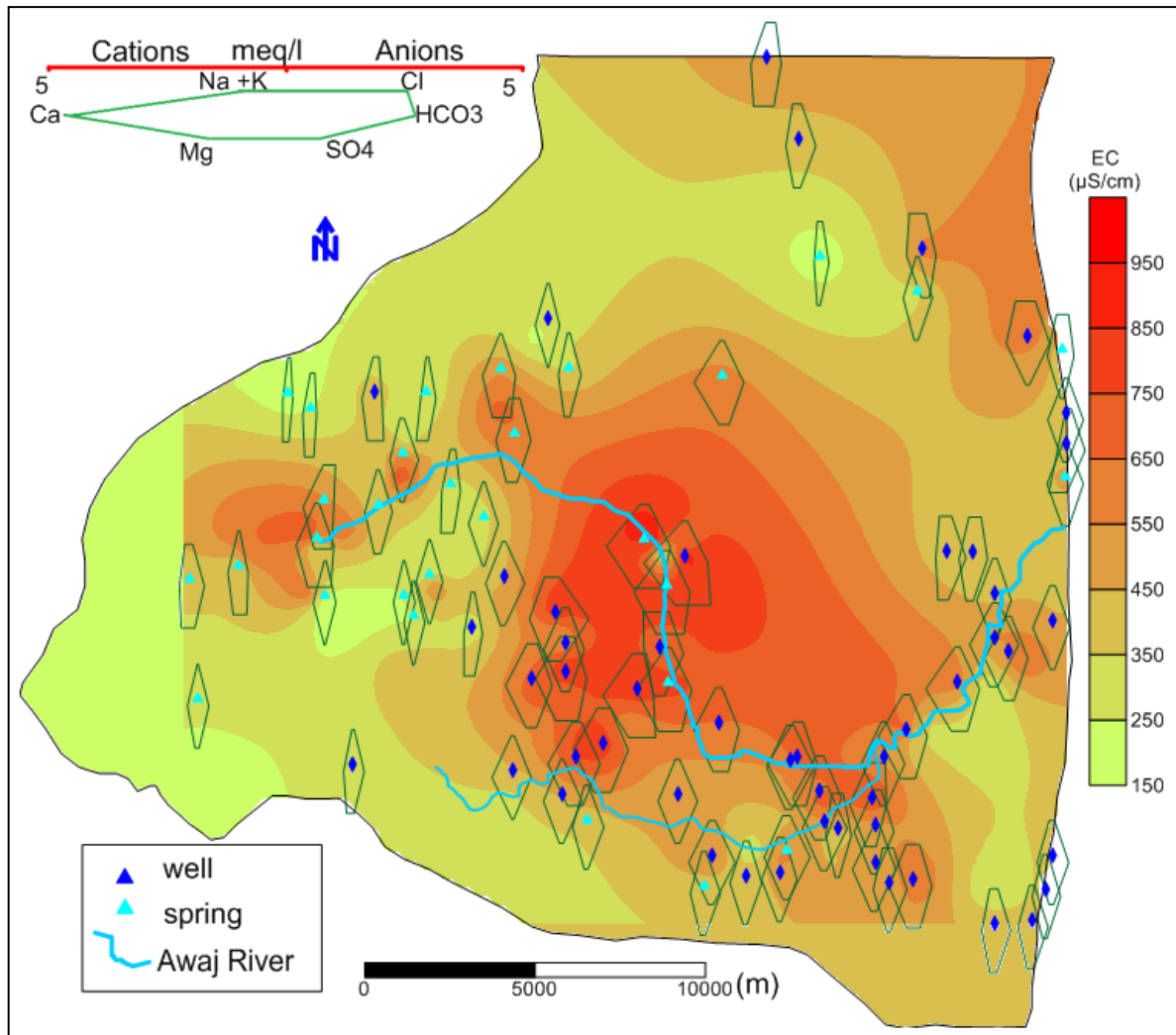


Fig. 4 - 5 Representative stiff diagrams of selected samples for visual observation of spatial variation in their water chemistry. The spatial visualization of electrical conductivity (EC) is also shown in this figure.

4.1.3. Pollution Index (PI) and fecal contamination

The intensive uses of fertilizers and manure in the agricultural management systems have increased the nitrate pollution of groundwater which has adverse effects on ecosystems and human health (Anastasiadis 2003). Biodegradation of crop residues, agricultural and municipal wastes applied to agricultural fields and waste generated directly by animals are also considered as other sources of nitrate pollution. In addition to the presence or absence of potential sources, field characteristics such as soil conditions, recharge rates and depth to groundwater ultimately dictate an aquifer's vulnerability to nitrate contamination (Enwright and Hudak. 2009, Obeidat *et al.* 2013).

The domination of the karstic features in most parts of the study area increases its sensitivity to pollution, which is considered as a major problem in that area due to rapid developing of urbanization. There are 14 villages in the study area in whose wastewater is directly discharging onto sink holes or to the river, without any treatment. Wastewater can contain high concentration of pathogenic or indicator bacteria, which can act as a potential reservoir for contamination of groundwater. Pathogenic micro organic can be waterborn or foodborn, especially when the food crops are watered with contaminated water. The uninformed and excessive use of chemical fertilizers and organic input, to maintain high agricultural yields, as well as using of untreated waste water in irrigation lead to water quality degradation.

The pollution index (PI) calculated based on the concentration of nitrate and sulfate anions using the following formula (Stuyfzand 1989):

$$PI = (1.33 * ABS(pH - 7) + LN(10 * (SO_4 + NO_3))) / 1.7 \quad (12)$$

The spatial distribution of this factor, as shown in Fig. 4-6 (a) demonstrates highest localized values in Arneh and Bkassam villages. The elevated value found in Arneh is resulted from high concentration of sulfate driven by gypsum dissolution. Whereas the high values in Bkassam is resulted from the pollution by nitrate attributed to punctual pollution source mainly the existence of septic tank. The high vulnerability of karstic limestone in this region enhances quick infiltration of untreated wastewater and increases the nitrate concentration in the groundwater. On the other hand, the high value of this factor measured in the plain area, is caused by high nitrate concentration which results mainly from the extensive use of fertilizers. This area hosts a considerable number of irrigation wells and intensive agricultural activities where a massive input of nitrogenous fertilizers and manures are applied.

The total and fecal coliforms are used as indicators of possible sewage water contamination because they are commonly found in human and animal feces. Although they are generally not harmful themselves, they indicate the possible presence of pathogenic (disease-causing) bacteria, viruses, and protozoans that also live in human and animal digestive systems. Sources of these bacterial contaminations are mainly wastewater on-site septic systems and wild animal manure.

Available analysis results of these bacteria in three springs located in the plain area during March-April 2006 (RDWSSA 2006) were used to identify fecal pollution. As shown in Fig. 4-6 (b), three springs demonstrate pollution with total coliform and fecal coliform (*Escherichia coli*). This indicates that the recently ongoing bacteriological contamination from the untreated sewage or animals waste due to the relatively short life of both bacteria, consequently the recent recharge of these springs can be recognized.

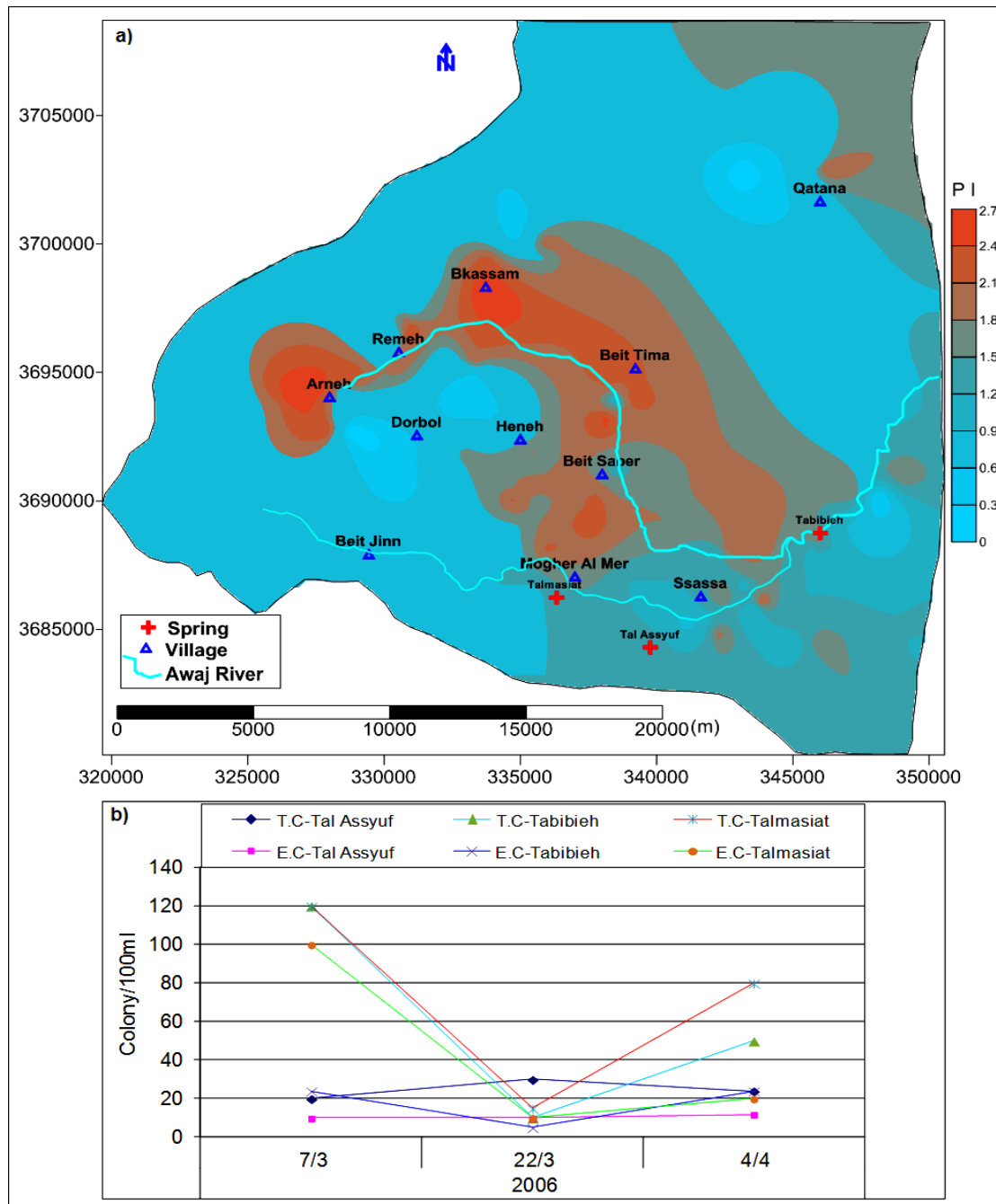


Fig. 4 - 6 Spatial visualization of the pollution index (PI) (a). The total coliform and fecal coliform (*Escherichia coli*) measured in 3 spring water samples during March-April 2006 are also shown (b).

The relationship between chloride and nitrate concentration is shown in the scatter plot on Fig. 4-7. This figure shows that a few samples are characterized by considerable chloride concentrations associated with relatively high nitrate concentrations. The high chloride concentration might be attributed to evaporites dissolution and the upward leakage from deeper aquifers, where these formations are located which leads to increase the chloride concentration.

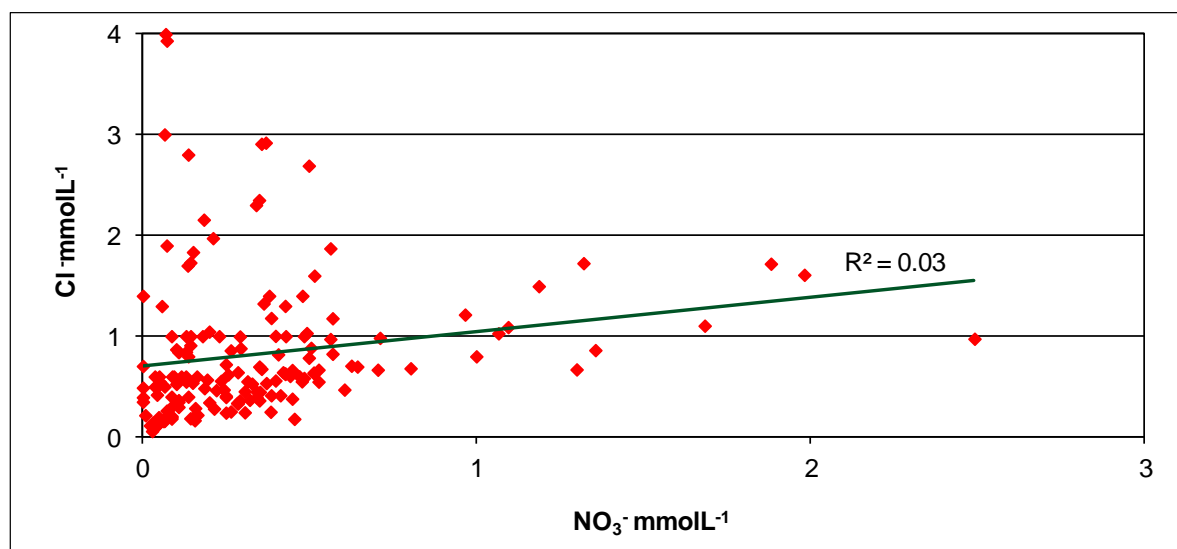


Fig. 4 - 7 Scatter plot shows the relationship between NO₃⁻ (mmolL⁻¹) vs. Cl⁻ (mmolL⁻¹)

4.1.4. Stable isotope composition of atmospheric precipitation and groundwater

4.1.4.1. Origin of air masses

The presence of two main parallel series of mountains, Anti-Lebanon and Coastal series, which is oriented from the southwest to the northeast, as well as the Syrian Desert and Palmyra Mountain chains, affects the isotope composition of precipitation in Syria. These topographic formations also control the distribution of precipitation amount throughout the country. According to (Eaid 2000, Abo Zakhem and Hafez 2010), there are several air masses trajectories influencing the rain events in Syria such as 1- Maritime tropical air masses transported from Atlantic Ocean and west Europe across the Mediterranean Sea. This mass causes high precipitation during wintertime. 2- Continental tropical air masses from North Africa Desert that becomes more humid across the

Mediterranean Sea and produce moderate rainfall in Syria. 3- The air mass coming from the Red Sea and Sinai desert characterized by hot and dry winds. This air mass causes sand storms with small amount of rainfall during springtime and is called the ‘Khamsin depression’ (El-Asrag, 2005, Abo Zakhem and Hafez 2010). 4- Continental polar air mass originated in Siberia that is cold and dry, especially when it is coming from northeast. 5- Continental tropical air masses from India producing hot and dry winds during the summer season.

4.1.4.2. Local meteoric water line

The measurement of $\delta^{18}\text{O}$ and $\delta^2\text{H}$ in precipitation often presents additional information for rainwater characterization and it helps to construct the local meteoric water line which provides key information for tracing a groundwater recharge (Barnes and Allison 1988, Saad *et al.* 2005). The position of meteoric waters on this line is controlled by a series of temperature-based mechanisms that drive the rainout process. This series includes vapour mass trajectories over the country, rising over topographic features, moving to high altitudes and seasonal effects. Each has a characteristic effect on the stable isotopic composition of precipitation (Clark and Fritz. 1997, Saad *et al.* 2005). However, and due to the worldwide variation in isotopic composition of precipitation, the long-term weighted mean value is taken as the input function into a hydrological system using the following formula (Dansgaard 1964; Yurtsever and Gat 1981):

$$\delta_w = \frac{\sum_i^n [p_i * \delta_i]}{\sum_i^n [p_i]} \quad (13)$$

Where (δ_w) is weighted mean, (p_i) is amount of monthly, weekly or daily precipitation and (δ_i) is isotopic composition of rainfall for the month, week or day (i).

The available historical data of the isotopic composition of atmospheric precipitation from 12 stations (Kattan 1997a, Selkhozpromexport 1986) were used to create local meteoric water line as well as to interpret the relationship between rainfall and groundwater in the study area. Most of these stations are located in or around this area. The Arneh, Remeh, Qatana, Bloudan and Damascus stations are located in the Barada and Awaj basin whereas the first three stations located in the study area (Fig. 4-8). Izraa, Al Suwieda, and Al Kounietra stations are located in Al Yarmouk basin while, Homs, Aleppo, Tartous and Palmyra stations are located in the Orontes, Euphrates, Coastal and Desert basins respectively (Fig. 4-8).

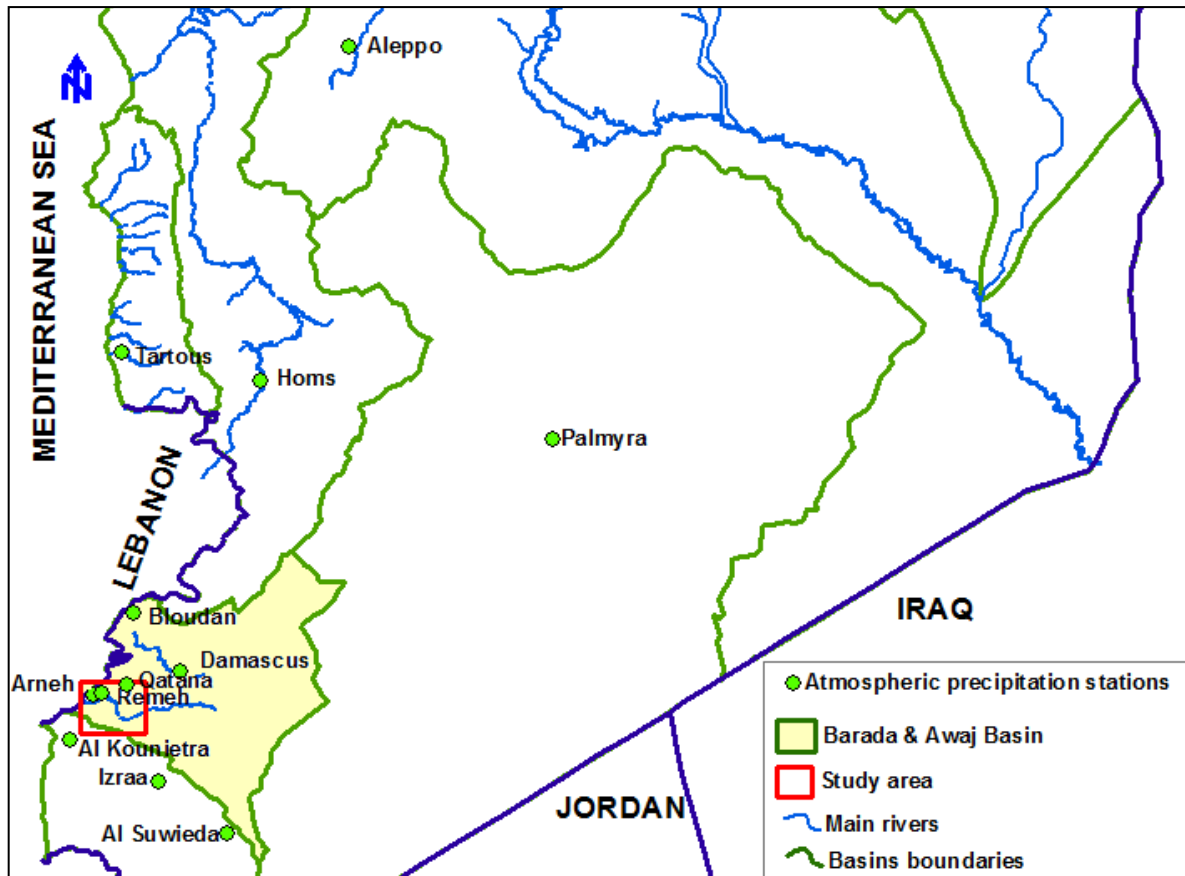


Fig. 4 - 8 The locations map of sampling sites of atmospheric precipitation in Barada and Awaj Basin and other basins in Syria.

The values of $\delta^{18}\text{O}$ and $\delta^2\text{H}$ measured in the groundwater samples are reported in table 4-3. The Fig. 4-9 shows the spatial distribution of these samples in the study area. The values of $\delta^{18}\text{O}$, $\delta^2\text{H}$ and ^3H (T U) as well as the amount of precipitation measured in the atmospheric precipitation stations are shown in table 4-4.

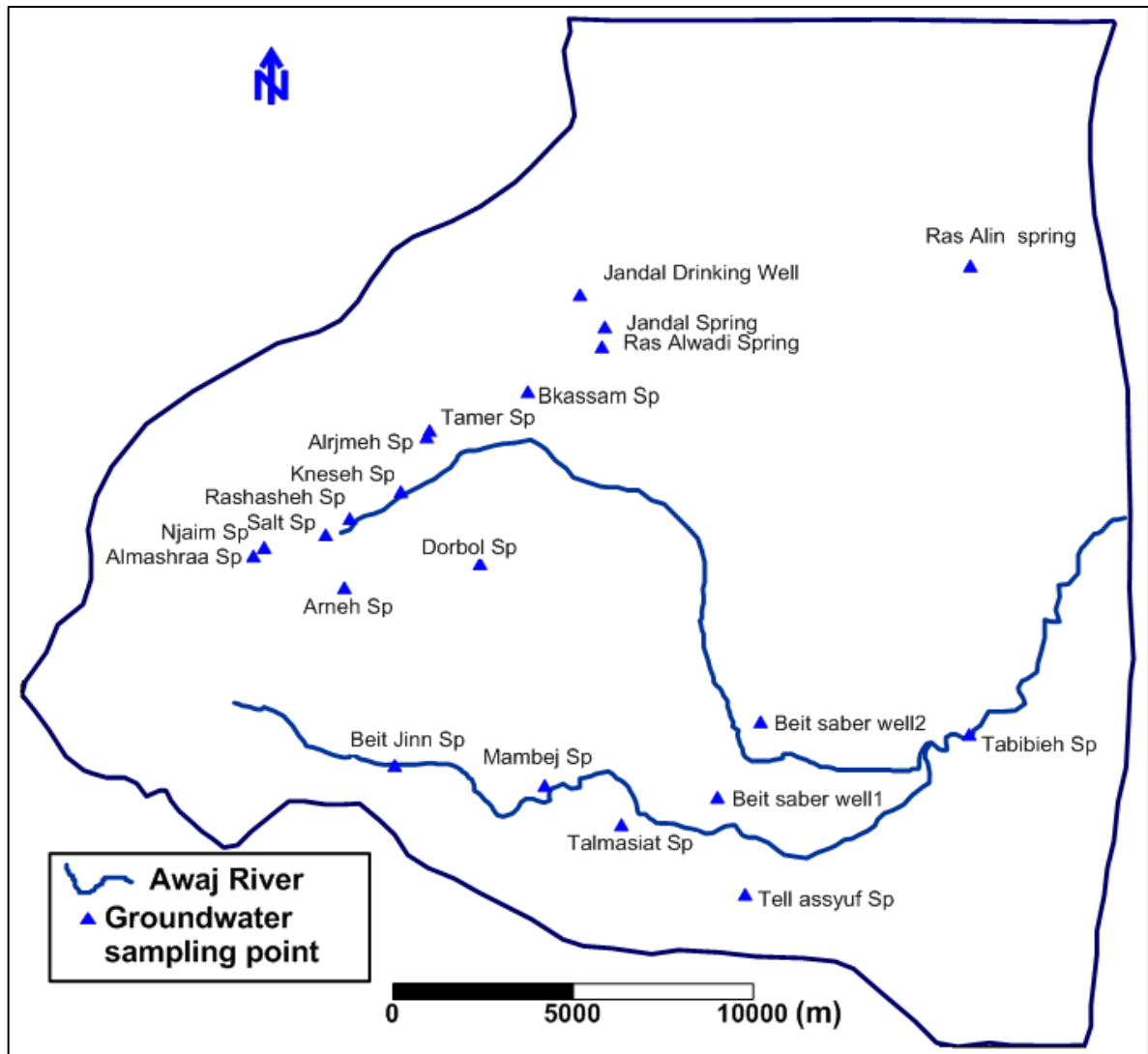


Fig. 4 - 9 The locations of groundwater sampling points for environmental isotopes investigations.

The variation in the isotopes composition of groundwater and the rainfall is used to identify the provenance of groundwater recharge and its flow regime. Fig. 4-10 shows the relationship between $\delta^{18}\text{O}$ and $\delta^2\text{H}$ in both atmospheric precipitation and groundwater samples. All the atmospheric precipitation stations are located between the Mediterranean Meteoric Water Line (MMWL) (Nir 1967) and the Global Meteoric Water Line (GMWL) (Craig 1961) which defined by the following two equations respectively.

$$\delta^2\text{H} = 8.\delta^{18}\text{O} + 22 \quad (14)$$

$$\delta^2\text{H} = 8.\delta^{18}\text{O} + 10 \quad (15)$$

The majority of these stations is located close to MMWL which indicates the effect of weather front originated from the Mediterranean Sea. The local meteoric water line (LMWL) indicates the relation of regional effects in precipitation and isotopes fraction process that occur during evaporation and condensation of air humidity along weather trajectories. The relationship between $\delta^{18}\text{O}$ and $\delta^2\text{H}$ determined for precipitation stations is given by the following equation:

$$\delta^2\text{H} = 7.9.\delta^{18}\text{O} + 17.9 \quad (16)$$

Kattan (1997a), has found this equation to be:

$$\delta^2\text{H} = 8.26.\delta^{18}\text{O} + 19.3 \quad (17)$$

The deuterium excess value was defined by Dansgaard (1964) according to the following formula

$$d = \delta^2\text{H} - 8\delta^{18}\text{O} \quad (18)$$

This value depends on the relative humidity of air masses at their origin and kinetic effects during evaporation (Merlivat and Jouzel 1979, Gat and Matsui 1991, Kattan 2006).

The d excess in our case is lower than the d excess in the Kattan equation, which might indicate a relatively less pronounced evaporation effect as a result of additional stations located at the higher altitude in Mt. Hermon.

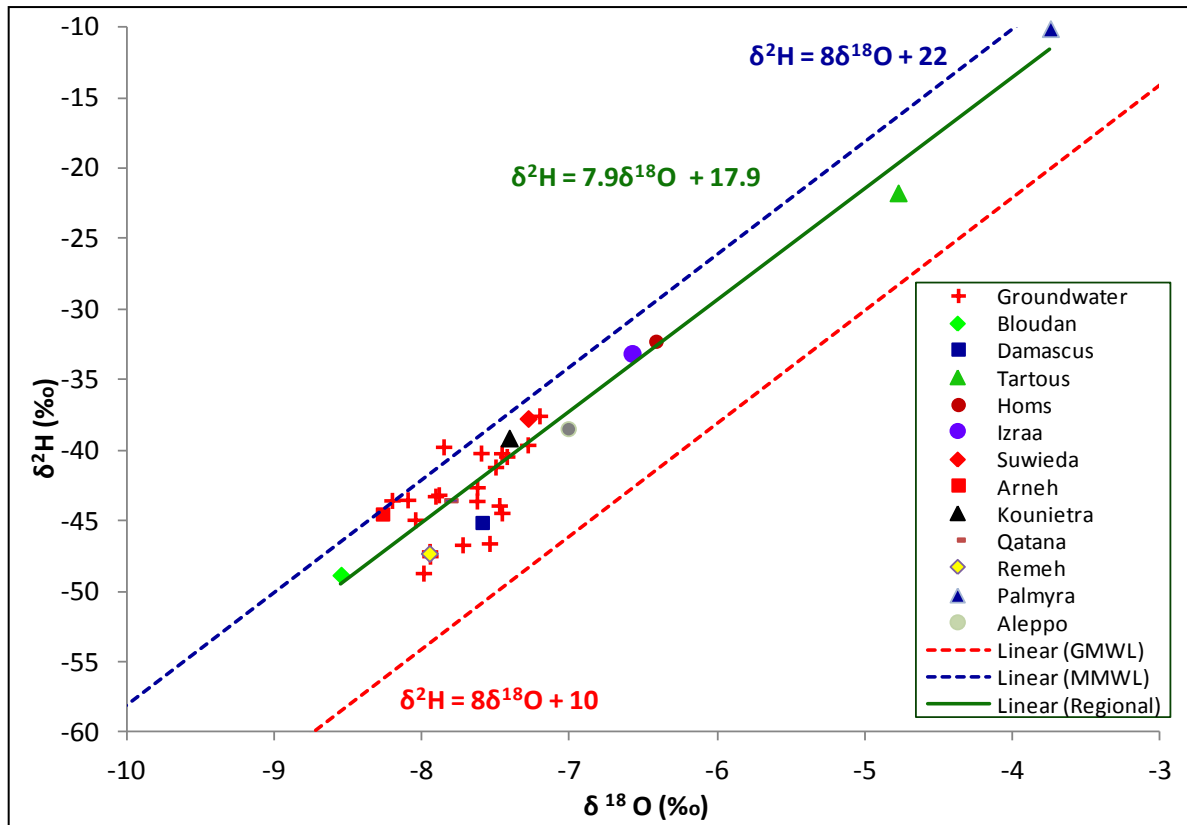


Fig. 4 - 10 The relationship between $\delta^{18}\text{O}$ and $\delta^2\text{H}$ in the atmospheric precipitation (Weighted Mean) and in the groundwater samples.

4.1.4.3. Altitude effect and tritium unit changes

The stable isotopic composition of precipitation decreases towards more depleted values with the increasing of altitude. The most depleted values of both ^{18}O and ^2H were measured in Bloudan atmospheric precipitation station which is situated at the higher altitude, while the most enriched values for these both stable isotopes were measured in the Palmyra station which is located in the central desert basin. The progressive depletion of heavy stable isotopes with altitude represents the local climate and topography effects, mainly the air temperature which decreases with altitude. As shown in the following two equations, these values were estimated to be -0.23‰ per 100 m for ^{18}O and -1.7‰ per 100 m for ^2H (Fig. 4-11).

$$\delta^2\text{H} = -0.0169 \cdot H - 22.6 \quad (19)$$

$$\delta^{18}\text{O} = -0.0023 \cdot H - 5 \quad (20)$$

Based on this gradient, the mean elevation of recharge zones of groundwater in the study area is calculated to be between 900 and 1,600 m. The deviation of Damascus, Aleppo and Palmyra stations from these two regression lines is caused by global, regional and/or seasonal effects such as the Khamasin rain originated from the North African dessert, or due to local and particular climatic conditions controlling rainfalls in the region.

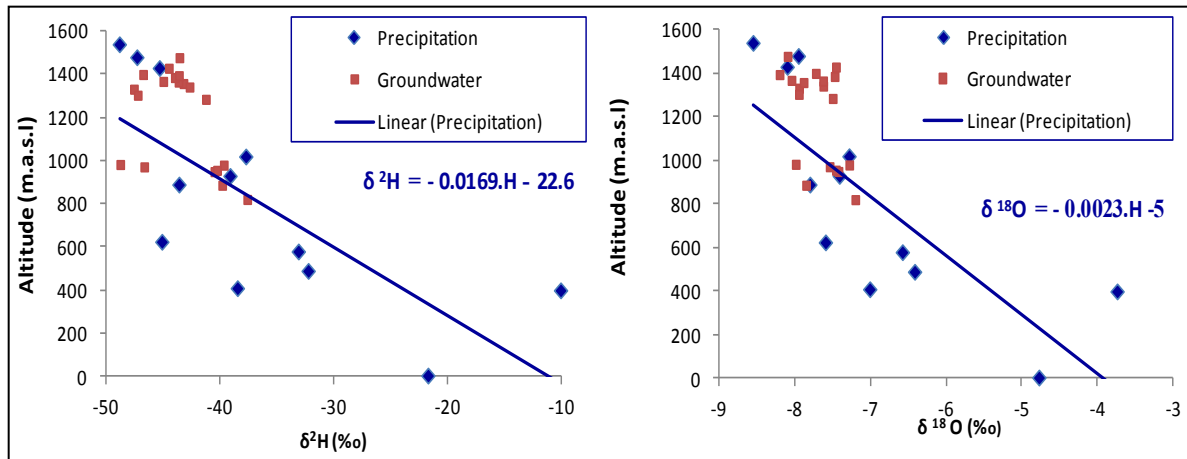


Fig. 4 - 11 The relationship between the both $\delta^{18}O$ and $\delta^{2}H$ and altitude for precipitation and groundwater samples.

Tritium (3H) is a naturally occurring radioactive isotope of hydrogen that has a half-life of 12.43 years and measured in tritium units (TU). 1 tritium unit is equivalent to one tritium atom in 10^{18} atoms of hydrogen (Izbicki *et al.* 2003, Taylor and Roether, 1982). The relationship between tritium units and distance from the Syrian shoreline (Fig. 4-12) shows a positive trend with moving inland as a result of increasing stratospheric influence. The build-up of tritium over land is a result of the cutting off from the supply of low activity oceanic vapour, while influx from aloft continues.

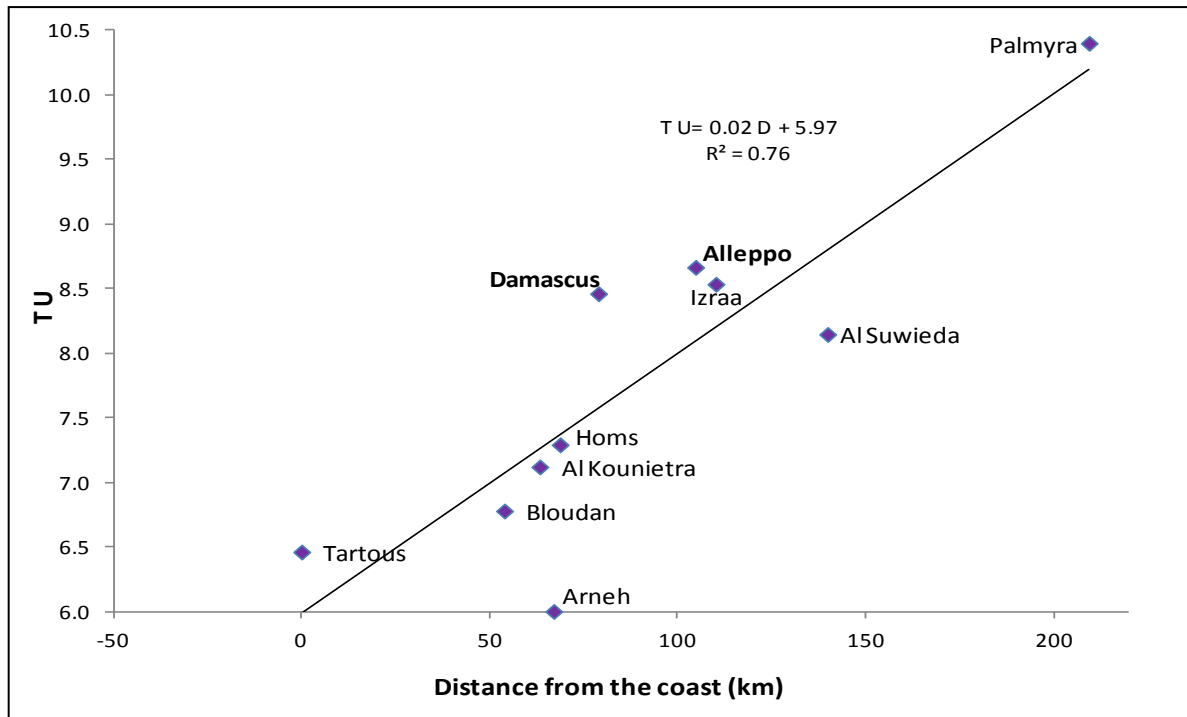


Fig. 4 - 12 The relationship between tritium unit and the distance from the Syrian shoreline.

4.1.4.4. Groundwater response to input precipitation

The environmental isotope compositions of groundwater studies were based on 21 samples including 18 springs, two shallow wells (Beit Saber well1,2, at depths of 40 and 60 m respectively) and one deep well (Jandal drink well, at 150 m depth-). The mean stable isotope composition of these samples ranged from -8.2 to -7.2 ‰ and -48.7 to -37.6 ‰ for $\delta^{18}\text{O}$ and $\delta^2\text{H}$ respectively, whereas deuterium excess value changes between 13.7 and 23 ‰ and most of these values are close to 20‰ (table 4-4). Meaning that these samples are originated by Mediterranean atmospheric moisture, which, due to the lower relative humidity conditions prevailing in this region, is more deficient in $\delta^{18}\text{O}$ compared to the moisture originating from the oceans. (Dinger and Payne, 1971).

All groundwater samples plot close to the meteoric water line ($\delta^2\text{H} = 7.9.\delta^{18}\text{O} + 17.9$) and MMWL (Fig. 4-10). This indicates the recent origin of these samples before a significant evaporation might take place earlier than or during the infiltration process. The rapid infiltration of precipitation is enhanced by the karstic environment that promotes infiltration through sinkholes and conduits. The springs which are located in the plain region and characterized by higher discharge tend to have slightly higher enriched stable isotope compositions compared with other springs in the mountain region. This might be

attributed to contribution recharge from an area of lower altitude (continuous recharge mechanism), as well as from an older component by water leaks upwards of deeper aquifers representing a mixture of several flow paths as a collective flow system. On the other hand, the small springs in the mountain area, can be attributed to point recharge assumption particularly to significant contribution of rainfall and melt waters originated on the high slopes of Mt. Hermon. These springs are more close to the MMWL line reflecting the effect of Mediterranean climate and they tend to have slightly depleted stable isotope as a result of altitude effect and cold temperature of melt waters infiltration. Consequently, the groundwater is fed by local rain in their nearby surrounding and the precipitation provides the major source of recharge to the upper part of Awajj River.

The concept behind gathering these samples close to each other is that the aquifers of these samples are fed from the same sources mainly the rainwater and snowmelt in the mountainous part and the hydraulic connection between those aquifers might occur.

Fig. 4-13 shows the change of $\delta^{18}\text{O}$ values in Beit Jinn spring during the year 1994 (RDWSSA, 2006). In the dry period, the $\delta^{18}\text{O}$ reaches the lowest value (-8.3) in this spring indicating that this spring is recharged by the water coming from higher elevation during this time. According to the relationship between the $\delta^{18}\text{O}$ and the altitude, this elevation estimated to be higher than 1500 m where the precipitation is mainly in the form of snow.

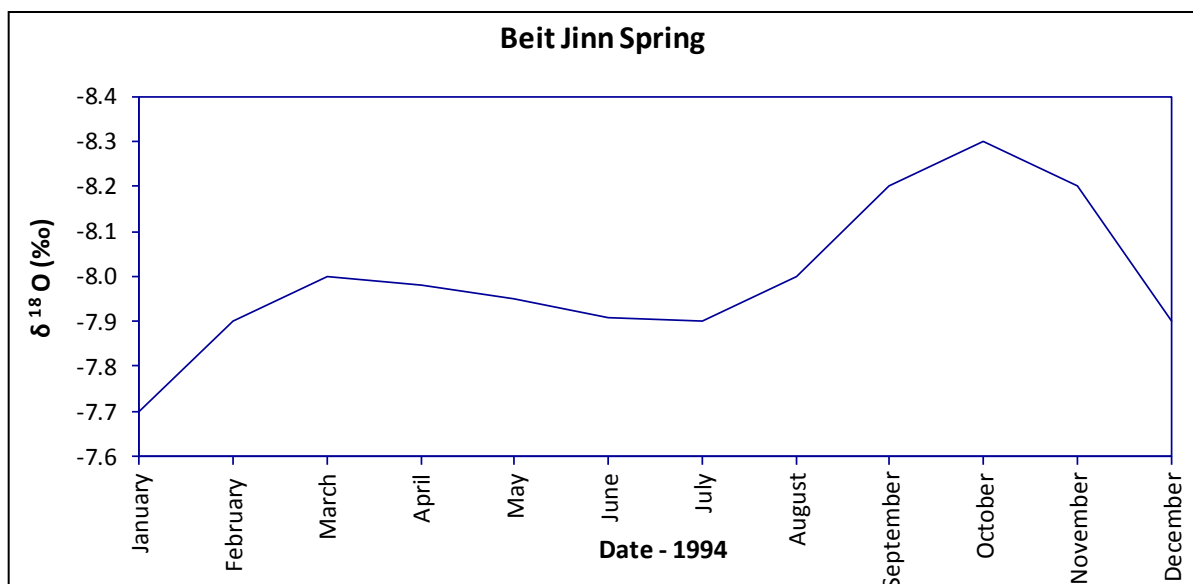


Fig. 4 - 13 Change of $\delta^{18}\text{O}$ in the Beit Jinn spring during the year of 1994.

4.1.5. Equipotential contour lines and hydrogeological subdivision of the study area

Based on available data of groundwater level measured in 31 groundwater monitoring wells obtained from Ministry of Irrigation of Syria, a preliminary equipotential contour lines map was constructed for October 2006 as shown on Fig. 4-14. The interpretation of this map indicates that the general groundwater flow is organized towards the east direction. Minor flow direction is also recognized from northwest to southeast where several springs with relatively high discharges emerge close to the limit between the basalt formation and other formations in the plain region. A stepper hydraulic gradient is observed in the western and northern mountainous parts, where the karsts and faults are more dominant.

According to water type classification, isotopes characteristics of groundwater and equipotential contour lines, the study area can be divided into two main sub-regions A and B (Fig. 4-14), each of them is characterized by different flow systems. The sub-region A is characterized by high amount of atmospheric precipitation and infiltration coefficient, the rainfall and snowmelt are the solely source of groundwater recharge in this sub-region. Groundwater flow is primarily controlled by the conduits, fractures and faults with a significant downward component. However, groundwater discharges in this sub-region is through many springs located along the foothill of Mt. Hermon in the Jurassic aquifer close to the Arneh Village. The two tributaries of Awaj River generated in this part. In the sub-region B, the Neogene and Quaternary aquifers form the main source of water supply for both domestic and agricultural purposes. In this part, there are two main sources of groundwater recharge. The first one is by direct infiltration of atmospheric precipitation mainly through Neogene outcropping formation, while the second one is by possible hydraulic exchange between the deep aquifers (Jurassic and Cretaceous) and the Neogene/Quaternary aquifers.

In the outcropping part of Jurassic aquifer, part of the infiltrated precipitation and snowmelt is flowing and circulating as deep groundwater through conduits and faults towards the upper aquifers by upward leakage. Water discharges in sub-region B through the major springs and groundwater withdrawals by numerous wells. The relatively high discharges of those springs indicate the drain of deeper aquifer and cannot be classified under perched springs. Rimmer and Salinger (2006) have mentioned that the springs which

emerge from lower topography in Mt. Hermon are characterized by higher discharge than the springs in higher altitude.

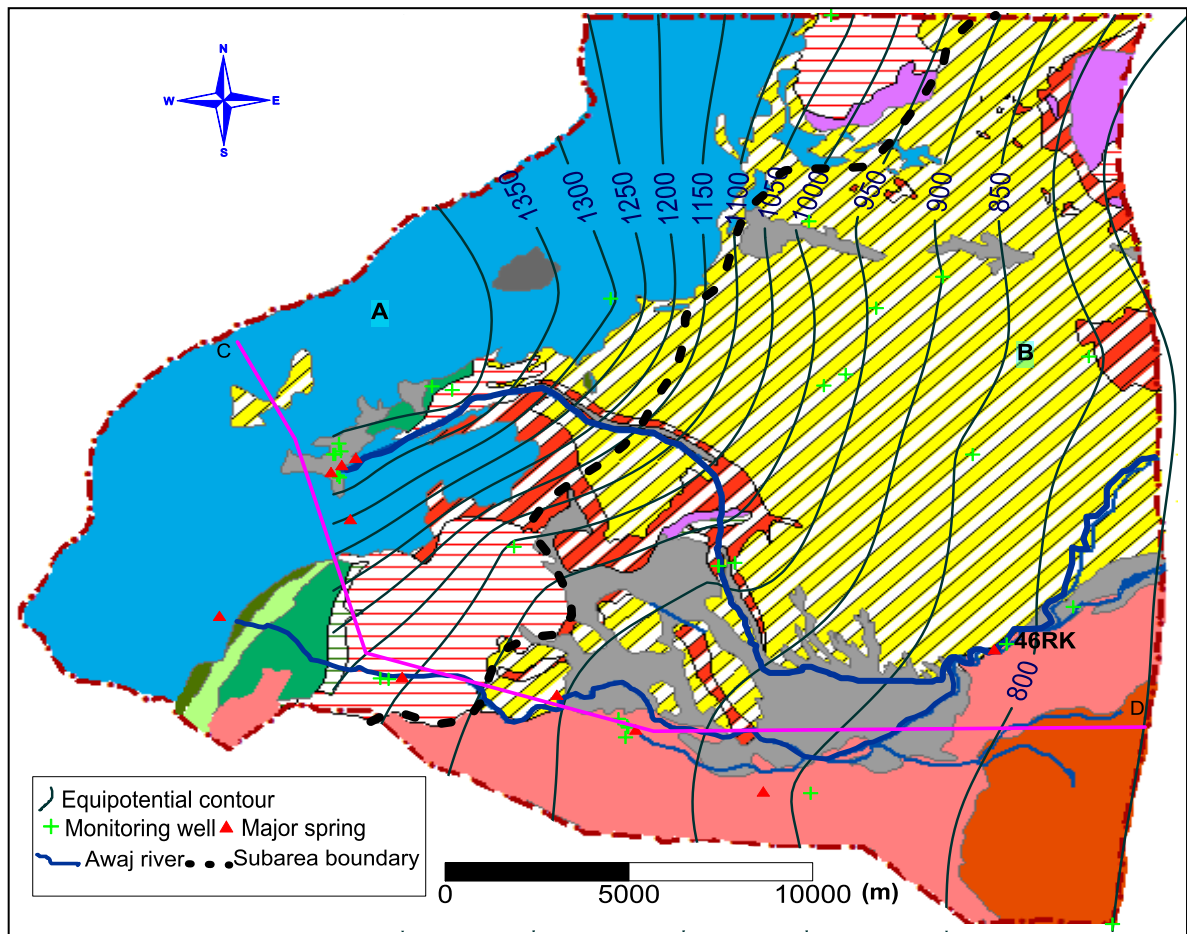


Fig. 4 - 14 Equipotential contours map based on groundwater level measured in 31 monitoring wells during October 2006. The associated hydrogeological sub-regions (A and B) as well as cross section C-D are depicted.

The fluctuations of monthly groundwater level of the well 46RK which is located in sub-region B during the period between 2004 and 2011 are shown in Fig. 4-15. The typical decline during the summer dry period and increase during the rainy winter period depict seasonal trends in the water level as well as the effect of groundwater withdrawal. The decreasing trend in groundwater level during the measured period is caused by groundwater overexploitation.

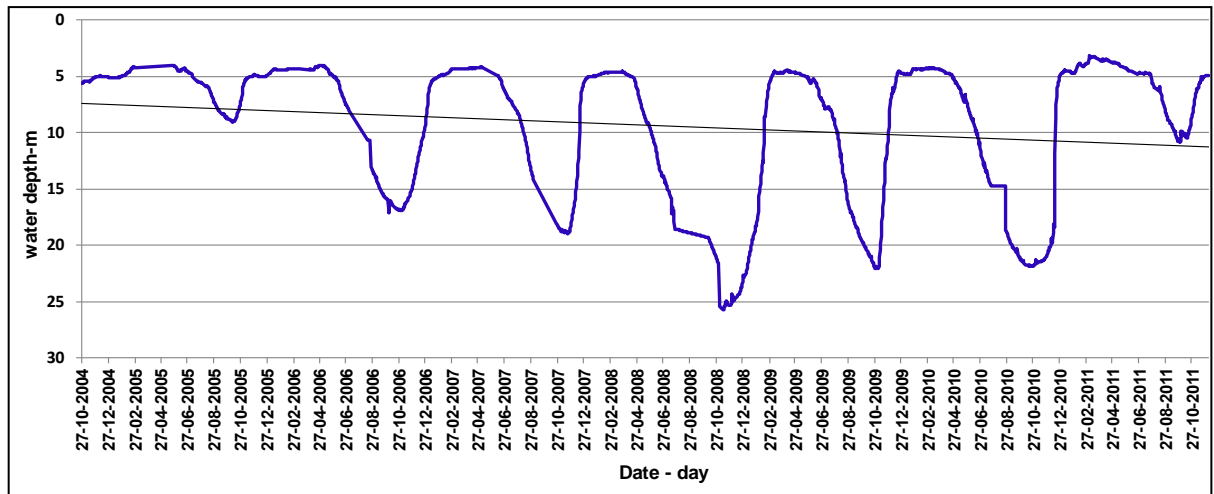


Fig. 4 - 15 The fluctuations of monthly groundwater level of the well 46RK from 2004 until 2011.

A published paper stemmed from this chapter is appended (Appendix B)

Chapter 5. Groundwater modeling approach to estimate the water budget of the upper aquifer horizon in the model domain and assess the hydraulic relationship between multilayered aquifers

Introduction

This chapter describes the development and calibration of the steady-state groundwater flow model. Among the available data on groundwater recharge and water consumption, the numerical model was applied for the water budget assessment in the upper aquifer horizon. This steady-state model was developed in this complex region primarily as a tool to assess groundwater flow behaviour between different aquifers and water bearing in the study area. This is significantly important since this relation is poorly understood and the hydrochemical evolution does not give enough information about the groundwater flow system in this area. The calculation of water budget of the upper aquifer horizon, which has a vital role in maintaining a stable agricultural life in this region, is another important purpose of developing this numerical model. The obtained result might be a valuable tool in order to select an optimum management scheme and sustainable use of groundwater resources in this semiarid region.

Groundwater modeling is recognized nowadays as a best tool to support management of groundwater resources (Lubczynski and Gurwin 2005, Mahmoudzadeh *et al.* 2012) and it is also considered to be as a significant alternative approach to overcome the lack of observational data. Groundwater model has been used as a scientific tool to examine the response of the aquifer system to an adequate level of details and understanding the flow patterns (Anderson and Woessner 1992, Chiang *et al.* 1998). Consequently, it provides a scientific answer to quantify water balance of the system under specified hydrological conditions. Bredehoeft (2002) has pointed out that the modeling is generally a preferred approach when studying a groundwater's system response to pumping. This is because it can include, explicitly, the spatio-temporal nature of the response of the system to imposed stresses, as well as the changes in boundary conditions and recharge and discharge rates that result from this response. Limiting uncertainty in groundwater models requires accurate determination of the spatial and temporal variations in hydraulic parameters of the aquifer such as the hydraulic conductivity and permeability (Su *et al.* 2004, Alkhaier 2011) The developed model in this case study will be used to calculate the water budget

component of the upper aquifer in the model domain which is considered a vital source for the intensive agricultural activities developed in the study area. However, this steady state model can be considered as a basis in order to predict the future changes in the groundwater system under various scenarios.

5.1. Conceptual model

The groundwater modeling is based on two key components which are a conceptual model and a mathematical model. The conceptual model is an idealised pictorial representation of our hydrogeological understanding which includes a delineation of system boundaries, inputs/outputs, hydrogeological units and flow patterns that are dominant in the system being studied. A mathematical model is a set of equations which, based on certain assumptions, quantify the active physical processes in the aquifer system(s) being modelled.

In order to simplify the field conditions of the model domain and based on the hydrogeological cross section C-D (Fig. 4-14), the design of the conceptual groundwater model (Fig. 5-1) was developed. The development of this model is based on the available geological and meteorological information as well as the obtained hydrogeological information from hydrochemistry and isotopic interpretation. The vertical and horizontal extent of the subsurface hydrogeological units and their connection is consistent with available boreholes information (Selkhozpromexport 1986). The recharge and discharge areas are delineated. The conceptual model assumed that the preferential groundwater flow occurs mainly in the Jurassic aquifer and discharges as a karstic springs into the upper part of the Arneh valley.

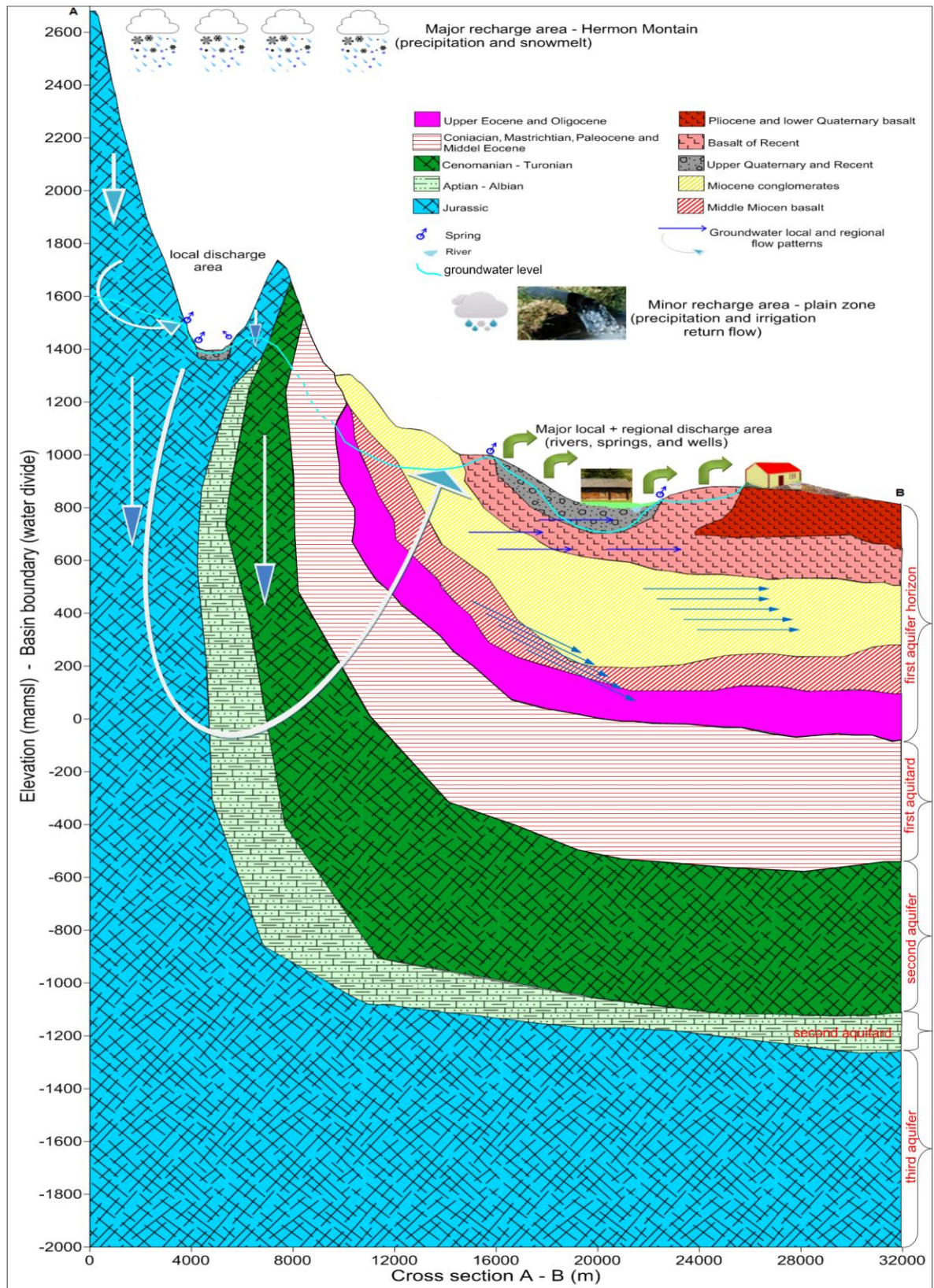


Fig. 5- 1 Schematic hydrogeological cross section C-D (Fig. 4-14) demonstrates conceptual hydrogeological model.

5.2. Boundary conditions

Defining suitable model boundary conditions is an essential step in building numerical groundwater models and largely responsible for how flow mechanisms in the system are occurring (Elango 2005). The boundary conditions were determined according to topography and hydro-geological conditions. The hinge axis of Mt. Hermon located at the western and north-western boundaries of the study area forms the western boundary of the model. From the south, the Quaternary basalt layer forms the southern boundary of the model domain at its limit with Yarmouk basin. This boundary was implemented as no flow boundary. The northern boundary of the model has been taken to the north of Qatana village to include all the springs located in the study area. This boundary also has been assigned as no flow boundary since the equipotential contours intersect with this boundary almost perpendicularly.

According to the geological and hydrogeological features as well as springs discharge and groundwater level fluctuations in the upper aquifer horizon and Jurassic aquifer, distinguished has made between different hydraulic behaviour that characterize each of them. We assume that there is a direct hydraulic connection between these two aquifers where the Neogene conglomerates come into direct contact with Jurassic limestone. This contact occurs in the model domain at the interface between these two aquifers.

Non-saturated zone in the exposed part of the Jurassic aquifer was determined based on available groundwater depths in the boreholes (Fig. 5-2) and the altitude of springs located in this part. By using topography and the thickness of this zone, we could interpolate the groundwater equipotential contours in this part. The highest value of these contours (1600 ma.s.l), was used as a constant hydraulic head (BC_s) in the Jurassic aquifer (Fig. 5-2). The intersection points of these contour lines with the western limit of the upper aquifer, together with water level measured in the boreholes located in this aquifer during the same period (September 2010), were used to construct the equipotential contour lines for this aquifer.

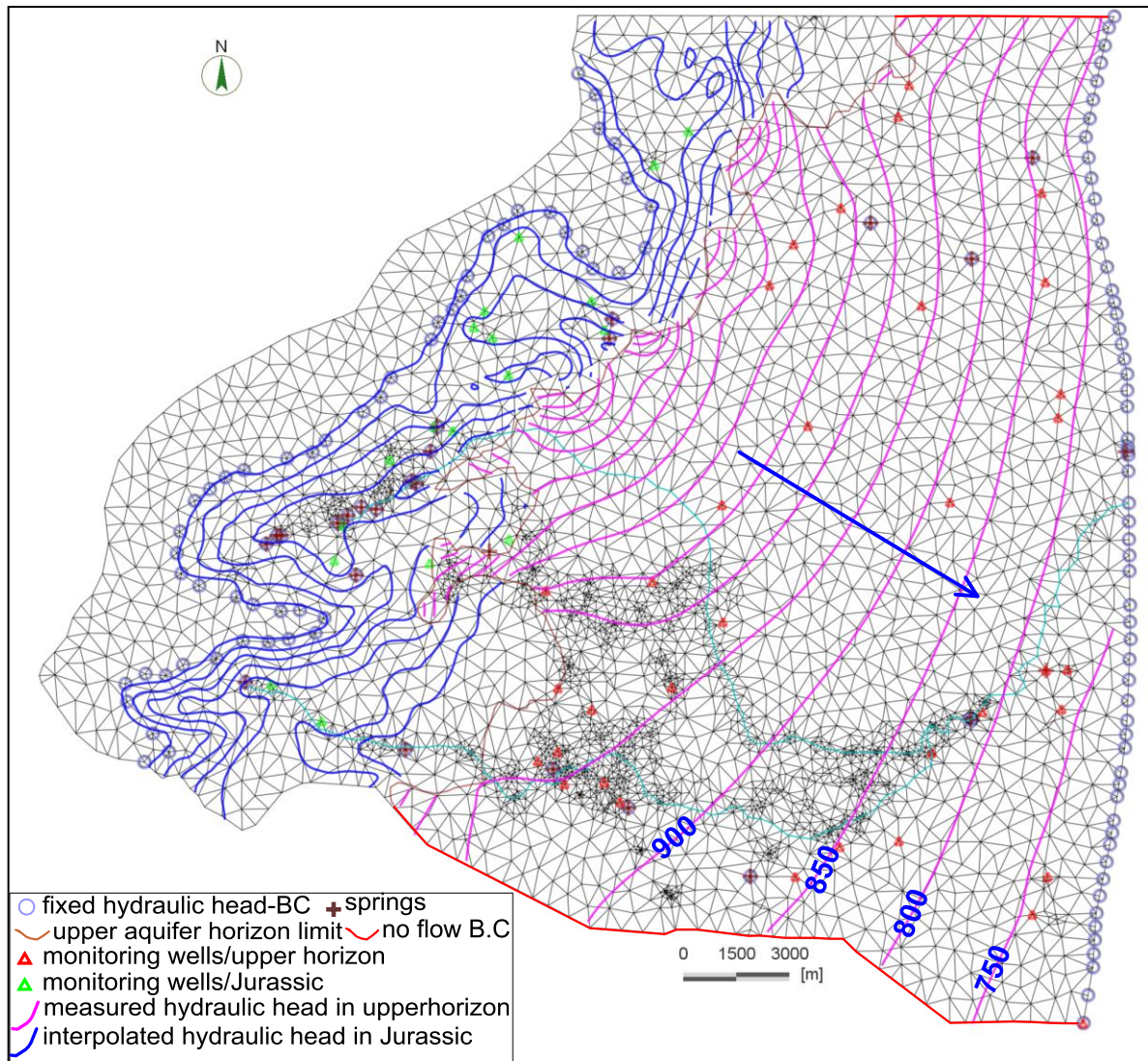


Fig. 5 - 2 Two dimensional (2D) FEFLOW mesh for the groundwater model and the spatial distribution of boundary conditions, springs and observation wells as well as the equipotential contours of measured initial hydraulic head for September 2010.

The contour lines were created by using ordinary kriging algorithm method (Krige 1951). This method requires a positive definite model of spatial variability which must be fitted to the data and approximately describes the spatial continuity of these data. The geostatistical analysis of measured groundwater levels resulted in a linear variogram model (Fig. 5-3), which has associated with performing the kriging interpolation.

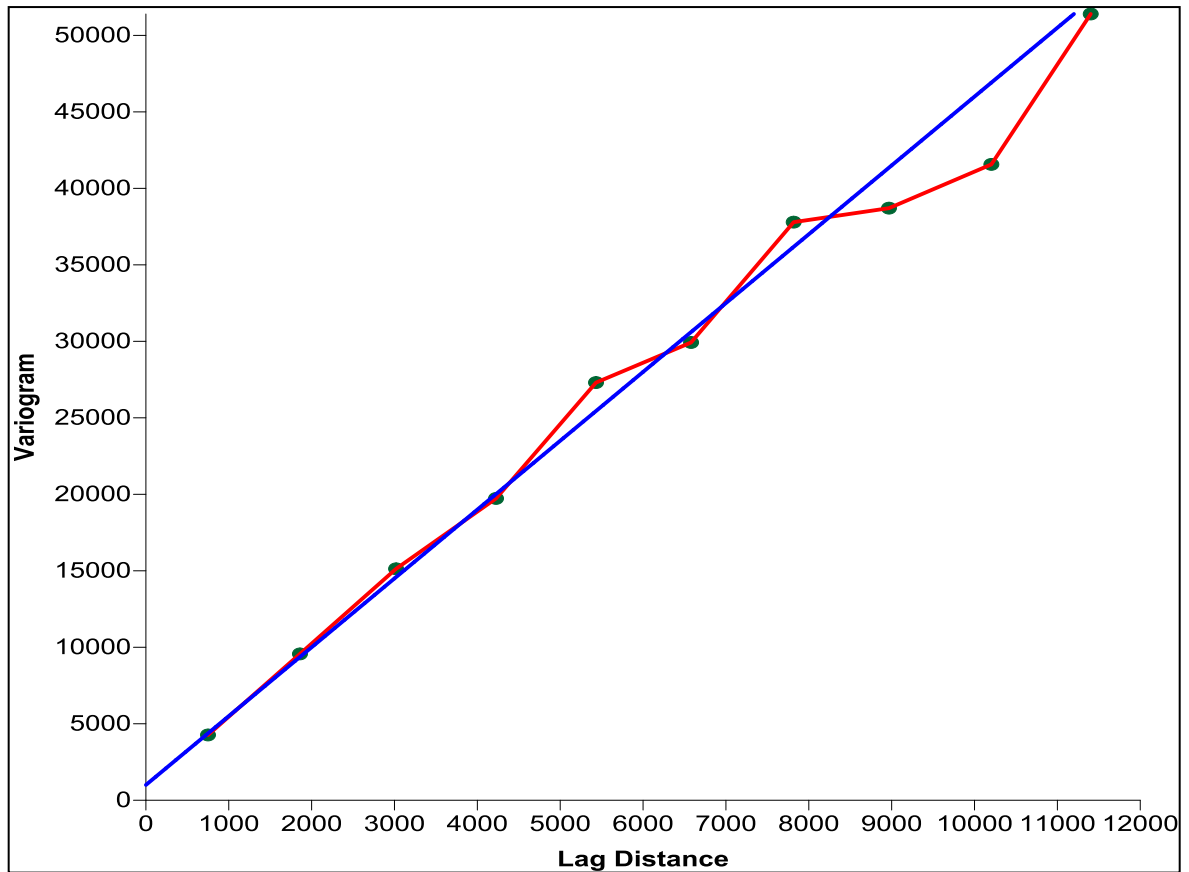


Fig. 5 - 3 Variogram associated with the performance of kriging interpolation method.

The resulted contours lines in the upper aquifer horizon as well as the simulated one in the exposed part of Jurassic (Fig. 5-4), were used as reference maps for the steady-state model simulation. The groundwater level interval was taken as 50 m for the upper aquifer horizon and 100 m for the exposed part of Jurassic aquifer. The hydraulic head changes between 700 and 775 m a.s.l in the outermost nodes of the eastern model boundary as well as the discrete altitudes of permanent springs discharge were simulated as constant head (BC_s) (Fig. 5-4).

The equipotential contours of the upper aquifer horizon are almost parallel to the boundaries between this horizon and the Jurassic aquifer. These boundaries were used to calculate the lateral groundwater flow amount from the Jurassic aquifer to the upper aquifer by implementing flux drive boundary conditions (Neumann type flux).

Under natural conditions, no important relationship between Sebarani tributary and groundwater in the plain region has been observed. The measured discharge of this tributary in the gauging station where it enters the plain region and in another one just

before its junction with Jenani tributary is almost the same. The Jenani tributary flows in the concrete canal which prevents the interaction between surface water and groundwater. Therefore, both tributaries were excluded from the simulation process. The evapotranspiration was also neglected because the groundwater level is situated at a depth of more than 5 m in general, where the evaporation and transpiration impossible.

5.3. Input data

The physical framework of the model was constructed, including the topographic surface, the layer's boundaries, the demission and thickness of each layer, hydraulic head boundaries based on a potentiometric map of September 2010. The hydraulic parameters for each layer were obtained from (Selkhozpromexport 1986) and the pumping test performed by (MOI 2005). These values were used as initial values for steady-state simulation. The initial and boundary conditions are defined on the mesh nodes, whereas the characteristics of the medium are assigned on elemental basis.

5.3.1. Recharge

Groundwater recharge rates vary with climate conditions. The other important factors controlling recharge are surface geology, surface topography, soils type, vegetation, and land use. The recharge amount includes the major input from precipitation and minor input from irrigation return flow over the irrigated areas. High amount of groundwater recharge occurs mainly by direct vertical percolation of rainfall and snowmelt through the unsaturated zone of the outcropping part of Jurassic formations. The Neogene/Quaternary aquifer receives a lower recharge portion from rainfall but an important recharge as lateral groundwater inflow from adjacent cavernous limestone in the western side and an additional recharge from irrigation return flow. The groundwater potentially leaks upward from deeper aquifers into this aquifer and forms another recharge component which is poorly understood and quantified.

The amount of recharge into the groundwater during the hydrological year 2009-2010 was calculated by using the isohyetal method to be $173 \text{ Mm}^3\text{y}^{-1}$ upon the model area based on available meteorological data in six stations located in the study area (Fig. 1-12). This year is considered as a moderate year in terms of precipitation amount. The total amount of precipitation, which recharges the upper aquifer horizon, was calculated to be $48 \text{ Mm}^3\text{y}^{-1}$. The recharge input was entered into the model as a specified flow through the top surface

of the first layer. Indirect recharge from, conveyance losses of irrigation canals and domestic water, exceeding irrigation water (return flow) and wastewater discharge were estimated to be $11.8 \text{ Mm}^3 \cdot \text{y}^{-1}$. This estimation is based on a certain percentage of water that evaporate or return to the water system according to (RDWSSA 2006).

5.3.2. Net Pumping

The percentage of the total irrigated area served by groundwater in Syria rose from 49% in 1985 to 60% in 2004 (MAAR 2006, Luijendijk and Bruggeman 2008). As a result of agricultural and urban development beginning few decades before, groundwater pumping became an important source of discharge from the study area. Water use and pumping data are essential in order to assemble a water budget or groundwater flow model. The accurate monitoring of agricultural water use is an important factor in order to reduce the uncertainty in water balance calculation. However, quantifying of groundwater abstraction is still a difficult but necessary challenge. Agriculture accounts for 87% of the water withdrawn from Syria's aquifers, rivers and lakes (FAO 2012, Aw-Hassan 2014). Groundwater abstraction for both agricultural and domestic uses is well developed in the study area. The total number of wells in this area is 931 from which 830 wells are used for irrigation purpose, while the remaining ones are used for domestic purposes. The majority of these wells are located in the plain region (Fig. 5-4). The dominating irrigation method in the study area is the surface irrigation, while recently the irrigation sprinkler method has started to be applied (Fig. 5-5).

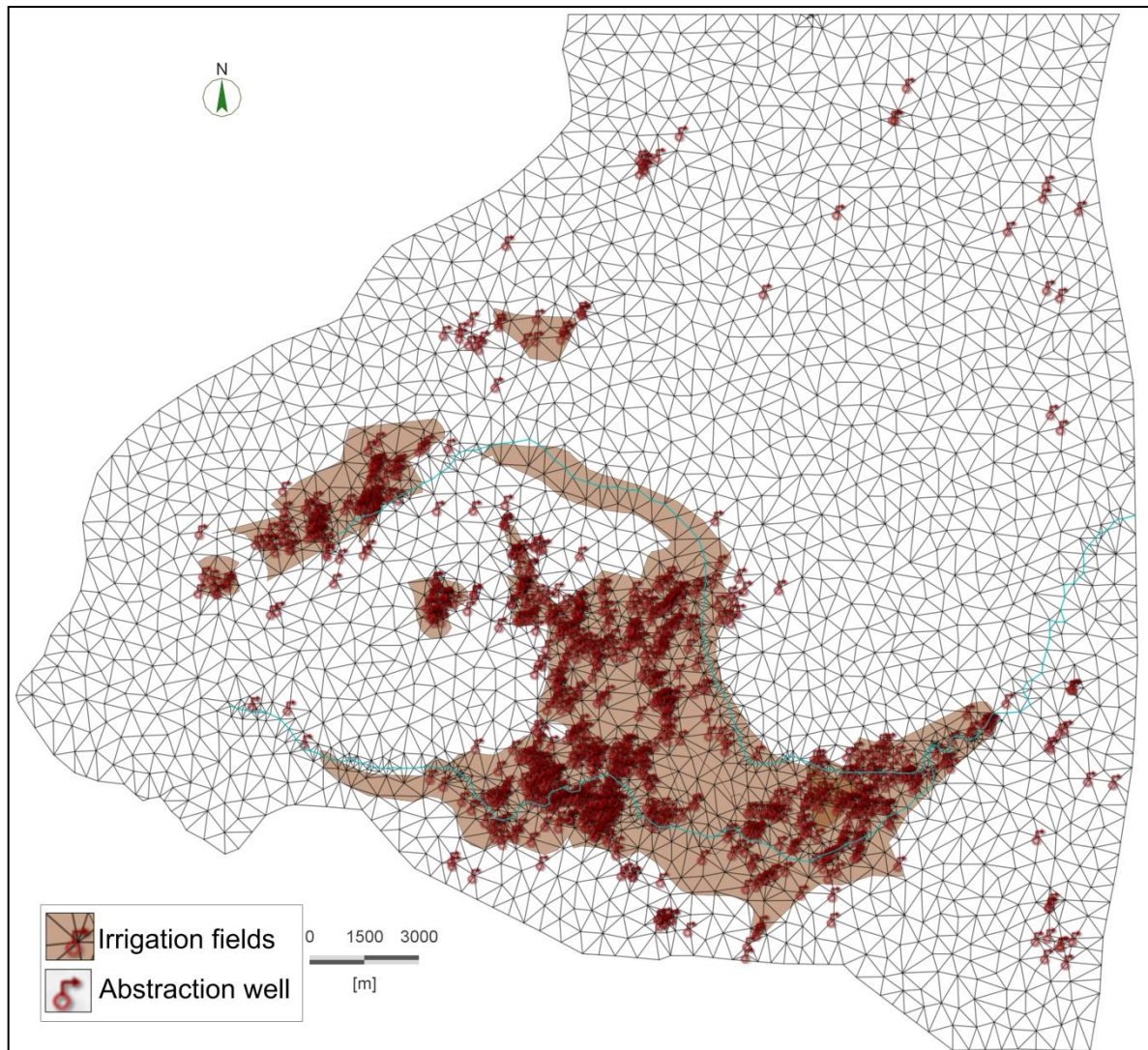


Fig. 5 - 4 Irrigation field location sites and spatial distribution of abstraction wells.

The annual amounts of groundwater abstraction from the wells, which are located in the upper aquifer horizon for agricultural and domestic purposes, were calculated to be 7 and 8 Mm^3y^{-1} respectively. About 85% of the groundwater abstraction wells are screened over the upper aquifer horizon, while 2% and 13% are penetrating the Cretaceous and Jurassic aquifer respectively. For modeling purpose the annual pumped volume for each well is converted to m^3d^{-1} and applied as a steady amount throughout the year. m^3d^{-1} .

The Awaj River is also used for irrigation purpose in the summer period. The amount of surface water used for irrigation purpose is about $35 \text{Mm}^3\text{y}^{-1}$ during the hydrological year 2009-2010. The total irrigated area by both groundwater and surface water is about 75km^2 of which about 21km^2 is irrigated by groundwater. The calculated amount of pumped groundwater is less than the required water for the irrigation purposes if the amount of 5000

$\text{m}^3\text{h}^{-1}\text{y}^{-1}$ has taken in consideration according to MOI (2005). The calculated total discharge of springs located in the upper aquifer was $37.5 \text{ m}^3\text{y}^{-1}$ for the hydrological year 2009-2010.



Fig. 5 - 5 The irrigations method applied in the study area (plain region).

5.3.3. Spatial distribution of hydraulic conductivity

The calibrated hydraulic conductivity for the upper aquifer horizon was varied within reasonable range based on literature values between 0.3 and 13 m.d^{-1} . For the other aquifers and aquitards, these values were assigned uniformly because there is not enough information about their spatial distribution across these layers. The uniform hydraulic conductivities for the Cretaceous and Jurassic aquifers were defined as 25 and 18 md^{-1} respectively, while these values were taken as 0.08 and 0.15 md^{-1} for the upper and second aquitards respectively. Fig. 5-6 shows the spatial distribution of the hydraulic conductivity in the upper aquifer horizon, taking into account the locations where this aquifer does not exist.

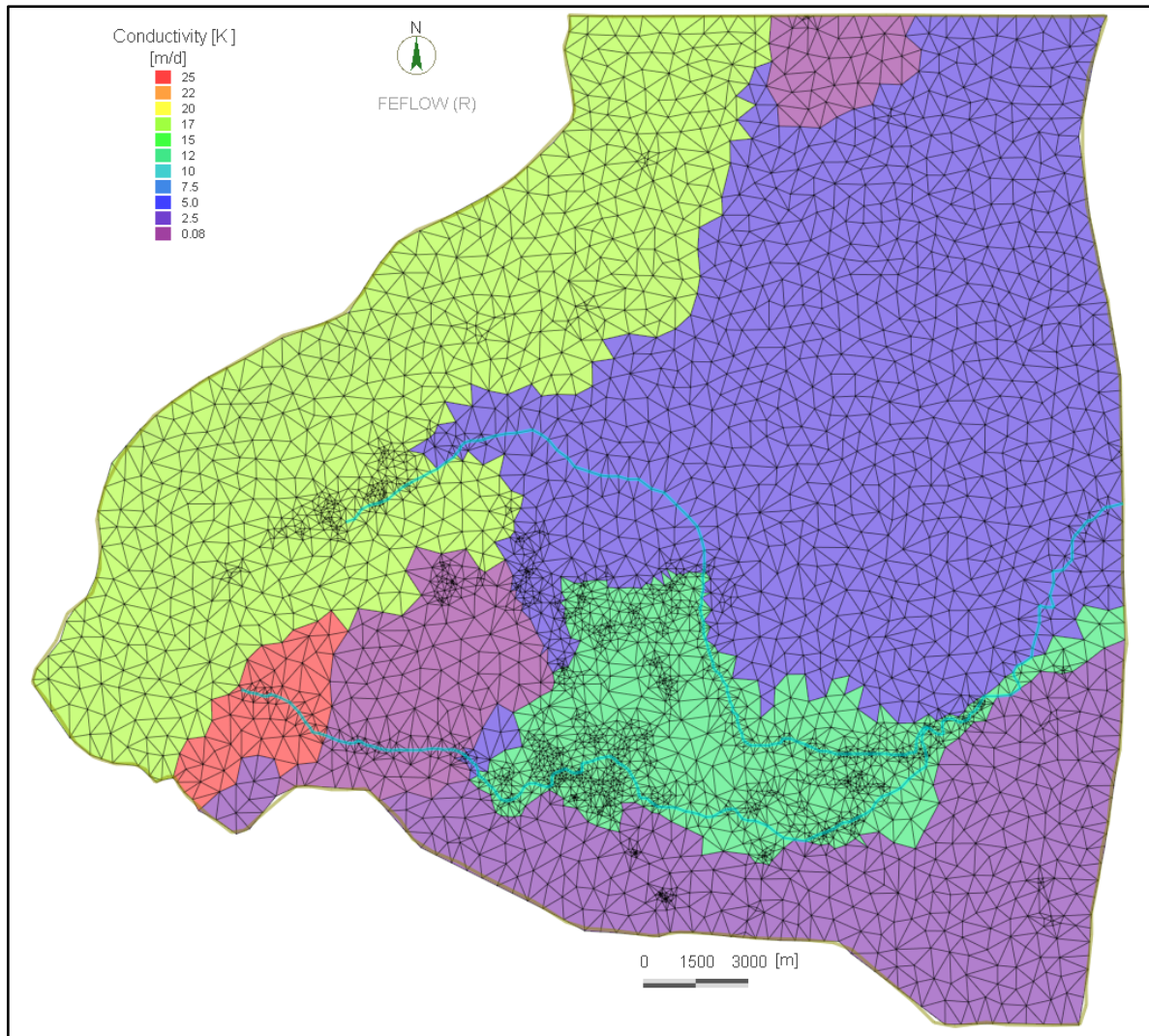


Fig. 5 - 6 Spatial distribution of the hydraulic conductivity in the model domain (upper aquifer horizon).

5.4. Steady-state calibration

Steady-state flow occurs when the magnitude and direction of flow is constant with time throughout the entire domain. The better agreement achieved between initial head observed with the hydraulic head simulated is called steady-state calibration. Calibration was performed by trial and error by changing the hydraulic conductivity of the model layers until achieving a reasonable agreement between the simulated and measured groundwater levels.

5.4.1. The result of simulated hydraulic head in the different aquifers

The measured and simulated groundwater level contours (Fig. 5-7) indicate fairly good agreement in the upper aquifer horizon. In the southern boundaries, where the basaltic layer and the zone which hosts numerous irrigation wells, less agreement between simulated and measured groundwater level was achieved. When the upper aquifer horizon gets in contact with the upper aquitard, it retards the groundwater flow, and thus the contour lines behaviour changes and becomes denser at this interface. This phenomenon can be observed at two places, in the southwest and the north of the study area where this aquitard is located and exposed to the surface. Furthermore, and due to the definition of no flow boundaries in the north and south part of the model domain, the contours in the model must be perpendicular to these boundaries, while the measured contours are not. This changes the performance of the model near these boundaries.

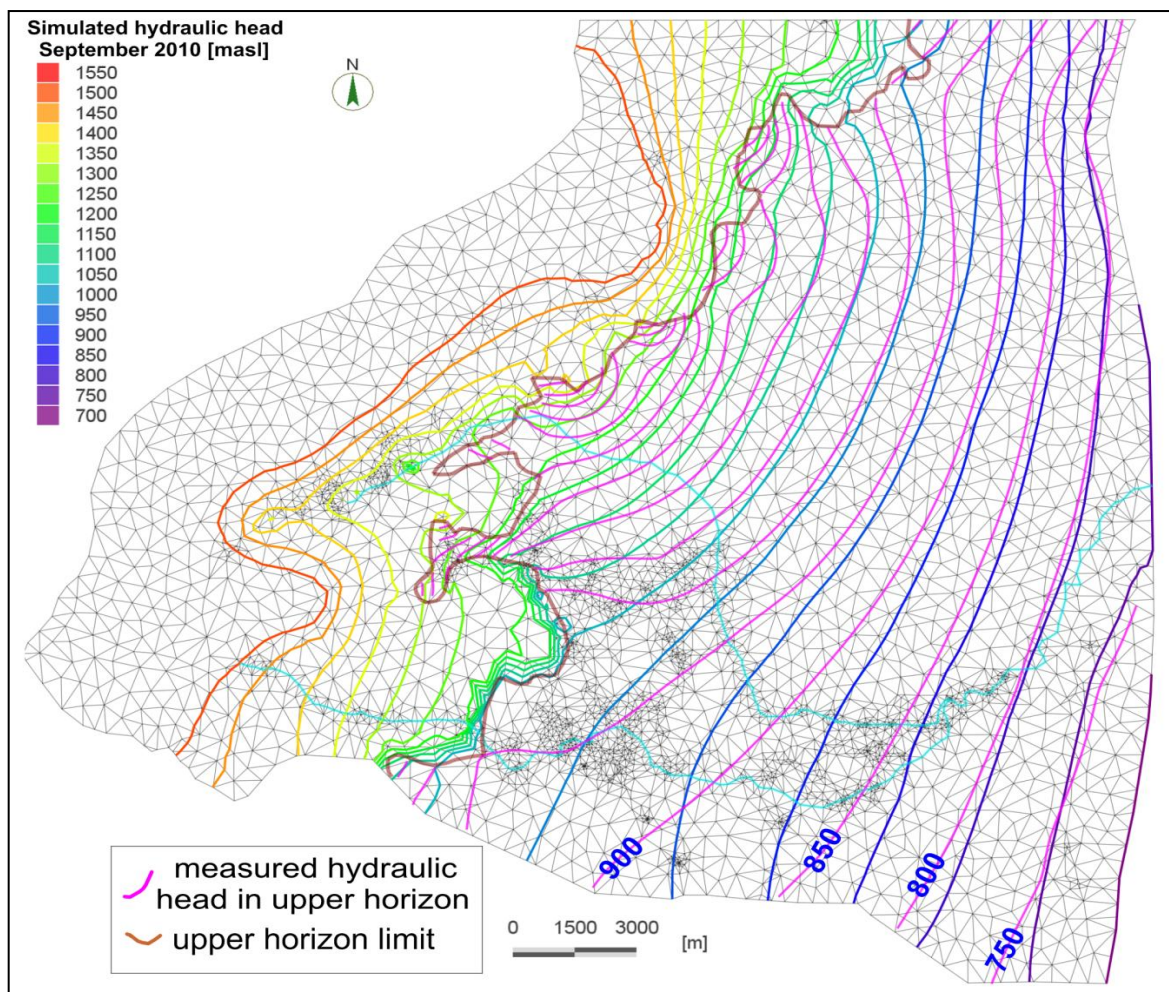


Fig. 5 - 7 The comparison between measured and simulated initial hydraulic head in the upper aquifer horizon, September 2010.

The scatter plot and regression analysis of computed and measured hydraulic head in the wells located in the upper aquifer horizon are shown in (Fig. 5-8). The result indicates that the agreement between simulated and measured hydraulic heads was reasonably good for the measured points.

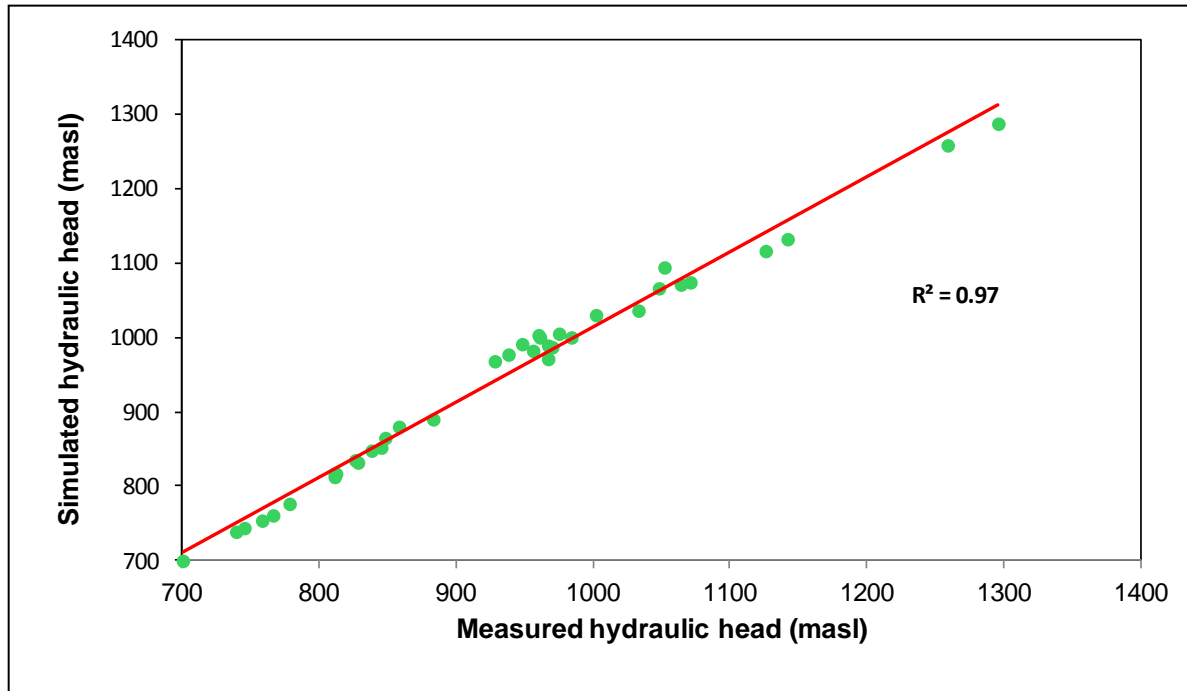


Fig. 5 - 8 Scatter plot of measured and simulated initial hydraulic head for September 2010.

The sensitivity of the model to input parameters was tested by changing the parameters of interest over the range of values in order to determine the most sensitive parameters identifying aquifer behaviour. During calibration, it was found that the most critical parameter that affects the simulated result is the spatial distribution of the hydraulic conductivity and to less extent the amount of recharge.

The flow regime in the upper aquifer horizon shows that the flow direction is organized toward the east direction with a higher hydraulic gradient in the western part and moderate hydraulic gradient in the plain region. The map also shows that a part of groundwater of the major valleys tends toward the southeast direction. This flow can be considered as a part of the lateral flow where the conduits of Jurassic aquifer are laced through the porous medium of Neogene aquifer. Calibration of the groundwater flow in the other aquifers was not possible due to the lack of groundwater level measurement in these aquifers. However, the simulated of groundwater level of these aquifer were performed with a limited certainty.

The hydraulic connections between the model aquifers depend on the hydraulic gradient difference in these aquifers. According to the simulation result, this gradient was high enough to permit hydraulic connections between the deep aquifers and the upper aquifer horizon. The amount of upward movement from the deep aquifers to the upper aquifer was calculated to be $31 \text{ Mm}^3 \cdot \text{y}^{-1}$.

The simulated groundwater level in the Cretaceous and Jurassic aquifers indicated that the major groundwater flow was organized toward the east direction. When both aquifers become at the considerable depth in south-eastern part of the model domain, a part of groundwater flow tends toward the southeast to the Yarmouk Basin. Fig. 5-9 and Fig. 5-10 show the equipotential contour lines in the Cretaceous and Jurassic aquifer respectively. In general the three aquifers of the model demonstrate almost the same flow behaviour which indicates a hydraulic connection between these aquifers.

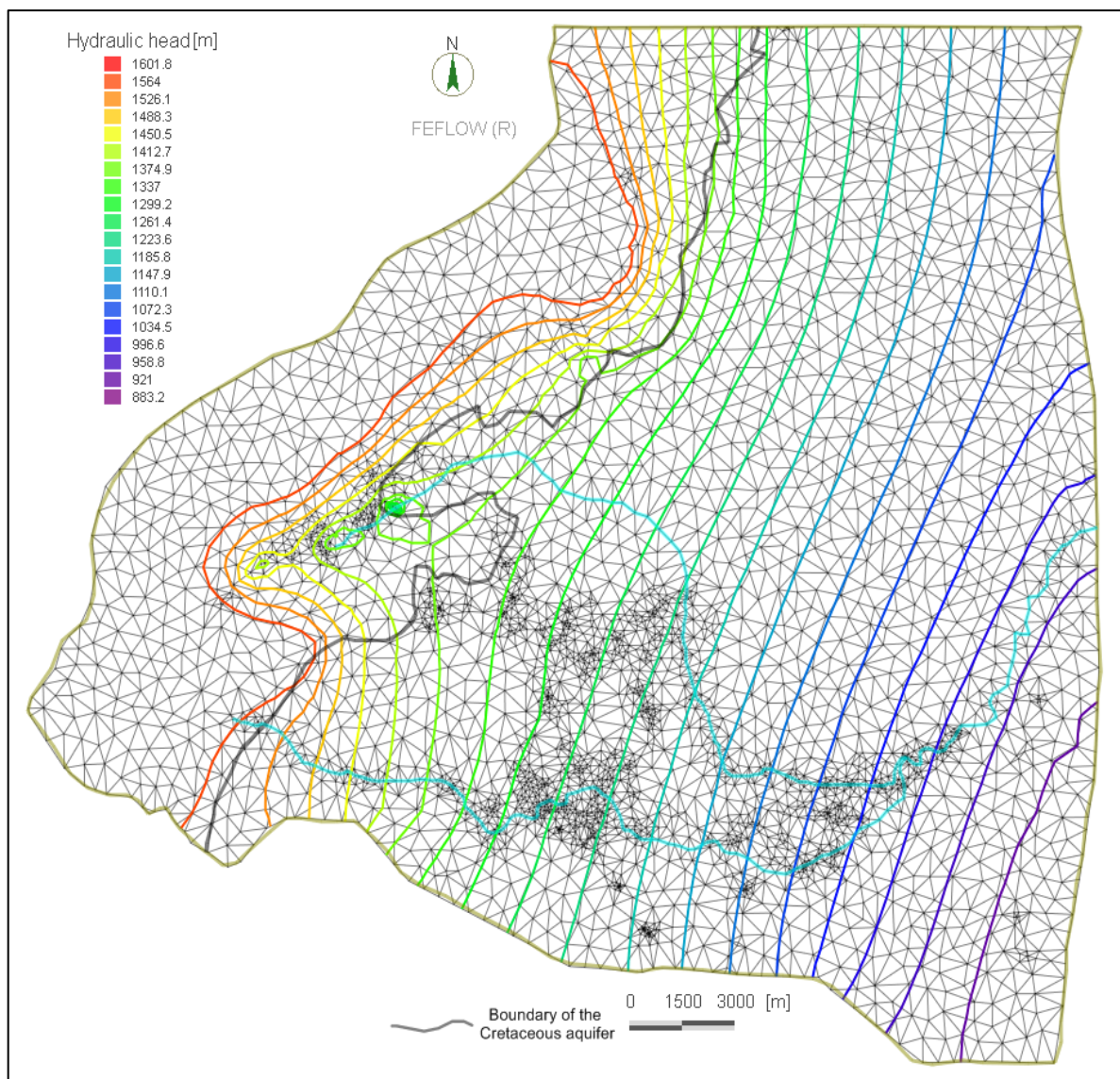


Fig. 5 - 9 Simulated equipotential contours lines in the Cretaceous aquifer, September 2010

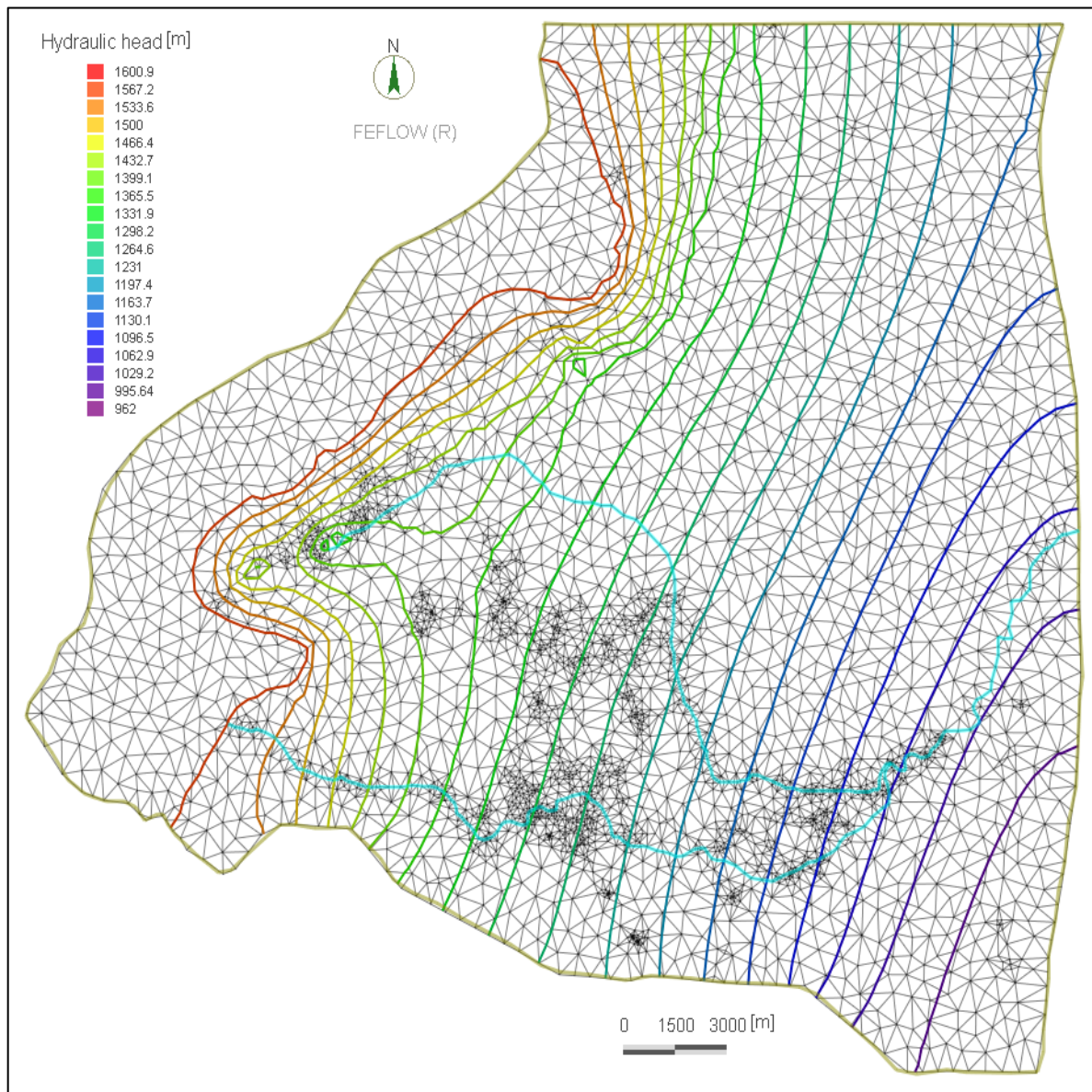


Fig. 5 - 10 Simulated equipotential contours lines in the Jurassic aquifer, September 2010.

5.4.2. Integrated water budget for the upper aquifer horizon

The evaluation of water resources is the cornerstone in estimating of the potential of the area for better water resource management and further groundwater development. Under predevelopment conditions and in long term, the groundwater system is equilibrium. The recharge and the discharge are the input and output from a groundwater system and both quantities are important in understanding how a particular groundwater system functions. Computing water budget provides information on whether the aquifer system is being depleted or not and allows calculating the amount of water exchange at the model

boundaries. This helps to use the available groundwater resources in a sustainable way. The water budget and flow tools in FEFLOW as well as the FEFLOW classic version can be used to quantify the volume of water across lines (aquifer boundaries), polygons (model layers), and boundary conditions (flow in or out of the model). The steady-state calibration result was used to calculate the preliminary water balance in the upper aquifer horizon. The change in groundwater storage can be estimated based on the quantity of water entering and leaving this aquifer during a certain period of time using the following equation:

$$\frac{dV}{dT} = R - (P + Q) \quad (21)$$

Where dV/dT is the change in storage ($m^3.y^{-1}$), R is the groundwater recharge by precipitation, lateral inflow, upward leakage, conveyance loss of irrigation and domestic water, irrigation return flow and wastewater discharge ($m^3.y^{-1}$). P is the total groundwater pumping ($m^3.y^{-1}$), and Q represents the springs discharges and cross-boundary groundwater outflow from the model area ($m^3.y^{-1}$). The groundwater balance was calculated based on available recent data of the hydrological year 2009-2010. The precipitation during this year is near the long-term average (MOI. 2005). The groundwater used for irrigation does not depend on the rainfall because there is no rainfall during the summer period.

The indirect recharge component of this budget was developed based on various assumptions which were drawn upon a hydrogeological and meteorological conditions dominated in the model area and mainly the fractions that evaporate or recharge the system.

The water budget of the calibrated model domain is balanced. However, the water budget applied on the upper aquifer horizon indicates an imbalance between the simulated and estimated components of inflow and outflow (table 5-1) in this aquifer equal to $4.6 \text{ Mm}^3.y^{-1}$. The lateral and upward inflow ensemble is the most important input to this horizon while the atmospheric precipitation is the second important recharge component. The largest outflow component is through the eastern boundary. Even with the fact that groundwater flows across the eastern boundary of the model area, the groundwater system in the adjacent eastern region is under a great stress than of the model region. Based on the FEFLOW numerical model and the other primarily information utilized within this study, the different components of the water budget of the upper aquifer horizon are shown in table (5-1).

Table 5 - 1 Possible amounts of water entering and leaving a groundwater system of the upper aquifer horizon and the primary information used to calculate different components of the groundwater budget in this horizon. Units are in Mm³.y-1

Recharge Components			
Indirect recharge (conveyance losses of domestic and irrigation water, wastewater discharge and irrigation return flow)	Direct recharge from meteoric infiltration	Lateral inflow from Jurassic aquifer- corresponds to FEFLOW simulation	Upward leakage from deeper aquifers corresponds to FEFLOW simulation
(Mm ³ y ⁻¹)	(Mm ³ y ⁻¹)	(Mm ³ y ⁻¹)	(Mm ³ y ⁻¹)
11.8	48	52	31
Discharge Components			
Lateral outflow from southern boundary to Yarmouk Basin corresponds to FEFLOW simulation	Spring discharges	Lateral outflow from eastern boundary- corresponds to FEFLOW simulation	Abstraction water for agricultural and domestic use
(Mm ³ y ⁻¹)	(Mm ³ y ⁻¹)	(Mm ³ y ⁻¹)	(Mm ³ y ⁻¹)
3.9	37.5	81.8	15

The different flow components for the water budget in the upper aquifer horizon are shown in Fig. 5-11 measured in Mm³.y⁻¹.

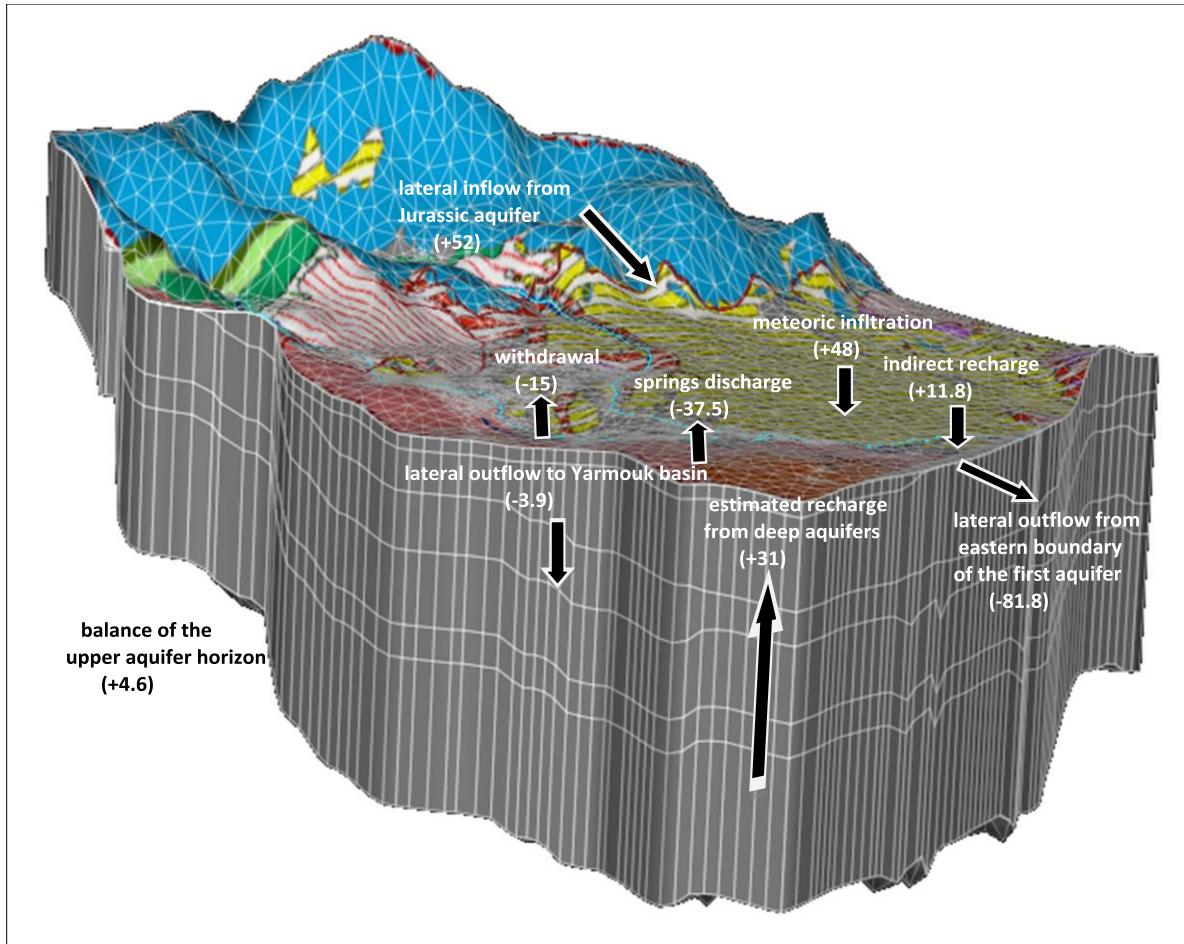


Fig. 5 - 11 Three dimensional (3D) numerical model showing computed water budget in the upper aquifer horizon applied for steady-state simulation during September 2010. The positive inflow and negative outflow values are expressed in Mm³y⁻¹.

A published paper stemmed from this chapter is appended (Appendix C)

Chapter 6. General conclusion and Prospective

6.1. General conclusion

The main objectives of this study were to evaluate groundwater flow behavior and assess the recharge and discharge mechanisms in the upper part of Awaj River which occupies the eastern part of Mt. Hermon. The dynamic controlling groundwater flow system in this area has been investigated. To achieve these objectives, the integration between hydrochemical, isotopic and hydrodynamic characteristics of groundwater were used. However, the aquifers system was interpreted based on obtained information on the flow paths and volumes of groundwater flow. Based on that, the water budget of the upper aquifer horizon, where the most anthropogenic activities are concentrated, is a considerable result of this study.

The hydrochemical characteristics of groundwater have provided useful information about different mechanisms characterising and controlling groundwater flow as a result of its interaction with the hosting rocks. Based on that and on the discharge of major springs, the discrimination between different main behavioural trends in groundwater flow pattern has been distinguished and thus the study area has been divided into four sub-areas. The dissolution/precipitation of carbonate minerals is the major process dominating water-rocks interaction and thus controlling groundwater composition not only in the mountainous part but also in the plain region. This was evidenced by the saturation indices of calcite and dolomite. However, and to less extent, the silicate hydrolysis and reverse ion exchange, involving clay minerals, were recognized to play a considerable role in groundwater composition. The dissolution of gypsum is recognized in some places, mainly in the Jurassic aquifer.

It is likely that the geochemistry of the groundwater at the upper part of the Awaj River is controlled by the geogenic process rather than the effect of anthropogenic activities. The interpretation of hydrogeochemical data reveals a large degree of variability that results from its marked hydrogeological and lithological complexity. Consequently, hydrochemical patterns did not give enough evidences for the expecting of huge feeding flow from Jurassic aquifers towards the other aquifers.

Nevertheless, the hydrochemical facies of groundwater show that about 70% of water samples, tend to have anion chemistry dominated by HCO_3^- and cation composition

dominated by Ca^{2+} (Ca- HCO_3 water type). This confirms the dissolution/precipitation of carbonate rocks and the recent recharge of groundwater from atmospheric precipitation. The similarity in water type tends to express the existence of a unique hydrochemical system where the individualised groundwater flow paths are difficult to delineate within the different hydro-stratigraphic units.

A remarkable anthropogenic influence on the groundwater quality was observed through the infiltration of irrigation water and the effect of fertilizers on nitrate level as well as the contamination by sewage water and animal waste disposal. This impact has been detected in some villages in the mountainous part as well as in the plain area through the substantial increases of nitrate and fecal concentrations.

In general, the result of hydrochemical evolution is not clear enough to provide an effective approach to delineate the flow pattern, indicating that this area is much more dominated by recharge than discharge processes. Thus, it could be considered as a part of a main intermediate or regional flow system rather than a local one. The flow pattern is clear from the potentiometric map but that does not tell the whole story about the groundwater behaviour.

The isotope compositions of precipitation were used to construct a local meteoric water line in the study area ($\delta^2\text{H} = 7.9\delta^{18}\text{O} + 17.9$) as well as the relationship between stable isotope depletion and altitude. This relation indicated that the altitude effect causes a depletion of -0.23‰ per 100 m for ^{18}O and -1.7‰ per 100 m for ^2H . Comparing the isotope composition of groundwater and precipitation implies an important rapid infiltration of atmospheric precipitation before significant evaporation takes place prior to or during the infiltration. These data also show that groundwater recharge takes place all over the study area but the main recharge occurs over the mountainous parts. The karstic springs along Arneh valley show similar isotopic composition to the precipitation of that area. This indicates that these springs issued water is originated from the direct local recharge of this precipitation. All the groundwater samples are situated to the left of GMWL suggesting input of local rainfall that derives from weather front originating from the Mediterranean Sea. The infiltrated precipitation provides the main source of recharge to the aquifers system through the karst landscape and fractured rocks in the mountainous part (Jurassic aquifer). It also, but to a less extent, contributes to the recharge of Neogene

conglomerate, Quaternary alluvial and basalt formations in the plain region where the mixing of groundwater flow paths has been recognized.

Nevertheless and based on the hydrochemical and isotopic characteristics of groundwater, the study area can be divide into two main sub-region A and B. The sub-region A constitutes the western, south-western, and north-western parts (Jurassic aquifer) where the main groundwater recharge is occurring. In this part, the karstic features are well developed in the upper and deeper parts facilitated by cracks and fissures. This leads to increase the permeability characteristics and enhance the infiltration and dissolution mechanisms; hence this part is characterized by a high vulnerability of groundwater to pollution evidenced by high rates of nitrates resulting from sewage water infiltration. The hydrochemical processes are highly irregular in this part which is suggestive of an active dissolution phenomenon and a deep vertical groundwater flow.

The sub-region B occupies the south, central and eastern part (Neogene conglomerates and Quaternary alluvial aquifers). This part is characterized by a shallow horizontal flow component associated with active interaction between groundwater and hosting rocks, evidenced by water chemistry evolution. The upward movement from deep aquifers seem to be an important component to maintain the Neogene/Quaternary aquifer in this sub-region where the discharge occurs mainly through the major springs and groundwater abstraction wells. The springs which are distributed in the recent basalt or close to its border with the other formations in this sub-region, yield significantly high discharge and cannot be classified under the perched springs. This indicates that these springs are draining the deeper regional aquifers.

Fluctuation of groundwater level is strongly controlled by atmospheric precipitation and anthropogenic influence through the increasing of groundwater abstraction.

The development of numerical model which simulated the groundwater system behavior of the upper part of Awaj River was a useful alternative tool to evaluate groundwater resources in this region. The result of the calibrated model shows reasonable agreement between measured and calculated water level in the observed wells. However, the model has predicted water level in the deep aquifers and the hydraulic connection between these aquifers and the upper one. Based on the simulation result, the calculation of the groundwater budget of the upper aquifer horizon was developed.

The model result indicates that the elevated Jurassic and Cretaceous aquifers become confined where they are extended toward the east in the plain region where they are overlaid by the recent formations. The hydraulic gradient of these aquifers was high enough to permit hydraulic connections between them and the overlying upper aquifer horizon through the upward leakage of groundwater. In the upper aquifer horizon, the groundwater flow system is affected by different mechanisms in terms of recharge and discharge. The recharge is originated from different sources such as direct meteoric recharge, lateral recharge along the contacts between Jurassic aquifer and the escarpment conglomerate of Neogene aquifer and the upward leakage of deep artesian water as well as the indirect recharge from the irrigation return flow. The discharge is occurred mainly through the lateral outflow at the eastern and south-eastern boundaries as well as groundwater withdrawal. The highlands Jurassic aquifer is recharged solely by the infiltration of intensive rainfall and snowmelt.

Consequently, groundwater flow system in the model domain can be divided into two different systems. The first is shallow and develops in the unconsolidated or semi-consolidated Quaternary/Neogene formations in the plain region. The second is deep and develops in the Cretaceous and Jurassic carbonate strata where the preferential flow mechanism contributes potentially to the groundwater flow patterns. The hydraulic connection between the two systems was observed. Groundwater flow in the first system seems to be controlled by bedding and lithostratigraphic units with a minor downward component. While in the second system, groundwater flow pathways constitute of two main components. The first component is controlled by local conduits and an active fault zones. This component discharges either as a preferential flow throughout several karstic springs or recharges the upper aquifer horizon through the cavernous limestone as a lateral groundwater flow. The second component is recognized to be regional which is controlled by the geological structures as deep vertical groundwater flow. Accordingly, the local flow and deep circulation of groundwater seem to be dominating and controlling the flow system in the study area.

Due to the complexity of the geology/hydrogeology and the uncertain accuracy of hydraulic parameters of deep aquifer (Cretaceous and Jurassic), this groundwater model was limited in developing a general insight about groundwater system and water budget in the upper aquifer horizon. However, the most important components of this budget had been determined. The result indicates that the lateral discharge from the Jurassic karstic

aquifer as well as the meteoric infiltration is the most important recharging component of this budget. The upward movement of groundwater from deeper aquifers plays an important role in recharging this aquifer. However, the lateral discharge from the eastern model domain boundary is the most important discharge component which indicates that the study area can be considered as a main recharge region of the western side in Barada and Awaj Basin. Nonetheless, the simulated groundwater level in the Cretaceous and Jurassic aquifer indicated that the major groundwater flow was organized toward the east direction. In general, the natural characteristics of the hydrogeological dynamic of the study area seem to play a key role in the groundwater flow system despite of the development of intensive agricultural/domestic activities in this area.

The obtained result of groundwater modeling is in well agreement with that one achieved by the interpretation of groundwater hydrochemical characteristics of the study area. This result clarifies the recharge/discharge mechanisms between two different but linked hydrogeological systems (shallow and deep), and helps to quantify the different components of the water budget in the shallow one. The simulated result, which indicates a relatively high amount of lateral inflow and upward leakage of groundwater into the upper aquifer horizon, supports the suggestion based on hydrochemical analysis to extend the orographic basin boundary towards the west. This leads to increase the subsurface recharge area and justify the considerable quantity ($31\text{Mm}^3\cdot\text{y}^{-1}$) of upward leakage from deeper aquifers to the upper aquifer horizon.

6.2. Prospective

In the dry developing agricultural countries such as Syria, the achieving balance between short-term productivity growths with the long-term negative impacts of groundwater depletion is a challenge facing policy makers.

Further additional survey of the aquifer mineralogy, more frequent sampling for geochemical characterization, isotopes analysis and age-dating techniques as well as increasing of groundwater model efficiency would help as significant tools for better understanding of the aquifer system behaviour. However, more accurate geological and hydrogeological information, in particular the hydraulic and dispersive characteristics of deep aquifers and karst setting, could give more accurate result in terms of groundwater

modeling. Obtaining necessary data during a considerable period will allow running the model in transient state and applying, probably, different scenarios to predict future changes in the groundwater system in the study area.

Due to the complexity and lack of hydrodynamic data, the investigations of the aquifers system in the study area should focus on the isotope techniques that are very useful to characterize the aquifers system. The accurate information concerning groundwater level fluctuations, irrigation water losses, crops productivity as well as meteorological data would help to overcome the policy makers' challenge.

Nonetheless, more accurate results could be obtained by improving the quality of site-specific information, in particular more accurate information about the hydraulic and dispersive characteristics of deep aquifers and karst setting (e.g., drilling data, tracer tests, pumping tests, and additional groundwater level data). However, extending the study area over the entire Barada and Awaj Basin, and applying regional groundwater flow modeling might give significant insight about groundwater system in this basin. Immediate reaction must be taken to reduce water losses throughout the distribution system and the application of modern irrigation techniques instead of traditional surface ones.

Improving the efficiency of water system data monitoring as well as the communication between different water authorities will help in accurate determination of renewable water resources and furthermore in better water resources management strategy. The co-ordination between the neighboring countries and exchange the experience in terms of investigations, exploitation, transfer and protection of water resources will give a significant effort in terms of water management in this semiarid zone.

6.3. Conclusion générale

Les principaux objectifs de cette étude étaient de préciser le fonctionnement hydrodynamique du système aquifère en utilisant notamment la physico-chimie des écoulements des eaux souterraines et en précisant l'aspect quantitatif des mécanismes de recharge et de décharge de la partie supérieure du bassin versant de la rivière Awaj (zone orientale du Mt. Hermon, Syrie).

La dynamique des écoulements des eaux souterraines du système a été précisée en utilisant à la fois les caractéristiques hydrochimiques (nature et qualification des eaux), isotopiques (origine et nature) et hydrodynamiques des eaux (balance des eaux et modèle numérique de quantification).

Un des résultats a été l'identification des directions et sens d'écoulement au sein des différentes unités hydrogéologiques du bassin versant d'Awaj ainsi que l'estimation des volumes et stocks de masses d'eau propres à cet aquifère. Ces éléments sont indispensables pour déterminer les capacités de la ressource en eau de l'aquifère du Quaternaire-Néogène (aquifère phréatique libre local) à répondre aux besoins humains et agricoles (eau potable et irrigation). L'étude intègre également l'influence des activités anthropiques concentrées dans la zone alluviale de la plaine et pouvant affecter la qualité des eaux.

Les caractéristiques hydrochimiques des eaux souterraines ont fourni des informations essentielles sur les différents mécanismes caractérisant ces eaux. Notamment l'interaction eau-roche, qui contrôle en grande partie la dissolution-précipitation des ions (majeurs et mineurs), a permis de préciser la nature des flux d'eaux circulant au sein des différentes unités géologiques. La dissolution/ précipitation des minéraux carbonatés est le phénomène dominant et marque la chimie des eaux souterraines tant dans la partie montagneuse que dans la zone de plaine. Ceci a été démontré par le calcul des indices de saturation de la calcite et la dolomite. Cependant, et dans une moindre mesure, l'hydrolyse des silicates (type argiles) peut inverser localement les échanges ioniques et modifier localement l'hydrochimie des eaux souterraines. Au vu de ces résultats, il est possible de conclure que les eaux souterraines de la partie supérieure du bassin de la rivière Awaj sont contrôlées par des processus géogéniques et non anthropiques. Les données hydrogéochimiques révèlent une grande variabilité, conséquence d'une complexité hydrogéologique et lithologique. De ce fait, il est difficile de pouvoir clairement identifier les importants flux migrant depuis l'aquifère du Jurassique vers les autres aquifères surincombants au sein du bassin sédimentaire.

Les principaux résultats hydrochimiques montrent que plus de 70% des échantillons d'eau analysés ont une composition anionique de type HCO_3^- et cationique de type Ca^{2+} propre aux eaux carbonatées (Ca- HCO_3). Ce résultat confirme d'une part le mécanisme de dissolution/ précipitation des roches carbonatées et d'autre part une recharge plus récente de l'ensemble du système aquifère par les précipitations atmosphériques. Les similarités

entre les différents types d'eau des aquifères de la zone d'étude tendent à démontrer l'existence d'un système hydrochimique unique, où la délimitation des chemins d'écoulement propres aux eaux souterraines sont difficiles à identifier au sein des différentes unités hydro-stratigraphiques. A noter également, l'influence des activités anthropiques sur la qualité des eaux du fait de l'infiltration des eaux d'irrigation fortement chargées en fertilisants (niveau de nitrates élevé) mais également par les eaux usées issues des décharges de déchets organiques (élevages). Ces impacts ont été identifiés localement dans certains villages de montagne et de plaine.

Si d'une façon générale, l'évolution de la signature hydrochimique n'est pas suffisante pour orienter les sens d'écoulement des différentes masses d'eaux considérées le recours aux cartes piézométriques permettent de préciser clairement les écoulements et de proposer un modèle de fonctionnement intégrateur. Notre système est à priori caractérisé par un taux de recharge supérieur la décharge et peut être considéré comme faisant partie d'un système intermédiaire ou régional plus que local.

La composition isotopique des eaux des précipitations a été utilisée pour construire localement la ligne d'eau météorique de la zone d'étude ($\delta^2\text{H} = 7.9.\delta^{18}\text{O} + 17.9$) ainsi que la corrélation entre l'appauvrissement en isotopes stables et l'altitude. Cette relation indique qu'en fonction de l'altitude un appauvrissement de -0,23% par hm pour ^{18}O et -1,7% par hm pour ^2H . Les résultats de la comparaison entre la composition isotopique des eaux souterraines à celle des précipitations, impliquent une infiltration rapide des précipitations atmosphériques avant qu'une évaporation des eaux ne se produise. Ces données montrent également que la recharge des nappes a lieu dans toute la zone d'étude, mais que la recharge se produit principalement en zone montagneuse. Cela est démontré par le fait que les sources karstiques le long de la vallée Arneh montrent une composition isotopique similaire à celle des eaux de précipitation. Ceci indique que ces émergences sont directement alimentées par les eaux infiltrées précédemment. Tous les échantillons d'eau souterraine, ont une composition isotopique située à gauche du GMWL suggérant une contribution des précipitations locales dérivant des intempéries provenant de la mer Méditerranée.

L'infiltration des précipitations contribue principalement à la recharge de l'aquifères du Jurassique et plus spécifiquement de sa partie karstique localisée dans les formations de roches fracturées, en montagne. Elle contribue également, mais dans une moindre mesure, à la recharge du système des aquifères conglomératiques du Néogène ainsi que des aquifères

alluviaux dans les formations basaltiques de la plaine. Dans ce dernier aquifère, un mélange des flux souterrains a été observé.

Néanmoins, et en fonction des caractéristiques hydrochimiques et isotopiques des eaux souterraines, la zone d'étude peut être divisée en deux principales sous-région : A et B. La sous-région A est constituée par la partie occidentale, sud-ouest et nord-ouest, de l'aquifère jurassique et constitue la principale zone de recharge des nappes souterraines. Dans cette partie, les caractéristiques karstiques sont bien exprimées aussi bien dans la zone supérieure qu'en profondeur du fait de l'existence de fissures et de fractures. Cela conduit à augmenter la conductivité hydraulique de l'aquifère, ce qui induit une prédominance de l'infiltration ainsi que de la dissolution. D'un autre côté, cette sous-région A est caractérisée par une forte vulnérabilité des eaux souterraines à la pollution, comme en témoignent les taux élevés de nitrates issus de l'infiltration des eaux usées. L'irrégularité des processus hydrochimiques dans cette zone suggère d'actifs phénomènes de dissolution associés à des écoulements verticaux en profondeur.

La sous-région B occupe le sud, le centre et la zone orientale avec des aquifères dans les formations conglomératiques du Néogène et alluviales du Quaternaire. Cette partie est caractérisée par une composante d'écoulement horizontal de sub-surface associée à une interaction active entre les eaux souterraines et les roches encaissantes, comme en témoigne l'évolution de la chimie des eaux souterraines. Une circulation de flux ascendant au sein des aquifères semblent être un élément important pour maintenir le niveau piézométrique de l'aquifère du Néogène-Quaternaire où la décharge est essentiellement fonction des émergences (sources) et des prélèvements (puits et forages). Ces sources, présentes dans les formations basaltiques récentes et aux interfaces avec les autres formations, affichent un rendement de flux sortants importants et ne peuvent être classées comme des sources perchées. Ceci indique que ces sources drainent les aquifères régionaux plus importants et plus profonds.

La fluctuation du niveau piézométrique des eaux souterraines est fortement contrôlée par les précipitations atmosphériques et l'influence anthropique du fait de l'augmentation des captages d'eaux souterraines.

Le développement d'un modèle numérique pour simuler le devenir du système d'eaux souterraines de la partie supérieure du bassin versant de la rivière Awaj est une alternative

utile pour évaluer les ressources en eau de la région. Le résultat du modèle calibré montre un accord raisonnable entre les niveaux observés dans les puits et calculés par simulation. Le modèle a permis de simuler la hauteur piézométrique dans tous les aquifères profonds en précisant la nature de la connexion hydraulique avec le premier aquifère de surface du Quaternaire-Néogène ainsi que ses débits entrants/sortants.

Le résultat du modèle indique que les aquifères Jurassique et du Crétacé supérieur (Cénomaniens-Turonien) sont captifs quand ils s'étendent vers la plaine et surmontés par les formations plus récentes. Le gradient hydraulique de ces aquifères est suffisamment élevé pour permettre des connexions hydrauliques entre eux et l'aquifère directement surincombant par drainance ascendante. Dans l'aquifère superficiel libre du Néogène-Quaternaire, le système d'écoulement des eaux souterraines est affectée par des mécanismes différents en termes de réalimentation et de déversement. Le flux de recharge provient de différentes origines telles que l'infiltration directe par les eaux météoritiques, les recharges latérales le long des contacts hydrauliques avec l'aquifère du Jurassique et de l'aquifère conglomératique du Néogène. Cet aquifère libre bénéficie également du flux ascendant par drainance des eaux profondes mais également indirectement d'une recharge induite par les flux en retour d'irrigation. L'écoulement sortant se produit principalement par les flux latéraux aux limites est et sud-est ainsi que par le prélèvement direct des eaux souterraines. L'aquifère du Jurassique de la partie montagneuse se recharge uniquement par l'infiltration des importantes précipitations et la fonte des neiges.

Par conséquent, le système d'écoulement des eaux souterraines dans le domaine modélisé peut être divisé en deux systèmes différents. Le premier est superficiel et se développe dans les formations non consolidées du Quaternaire et du Néogène de la plaine. Le second est profond et se développe dans les horizons carbonatés du Crétacé et du Jurassique. La liaison hydraulique entre les deux systèmes par drainance a été observée. L'orientation des flux d'eaux souterraines dans le premier système semble être contrôlée par l'organisation lithologique et les unités stratigraphiques sédimentaires. En revanche, dans le second système, les écoulements des eaux souterraines ont deux composantes principales. La première plus locale est contrôlée localement par les chemins au sein des zones de failles actives, par écoulements préférentiels, et émerge au travers de plusieurs sources karstiques et par alimentation latérale du premier horizon de l'aquifère au travers les calcaires caverneux. La seconde plus régionale s'effectue selon un flux ascendant contrôlé par les structures géologiques. En conséquence, le flux local et la circulation des

eaux souterraines en profondeur semblent dominer et contrôler le système d'écoulement global de la zone d'étude.

En raison de la complexité de la géologie et de l'hydrogéologie et de l'incertitude sur la précision des paramètres hydrauliques de l'aquifère profond (du Crétacé et du Jurassique), la finalité du modèle hydrodynamique du système aquifère général est de donner un aperçu du fonctionnement du système des eaux souterraines et une estimation de la balance des eaux de la première nappe (aquifère superficiel). Les principales composantes du bilan volumique des eaux ont été déterminées. Le résultat indique que les flux latéraux de la partie karstique du Jurassique ainsi que l'infiltration sont les deux principales contributions du bilan. Le mouvement ascendant des eaux souterraines des aquifères profonds par drainance joue un rôle important dans la recharge cet aquifère. Pour les sorties, l'exhaure latéral en limite orientale du domaine est le flux le plus important, qui indique que la zone d'étude peut être considérée comme la principale zone d'alimentation de la partie ouest du grand bassin de Barada et Awaj.

Le résultat obtenu par la modélisation des eaux souterraines concorde avec celui obtenu par l'interprétation des caractéristiques hydrochimiques de la zone d'étude. Ce résultat clarifie les mécanismes de recharge / décharge entre les deux systèmes hydrogéologiques différents (profond et superficiel), mais étroitement liés et a permis de quantifier les différentes composantes de la balance des eaux de l'aquifère superficiel. Le résultat de la simulation indique une proportion relativement élevée de flux latéraux d'eaux entrantes avec une drainance ascendante des eaux souterraines profondes vers l'aquifère de superficiel. Ces observations soutiennent l'hypothèse, issue de l'analyse hydrochimique d'étendre les limites du bassin orographique vers l'ouest. Cela conduit à augmenter la zone de recharge de sub-surface et justifie le volume conséquent ($31 \text{ Mm}^3 \cdot \text{y}^{-1}$) du flux ascendant issu des aquifères plus profonds.

6.4. Perspectives

Dans les pays en développement, tels que la Syrie, l'équilibre - entre l'amélioration de l'augmentation de la productivité de agriculture en climat aride - à court terme avec les impacts négatifs à long terme liés à la sur exploitation des eaux souterraines est un défi pour les décideurs politiques.

En complément, une étude de la minéralogie du réservoir, avec une fréquence d'échantillonnage plus élevée pour l'analyse des isotopes et des techniques de datation additionnelles permettraient d'améliorer la précision du modèle hydrogéologique et la compréhension d'un système complexe. Des données géologiques et hydrogéologiques plus précises en particulier les caractéristiques hydrauliques et de dispersion de l'aquifère profond permettraient d'affiner le calage du modèle hydrogéologique en zone hétérogène. L'obtention de ces données sur une période suffisamment longue permettrait d'utiliser le modèle développé en régime transitoire. Celui-ci pourrait alors être utilisé en déclinant différents scénarios afin prévoir et évaluer les possibles changements dans le fonctionnement du système hydrogéologique de la zone d'étude. Ceci tant pour l'aspect qualitatif que quantitatif.

En raison de la complexité et le manque de données hydrodynamiques, les performances du modèle hydrogéologique de la zone d'étude ne permettent pas de répondre à l'ensemble des questionnements. A des fins de calage, le modèle doit intégrer les résultats issus de l'isotopie qui sont très utiles pour améliorer la compréhension du comportement des aquifères. Les informations précises concernant les fluctuations piézométriques de la nappe phréatique, les pertes en eau liées à l'irrigation, l'augmentation de la productivité des cultures ainsi que les données météorologiques sont un des enjeux majeur en vue de surmonter le défi d'un développement durable et raisonné de la zone envisagé par les décideurs et le politique.

L'extension de la zone d'étude à l'ensemble du bassin de Barada et Awaj, en vue de modéliser régionalement le bilan hydrique, permettrait une meilleure gestion des ressources en eaux du bassin.

Une des premières mesures à envisager porte sur la réduction des pertes en eau du système de distribution et l'application de techniques d'irrigation modernes en lieu et place de l'irrigation de surface traditionnelle.

L'eau domestique est la première priorité en termes de gestion des ressources du bassin du fait de l'augmentation de cette demande en compensant par une diminution équivalente des prélèvements pour l'irrigation. Ainsi, les politiques futures doivent tenir compte des utilisateurs finaux des ressources hydriques. En particulier le domaine agricole, plus grand consommateur d'eau, a besoin d'un système d'informations précis et optimisé pour tous. Ceci passe également par une politique de soutiens en action de formations de la main d'œuvre, des propriétaires et des acteurs régionaux. Ces actions passent par le déploiement

de système d'irrigation moderne en accord avec une politique agricole réfléchi. Cela aidera à réduire la quantité des prélèvements par captage des eaux souterraines à des fins d'irrigation tout en augmentant l'efficacité des usages de l'eau.

En termes d'eau potable, du fait de ressources limitées dans la zone d'étude, la seule stratégie adaptée qui devrait être développée, est d'investir dans la protection et l'amélioration des techniques de prélèvements. L'analyse des coûts et conséquences du laisser-faire doivent conduire à modifier le modèle économique concernant la ressource afin de tendre vers une gestion régionale afin d'épargner les eaux à usage domestique.

La coordination entre les pays voisins ainsi que le partage des connaissances et d'expériences en matière de protection, de transfert et d'exploitation des ressources en eau, permettraient également d'améliorer significativement une gestion de l'eau concertée en zone semi-aride.

References

- Abed Rabboh, R. Water demand management, progress and policies: Proceedings of the 3rd Regional Workshop on Water and Sustainable Development in the Mediterranean. Zaragoza, Spain, 19 - 21 March 2007.
- Abou Zakhem, B.; Hafez, R. Climatic factors controlling chemical and isotopic characteristics of precipitation in Syria. *Hydrol Process.* **2010**, *24*, 2641-2654.
- Adar, E.M.; Dody, A.; Geyh, M.A.; Yair, A.; Yakirevich, A.; Issar, A.S. Distribution of stable isotopes in arid storms. I. Relation between the distribution of isotopic composition in rainfall and in the consequent runoff. *Hydrogeol J.* **1998**, *6*, 50-65.
- Aghazadeh, N.; Mogaddam A.A. Investigation of hydrochemical characteristics of groundwater in the Harzandat aquifer, Northwest of Iran. *Environ Monit Assess* **2011**, *176*,183-195.
- Al-Charideh, A. Environmental isotopic and hydrochemical study of water in the karst aquifer and submarine springs of the Syrian coast. *Hydrogeol J.* **2007**, *15*, 351-364.
- Al-Charideh, A. Environmental isotope study of groundwater discharge from the large karst springs in West Syria:a case study of Figehe and Al-sin springs. *Environ Earth Sci.* **2011**, *63*,1-10.
- Al-Charideh, A. Geochemical and isotopic characterization of groundwater from shallow and deep limestone aquifers system of Aleppo basin (north Syria). *Environ Earth Sci.* **2012^a** *65*, 1157-1168.
- Al-Charideh, A. Recharge rate estimation in the Mountain karst aquifer system of Figehe spring, Syria. *Environ Earth Sci.* **2012^b** *65*, 1169-1178.
- Al-Charideh, A.; Abou Zakhem, B. Distribution of tritium and stable isotopes in precipitation in Syria. *Hydrol Sci J.* **2010^a**, *55*, 832-843.
- Al-Charideh, A.; Abou-Zakhem, B. Geochemical and isotopic characterization of groundwater from the Paleogene limestone aquifer of the Upper Jezireh, Syria. *Environ Earth Sci.* **2010^b**, *59*, 1065-1078.
- Al-Charideh, A.; Hasan, A. Use of isotopic tracers to characterize the interaction of water components and nitrate contamination in the arid Rasafeh area (Syria). *Environ Earth Sci.* **2013**, *70*, 71-82.

- Alkhaier, F. Shallow groundwater effect on land surface temperature and surface energy balance: description, modeling, and remote sensing application. Ph.D. Thesis, University of Twente. The Netherlands, 2011.
- Alpert, P.; Krichak, D.O.; Sharif, H.; Haim, D.; Osetinsky, I. Climatic trends to extremes employing regional modeling and statistical interpretation over the E. Mediterranean. *Global planet change*. **2008**, *63*, 163-170.
- Anderson, M.P.; Woessner W.W. *Applied groundwater modeling, simulation of flow and advective transport*, Academic press, New York, USA, 1982.
- Anastasiadis, P. Vulnerability of groundwater to agricultural activities Pollution, Proceedings of the 8th International Conference on Environmental Science and Technology Lemnos Island, Greece, 8- 10 September. 2003. Full paper Vol. B, p: 24-30.
- Aouad-Rizk, A.; Job, J.-O.; Khalil, S.; Touma, T.; Bitar, C.; Boquillon, C.; Najem, W. Snow in Lebanon: A preliminary study of snow cover over Mount Lebanon and simple snowmelt model. *Hydrolog Sci J*. **2005**, *50* (3), 555-569.
- Appelo, C.A J.; Postma, D. *Geochemistry, Groundwater and Pollution*. A.A. Balkema, 1993, Rotterdam. The Netherlands.
- Appelo, C.A.J.; Postma, D. *Geochemistry, groundwater and pollution*. 1996, (p. 536). Rotterdam-Balkema.
- Appelo, C.A.J, Postma, D. *Geochemistry, Groundwater and Pollution*, 2nd edition. 2005, Amsterdam, The Netherlands.
- Asfahani, J.; Abdul Ghani, B. Automated interpretation of nuclear and electrical well loggings for basalt characterization (case study from southern Syria). *Appl Radiat Isot*. **2012**, *70*, 2500-2506.
- Asmael, N.M.; Huneau, F.; Garel, E.; Celle-Jeanton, H.; Le Coustumer, P.; Dupuy, A. Hydrochemistry to delineate groundwater flow conditions in the Mogher Al Mer area (Damascus Basin, Southwestern Syria). *Environ Earth Sci*. **2014**, *72*, 3205-3225.
- Aw-Hassan, A.; Rida, F.; Telleria, R.; Bruggeman, A. The impact of food and agricultural policies on groundwater use in Syria. *J. Hydrol*. **2014**, *513*, 204-215.
- Bajjali, W. Evaluation of groundwater in a three-aquifer system in Ramtha area, Jordan: recharge mechanisms, hydraulic relationship and geochemical evolution. *Hydrogeol J*. **2008**, *16*, 1193-1205.

- Bajjali, W. Recharge mechanism and hydrochemistry evaluation of groundwater in the Nuaimah Area, Jordan using environmental isotope techniques. *Hydrogeol J* **2006**, *14*, 180-191.
- Bakalowicz, M.; El Hakim, M.; El-Hajj, A. Karst groundwater resources in the countries of eastern Mediterranean: the example of Lebanon. *Environ Geol.* **2008**, *54*, 597-604.
- Barbieri, P.; Adami, G.; Favretto, A.; Lutman, A.; Avoscan, W.; Reisenhofer, E. Robust cluster analysis for detecting physicochemical typologies of freshwater from wells of the plain of Friuli (north-eastern Italy). *Anal Chim Acta* **2001**, *440*, 161-170.
- Barnes, C.J.; Allison, G.B. Tracing of water movement in the unsaturated zone using stable isotopes of hydrogen and oxygen. *J. Hydrol.* **1988**, *100*, 143-176.
- Bartov, Y.A. structural and paleogeographical study of central Sinai faults and domes, Ph.D. thesis, Hebrew Univ Jerusalem. 1974, 143 p.
- Bartov, Y.; Steinitz, G.; Eyal, Y. Sinistral movement along the Gulf of Aqaba - its age and relation to the opening of the Red Sea, (letter), *Nature* **1980**, *285*, 220-222.
- Batiot, C.; Emblanch, C.; Blavoux, B. Carbone organique total (COT) et magnésium (Mg^{+2}): deux traceurs complémentaires du temps de séjour dans l'aquifère karstique Total Organic Carbon (TOC) and magnesium (Mg^{+2}): two complementary tracers of residence time in karstic systems. *CR Geosci* **2003**, *335* (2): 205-214.
- Berkoff, J.A. Strategy for managing water in the Middle East and North Africa. WORLD BANK, WASHINGTON, D.C. (USA). 1994. 96 pp.
- Bicalho, CC.; Batiot-Guilhe, C.; Seidel, J.L.; Exter, S.V.; Jourde, H. Geochemical evidence of water source characterization and hydrodynamic responses in a karst aquifer. *J Hydrol.* **2012**, *450-451*: 206-218.
- Bijay-Singh.; Yadvinder-Singh.; Sekhon, G.S. Fertilizer-N use efficiency and nitrate pollution of groundwater in developing countries. *j contam hydrol.* **1995**, *20*, 167-184.
- Bredehoeft, J.D. The water budget myth revisited: why hydrogeologists model. *Groundwater.* **2002**, *4*, 340-345.
- Brielmann, H. Recharge and discharge mechanism and dynamics in the mountainous northern Upper Jordan River Catchment, Israel. Ph.D. Thesis, Ludwig-Maximilians-University, Munich, Germany, 2008.

- Burdon, D.J.; Safadi, C. Ras-El-Ain: The great karst spring of Mesopotamia, an hydrogeological study. *J Hyrol* **1963**, *1*, 58-95.
- Burdon, D.J.; Safadi, C. The Karst Groundwater of Syria. *J Hyrol* **1964**, *2*, 324-347.
- Capaccioni, B.; Didero, M.; Paletta, C.; Salvadori, P. Hydrochemistry of Groundwater from Carbonate Formation with Basal Gypsiferous Layers. *J Hydrol.* **2001**, *253*, 14-26.
- CBS (Central Bureau of Statistics), 2010. Statistical Abstract, 2003–2010. Central Bureau of Statistics, Damascus, Syria.
- Celle-Jeanton, H.; Gonfiantini, R.; Travi, Y.; Sol, B. Oxygen-18 variations of rainwater during precipitation: application of the Rayleigh model to selected rainfalls in Southern France. *J Hydrol.* **2004**, *289*, 165-177.
- Chiang, W.H.; Kinzelbach, W.; Rausch, R. Aquifer Simulation Model for Windows - Groundwater flow and transport modeling, an integrated program. 1998. 137 p. Berlin, Stuttgart (Borntraeger).
- Clark, I.D.; P. Fritz. Environmental isotopes in hydrogeology. New York, Lewis Publishers. 1997, 328 p.
- Coetsiers, M.; Walraevens, K. Chemical characterization of the Neogene Aquifer, Belgium. *Hydrogeol J.* **2006**, *14*, 1556-1568
- Craig, H. Isotopic variations in meteoric waters. *Science.* **1961**, *133*, 1702-1703.
- Dansgaard, W. Stable isotope in precipitation. *Tellus.* **1964**, *216*, 436-468.
- Datta, P.S, Tyagi, S.K. Major Ion Chemistry of Groundwater in Delhi Area: Chemical Weathering Processes and Groundwater Flow Regime. *J Geol Soc India.* **1996**, *47*, 179-188.
- Dehnavi, A.G.; Sarikhani, R.; Nagaraju, D. Hydro geochemical and rock water interaction studies in East of Kurdistan, N-W of Iran. *Int J Environ Sci Res* **2011**, *1*(1), 16-22.
- Deutsch, W.J. Groundwater geochemistry: fundamentals and application to contamination. 1997 CRC Press, Boca Raton.
- DHI-WASY GmbH. FEFLOW 6. Finite elements subsurface flow and transport simulation system. User's manual, Berlin. 2010.
- Dinçer, T.; Payne, B.R. An environmental isotope study of the south-western part karst region of Turkey. *J Hydrol.* **1971**, *14*, 233-258.
- Domenico, P.A.; Schwartz, F.W. Physical and chemical hydrogeology. (p. 824). 1990. New York.

- Drever, J.I. The Geochemistry of Natural Waters, Prentice-Hall, Upper Saddle River. 1988.
- Drever, J.I. The Geochemistry of Natural Waters: Surface and Groundwater Environments. 3rd ed., Prentice-Hall, Upper Saddle River, NJ. 1997, 436pp.
- Dubertret, L. L'Hydrologie et aperçu sur l'Hydrographie de la Syrie et du Liban dans leurs relations avec la géologie. Rev Géogr Phys Géol Dynamique. 1932, TVI fas.4.
- Eaid, E. Meteorological Conditions in Mediterranean Basin. General Meteorological Department. 2000, Damascus, Syria; 41.
- Edmunds, W.M.; Carrillo-Rivera, J.J.; Cardona, A. Geochemical evolution of groundwater beneath Mexico City. *Hydrogeol J.* **2002**, 258, 1-24.
- Edmunds, W.M.; Ma, J.Z.; Aeschbach-Hertig, W.; Kipfer, R.; Darbyshire, D.P.F. Groundwater recharge history and hydrogeochemical evolution in the Minqin Basin, North West China. *Appl Geochem.* **2006**, 21, 2148-2170.
- Edmunds, W.M.; KAY, R.L.F.; McCartney, R.A. Origin of saline groundwater in the carnmenellis granite (cornwall, england): natural processes and reaction during hot dry rock reservoir circulation. *Chem Geol.* **1985**, 49, 287-301.
- Edmunds, W.M.; Smedley, P.L. Residence time indicators in groundwater: the East Midlands Triassic sandstone aquifer. *Appl Geochem.* **2000** 15, (6), 737-752.
- Elango, L. Numerical Simulation of Groundwater Flow and Solute Transport, 1st ed. 2005. New Delhi, India.
- El-Asrag, A.M. Effect of synoptic and climatic situations on fractionation of stable isotopes in rainwater over Egypt and east Mediterranean. 2005. IAEA-TECDOC-1453. 51–73.
- Elhadj, E. The household water crisis in Syria's Greater Damascus Region. 2004. School of Oriental & African Studies and King's College London, University of London.
- El-Hakim, M.; Bakalowicz, M. Significance and origin of very large regulating power of some karst aquifers in the Middle East. Implication on karst aquifer classification. *J Hyrol.* **2007**, 333, 329-339.
- Enwright, N.; Hudak, P.F. Spatial distribution of nitrate and related factors in the High Plains Aquifer, Texas. *Environ Geol.* **2009**, 58, 1541-1548.
- Fairchild, I.J.; Borsato, A.; Tooth, A.F.; Frisia, S.; Hawkesworth, C.J.; Huang, Y.; McDermott, F.; Spiro, B. Controls on trace element (Sr-Mg) compositions of

- carbonate cave waters: implications for speleothem climatic records. *Chem Geol.* **2000**, *166* (3–4), 255-269.
- FAO (Food and Agriculture Organization of the United Nations). 2012. AQUASTAT: <http://www.fao.org/nr/water/aquastat/main/index.stm> (accessed on 11 February 2013).
 - Flakova, R. Formation and changes of groundwater chemical composition of the Western Carpathian carbonate systems. *ACTA Geologica Universitatis Comenianae* Nr. 53, 5 – 25. 1998. Bratislava, Slovakia.
 - Freeze, R.A.; Cherry, J.A. Groundwater. Published by: Prentice-Hall, Englewood Cliffs, N.J. 1979.
 - Freund, R.A. Model of the structural development of Israel and adjacent areas since Upper Cretaceous times. *Geol Mag.* **1965**, *102*, 189-205.
 - Fritz, P.; Suzuki, O.; Silva, C.; Salati, E. Isotope hydrology of groundwater in the Pampa del Tamarugal, Chile. *J Hydrol.* **1981**, *53*, 161-184.
 - Fröhlich, C.J. Water: Reason for Conflict or Catalyst for Peace? The Case of the Middle East. *L'Europe en Formation.* **2012**, *365*, 139-161. DOI: 10.3917/eufor.365.0139.
 - Frumkin, A.; Shimron, A.E.; Miron, Y. Karst morphology across steep climate gradient southern Mount Hermon. Israel. *Z Geomorphol.* **1998**, *109*, 23-40.
 - Garfunkel, Z. Internal structure of the Dead Sea leaky transform (Rift) in relation to plate kinematics. *Tectonophysics.* **1981**, *80*, 81-108.
 - Garfunkel, Z. Tectonic setting of Phanerozoic magmatism in Israel. *Isr. J. Earth Sci.* **1989**, *38*, 51-74.
 - Gat, J.R. Comments on the stable isotope method in regional groundwater investigations. *Water Resour Res.* **1971**, *7*, 980-993.
 - Gat, J.R.; Matsui, E. Atmospheric water balance in the Amazon Basin. An isotopic evapo-transpiration model. *J Geophys Res.* **1991**, *96*, 13179-13188
 - Guendouz, A.; Moulla, A. S.; Edmunds, W.M.; Zouari, K.; Shand, P.; Mamou, A. Hydrogeochemical and isotopic evolution of water in the Complexe Terminal aquifer in the Algerian Sahara. *Hydrogeol J.* 2003, *11*, 483-495.
 - Guler, C.; Thyne, G.D. Delineation of hydrochemical facies distribution in a regional groundwater system by means of fuzzy c-means clustering. *Water Resour Res.* **2004**^a, *40*, 1-11.

- Guler, C.; Thyne, G.D. Hydrologic and geologic factors controlling surface and groundwater chemistry in Indian Wells-Owens Valley area, southeastern California, USA. *J Hydrol* 2004^b 285, 177-198.
- Guler, C.; Thyne, G.D.; McCray, J.E.; Turner, K.A. Evaluation of graphical and multivariate statistical methods for classification of water chemistry data. *Hydrogeol J* **2002**, 10, 455-474.
- Han, G.; Liu, C. Water geochemistry controlled by carbonate dissolution: a study of the river waters draining karst-dominated terrain, Guizhou Province, China. *Chem Geol* **2004**, 204, 1-21.
- Hartmann, A. Process-based modeling of karst springs in Mt. Hermon, Israel. Ph.D. Thesis. 2008 Albert-Ludwigs-Universität Freiburg im Breisgau, Breisgau, Germany.
- Heathcote, J.A.; Lloyd, J.W. Factors affecting the isotopic composition of daily rainfall at Driby, Lincolnshire. *J Climatol.* **1986**, 6 (1), 97-106.
- Hem, J.D. Study and interpretation of the chemical characteristics of natural water, 3rd Edn. 1985 U.S. Geol. Surv. Water Supply Paper: 2254.
- Higano, Y.; Melhem, R. Endogenous derivation of the optimal policy measures to improve the water quality in the Barada Basin, Syria. 2002, In: ERSa conference papers. RePEc:wiiw:wiwrsa:ersa02p249.
- Hsu, K.J. Solubility of dolomite and the composition of Florida groundwater. *J Hydrol.* **1963**, 1, 288-310.
- INECO. Studies and Integration Consulting (2009) Institutional framework and decision-making practices for water management in Syria. Towards the development of strategy for water pollution prevention and control in the Barada River Basin, Greater Damascus area. Contract No: INCO-CT-2006-517673.
- Integrated Regional Information Networks (IRIN). Syria: Drought pushing millions into poverty. Damascus 9 September 2010. Available at <http://www.irinnews.org/Report/90442/SYRIA-Drought-pushing-millions-into-poverty>.
- IPCC, Climate Change. The Scientific Basis, Contribution of WG I to the Third Assessment Report of the Intergovernmental Panel on Climate Change. 2001. Cambridge Univ. Press.
- Issar, A.S. Climatic Changes and Water Resources in the Middle East and North Africa 2008. Book, pp: 145-164. DOI: 10.1007/978-3-540-85047-2_12
- Izbicki, J.A.; Borchers, J.W.; Leighton, D.A.; Kulongoski, J.; Fields, L.; Galloway, D.L.; Michel, R.L. Hydrogeology and Geochemistry of Aquifers Underlying the

- San Lorenzo and San Leandro Areas of the East Bay Plain, Alameda County, California. 2003. U.S. Geological Survey, Water-Resources Investigations Report 02-4259.
- Jianhua, S.; Qi, F.; Xiaohu, W.; Yonghong, S.; Haiyang, X.; Zongqiang, C. Major ion chemistry of groundwater in the extreme arid region northwest China. *Environ Geol* **2009**, *57* 1079-1087.
 - JICA (Japan International Cooperation Agency) The study on water resource development in Northern and Central Basins in the Syrian Arab Republic: final report. 1997, Nippon Koei, Tokyo.
 - JICA (Japan International Cooperation Agency). The study of water resources development in the western and central basins in Syrian Arab Republic, phase I. 2001, unpublished report, in Arabic.
 - Jumaa, V.; Naji, M.; Pala, M. Review paper on optimizing soil water use in Syria. 1999. In: Van Dulmkwden, N.; Pala, M.; Studer, C.; Bieldes, C.L. (eds) Proceedings of workshop on efficient soil water use. Soil Water Use Consortium, Niamey, Niger, 26-30 April 1998; Amman, Jordan.
 - Kaisi, A.; Al-Chayeb, R.; Al-Zoughbi, S. Water resources in Syria: management, development and women role. 2006. 3rd Arab Water Regional Conference: Research Advancement in Managing Monitoring and Evaluation Limited Water Resources.
 - Kattan, Z. Chemical and environmental isotopes study of precipitation in Syria. *J Arid Environ.* **1997**^a *35*, 601-615
 - Kattan, Z. Environmental isotope study of the major karst springs in Damascus limestone aquifer systems: case of the Figeih and Barada springs. *J Hydrol.* **1997**^b *193*, 161-182.
 - Kattan, Z. Characterization of surface water and groundwater in the Damascus Ghotta basin: hydrochemical and environmental isotopes approaches. *Environ Geol.* **2006** *51*, 173-201.
 - Kattan, z.; Kadkoy, N.; Nasser, S. Effects of artificial recharge via injection wells on groundwater quality in a shallow alluvial aquifer, central Damascus Basin. ISMAR, MAR, in Arid Environment. 7th International Symposium, 9-13 October 2010, Abu Dhabi, UAE.
 - Kattan, z. Estimation of evaporation and irrigation return flow in arid zones using stable isotope ratios and chloride mass-balance analysis: Case of the Euphrates River, Syria. *j. arid environ.* **2008**, *72*, 730-747.

- Kennedy, V.C. Silica variations in stream water with time and discharge. In: Hem, J. D. (Ed.). Nonequilibrium systems in natural water chemistry. Advances in Chemistry Series American Chemical Society, Washington, DC, 1971, pp. 106-130.
- Kløve, B.; Ala-Aho, P.; Bertrand, G.; Gurdak, J.J.; Kupfersberger, H.; Kvaerner, J.; Muotka, T.; Mykrä, H.; Preda, E.; Rossi, P.; Uvo, C. B.; Velasco, E.; Pulido-Velazquez, M. Climate change impacts on groundwater and dependent ecosystems. *J. Hydrol.* **2013**, *518*, 250-266.
- Konikow, L.; Kendy, E. Groundwater depletion: a global problem. *Hydrogeol J.* **2005**, *13*, 317-320.
- Kortatsi, B.K. Hydrochemical framework of groundwater in the Ankobra Basin, Ghana. *Aquat Geochem.* **2007**, *13*, 41-74.
- Krige, D.G. A statistical approach to some basic mine valuation problems on the Witwatersrand. *J Chem Metall Min Soc S Afi.* **1951**, *52*, 119-139.
- Kubota, T.; Tsuboyama, Y. Estimation of evaporation rate from the forest floor using oxygen-18 and deuterium composition of throughfall and stream water during a non-storm runoff period. *J Forest Res.* **2003**, *9*(1), 51-59.
- Kumar, C. P. Climate Change and Its Impact on Groundwater Resources. *Ent J Eng Sci.* **2012**, *1*(5), 43-60.
- Kumar, M.; Ramanathan, A.L.R.; Kumar, M.S.B. Identification and evaluation of hydrogeochemical processes in the groundwater environment of Delhi, India. *Environ Geol.* **2006**, *50*, 1025-1039.
- La-Moreaux, P.E.; Hughes, T.H.; Memon, B.A.; Lineback, N. Hydrogeologic assessment-Figeh Spring, Damascus, Syria. *Environ Geol Water Sci* **1989**, *13* (2), 73-127.
- Langmuir, D. Aqueous environmental geochemistry (p. 601). Prentice Hall, Inc. 1997
- Langmuir, D. The geochemistry of some carbonates groundwater in central Pennsylvania. *Geochim Cosmochim Ac.* **1971**, *35*, 1023-1045.
- Lawrence, A.R.; Gooddy, D.C.; Kanatharana, P.; Meesilp, M.; Ramnarong, V. Groundwater evolution beneath Hat Yai, a rapidly developing city in Thailand. *Hydrogeol J.* **2000**, *8*, 564-575.
- Litaor, M. I.; Brielmann, H.; Reichmann, O.; Shenker, M. Hydrochemical analysis of groundwater using a tree-based model. *J Hydrol.* **2010**, *387*, 273-282.

- López-Chicano, M.; Bouamama, M.; Vallejos, A.; Pulido-Bosch, A. Factors which determine the hydrogeochemical behaviour of karstic springs. A case study from the Betic Cordilleras, Spain. *Appl Geochem* **2001**, *16* (9–10): 1179-1192.
- Luijendijk, E.; Bruggeman, A. Groundwater resources in the Jabal Al Hass region, northwest Syria: an assessment of past use and future potential. *Hydrogeol J* **2008**, *16*, 511-530. doi: 10.1007/s10040-008-0282-5.
- Lubczynski, M. W.; Gurwin, J. Integration of various data sources for transient groundwater modeling with spatio-temporally variable fluxes - sardon study case, Spain. *J Hydro.* **2005**, *1306*, 71–96.
- Ma, J.Z.; Wang, X.S.; Edmunds, W.M. The characteristics of groundwater resources and their changes under the impacts of human activity in the arid Northwest China, a case study of the Shiyang River Basin. *J Arid Environ.* **2005**, *61*:277-295.
- Ma, J.Z.; Edmunds, W.M. Groundwater and lake evolution in the Badain Jaran desert ecosystem, Inner Mongolia. *Hydrogeol J.* **2006**, *14*, 1231-1243.
- MAAR (Ministry of Agriculture and agrarian reform) syrian agriculture database. 2006. Damascus, Syria.
- Mahmoudzadeh M.R.; Francés, A.P.; Lubczynski. M.; Lambot. S. Using Ground Penetrating Radar to investigate the water table depth in weathered granites - Sardon case study, Spain. *J Appl Geophys.* **2012**, *79*, 17-26.
- Malkawi, A.H.; Liang, R.Y.; Nusairat, J.H.; Al-Homoud, A.S. Probabilistic Seismic Hazard Zonation of Syria. *Nat Hazards.* **1995**, *12*, 139-151.
- Matthes, G. Properties of groundwater. Wiley, 1982. New York. Translated by John C. Harvey.
- McMahan, P.B.; Böhlke, J.K.; Christenson, S.C. Geochemistry, radiocarbon ages, and paleorecharge conditions along a transect in the central High Plains aquifer, southwestern Kansas, USA. *Appl Geochem.* 2004, *19* (11), 1655-1686
- Melhem, R.; Higano, Y. Policy measures for river water management in Barada Basin, Syria. *Stud Region Sci.* 2001 *32*, 1-23, DOI:10.2457/srs.32.3_1.
- Merlivat, L.; Jouzel, J. Global climatic interpretation of deuterium-oxygen 18 relationship for precipitation. *J Geophys Res.* **1979**, *84*, 5029-5033.
- MOI. Annual Water Resources Report of Barada and Awaj Basin, Damascus, Syria. 2005. (In Arabic), (Unpublished report).
- MOI, Hermon Project Report. 1994. (In Arabic).

- Mor, D. A time-table for the Levant Volcanic Province, according to K-Ar dating in the Golan Heights, Israel. *J Afr Earth Sci.* **1993**, *16*, 223-234.
- Moral, F.; Cruz-Sanjulián, J.J.; Olías, M. Geochemical evolution of groundwater in the carbonate aquifers of Sierra de Segura (Betic Cordillera, southern Spain). *J Hydrol.* **2008** *360*, 281-296.
- Mourad, K.A.; Berndtsson, R. Water Status in the Syrian Water Basins. *Open J Mod Hydrol.* **2012**, *2*, 15-20.
- Mourad, K.A.; Berndtsson, R. Syrian Water Resources between the Present and the Future. *Air, Soil Water Res* **2011**, *4*, 93-100. DOI: 10.4137/ASWR.S8076.
- Mouty, M.; Delalaye, M.; Fontignie, D.; Piskin, O.; Wagner, J.J. The volcanic activity in Syria and Lebanon between Jurassic and Actual. *Schweiz mineral und petrogr Mitt.* **1992**, *72*, 91-105.
- Nativ, R.; Mazor, E. Rain events in an arid environment-their distribution and ionic and isotopic composition patterns: Makhtesh Ramon Basin. *Israel Journal of Hydrology.* **1987**, *89*, 205-237.
- Nir, A. Development of isotope methods applied to groundwater hydrology. *Proceedings of a Symposium on Isotope Techniques in the Hydrological Cycle.* Am Geophys Union Monogr Series. 1967 no° 11, pp 1-109.
- Obeidat, M.M.; Awawdeh, M.; Abu Al-Rub, F. Multivariate statistical analysis and environmental isotopes of Amman/Wadi Sir (B2/A7) groundwater, Yarmouk River Basin, Jordan. *Hydrol Process.* **2013**, *27*, 2449-2461.
- Parkhurst, D.L.; Appelo, C.A.J PHREEQC for windows version 1.4.07. A hydrogeochemical transport model. 1999. U.S. Geological Survey Software.
- Piper, A.M. A graphic procedure in the geochemical interpretation of water analyses. *Trans Amer Geophys Union.* **1944**, *25*, 914-923.
- Plummer, L.N. Defining reactions and mass transfer in part of the Floridan aquifer. *Water Resour Res* **1977**, *13* (5), 801-812.
- Plummer, L.N.; Wigley, T.M.L.; Parkhurst, D.L. The kinetics of calcite dissolution in CO₂ water systems at 5–60 C° and 0.0–1.0 atm CO₂. *Am J Sci* **1978**, *278* (2) 179-216.
- Plummer, L.N.; Busby, J.F.; Lee, R.W.; Hanshaw, B.B. Geochemical Modeling of the Madison Aquifer in parts of Montana, Wyoming, and south Dakota. *Water Resour Res.* **1990**, *26* (9): 1981-2014.

- Ponikarov, V.O. The geology of Syria, explanatory notes on the map of Syria, Scale 1:500,000. Part II. Mineral deposits and underground water resources 1967 Technoexport, Moscow.
- Quennell, M. Tectonics of the Dead Sea Rift. 20th International Geological Congress. Mexico, *Assoc Serv Geol Africa*. **1959**, pp: 385-405.
- Rakhmatullaev, S.; Huneau, F.; Kazbekov, J.; Celle-Jeanton, H.; Motelica-Heino, M.; Le Coustumer, P.; Jumanov, J. Groundwater resources of Uzbekistan: an environmental and operational overview. *Cent Eur J Geosci* **2012**, *4*, 67-80.
- RDWSSA (Damascus Rural Water Supply and Sanitation Authority, Damascus, Syria) Interim Report - Hydrogeological study of Mogher Al Mer area. 2006, Damascus rural water and sanitation project (Unpublished report, in Arabic),.
- Ribolzi, O.; Andrieux, P.; Valles, V.; Bouzigues, R.; Bariac, T.; Voltz, M. Contribution of groundwater and overland flows to storm flow generation in a cultivated Mediterranean catchment. Quantification by natural chemical tracing. *J Hydrol*. **2000**, *233*, 241-257.
- Rimmer, A.; Salinger, Y. Modelling precipitation-streamflow processes in karst basin: The case of the Jordan River sources, Israel. *J Hydrol* **2006**, *331*, 524-542.
- Rindsberger, M.; Jaffe, S.; Rahamim, S.; Gat, J.R. Patterns of the isotopic composition of precipitation in time and space: data from the Israeli storm water collection program. *Tellus*. **1990**, *42B*, 263-271.
- Rosegrant, M.W.; Cline, S.A. Global food security: challenges and policies. *Sci*. **2003**, *302*, 1917-1919. DOI: 10.1126/science.1092958.
- Saad, Z.; Kazpard, V.; El Samrani, A.G, Slim, K. Chemical and isotopic composition of rainwater in coastal and highland regions in Lebanon. *J Environ Hydrol*. **2005**, *13*.
- Scanlon, B.R.; Keese, K.E.; Flint, A.L.; Flint, L.E.; Gaye, C.B.; Edmunds, W.M.; Simmers, I. Global synthesis of groundwater recharge in semiarid and arid regions. *Hydrol. Process*. **2006**, *20*, 3335-3370.
- Schoeller, H. Geochemie des eaux souterraines. Application aux eaux des gisements de petrole. Soc Ed Technip, Paris. 1956, 213 pp.
- Seiler, K.P.; Gat, J.R. Groundwater recharge from run-off and infiltration. 2007, 241pp. Springer Verlag, Dordrecht. DOI: 10.1007/978-1-4020-5306-1

- Selkhozpromexport. Water resources use in Barada and Awaj Basins for irrigation of crops, Syria Arab Republic. 1986. USSR. Ministry of Land Reclamation and Water Management, Moscow.
- Shimron, A.E. Tectonic evolution of the southern Mount Hermon. Report Geol Surv Isr Rep GSI. 1998, 10, 98.
- Stadler, S.; Geyh, M.A.; Ploethner, D.; Koeniger, P. The deep Cretaceous aquifer in the Aleppo and Steppe basins of Syria: assessment of the meteoric origin and geographic source of the groundwater. *Hydrogeol J.* **2012**, *20* 1007-1026.
- Stiff, H.A. The Interpretation of Chemical Water Analysis by Means of Patterns. *J Petrol Technol.* **1951** 3(10).
- Stumm, W.; Morgan, J.J. Aquatic chemistry; an introduction emphasizing chemical equilibria in natural waters. 1981, Wiley, New York.
- Stuyfzand, P.J. A new hydrochemical classification of water type. IAHS Red books 1989, 182: 89-98
- Su, G.W.; Jasperse, J.; Seymour, D.; Constantz, J. Estimation of Hydraulic Conductivity in an Alluvial System Using Temperatures. *Groundwater.* **2004**, *42*, 890-901.
- Suk, H.; Lee, K-K. Characterization of a ground water hydrochemical system through multivariate analysis: Clustering into groundwater zones. *Groundwater.* **1999**, *37*, 358-366.
- Suppan, P.; Kunstmann, H.; Heckl, A.; Rimmer, A. Climatic Changes and Water Resources in the Middle East and North Africa. 2008. Book, pp: 47-58. DOI: 10.1007/978-3-540-85047-2_12.
- Taylor, C.B.; Roether, W. A uniform scale for reporting low-level tritium in water. Methods of low-level counting and spectrometry. 1982 Vienna, International Atomic Energy Agency, p: 303-323.
- United Nations Groundwater in the Eastern Mediterranean and Western Asia, natural resources, water series 1982. n° 9, United Nations, New York.
- U.S. Department of Agriculture (USDA), Foreign Agricultural Service Middle East and Central Asia: Continued drought in 2009/2010 threatens greater food grain shortages. 2008, available at http://www.pecad.-fas.usda.gov/highlights/2008/09/mideast_cenasia_drought/, accessed 16 September.

- Varol, S.; Davraz, A. Assessment of geochemistry and hydrogeochemical processes in groundwater of the Tefenni plain (Burdur/Turkey). *Environ Earth Sci.* **2014**, *71*, 4657-4673.
- Vengosh, A.; Rosenthal, E. Saline groundwater in Israel: its bearing on the water crisis in the country. *J Hydrol.* **1994**, *156*, 389-430.
- Voss, K. A.; Famiglietti, J.S.; Lo, M.; de Linage, C.; Rodell, M.; Swenson, S.C. Groundwater depletion in the Middle East from GRACE with implications for transboundary water management in the Tigris-Euphrates-Western Iran region. *Water Resour Res.* **2013**, *49*, 904-914.
- Wen, X.; Wu, Y.; Zhang, Y.; Liu, F. Hydrochemical characteristics and salinity of groundwater in the Ejina basin, northwestern China. *Environ Geol.* **2005**, *48*, 665-675.
- White, W. *Geomorphology and Hydrology of Karst Terrains*. Oxford Univ. Press, New York. 1988, 464 pp.
- Wilson, M.; Shimron, A.E.; Rosenbaum, J.M.; Preston, J. Early Cretaceous magmatism of Mount Hermon, Northern Israel. *Contributions to Mineralogy and Petrology. Contrib Mineral Petr.* **2000**, *139*, 54-67.
- Wolfart, R. Hydrogeology of the Damascus Basin (southwest-Syria). *Internat, Assoc. Sci. Hydrology.* **1964**, *64*, 402-413.
- Yurtsever, Y.; Gat, J.R. Atmospheric waters. Stable isotopes hydrology, deuterium and oxygen-18 in the water cycle. 1981, IAEA, Vienna, Tech Rep Ser no 210.
- Zhou, Y.; Zwahlen, F.; Wang, Y.; Li, Y. Impact of climate change on irrigation requirements in terms of groundwater resources. *Hydrogeol J*, **2010**, *18*, 1571-1582.
- Zhu, G.F.; Li, Z.Z.; Su, Y.H.; Ma, J.Z.; Zhang, Y.Y. Hydrogeochemical and isotope evidence of groundwater evolution and recharge in Minqin Basin, Northwest China. *J Hydrol.* **2007**, *333*, 239-251.

Supplemental data tables

Supplementary data table associated with this thesis can be found in below:

Table 3 - 1 List of sampling sites and chemical composition of water samples collected during November and December 2006 and the historical data based on Selkhozpromexport study performed on 1986.

Name	Location	Date	Type	EC μS/cm	pH (-)	T (C°)	Na ⁺ (mg/L)	K ⁺ (mg/L)	Mg ²⁺ (mg/L)	Ca ²⁺ (mg/L)	Cl ⁻ (mg/L)	HCO ₃ ⁻ (mg/L)	SO ₄ ²⁻ (mg/L)	NO ₃ ⁻ (mg/L)	SiO ₂ (mg/L)	σ (%)	Water type (Stuyfzand)
Artesian well	Arneh	Dec-06	W	660	7.5	14.4	4.9	0	20	120	5.7	238	196.5	4	6.6	-2.6	g2-CaSO4
drink well	Harfa	Nov-06	W	462	7.3	17.8	15.6	13.8	4	67	24.2	162.3	9.6	49.7	14.4	4.0	g2-CaHCO3
Artesian well	Harfa	Nov-06	W	431	7.8	15.5	10.9	5.7	23	31	7.7	244	0.7	0.4	10.2	-2.2	g2-MgHCO3
well6	Heneh	Nov-06	W	570	7.6	18.7	20.7	1	25	59	29.1	223.3	63	25.1	22.6	-2.3	g2-CaHCO3
well1	Heneh	Nov-06	W	443	7.3	17.4	9.2	0	10	72	14.1	231.8	9.5	15.4	26.6	1.9	g2-CaHCO3
well5	Heneh	Nov-06	W	708	7.2	18.4	22.3	2	16	101	36.5	247.7	42.6	66	18.8	2.4	F3-CaHCO3
MJ Alshekh	Heneh	Nov-06	W	681	7.3	13.4	20.3	1.1	14	106	43.1	253.8	47	59.8	15.6	0.1	F3-CaHCO3
well1	Kleaa	Dec-06	W	530	7.2	17.2	16.4	3.7	10	87	24	264.7	14.7	22	14	2.6	g3-CaHCO3
well2	Kleaa	Dec-06	W	532	7.3	16.9	11.9	1.7	11	94	35.6	249	8	24.6	11.4	4.4	F3-CaHCO3
well3	Kleaa	Dec-06	W	685	7.4	17.5	30.3	2.7	15	98	47	234.2	69.1	22.4	13	4.0	F2-CaHCO3
well1	Remeh	Dec-06	W	350	7.5	13.1	3.3	0	3	65	5.9	207.4	5.2	9.6	5.6	-2.7	g2-CaHCO3
well1	Dorbol	Nov-06	W	480	7.5	13.6	7.8	0	6	86	17.2	253.8	11.7	11.4	24.2	0.5	g3-CaHCO3
well2	Dorbol	Nov-06	W	430	7.3	14.8	5.8	0	5	86	7.4	261	5.4	5.3	22	2.9	g3-CaHCO3
well1	Drossha	Dec-06	W	424	7.4	18.4	7.5	1.4	8	75	12	211.1	15.7	17.5	10.2	4.0	g2-CaHCO3
well2	Heneh	Nov-06	W	842	7	18.2	42.8	15.5	21	106	29.3	414	59	35.2	31.6	-0.7	g3-CaHCO3
well1	Knaker	Dec-06	W	418	7.7	17.4	22.6	1.7	12	53	22	196.4	19.6	15.8	15	1.8	g2-CaHCO3
well2	Knaker	Dec-06	W	386	7.6	18.3	12.2	1.5	12	58	16.7	197.6	11.6	15	12.8	3.1	g2-CaHCO3

well3	Knaker	Dec-06	W	378	7.4	16.1	13.3	1.8	8	56	16.5	183	12.5	13.6	13.2	1.7	g2-CaHCO3
well4	Knaker	Dec-06	W	387	7.5	17.1	14.8	1.8	9	63	14	198.9	8.9	21.1	12.8	4.6	g2-CaHCO3
well1	Saasaa	Nov-06	W	685	7.3	16.6	14	2.3	11	100	103.6	213.5	5.7	22.8	12.6	-2.6	F2-CaHCO3
well2	Saasaa	Dec-06	W	633	7.5	17.2	17.2	2	11	99	35.4	294	43	18	12.8	-2.7	F3-CaHCO3
well3	Saasaa	Dec-06	W	625	7.2	17.1	15.6	2	12	108	30.5	274.5	59.6	16.3	13	1.8	F3-CaHCO3
well4	Saasaa	Dec-06	W	542	7.3	15.7	14	1.8	8	87	34.5	262.3	12.1	34.8	11	-3.8	F3-CaHCO3
well5	saasaa	Dec-06	W	515	7.2	15.1	11.7	1.5	9	90	21.5	280.6	21.2	27.3	11.8	-2.7	g3-CaHCO3
well6	Saasaa	Dec-06	W	551	7.2	16.1	12.7	1.6	9	97	16.7	283	7.1	37.4	12.4	2.7	g3-CaHCO3
well7	Saasaa	Dec-06	W	350	7.6	17.9	17.2	1.7	5	53	13	190.3	6.3	6.6	11	1.7	g2-CaHCO3
well8	Saasaa	Dec-06	W	430	7.4	18.6	13	1.9	7	58	34.6	48.8	5.2	154.4	11.6	-3.4	F0-CaNO3
well9	Saasaa	Dec-06	W	434	7.7	18.9	27.7	2.4	7	50	36.6	163.5	10.6	30.4	13	-1.0	F2-CaHCO3
well10	Saasaa	Dec-06	W	385	7.5	17.1	13.9	1.9	6	55	19.1	176.9	4.9	9.2	10.6	2.7	g2-CaHCO3
well12	Saasaa	Dec-06	W	443	7.7	17.1	29.6	2.3	6	65	29.9	219.6	9.5	6.6	11.4	3.5	g2-CaHCO3
well14	Saasaa	Dec-06	W	410	7.4	16.6	10.1	2.3	7	66	19.8	194	7	14.5	11.6	3.0	g2-CaHCO3
well15	Saasaa	Dec-06	W	510	7.5	16.6	17.6	2.1	10	70	37.1	224.5	13	12.3	13.2	-0.6	F2-CaHCO3
well16	Saasaa	Dec-06	W	482	7.4	17.4	12.3	2.3	7	76	31.4	207.4	10.2	31.2	12.2	-0.4	F2-CaHCO3
well17	saasaa	Dec-06	W	587	7.1	17.7	15.1	0	10	98	23.7	275.7	13.6	32.6	13.6	3.1	g3-CaHCO3
well18	Saasaa	Dec-06	W	535	7.2	16.4	16.1	3	9	89	21.4	272.1	14.4	29	13.4	1.1	g3-CaHCO3
well19	Saasaa	Dec-06	W	557	7.1	17.1	17.2	5.9	10	93	22.2	285.5	16.6	26.4	14	2.4	g3-CaHCO3
well21	Saasaa	Dec-06	W	688	7.2	16.5	11.2	2	12	116	103.2	236.7	6	22	13.2	0.3	F2-CaHCO3
well22	Saasaa	Dec-06	W	510	7.3	18.2	10.3	1.7	11	87	41.9	225.7	7.9	23.8	12.4	2.8	F2-CaHCO3
well23	Saasaa	Dec-06	W	791	7.1	17.5	16	2.4	16	91	95.5	174.5	39.1	30.8	13.6	-1.9	F2-CaMIX
well3	Dorbol	Nov-06	W	560	7.4	14.2	7.4	0	5	107	22.8	274.5	18.2	17.6	14.2	2.3	g3-CaHCO3
well2	AboKaook	Dec-06	W	506	7.2	15.7	10.1	3.8	9	93	14.7	256.2	23.5	25.5	11.6	3.6	g3-CaHCO3
well3	AboKaook	Dec-06	W	466	7.3	15.6	10.4	2.1	8	85	16	246.4	15	21.1	11.8	2.6	g3-CaHCO3
well6	BeitSaber	Nov-06	W	756	6.6	15.6	17.8	1.1	17	121	41.8	246.4	87.2	35.2	10.6	4.3	F3-CaHCO3
well2	BeitTima	Nov-06	W	710	6.7	16.7	10.5	1.2	23	121	12.9	224.5	174.6	21.6	14.6	2.7	g2-CaMIX
well3	BeitTima	Nov-06	W	930	6.5	16.7	9.1	1.6	24	167	18.7	285.5	250.7	6.2	10.6	1.2	g3-CaSO4
well1	Hosenieh	Dec-06	W	648	7.2	17	13.5	1.6	15	99	23.7	292.8	52.8	43.6	11.4	-3.5	g3-CaHCO3

well2	Hosenieh	Dec-06	W	587	7.3	18.4	10.2	1.2	11	96	19.5	242.8	56.2	32.6	10.6	-0.5	g2-CaHCO3
well3	Hosenieh	Dec-06	W	582	7.3	18.7	10.4	1.2	11	90	19.9	240.3	63	24.6	11.4	-2.9	g2-CaHCO3
well1	Tabibieh	Nov-06	W	624	7.5	16.3	10.3	1.1	13	104	23.6	240.3	87.3	27.7	9.6	-1.0	g2-CaHCO3
well1	Ainashara	Nov-06	W	440	7.3	17.9	8.8	0	10	76	9.3	253.8	5	4.4	27	4.3	g3-CaHCO3
well4	BeitSaber	Nov-06	W	588	7.2	14.6	15.2	2.1	13	97	22.4	296.5	15.6	26.4	13.8	3.1	g3-CaHCO3
well5	BeitSaber	Nov-06	W	646	7.2	17.3	14.1	1.6	14	102	22.7	251.3	90.4	31.7	11.8	-1.9	g3-CaHCO3
well7	BeitSaber	Dec-06	W	473	7.3	15.9	11.5	1.7	7	81	11.8	240.3	17.3	17.6	11.8	2.5	g2-CaHCO3
well9	BeitSaber	Dec-06	W	855	7.3	18.8	22.9	0.6	21	140	66.4	198.9	179.8	34.8	19.6	1.7	F2-CaMIX
well1	KaferHour	Nov-06	W	818	7.5	13.3	13	0.8	25	146	14.7	211	314.9	23.8	11	-5.0	g2-CaSO4
well2	KaferHour	Nov-06	W	697	7.5	18.9	11	0	20	116	19.6	240.3	162	19.4	16.4	-1.8	g2-CaMIX
well3	KaferHour	Nov-06	W	673	7.3	19.1	14.8	0.7	17	97	25.1	248.9	78	38.7	17.4	-1.0	g3-CaHCO3
well1	Khazrajeh	Dec-06	W	578	7.1	17.2	11	3.1	9	95	22.8	284.3	11.9	26	13.2	0.6	g3-CaHCO3
well3	MogherAlMer	Nov-06	W	560	7.4	18	10.4	0	13	85	20.8	297.7	13.9	29.9	12.6	-4.1	g3-CaHCO3
well2	Tabibieh	Dec-06	W	662	7.1	17.9	12.6	1.8	15	115	27.9	261.1	89.2	30.8	12	1.0	g3-CaHCO3
well1	Talmasiat	Nov-06	W	385	7.4	17	7.1	1.5	7	60	8.7	207.4	6.7	18.9	9.8	-2.2	g2-CaHCO3
well2	Talmasiat	Nov-06	W	466	7.4	15.4	6.7	1.3	7	77	8.9	244.1	9.5	23.7	9.2	-0.9	g3-CaHCO3
well1	KhanElshekh	Dec-06	W	407	7.4	17.9	9	1	5	73	15.9	203.7	8.3	21.7	10.6	1.9	g2-CaHCO3
well2	KhanElshekh	Dec-06	W	625	6.8	17.9	9	1.1	15	128	19.6	274.5	100.6	29.5	11.2	2.9	g3-CaHCO3
well4	KhanElshekh	Dec-06	W	443	7.5	19.2	8.6	0.7	5	84	16.1	219.6	16.6	18.9	10.2	3.1	g2-CaHCO3
well7	KhanElshekh	Dec-06	W	575	7.1	17.6	11.5	1	13	102	24.8	295.2	26.6	21.6	10.8	2.0	g3-CaHCO3
well8	KhanElshekh	Dec-06	W	456	7.4	17.1	11.3	0.8	5	81	19	213.5	17.7	22.9	10.6	2.0	g2-CaHCO3
well1	MazratNafor	Dec-06	W	415	7.4	17.7	13.2	1.8	7	62	14.5	214.7	10.1	15.4	11.4	-1.1	g2-CaHCO3
well1	Mogher-Hene	Nov-06	W	655	7.2	18.8	16.5	0	15	97	34.9	244	44	44	15.8	1.4	F2-CaHCO3
well2	Mogher-Hene	Nov-06	W	884	7.1	17.2	26.3	0	24	122	61.2	259.9	122.1	81.8	18.6	-3.6	F3-CaMIX
well3	Mogher-Hene	Nov-06	W	541	7.3	18.8	15.3	0.6	10	89	22.5	230.6	35.1	31.7	15.2	2.6	g2-CaHCO3
well4	MogherAlmer	Nov-06	W	849	7.2	16.4	27.6	0.7	23	121	53.1	311.1	77	73.5	23	-1.3	F3-CaHCO3
well5	MogherAlmer	Nov-06	W	766	7.6	18.1	16.8	0	21	114	38.7	301.1	66	67.8	18.2	-2.2	F3-CaHCO3
well6	MogherAlMer	Dec-06	W	529	7.7	19	17.5	0.7	11	75	30.6	173.2	31.2	84	22.4	-2.6	F2-CaMIX
well7	MogherAlMer	Dec-06	W	732	7.3	19.3	22.3	0.8	18	103	61	185.4	35.6	116.6	18.8	1.5	F2-CaMIX

MambejWell	MogherAlmer	Nov-06	W	451	7.2	18.4	6.4	0.8	2	85	9	226.9	7.2	16.3	10.4	3.6	g2-CaHCO3
8k	Arneh	Jun-82	W	-	6.9	12.8	9.7	0.7	4.9	22	10.6	91.5	4	6.6	-	0.0	g1-CaHCO3
43k	OmSharatet	Oct-84	W	-	7.4	-	6	1.8	18.3	38	21.3	195.2	13	7.1	-	-3.2	g2-CaHCO3
46k	AboKaook	Sep-83	W	-	7.1	18	12.2	5	40.2	12	24.8	231.8	2	39.8	-	-1.9	g2-MgHCO3
48K	Arneh	Oct-84	W	-	7.4	14	23.9	1.5	18.3	40	14.2	146.4	95	5.3	-	-1.3	g2-CaMIX
49k	Arneh	Oct-83	W	-	7.4	13.5	8.5	0.7	25.6	34	35.5	183	9	5.3	-	-0.2	F2-MgHCO3
52K	Beit Tima	Jul-83	W	-	6.5	14.6	29	2	13.4	22	19.5	134.2	32	8	-	-0.3	g2-MgHCO3
53K	Beit Tima	Oct-84	W	-	7.5	14.6	8	1.8	12.2	20	17.8	109.8	2	4	-	-0.1	g1-MgHCO3
55K	Beit Jinn	May-83	W	-	7.3	11.2	16.6	1.5	9.8	24	14.2	122	23	8.4	-	-0.5	g1-CaHCO3
57K	Beit Jinn	May-84	W	-	7.3	10.3	2.5	0.5	14.6	36	12.4	146.4	16	6.6	-	1.6	g2-CaHCO3
133K	KhanElshekh	Oct-83	W	-	6.7	20	9.7	9	29.3	20	21.3	207.4	3	2.2	-	-0.3	g2-MgHCO3
150k	JdedetArtoz	Aug-83	W	-	7	18	61.6	11	19.5	68	46.1	36.6	300	3.5	-	-1.4	F0-CaSO4
154k	JdedetAartoz	Oct-84	W	-	7.5	-	57.7	4.7	42.7	26	106.5	292.8	9	4	-	-1.9	F3-MgHCO3
165k	Dorbol	Apr-85	W	-	8.1	-	2.1	0	19.2	32	21.3	134.2	28	3	-	-1.0	g2-CaHCO3
176	JdedetArtoz	Oct-84	W	-	7.5	-	23.5	0.5	17.1	56	49.7	146.4	43	29.6	-	0.1	F2-CaMIX
181	Artouz	Oct-82	W	-	7.3	17.5	29	6.6	18	88	30	260	100	6.6	-	0.1	F3-CaHCO3
184K	Beit Saber	Aug-85	W	-	7.4	-	69	12.5	14.4	64	67.4	292.8	45	4.4	-	-0.1	F3-CaHCO3
179	Artouz	Oct-82	W	-	8.2	18	17	2.5	24.3	52	30	165	80	8	-	0.5	F2-CaHCO3
186	KhanElshekh	Apr-83	W	-	6.2	-	62.1	1.3	19.5	60	35.5	237.9	104	14.1	-	0.3	F2-CaHCO3
265k	KaferQuaq	Dec-84	W	-	7.3	18	2.3	3.1	32.2	64	65.1	179.8	72	9.3	-	-3.3	F2-CaMIX
275k	Arneh	Oct-85	W	-	7.5	-	18.4	4.3	31.2	124	49.7	317.3	150	0	-	-0.1	F3-CaHCO3
300	KhanElshekh	Oct-84	W	-	7.6	16.5	37.5	2.3	19.5	52	28.4	244	42	8.4	-	0.1	g2-CaHCO3
720	KhanElshekh	Mar-85	W	-	7.3	20	0.9	0	43.2	36	35.5	231.9	5	26.5	-	0.3	F2-MgHCO3
721	Qatana	Apr-85	W	-	7.7	19	48	21.5	2.4	64	28.4	170.8	70	61.9	-	0.6	g2-CaMIX
721a	Qatana	Apr-85	W	-	7.4	-	11.5	2.3	7.2	64	35.5	183	15	8.8	-	-0.7	F2-CaHCO3
740	KhanElshekh	Aug-85	W	-	7.4	20	16.1	2.3	16.8	56	60.35	183.1	4	8.3	-	0.0	F2-CaHCO3
744	KhanElshekh	Aug-85	W	-	7.4	-	31.8	3.1	21.6	44	35.5	239	15	11.1	-	0.5	F2-CaHCO3
3032	Kafer Qouq	May-84	W	-	8.2	-	27.6	0.5	12.2	52	21.3	213.5	17	8	-	2.3	g2-CaHCO3
3036	Qatana	Oct-84	W	-	7.3	17	53.8	3.2	3.7	86	56.8	274.5	18	31.8	-	0.1	F3-CaHCO3

3050	Saasaa	Jun-82	W	-	8.4	17.4	35	1.8	35	11.6	70	128	18	13	-	3.9	F2-MgHCO3
3055	Kleaa	May-84	W	-	8.2	-	12.2	1.5	9.8	28	10.7	128.1	10	5.3	-	1.9	g2-CaHCO3
3072	Heneh	May-84	W	-	7.5	14.4	61.9	0.3	25.6	58	49.7	176.9	145	23.4	-	0.2	F2-CaMIX
Almalha	Arneh	Nov-06	S	972	7.1	13.4	5.1	0.8	29	183	4.2	234	395	2.6	5.6	-2.3	G2-CaSO4
Albardeh	Arneh	Nov-06	S	640	7.4	13.7	5	1.2	15	120	6.5	248	164.5	5.3	6.2	-2.1	g3-CaHCO3
Dorbol1	Dorbol	Nov-06	S	295	7.8	17.6	3.6	0	2.5	54	7	164.7	7.6	2.9	6.6	-0.7	g2-CaHCO3
Dorbol4	Dorbol	Nov-06	S	251	7.9	14.5	2.8	0	4	42	6.4	139	3.7	4	4.8	-1.1	g2-CaHCO3
Dorbol3	Dorbol	Nov-06	S	245	7.7	15.2	2.8	0	3	40	5.6	136.6	4.3	3.8	5.4	-3.8	g2-CaHCO3
RasAlin	Qatana	Nov-06	S	330	7.4	17.6	5.8	0.7	8	58	7.8	185	6.1	10.1	6.6	3.9	g2-CaHCO3
Hamana	BeitTima	Nov-06	S	789	7.1	17.6	12.4	1.7	25.5	133	25.6	289.1	168	15.4	22	0.7	g3-CaHCO3
Beitsaber1	Beitsaber	Nov-06	S	762	7.1	17.2	10.2	0.8	23.5	131	20.2	290.4	132	11.9	12.4	4.2	g3-CaHCO3
Beitsaber2	Beitsaber	Nov-06	S	767	7.1	16.7	11.6	0.9	23	132	18.8	307.4	136	20.2	12.6	1.7	g3-CaHCO3
Alla	Ainashara	Nov-06	S	327	8.1	16.1	8.3	2.2	2.5	52	13.5	109.8	14.9	27.7	6.8	4.7	g1-CaHCO3
KaferHour1	KaferHour	Nov-06	S	887	7.3	15.8	13.6	6.6	25.5	153	35.5	327	171	29.9	13.8	0.5	F3-CaHCO3
Ganat	Hasebe	Dec-06	S	462	7.4	18.1	7.6	2	8	74	12.9	224.5	36.3	18	9.2	-3.8	g2-CaHCO3
AinAljoz	Kalaetjandal	Nov-06	S	219	7.8	14	2.9	0.5	9.5	30	3.8	137	2.9	1.9	5	-0.5	G2-CaHCO3
HighBeitJinnn	BeitJinnn	Nov-06	S	260	8.4	11.2	1.8	0.5	7	42	2.1	136.6	13	1.7	3.6	3.2	G2-CaHCO3
Morkos	Arneh	Dec-06	S	610	7.6	12.4	2.1	0	14	107	4.1	153.7	196.2	2.6	5	-1.5	G2-CaSO4
Dorbol2	Dorbol	Nov-06	S	298	7.3	16.8	3.5	0	2	57	6.6	172	5.2	4	5.8	-0.3	g2-CaHCO3
Saasaa	Saasaa	Nov-06	S	237	7	18.4	19.7	4.5	8.5	15	13.1	80.5	8.9	19.8	27.6	5.0	g1-CaHCO3
Bkassam3	Bkassam	Nov-06	S	535	7.7	12.1	5.1	0	21	75	6.4	180.6	95.8	28.1	6.6	1.0	g2-CaHCO3
AinBala	Qatana	Nov-06	S	582	7.4	17.4	10.5	0.7	8	115	12.2	266	67	12.3	12	4.6	g3-CaHCO3
Bkassam2	Bkassam	Nov-06	S	633	8.1	16.4	22	5.9	20	76	39.2	201.3	25.2	104.3	8.6	-0.5	F2-CaMIX
Asfal	Ainshara	Nov-06	S	318	7.5	15.4	4.7	1.3	3	63	7	178.1	6.3	5.3	6.4	4.3	g2-CaHCO3
KhrbtSouda	KhrbtSouda	Nov-06	S	262	8.1	13.4	3.5	0	1	41	6.3	127	8.5	3.1	5.4	-4.4	g2-CaHCO3
33	Tal Assyuf	Jun-83	S	-	7.5	-	142.9	0	41.5	108	140	280.6	59	4.2	-	1.1	F3-CaCl
41	Ain Saba	Dec-77	S	-	7.5	-	10	0	23	85	14	207.4	134.1	0	-	0.8	g2-CaHCO3
43	Rashasheh	Sep-77	S	-	7.2	-	13	0	26	89	17.4	231.8	135	0	-	0.4	g2-CaHCO3
44	Rijmeh	May-83	S	-	8.1	-	9.2	0	18.3	18	12.4	134.2	7	0	-	2.0	g2-MgHCO3

45	Ras Alwadi	Jul-78	S	-	7	-	20	0	12	38	25	170.8	10.7	0	-	0.4	g2-CaHCO3
46	Tabibieh	Aug-82	S	-	8.2	-	14.7	0	7.2	52	10	150	42	13.2	-	0.0	g2-CaHCO3
47	Husenieh	Oct-83	S	-	6.9	-	15.6	0	3.6	32	19.5	109.8	6	3.1	-	1.0	g1-CaHCO3
49	Mbaya	Oct-83	S	-	7.6	-	13.3	0	7.3	24	17.8	109.8	2	2.2	-	0.0	g1-CaHCO3
51	Artouz Qanat	Aug-84	S	-	7.5	-	26.4	0	4.9	60	46.2	145.2	18	26.4	-	0.7	F2-CaHCO3
61	Alfouar spring	Oct-83	S	-	6.9	-	11.7	0	4.9	12	17.8	48.8	2.5	2.7	-	3.9	g0-CaHCO3
10276	Mt Hermon	Oct-84	S	-	7.3	-	21.6	2	20.7	47	21.3	183	50	10	-	-0.1	σ^2 -CaHCO3
10285	Shabaanet	Oct-84	S	-	7.6	-	73.6	0.5	25.6	66	21.3	256.2	180	5.4	-	-0.1	g3-CaMIX
10291	Mt Hermon	Oct-84	S	-	7.7	-	1.4	0.4	25.5	60	99.4	128.14	4	8.4	-	0.5	F2-CaCl
10292	Ain Najeem	Oct-84	S	-	7.8	-	4.6	0	19.3	116	61.4	97.6	190	8.8	-	1.3	F1-CaSO4
10297	Almashraa	Oct-84	S	-	8.3	-	23	0	24.3	50	76.5	122	33.4	11.3	-	4.6	F1-CaMIX
10308	Beit Tima1	Oct-84	S	-	7	-	6.7	0.4	34.8	72	31.3	176.9	130	18.1	-	0.2	F2-CaMIX
10309	Beit Tima2	Oct-84	S	-	7.1	-	4.6	3.5	60	104	139.5	30.5	283.4	4.4	-	0.6	F*-CaSO4
10310	Mt Hermon	Oct-84	S	-	7.7	-	0	0	24.3	22	17.8	122	20	2.6	-	2.1	g1-MgHCO3
10311	Mt Hermon	Oct-84	S	-	7.3	-	4.6	3.5	18.2	52	32.3	91.5	88.9	8.8	-	-0.3	F1-CaMIX
10322	Mt Hermon	Dec-84	S	-	7.7	-	2.7	0	24.3	84	83.4	122	76.8	21.6	-	0.1	F1-CaMIX
10325	Mt Hermon	Dec-84	S	-	7.7	-	0.5	0	14.6	32	30.9	74.4	31.2	6.2	-	-0.3	F1-CaMIX
10326	Mt Hermon	Dec-84	S	-	8.1	-	0.2	0	12.2	20	21.3	62	10	5.7	-	2.3	g1-MgHCO3
10327	Albardeh(Remeh)	Dec-84	S	-	8.3	-	2.3	0.8	23.1	64	81.7	115.9	38.9	21	-	-1.3	F1-CaMIX
10333	Ain Badran	Dec-84	S	-	7.9	-	0.3	0.8	24.3	36	35.5	122	29.7	8	-	1.2	F1-MgHCO3

EC electrical conductivity, *T* temperature, *W* well, *S* spring, σ chemical analyses error.

Table 4 - 2 List of sampling sites and chemical composition of water samples collected during August 2012.

Name	Locations	Date	Type	EC μS/cm	pH	Na ⁺ (mg/L)	K ⁺ (mg/L)	Mg ²⁺ (mg/L)	Ca ²⁺ (mg/L)	Cl ⁻ (mg/L)	HCO ₃ ⁻ (mg/L)	SO ₄ ²⁻ (mg/L)	NO ₃ ⁻ (mg/L)	σ (%)	Water type (Stuyfzand)
Beit Jinn	Beit Jinn	16/08/2012	S	310	7.97	3.4	1.0	8.2	48.7	4.9	176	7.1	2.6	1	G2-CaHCO3
Arneh	Arneh	20/08/2012	S	272	7.90	2.9	0.2	1.7	47.7	9.5	137	3.8	0.7	1	g2-CaHCO3
Almashraa	Arneh	20/08/2012	S	352	7.96	3.1	0.5	13.5	44.0	8.3	115	77.7	1.6	-4	g1-CaHCO3
Talmasiat	Mogher Al Mer	16/08/2012	S	384	8.05	11.1	2.6	7.1	59.3	8.7	207	8.3	10.4	1	g2-CaHCO3
Jandal	Kalet Jandal	17/08/2012	S	358	7.99	9.9	1.4	13.4	34.7	19.9	112	18.2	44.2	-3	g1-CaHCO3
Mambej	Mogher Al Mer	16/08/2012	S	360	8.03	11.9	2.8	6.1	53.2	8.3	194	7.1	10.2	0	g2-CaHCO3
Bkassam1	Bkassam	17/08/2012	S	697	8.04	31.0	5.8	25.8	60.0	49.8	157	39.4	108.6	0	F2-CaMIX
Kneseh	Remeh	20/08/2012	S	380	7.82	5.7	2.6	10.3	54.7	8.6	173	24.1	10.4	2	g2-CaHCO3
Tamer	Remeh	20/08/2012	S	330	7.98	4.2	0.4	11.9	45.2	7.7	172	10.7	6.7	1	g2-CaHCO3
Tal Assyuf	Mogher Al Mer	16/08/2012	S	396	7.87	10.4	2.1	9.8	56.7	10.9	201	11.7	15.9	0	g2-CaHCO3
Rashasheh	Arneh	20/08/2012	S	600	7.87	4.1	0.5	18.8	92.2	9.7	167	171.1	2.8	-2	g2-CaSO4
Alrjimeh	Remeh	20/08/2012	S	573	7.89	19.0	4.9	20.0	58.2	32.5	181	26.6	71.6	-1	F2-CaHCO3
Ras Alwadi	Kalet Jandal	17/08/2012	S	323	8.02	4.8	1.1	11.4	42.4	8.3	154	11.6	8.4	2	g2-CaHCO3
Njaim Spring	Arneh	20/08/2012	S	609	7.92	2.9	0.5	15.9	100.8	8.5	150	189.6	1.4	-2	g2-CaSO4
Jandal Drink Well	Kalet Jandal	17/08/2012	W	278	8.01	2.9	0.3	0.9	52.0	9.2	145	5.3	0.0	1	g2-CaHCO3

EC electrical conductivity, W well, S spring, σ chemical analyses error.

Table 4 - 3 Environmental stable isotopic composition measured in groundwater samples collected from 18 sites in the study area during August 2012 as addition to 3 samples from Selkhozpromexport 1986.

Station name	Analysis date	Type	X coord	Y coord	$\delta^2\text{H}$ Reportable value (‰ permil)	$\delta^2\text{H}$ Standard deviation (‰ permil)	$\delta^{18}\text{O}$ Reportable value (‰ permil)	$\delta^{18}\text{O}$ Standard deviation (‰ permil)	d (‰)	Altitude (m)
Beit Saber1	17/08/2012	W	339000	3687000	-48.76	0.57	-7.99	0.04	15.14	983
Beit Saber2	17/08/2012	W	340200	3689100	-46.65	0.72	-7.54	0.10	13.66	972
Jandal	17/08/2012	S	335870	3700080	-47.55	0.60	-7.94	0.09	15.98	1332
Ras Alwadi	17/08/2012	S	335790	3699530	-47.22	0.49	-7.94	0.03	16.34	1304
Jandal Drink Well	17/08/2012	W	335180	3700980	-44.98	1.04	-8.04	0.12	19.36	1368
Bkassam	17/08/2012	S	333730	3698280	-46.75	0.29	-7.72	0.05	15.02	1400
Njaim	20/08/2012	S	326400	3693950	-43.30	0.94	-7.91	0.11	19.94	-
Almalha	20/08/2012	S	328110	3694300	-43.20	0.67	-7.88	0.11	19.86	1358
Arneh	20/08/2012	S	328630	3692830	-43.56	0.32	-8.09	0.10	21.19	1478
Almashraa	20/08/2012	S	326100	3693710	-40.24	0.28	-7.60	0.05	20.53	-
Rashasheh	20/08/2012	S	328780	3694750	-42.67	0.85	-7.62	0.10	18.31	1342
Kneseh	20/08/2012	S	330200	3695500	-43.64	0.94	-7.62	0.09	17.35	1365
Alrjmeh	20/08/2012	S	330920	3697020	-44.49	0.25	-7.45	0.06	15.15	1429
Tamer	20/08/2012	S	331000	3697200	-43.97	0.53	-7.47	0.08	15.82	1386
Mambej	16/08/2012	S	334200	3687330	-39.66	1.04	-7.28	0.12	18.58	980
Talmasiat	16/08/2012	S	336330	3686240	-40.49	0.68	-7.42	0.08	18.89	950
Tal Assyuf	16/08/2012	S	339770	3684300	-40.26	0.69	-7.46	0.08	19.40	956
Beit Jinn	16/08/2012	S	330030	3687890	-41.23	0.51	-7.50	0.05	18.75	1285
dorbol	1984	S	331240	3692240	-43.6		-8.2		22	1394
Tabibieh	1984	S	346000	3688750	-37.6		-7.2		20	821
Ras Alin	1984	S	346030	3701780	-39.8		-7.85		23	887

W Well, S Spring, d Deuterium excess. The coordinates system is special for Syrian Arab Republic

Table 4 - 4 Environmental stable isotopic composition and amount of precipitation measured in different meteorological stations in Syria. 1989-1990 data from Kattan (1997a), 1983-1984 data from Selkhozpromexport (1986) and Arneh data from Kattan (2006).

Station name	Altitude (m)	Distance from the coast (km)	Date	P (mm)	$\delta^{18}\text{O}$ (‰)	$\delta^2\text{H}$ (‰)	^3H (T U)	d (‰)
Bloudan	1540	55	Dec-89	48.1	-8	-44.1	4.3	20.1
			Jan-90	46.1	-7.8	-40.2	6.9	22
			Feb-90	101.9	-8.7	-48.7	7.3	20.7
			Mar-90	51.5	-8.2	-47.8	7	17.9
			Apr-90	18	-12.2	-87.4	9.5	10.4
weighted mean					-8.6	-48.8	6.8	19.6
Damascus	625	80	Dec-89	4.8	-7.3	-47.8	5.5	10.8
			Jan-90	14.9	-9.6	-62.6	9	14.5
			Feb-90	30.6	-7.2	-35.5	8.6	21.9
			Mar-90	28.2	-6.5	-37.9	7	13.8
			Apr-90	8.4	-9.4	-71.7	13.6	3.8
weighted mean					-7.6	-45.1	8.5	15.7
Kounietra	930	64	Dec-89	55.6	-6.4	-30.6	6.5	20.9
			Jan-90	70.3	-8.5	-48.8	7.5	19.1
			Feb-90	115.9	-7	-34.6	7.6	21.7
			Mar-90	86.6	-7.7	-42.3	6.5	19.1
			Apr-90	7.3	-7.2	-44.5	7.9	13.3
weighted mean					-7.4	-39.1	7.1	20.2
Tartous	5	0	Dec-89	96.6	-4.6	-18.5	5.1	18.4
			Jan-90	72.4	-5.4	-24.9	7.3	18.1
			Feb-90	132.2	-3.8	-14.2	5.4	16.4
			Mar-90	95	-4.1	-17.3	5.6	15.3

			Apr-90	54.8	-7.8	-49	11.8	13.3
			weighted mean		-4.8	-21.7	6.5	16.5
Homs	490	70	Dec-89	49.6	-6.6	-32.9	5.1	19.8
			Jan-90	40.8	-6.4	-29.7	7	21.8
			Feb-90	36.6	-6.5	-30.1	7.9	22.2
			Mar-90	10.5	-5.1	-30.1	9.2	10.6
			Apr-90	19.5	-6.4	-41.1	11.3	10.2
			weighted mean		-6.4	-32.2	7.3	19.1
Izrra	580	111	Dec-89	37	-7.1	-36.9	5.6	20.1
			Jan-90	65.9	-7.1	-41.6	9.7	14.8
			Feb-90	60.9	-6.8	-29.6	9.4	24.4
			Mar-90	55.4	-5.2	-21.5	8	20.3
			Apr-90	10.1	-7.8	-48.7	9.4	14
			weighted mean		-6.6	-33.1	8.5	19.5
Suwieda	1020	140	Dec-89	44.7	-7.8	-40.2	4.6	22.1
			Jan-90	100	-8.8	-52.5	9.2	17.6
			Feb-90	65.8	-6.9	-31.7	8.7	23.3
			Mar-90	76.3	-5	-17.6	7.5	22.3
			Apr-90	30.6	-8.3	-49	10.3	17.6
			weighted mean		-7.3	-37.7	8.1	20.5
Palmyra	400	211	Dec-89	11.5	-7	-45.2	7.1	10.5
			Jan-90	3.8	-6.4	-38.7	12.4	12.2
			Feb-90	29	-6.3	-22.2	11.4	28
			Mar-90	24.2	-0.4	16.4	9.8	19.5
			Apr-90	11.4	-0.3	9.6	11.8	12.1
			weighted mean		-3.7	-10.1	10.4	19.9
Aleppo	410	105	Dec-89	45.1	-7.1	-37.8	6.7	19.2
			Jan-90	24.9	-10.7	-65	10.8	20.9

			Feb-90	47.1	-7.1	-38.9	9.1	18.1
			Mar-90	20.5	-2.8	-10.9	9	11.6
			Apr-90	3.5	-2	-14	11	2
weighted mean					-7	-38.5	8.7	17.6
Qatana	890	-	Feb-83	63	-6.7	-29.6		24
			Mar-83	43.5	-9.4	-55.2		20
			Jan-84	56.5	-9.3	-49.4		25
			Mar-84	64	-6.4	-44.2		7
weighted mean					-7.8	-43.6		18.7
Remeh	1480	-	Feb-83	51	-5.8	-23.4		23
			Mar-83	64	-11	-71		17
			Mar-84	100	-7.4	-44.2		15
			Apr-84	40	-7.2	-47.6		10
weighted mean					-8	-47.3		16.3
Arneh	1430	-	1989 - 1993		-8.3	-44.5	6	21.7

Appendices

Appendix A Published Article

Article published in the journal of Environmental Earth Sciences

Hydrochemistry to delineate groundwater flow conditions in the Mogher Al Mer area (Damascus Basin, Southwestern Syria)

Hydrochemistry to delineate groundwater flow conditions in the Mogher Al Mer area (Damascus Basin, Southwestern Syria)

N. M. Asmael · F. Huneau · E. Garel · H. Celle-Jeanton · P. Le Coustumer · A. Dupuy

Received: 11 February 2013 / Accepted: 20 March 2014 / Published online: 13 April 2014
© Springer-Verlag Berlin Heidelberg 2014

Abstract The hydrochemistry of groundwater from the Mogher Al Mer area, located in southwestern Syria, has been used as a tool to identify and assess the hydrogeological systems and associated conditions. In this arid region of Syria, groundwater is considered as the main source of water supply for both drinking and irrigation purposes. The detailed description of hydrogeochemical conditions, including major ions, physico-chemical and in situ field parameters, has underlined the very complex

variability of the stratigraphic sequences and hence the numerous hydrogeological units within the study area. On the one hand, groundwater chemical signature is found to be mainly controlled by the water–rock interaction processes in the mountainous western part of the study area. On the other hand, anthropogenic influences are observed in the eastern plain. In terms of recharge mechanisms, the region can be considered as a part of a main intermediate or even regional flow system instead of a local one.

N. M. Asmael
Department of Geology, Faculty of Sciences, University of Damascus, P.O. Box 32022, Damascus, Syria

N. M. Asmael · P. Le Coustumer · A. Dupuy
EA 4592 Géoressources & Environnement, Université de Bordeaux, 1 allée F. Daguin, 33607 Pessac, France

F. Huneau (✉) · E. Garel
Laboratoire d'Hydrogéologie, Faculté des Sciences et Techniques, Université de Corse Pascal Paoli, Campus Grimaldi, BP 52, 20250 Corte, France
e-mail: huneau@univ-corse.fr

F. Huneau · E. Garel
CNRS, UMR 6134, SPE, 20250 Corte, France

H. Celle-Jeanton
Laboratoire Magmas et Volcans, Clermont Université, Université Blaise Pascal, BP 10448, 63038 Clermont-Ferrand, France

H. Celle-Jeanton
CNRS, UMR 6524, LMV, 63038 Clermont-Ferrand, France

H. Celle-Jeanton
IRD, R 163, LMV, 63038 Clermont-Ferrand, France

A. Dupuy
ENSEGID-IPB, 1 allée F. Daguin, 33607 Pessac, France

Keywords Aquifer · Groundwater · Hydrochemistry · Arid region · Syria

Introduction

In the former days, the Barada and Awaj Rivers, mainly fed by karst springs (Wolfart 1964), were considered as a vital socioeconomic resource, sustaining the Ghouta Oasis and agricultural activities in the Damascus Basin (Barada and Awaj Basin) (INECO 2009).

Due to the decrease in surface water supplies in the study area, groundwater remains the only option to supplement the ever-growing demand for water to meet the requirement of human activities (Al-Charideh 2011, 2012a, b). Therefore, additional threat is put on all fresh groundwater resources. The protection and management sustainable of groundwater resources is a priority objective in both industrialized and developing countries (European Commission 1995; Barbieri et al. 2005). Groundwater management in Syria is an issue of great concern to water policy makers, planners, and legislators, with respect to pollution and resources sustainability (FAO 1993; Angelakis 2000).

Consumption rates greater than recharge rates are common in the last 20 years in most regions of Syria. Consequently, groundwater levels have started to decrease dramatically and negative water balance has been detected. Several springs have dried up and a large number of rivers have become seasonal or have been converted to wastewater canals (Al-Charideh and Abou-Zakhem 2009; Meslmani and Wardeh 2010). From a holistic perspective, a conceptual approach that encompasses human pressures must recognize the hydrogeological heterogeneity caused by the complexity of the geological structure. Also the potential contributions of distinct recharge areas have to be identified once groundwater withdrawal has begun (Mahlknecht et al. 2006; Palmer et al. 2007; Li et al. 2008; Folch et al. 2011).

The characterization of the flow conditions within the local aquifers is an important step towards a better management of water resources. Hydrochemistry can provide an important information and independent method for identifying recharge areas and delineating preferential flow paths. Groundwater carries chemical signatures of recharge precipitation and interactions along flow paths with aquifers rocks as well as anthropogenic activities (Rakhmatulaev et al. 2010, 2012; Huneau et al. 2011).

Groundwater in the Mogher Al Mer area is the main source of water supply for small population centres as well as for private use in agriculture and cattle supply. However, the processes (natural or anthropogenic) controlling the chemistry and quality of groundwater in this area is not yet well understood. Therefore, the main objectives of the present study are to (1) evaluate relevant rock–water interactions that influence water quality in the study area within the framework of its complex geology and morphology, (2) determine predominant water type based on their chemical compositions and ionic ratios, (3) interpret the groundwater flow system conditions to update and improve the knowledge on the groundwater flow behaviour.

General setting of the study area

The Damascus Basin occupies the southwestern part of the Syrian Arab Republic (SAR). The climate of SAR is characterized by warm dry summers and cool rainy winters. SAR has scarce water resources with more than 60 % of the country receiving less than 250 mm/year of rainfall (Mourad and Berndtsson 2011). Annual precipitation in the Damascus Basin varies in the range of 86–900 mm/year and this basin is classified into four climatic zones: hot desert, arid, semiarid, and moderate (RDAWSA 2006).

A high variation in the air temperature is observed between winter and summer. Temperatures can drop down

below freezing point at high altitudes (1,500–2,000 m) in winter and can reach 42 °C during summer. The relative humidity is usually about 24–50 % during summer (July and August) and may reach up to 60–70 % during winter (January and February). The annual average potential evaporation varies between 1,500 mm/year in the flatlands and 1,100 mm/year in the mountainous areas. Evapotranspiration in the mountainous area varies between 300 and 400 mm/year and it is close to precipitation in the flatland area (Selkhozpromexport 1986; Kattan 1997).

Mogher Al Mer and its surrounding areas (Fig. 1) cover an area of approximately 400 km². This region is considered as a main recharge area of Awaj River which is the main watercourse in this area. The annual average discharge of Awaj River is 4.7 m³/s (MOI 2005). Topographically, the area is characterized by mountains in the west and northwest with sharp deep valleys in between, and by a flat area in the east and southeast. The relief varies between 800 and 1,800 m.a.s.l.

Geological and hydrogeological setting

Geology

The main formations outcropping in the study area range from the Middle Jurassic up to the Quaternary period. The major Jurassic deposits are found in the Mt Hermon (western and northwestern parts), whereas the plain areas are characterized by outcroppings of the Paleogene, Neogene, and Quaternary deposits. The Cretaceous formation is exposed in a small part southwest of the study area. The Paleogene formation is found in the southern part. The thickness of Paleogene is about 1,500 m and is composed of limestone characterized by nummulites and interbedded with marl layers and clayey marls in the upper part of the Eocene. The Neogene formation is outcropping in the central and eastern parts of the study area with a thickness of about 500 m. The dark colored Miocene basalts, which are characterized by fractures filled with calcite, are found locally beneath the conglomerates of Pliocene age. The Quaternary deposits are mainly found in the plain area around the Awaj River. Its thickness varies between 1 and 10 m. Figure 2 displays three cross sections showing subsurface lithology as well as the major structures within the study area and the logs of wells penetrating Neogene, Palaeogene, Cretaceous, and Jurassic formations.

In terms of tectonic, the area is strongly affected by faulting and folding resulting in several folded structures such as Mt. Anti-Lebanon (up to 2,466 m) and Mt. Hermon (2,814 m) (Dubertret 1932; Ponikarov 1967; Selkhozpromexport 1986; La-Moreaux et al. 1989; Kattan 2006). Generally, most strata from Jurassic to Cretaceous age are

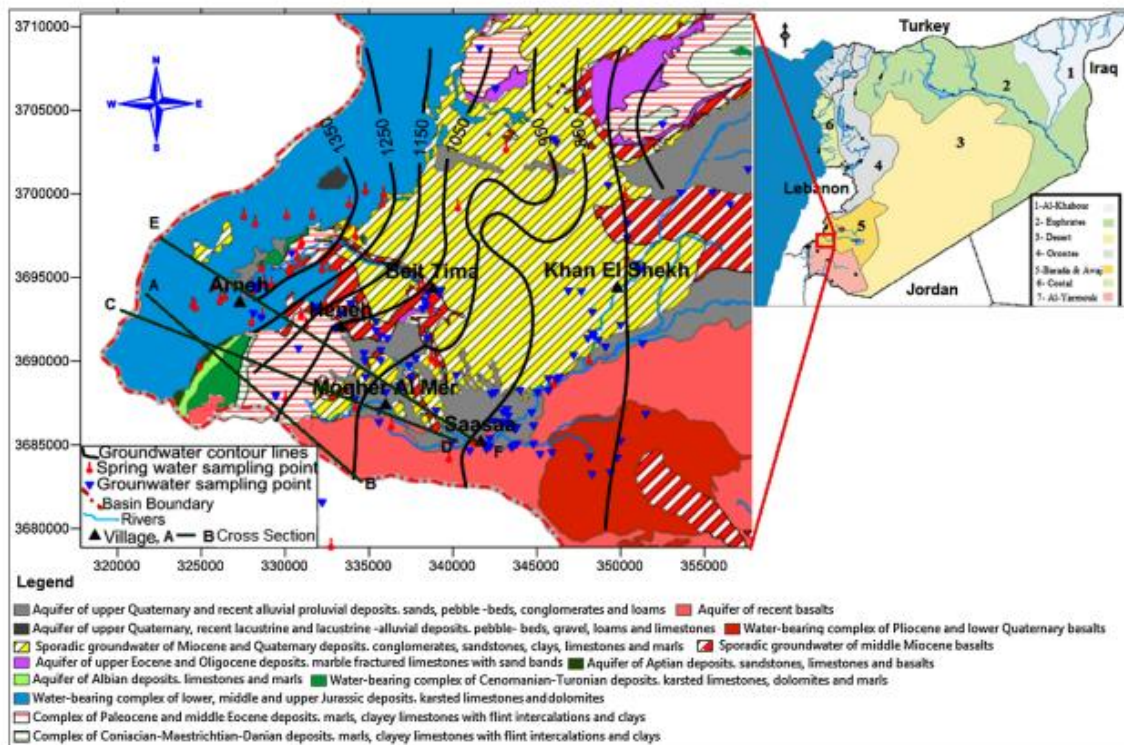


Fig. 1 Map of Syria divided into seven basins with the location of study area in the Barada and Awaj Basin. The locations of sampling sites, groundwater equipotential contours, and three geological cross sections presented in Fig. 2 are shown on hydrogeological map of the study area

dipping in the southeast direction to the east Mt. Hermon. The tectonic activities, mainly fault zones, together with karstic features, seem to play a significant role in this area in terms of increasing infiltration coefficient and controlling groundwater flow behaviour, and recharge/discharge mechanisms (Burdon and Safadi 1964).

Hydrogeology

The aquifers in the study area can be classified into karstic and porous aquifers.

The karstic aquifers consist of limestones and dolomites, which upon dissolution along faults and fractures create a secondary porosity. Such aquifers belong to the Jurassic, the Cenomanian–Turonian, and the Upper Eocene units (Al-Charideh 2012a). Porous formations consist of unconsolidated or semi-consolidated sediments, such as the Pliocene conglomerate units and the Quaternary aquifer. The basalts, if not intensely fractured, can be considered to a certain extent as an aquiclude (Kattan 1997, 2006).

Figure 1 shows the hydrogeological map of the study area with major aquifers. The major hydrogeological units

in the study area are classified and described below (Selkhozpromexport 1986):

Jurassic unit

The karstic limestone layer containing gypsum infilling (about 2,000 m thick) interbedded with dolomite, dolomitic limestone, and marls layers forms this unit. The hydraulic conductivity varies between 2 and 99.3 m/day, and the transmissivity is about 3,085 m²/day (RDAWSA 2006).

Cretaceous unit

The limestone, dolomitic limestone, and crystalline dolomite interbedded with argillaceous limestone, marl, and sandstone formations compose the aquifer member of this unit (400–1,000 m). This unit together with the Jurassic unit represents the most important water-bearing system in the Damascus Basin and even in the SAR in terms of storage capacity and discharge of springs (JICA 2001). The hydraulic conductivity is up to 80 m/day and transmissivity varies between 12 and 7,435 m²/day (La-Moreaux et al. 1989).

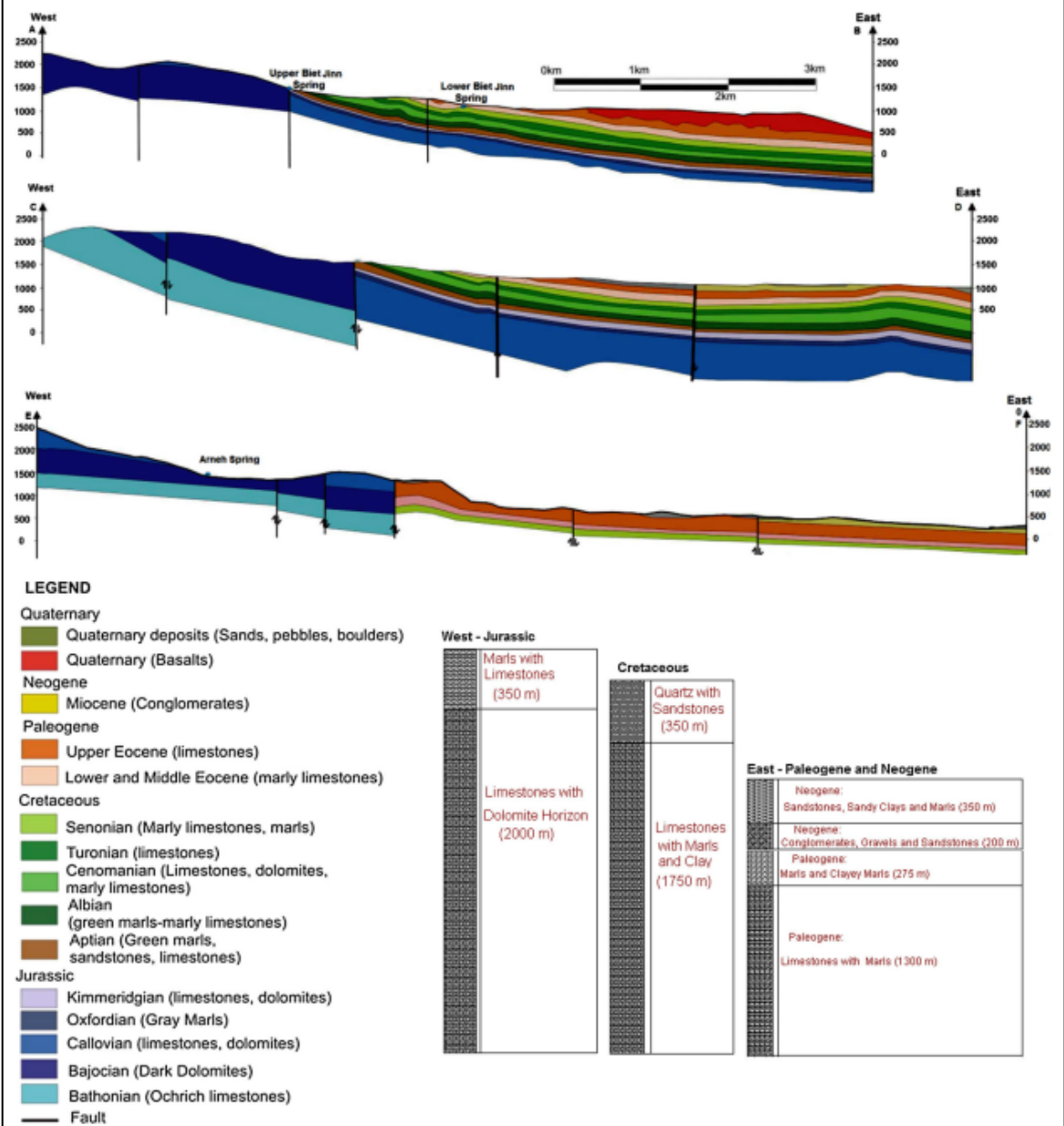


Fig. 2 Three geological cross sections showing subsurface lithology as well as the major structure within the study area and the logs of wells tapping Neogene, Paleogene, Cretaceous, and Jurassic formations

Sedimentary Mio-Quaternary aquifer

The rocks of this complex (140–630 m thick) are widespread on the foothill of Mt. Hermon and in the plain area.

They consist of gravels and conglomerates interbedded with clay, sandstone, and limestone. As clay content increases and/or aquifer thickness decreases, the transmissivity value can drop down from 756 to 0.05 m²/day.

Volcanic middle Miocene aquifer

The Basaltic aquifer (500 m) consists of fissured basalts associated with thin beds and lenses of sand and sandstone. This aquifer overlays the Neogene conglomerates. The transmissivity of this aquifer is about 30–60 m²/day. Almost all the springs emerging from the basalts aquifer originate from deeper aquifers, such as the Neogene conglomerates or other related aquifers.

Groundwater contour map

Based on available water level data on 33 groundwater monitoring points obtained from Ministry of Irrigation of Syria, a preliminary potentiometric map was constructed for November 2006 as shown in Fig. 1. The interpretation of equipotential contours indicates that the general groundwater flow is organized towards the east direction. Minor flow direction is also recognized from northwestern to southeastern where several springs characterized by relatively high discharge rates are emerging. A steeper hydraulic gradient is observed in the western and northern mountainous parts, where the karsts and faults are more developed.

Sampling, analysis, and database preparation

A total of 107 water samples from springs and wells (Fig. 1) were collected during the fieldwork campaign in November and December 2006. Wells depths range between 35 and 160 m and are owned by the Ministry of Irrigation and farmers. Samples were collected in polyethylene bottles, which were rinsed twice with sample water. Two bottles of each water point were collected. One bottle was filtered (0.45 µm) and acidified with two drops of nitric acid, (HNO₃) for cations determination.

Field parameters such as electrical conductivity (EC), pH, and alkalinity (HCO₃⁻) were measured onsite. Within 30 days of sampling, all samples were analysed in the UNESCO-IHE Institute laboratory in The Netherlands. Cation concentrations were measured using an Absorption Spectrophotometer (AAS), whereas the anions were measured with Dionex Ion Chromatograph (DIOEX ICC-1000). Silica (as SiO₂) was measured using HACH colorimeter. In addition, the database was completed with other available related data from different sources (RDAWSA 2006; Selkhozpromexport 1986). Using PHREEQC (Parkhurst and Appelo 1999), different calculations were performed to determine water types according to Stuyfzand classification (Stuyfzand 1989), and the saturation indices of a selection of minerals and the partial pressure of carbon dioxide. Field parameters and majors ions for the different sampling points are displayed in Table 1.

Results and discussion

To protect valuable water resources effectively and to predict any change in groundwater environments, it is necessary to understand the hydrochemical characteristics of the groundwater and its evolution under natural water circulation processes (Lawrence et al. 2000; Guendouz et al. 2003; Wen et al. 2005; Ma et al. 2005; Edmunds et al. 2006; Ma and Edmunds 2006; Jianhua et al. 2009). The motion of groundwater along its flow paths generally increases the concentration of the chemical species (Domenico and Schwartz 1990; Freeze and Cherry 1979; Kortatsi 2007; Aghazadeh and Mogaddam 2011).

Calcite, dolomite, and gypsum dissolution

The dissolution of limestones and dolomites is a dominant mineralization process for groundwater of carbonate systems. In many cases, the dissolution of gypsum has also a very important role (Flakova 1998). The most important factor determining the solubility of minerals is the abundance of carbon dioxide in the system. The process of calcite and dolomite dissolution takes place under conditions of open and closed systems, depending on the CO₂ pressure. Figure 3 shows the pure calcite and dolomite dissolution under both open and closed system dissolution as a function of CO₂ supply determined by PHREEQC (Parkhurst and Appelo 1999). The relationship between measured pH and calculated pCO₂ in the water samples is also shown on this figure. In the closed system, CO₂ is decreasing along the groundwater flow path. On the other hand, it remains constant in the open system (Appelo and Postma 2005). The ranges of calculated pCO₂ as a function of pH in the water samples comparing with those values of open and close system dissolution indicated that open system dissolution is prevailing in the study area.

During the contact between infiltrating water and limestones, dolomites and gypsum, congruent or incongruent dissolution of carbonate minerals can occur. Mineral equilibrium calculations for groundwater are useful in predicting the presence of reactive minerals in the groundwater system and estimating mineral reactivity (Deutsch 1997; Jianhua et al. 2009).

Since open system dissolution of carbonates is suspected, bicarbonate, calcium, and magnesium concentrations have been plotted as a function of calculated pCO₂ together with the pure calcite and dolomite dissolution determined with PHREEQC (Fig. 4a). The PHREEQC lines and the scatter plot determine the dissolution state of the carbonate system. Distinctly, this graph shows different sources of calcium in water samples because most of the samples are plotted above PHREEQC lines. In contrast, bicarbonate and magnesium for most samples are situated below those lines.

Table 1 List of sampling sites and chemical composition of water samples collected during November and December 2006 and the historical data based on Selkhozpromexport study performed on 1986

Name	Location	Date	Type	EC ($\mu\text{S}/\text{cm}$)	pH (–)	T ($^{\circ}\text{C}$)	Na^+ (mg/L)	K^+ (mg/L)	Mg^{2+} (mg/L)	Ca^{2+} (mg/L)	Cl^- (mg/L)	HCO_3^- (mg/L)	SO_4^{2-} (mg/L)	NO_3^- (mg/L)	SiO_2 (mg/L)	σ (%)
Artesian well	Arneh	Dec-06	W	660	7.5	14.4	4.9	0	20	120	5.7	238	196.5	4	6.6	-2.6
Drink well	Harfa	Nov-06	W	462	7.3	17.8	15.6	13.8	4	67	24.2	162.3	9.6	49.7	14.4	4.0
Artesian well	Harfa	Nov-06	W	431	7.8	15.5	10.9	5.7	23	31	7.7	244	0.7	0.4	10.2	-2.2
well6	Heneh	Nov-06	W	570	7.6	18.7	20.7	1	25	59	29.1	223.3	63	25.1	22.6	-2.3
well1	Heneh	Nov-06	W	443	7.3	17.4	9.2	0	10	72	14.1	231.8	9.5	15.4	26.6	1.9
well5	Heneh	Nov-06	W	708	7.2	18.4	22.3	2	16	101	36.5	247.7	42.6	66	18.8	2.4
MJ Alshekh	Heneh	Nov-06	W	681	7.3	13.4	20.3	1.1	14	106	43.1	253.8	47	59.8	15.6	0.1
well1	Kleaa	Dec-06	W	530	7.2	17.2	16.4	3.7	10	87	24	264.7	14.7	22	14	2.6
well2	Kleaa	Dec-06	W	532	7.3	16.9	11.9	1.7	11	94	35.6	249	8	24.6	11.4	4.4
well3	Kleaa	Dec-06	W	685	7.4	17.5	30.3	2.7	15	98	47	234.2	69.1	22.4	13	4.0
well1	Remeh	Dec-06	W	350	7.5	13.1	3.3	0	3	65	5.9	207.4	5.2	9.6	5.6	-2.7
well1	Dorbol	Nov-06	W	480	7.5	13.6	7.8	0	6	86	17.2	253.8	11.7	11.4	24.2	0.5
well2	Dorbol	Nov-06	W	430	7.3	14.8	5.8	0	5	86	7.4	261	5.4	5.3	22	2.9
well1	Drosha	Dec-06	W	424	7.4	18.4	7.5	1.4	8	75	12	211.1	15.7	17.5	10.2	4.0
well2	Heneh	Nov-06	W	842	7	18.2	42.8	15.5	21	106	29.3	414	59	35.2	31.6	-0.7
well1	Knaker	Dec-06	W	418	7.7	17.4	22.6	1.7	12	53	22	196.4	19.6	15.8	15	1.8
well2	Knaker	Dec-06	W	386	7.6	18.3	12.2	1.5	12	58	16.7	197.6	11.6	15	12.8	3.1
well3	Knaker	Dec-06	W	378	7.4	16.1	13.3	1.8	8	56	16.5	183	12.5	13.6	13.2	1.7
well4	Knaker	Dec-06	W	387	7.5	17.1	14.8	1.8	9	63	14	198.9	8.9	21.1	12.8	4.6
well1	Saasaa	Nov-06	W	685	7.3	16.6	14	2.3	11	100	103.6	213.5	5.7	22.8	12.6	-2.6
well2	Saasaa	Dec-06	W	633	7.5	17.2	17.2	2	11	99	35.4	294	43	18	12.8	-2.7
well3	Saasaa	Dec-06	W	625	7.2	17.1	15.6	2	12	108	30.5	274.5	59.6	16.3	13	1.8
well4	Saasaa	Dec-06	W	542	7.3	15.7	14	1.8	8	87	34.5	262.3	12.1	34.8	11	-3.8
well5	saasaa	Dec-06	W	515	7.2	15.1	11.7	1.5	9	90	21.5	280.6	21.2	27.3	11.8	-2.7
well6	Saasaa	Dec-06	W	551	7.2	16.1	12.7	1.6	9	97	16.7	283	7.1	37.4	12.4	2.7
well7	Saasaa	Dec-06	W	350	7.6	17.9	17.2	1.7	5	53	13	190.3	6.3	6.6	11	1.7
well8	Saasaa	Dec-06	W	430	7.4	18.6	13	1.9	7	58	34.6	48.8	5.2	154.4	11.6	-3.4
well9	Saasaa	Dec-06	W	434	7.7	18.9	27.7	2.4	7	50	36.6	163.5	10.6	30.4	13	-1.0
well10	Saasaa	Dec-06	W	385	7.5	17.1	13.9	1.9	6	55	19.1	176.9	4.9	9.2	10.6	2.7
well12	Saasaa	Dec-06	W	443	7.7	17.1	29.6	2.3	6	65	29.9	219.6	9.5	6.6	11.4	3.5
well14	Saasaa	Dec-06	W	410	7.4	16.6	10.1	2.3	7	66	19.8	194	7	14.5	11.6	3.0
well15	Saasaa	Dec-06	W	510	7.5	16.6	17.6	2.1	10	70	37.1	224.5	13	12.3	13.2	-0.6
well16	Saasaa	Dec-06	W	482	7.4	17.4	12.3	2.3	7	76	31.4	207.4	10.2	31.2	12.2	-0.4
well17	saasaa	Dec-06	W	587	7.1	17.7	15.1	0	10	98	23.7	275.7	13.6	32.6	13.6	3.1

Table 1 continued

Name	Location	Date	Type	EC ($\mu\text{S}/\text{cm}$)	pH	T ($^{\circ}\text{C}$)	Na ⁺ (mg/L)	K ⁺ (mg/L)	Mg ²⁺ (mg/L)	Ca ²⁺ (mg/L)	Cl ⁻ (mg/L)	HCO ₃ ⁻ (mg/L)	SO ₄ ²⁻ (mg/L)	NO ₃ ⁻ (mg/L)	SiO ₂ (mg/L)	σ (%)
well18	Saasaa	Dec-06	W	535	7.2	16.4	16.1	3	9	89	21.4	272.1	14.4	29	13.4	1.1
well19	Saasaa	Dec-06	W	557	7.1	17.1	17.2	5.9	10	93	22.2	285.5	16.6	26.4	14	2.4
well21	Saasaa	Dec-06	W	688	7.2	16.5	11.2	2	12	116	103.2	236.7	6	22	13.2	0.3
well22	Saasaa	Dec-06	W	510	7.3	18.2	10.3	1.7	11	87	41.9	225.7	7.9	23.8	12.4	2.8
well23	Saasaa	Dec-06	W	791	7.1	17.5	16	2.4	16	91	95.5	174.5	39.1	30.8	13.6	-1.9
well3	Dorbol	Nov-06	W	560	7.4	14.2	7.4	0	5	107	22.8	274.5	18.2	17.6	14.2	2.3
well2	AboKaook	Dec-06	W	506	7.2	15.7	10.1	3.8	9	93	14.7	256.2	23.5	25.5	11.6	3.6
well3	AboKaook	Dec-06	W	466	7.3	15.6	10.4	2.1	8	85	16	246.4	15	21.1	11.8	2.6
well6	BeitSabar	Nov-06	W	756	6.6	15.6	17.8	1.1	17	121	41.8	246.4	87.2	35.2	10.6	4.3
well2	BeitTima	Nov-06	W	710	6.7	16.7	10.5	1.2	23	121	12.9	224.5	174.6	21.6	14.6	2.7
well3	BeitTima	Nov-06	W	930	6.5	16.7	9.1	1.6	24	167	18.7	285.5	250.7	6.2	10.6	1.2
well1	Hosenieh	Dec-06	W	648	7.2	17	13.5	1.6	15	99	23.7	292.8	52.8	43.6	11.4	-3.5
well2	Hosenieh	Dec-06	W	587	7.3	18.4	10.2	1.2	11	96	19.5	242.8	56.2	32.6	10.6	-0.5
well3	Hosenieh	Dec-06	W	582	7.3	18.7	10.4	1.2	11	90	19.9	240.3	63	24.6	11.4	-2.9
well1	Tabibieh	Nov-06	W	624	7.5	16.3	10.3	1.1	13	104	23.6	240.3	87.3	27.7	9.6	-1.0
well1	Ainaashara	Nov-06	W	440	7.3	17.9	8.8	0	10	76	9.3	253.8	5	4.4	27	4.3
well4	BeitSabar	Nov-06	W	588	7.2	14.6	15.2	2.1	13	97	22.4	296.5	15.6	26.4	13.8	3.1
well5	BeitSabar	Nov-06	W	646	7.2	17.3	14.1	1.6	14	102	22.7	251.3	90.4	31.7	11.8	-1.9
well7	BeitSabar	Dec-06	W	473	7.3	15.9	11.5	1.7	7	81	11.8	240.3	17.3	17.6	11.8	2.5
well9	BeitSabar	Dec-06	W	855	7.3	18.8	22.9	0.6	21	140	66.4	198.9	179.8	34.8	19.6	1.7
well1	KaferHour	Nov-06	W	818	7.5	13.3	13	0.8	25	146	14.7	211	314.9	23.8	11	-5.0
well2	KaferHour	Nov-06	W	697	7.5	18.9	11	0	20	116	19.6	240.3	162	19.4	16.4	-1.8
well3	KaferHour	Nov-06	W	673	7.3	19.1	14.8	0.7	17	97	25.1	248.9	78	38.7	17.4	-1.0
well1	Khazrajeh	Dec-06	W	578	7.1	17.2	11	3.1	9	95	22.8	284.3	11.9	26	13.2	0.6
well3	MogherAlMer	Nov-06	W	560	7.4	18	10.4	0	13	85	20.8	297.7	13.9	29.9	12.6	-4.1
well2	Tabibieh	Dec-06	W	662	7.1	17.9	12.6	1.8	15	115	27.9	261.1	89.2	30.8	12	1.0
well1	Talmasiat	Nov-06	W	385	7.4	17	7.1	1.5	7	60	8.7	207.4	6.7	18.9	9.8	-2.2
well2	Talmasiat	Nov-06	W	466	7.4	15.4	6.7	1.3	7	77	8.9	244.1	9.5	23.7	9.2	-0.9
well1	KhanElshekh	Dec-06	W	407	7.4	17.9	9	1	5	73	15.9	203.7	8.3	21.7	10.6	1.9
well2	KhanElshekh	Dec-06	W	625	6.8	17.9	9	1.1	15	128	19.6	274.5	100.6	29.5	11.2	2.9
well4	KhanElshekh	Dec-06	W	443	7.5	19.2	8.6	0.7	5	84	16.1	219.6	16.6	18.9	10.2	3.1
well7	KhanElshekh	Dec-06	W	575	7.1	17.6	11.5	1	13	102	24.8	295.2	26.6	21.6	10.8	2.0
well8	KhanElshekh	Dec-06	W	456	7.4	17.1	11.3	0.8	5	81	19	213.5	17.7	22.9	10.6	2.0
well1	MazratNafor	Dec-06	W	415	7.4	17.7	13.2	1.8	7	62	14.5	214.7	10.1	15.4	11.4	-1.1
well1	Mogher-Hene	Nov-06	W	655	7.2	18.8	16.5	0	15	97	34.9	244	44	44	15.8	1.4

Table 1 continued

Name	Location	Date	Type	EC ($\mu\text{S}/\text{cm}$)	pH (-)	T ($^{\circ}\text{C}$)	Na^+ (mg/L)	K^+ (mg/L)	Mg^{2+} (mg/L)	Ca^{2+} (mg/L)	Cl^- (mg/L)	HCO_3^- (mg/L)	SO_4^{2-} (mg/L)	NO_3^- (mg/L)	SiO_2 (mg/L)	σ (%)
well2	Mogher-Hene	Nov-06	W	884	7.1	17.2	26.3	0	24	122	61.2	259.9	122.1	81.8	18.6	-3.6
well3	Mogher-Hene	Nov-06	W	541	7.3	18.8	15.3	0.6	10	89	22.5	230.6	35.1	31.7	15.2	2.6
well4	MogherAlmer	Nov-06	W	849	7.2	16.4	27.6	0.7	23	121	53.1	311.1	77	73.5	23	-1.3
well5	MogherAlmer	Nov-06	W	766	7.6	18.1	16.8	0	21	114	38.7	301.1	66	67.8	18.2	-2.2
well6	MogherAlmer	Dec-06	W	529	7.7	19	17.5	0.7	11	75	30.6	173.2	31.2	84	22.4	-2.6
well7	MogherAlmer	Dec-06	W	732	7.3	19.3	22.3	0.8	18	103	61	185.4	35.6	116.6	18.8	1.5
MambejWell	MogherAlmer	Nov-06	W	451	7.2	18.4	6.4	0.8	2	85	9	226.9	7.2	16.3	10.4	3.6
8k	Arneh	Jun-82	W	-	6.9	12.8	9.7	0.7	4.9	22	10.6	91.5	4	6.6	-	0.0
43k	OmSharatet	Oct-84	W	-	7.4	-	6	1.8	18.3	38	21.3	195.2	13	7.1	-	-3.2
46k	AboKaook	Sep-83	W	-	7.1	18	12.2	5	40.2	12	24.8	231.8	2	39.8	-	-1.9
48K	Arneh	Oct-84	W	-	7.4	14	23.9	1.5	18.3	40	14.2	146.4	95	5.3	-	-1.3
49k	Arneh	Oct-83	W	-	7.4	13.5	8.5	0.7	25.6	34	35.5	183	9	5.3	-	-0.2
52K	Beit Tima	Jul-83	W	-	6.5	14.6	29	2	13.4	22	19.5	134.2	32	8	-	-0.3
53K	Beit Tima	Oct-84	W	-	7.5	14.6	8	1.8	12.2	20	17.8	109.8	2	4	-	-0.1
55K	Beit Jinn	May-83	W	-	7.3	11.2	16.6	1.5	9.8	24	14.2	122	23	8.4	-	-0.5
57K	Beit Jinn	May-84	W	-	7.3	10.3	2.5	0.5	14.6	36	12.4	146.4	16	6.6	-	1.6
133K	KhanElshekh	Oct-83	W	-	6.7	20	9.7	9	29.3	20	21.3	207.4	3	2.2	-	-0.3
150k	JdedetArtoz	Aug-83	W	-	7	18	61.6	11	19.5	68	46.1	36.6	300	3.5	-	-1.4
154k	JdedetArtoz	Oct-84	W	-	7.5	-	57.7	4.7	42.7	26	106.5	292.8	9	4	-	-1.9
165k	Dorbol	Apr-85	W	-	8.1	-	2.1	0	19.2	32	21.3	134.2	28	3	-	-1.0
176	JdedetArtoz	Oct-84	W	-	7.5	-	23.5	0.5	17.1	56	49.7	146.4	43	29.6	-	0.1
181	Arrouz	Oct-82	W	-	7.3	17.5	29	6.6	18	88	30	260	100	6.6	-	0.1
184K	Beit Saber	Aug-85	W	-	7.4	-	69	12.5	14.4	64	67.4	292.8	45	4.4	-	-0.1
179	Arrouz	Oct-82	W	-	8.2	18	17	2.5	24.3	52	30	165	80	8	-	0.5
186	KhanElshekh	Apr-83	W	-	6.2	-	62.1	1.3	19.5	60	35.5	237.9	104	14.1	-	0.3
265k	KaferQuaq	Dec-84	W	-	7.3	18	2.3	3.1	32.2	64	65.1	179.8	72	9.3	-	-3.3
275k	Arneh	Oct-85	W	-	7.5	-	18.4	4.3	31.2	124	49.7	317.3	150	0	-	-0.1
300	KhanElshekh	Oct-84	W	-	7.6	16.5	37.5	2.3	19.5	52	28.4	244	42	8.4	-	0.1
720	KhanElshekh	Mar-85	W	-	7.3	20	0.9	0	43.2	36	35.5	231.9	5	26.5	-	0.3
721	Qatana	Apr-85	W	-	7.7	19	48	21.5	2.4	64	28.4	170.8	70	61.9	-	0.6
721a	Qatana	Apr-85	W	-	7.4	-	11.5	2.3	7.2	64	35.5	183	15	8.8	-	-0.7
740	KhanElshekh	Aug-85	W	-	7.4	20	16.1	2.3	16.8	56	60.35	183.1	4	8.3	-	0.0
744	KhanElshekh	Aug-85	W	-	7.4	-	31.8	3.1	21.6	44	35.5	239	15	11.1	-	0.5
3032	Kafer Qouq	May-84	W	-	8.2	-	27.6	0.5	12.2	52	21.3	213.5	17	8	-	2.3
3036	Qatana	Oct-84	W	-	7.3	17	53.8	3.2	3.7	86	56.8	274.5	18	31.8	-	0.1

Table 1 continued

Name	Location	Date	Type	EC ($\mu\text{S}/\text{cm}$)	pH	T ($^{\circ}\text{C}$)	Na^+ (mg/L)	K^+ (mg/L)	Mg^{2+} (mg/L)	Ca^{2+} (mg/L)	Cl^- (mg/L)	HCO_3^- (mg/L)	SO_4^{2-} (mg/L)	NO_3^- (mg/L)	SiO_2 (mg/L)	σ (%)
3050	Saasia	Jun-82	W	-	8.4	17.4	35	1.8	35	11.6	70	128	18	13	-	3.9
3055	Kleaa	May-84	W	-	8.2	-	12.2	1.5	9.8	28	10.7	128.1	10	5.3	-	1.9
3072	Heneh	May-84	W	-	7.5	14.4	61.9	0.3	25.6	58	49.7	176.9	145	23.4	-	0.2
BeitJinn	BeitJinn	Nov-06	S	284	8.1	12.3	3.6	1.3	8.5	47	14.9	156.2	8.7	2.6	5.4	0.5
Almalha	Arneh	Nov-06	S	972	7.1	13.4	5.1	0.8	29	183	4.2	234	395	2.6	5.6	-2.3
Arneh	Arneh	Nov-06	S	261	8	11.5	2.9	0.4	3.5	53	5.1	168	3.7	1.8	4.4	1.1
Albardeh	Arneh	Nov-06	S	640	7.4	13.7	5	1.2	15	120	6.5	248	164.5	5.3	6.2	-2.1
Almshraa	Arneh	Nov-06	S	470	7.6	10.7	3.1	0	15	74	4.1	144	116	1.3	4.2	1.6
Dorbol1	Dorbol	Nov-06	S	295	7.8	17.6	3.6	0	2.5	54	7	164.7	7.6	2.9	6.6	-0.7
Dorbol4	Dorbol	Nov-06	S	251	7.9	14.5	2.8	0	4	42	6.4	139	3.7	4	4.8	-1.1
Dorbol3	Dorbol	Nov-06	S	245	7.7	15.2	2.8	0	3	40	5.6	136.6	4.3	3.8	5.4	-3.8
RasAlin	Qatana	Nov-06	S	330	7.4	17.6	5.8	0.7	8	58	7.8	185	6.1	10.1	6.6	3.9
Hamana	BeitTima	Nov-06	S	789	7.1	17.6	12.4	1.7	25.5	133	25.6	289.1	168	15.4	22	0.7
Beitsaber1	Beitsaber	Nov-06	S	762	7.1	17.2	10.2	0.8	23.5	131	20.2	290.4	132	11.9	12.4	4.2
Beitsaber2	Beitsaber	Nov-06	S	767	7.1	16.7	11.6	0.9	23	132	18.8	307.4	136	20.2	12.6	1.7
Alla	Ainshara	Nov-06	S	327	8.1	16.1	8.3	2.2	2.5	52	13.5	109.8	14.9	27.7	6.8	4.7
KaferHour1	KaferHour	Nov-06	S	887	7.3	15.8	13.6	6.6	25.5	153	35.5	327	171	29.9	13.8	0.5
Talmasiat	MogherAlMer	Nov-06	S	345	7.4	15.9	13.1	3.4	6	53	10.2	195	7.2	9.7	16	-0.6
Ganat	Hasebe	Dec-06	S	462	7.4	18.1	7.6	2	8	74	12.9	224.5	36.3	18	9.2	-3.8
AinAljoz	Kalaetjandal	Nov-06	S	219	7.8	14	2.9	0.5	9.5	30	3.8	137	2.9	1.9	5	-0.5
jandal	Kalaetjandal	Nov-06	S	403	8	16.2	12.7	2.5	16.5	45	23.8	103.7	23.5	80.5	7.2	0.7
Mambej	MogherAlmer	Nov-06	S	325	7.7	16	13.9	3.7	6	51	6.6	190	5.7	8.8	15.2	2.5
Bkassam1	Bkassam	Nov-06	S	670	7.9	15.5	29.5	4	26	61	57.1	156.2	35.2	122.8	7.8	-2.4
BeitJinnn Ala	BeitJinnn	Nov-06	S	260	8.4	11.2	1.8	0.5	7	42	2.1	136.6	13	1.7	3.6	3.2
Morkos	Arneh	Dec-06	S	610	7.6	12.4	2.1	0	14	107	4.1	153.7	196.2	2.6	5	-1.5
Kneseh	Remeh	Dec-06	S	428	7.6	13.4	5.7	1.6	8	74	8.6	229.4	18.6	15.4	7.6	0.0
Tamer	Remeh	Dec-06	S	315	7.7	14.1	4	0	9	46	6.7	173.2	9	9.2	7	-2.4
Dorbol2	Dorbol	Nov-06	S	298	7.3	16.8	3.5	0	2	57	6.6	172	5.2	4	5.8	-0.3
Saasia	Saasia	Nov-06	S	237	7	18.4	19.7	4.5	8.5	15	13.1	80.5	8.9	19.8	27.6	5.0
Bkassam3	Bkassam	Nov-06	S	535	7.7	12.1	5.1	0	21	75	6.4	180.6	95.8	28.1	6.6	1.0
AinBala	Qatana	Nov-06	S	582	7.4	17.4	10.5	0.7	8	115	12.2	266	67	12.3	12	4.6
Bkassam2	Bkassam	Nov-06	S	633	8.1	16.4	22	5.9	20	76	39.2	201.3	25.2	104.3	8.6	-0.5
Asfal	Ainshara	Nov-06	S	318	7.5	15.4	4.7	1.3	3	63	7	178.1	6.3	5.3	6.4	4.3
KhrbtSouda	KhrbtSouda	Nov-06	S	262	8.1	13.4	3.5	0	1	41	6.3	127	8.5	3.1	5.4	-4.4
33	Tal Assyuf	Jun-83	S	-	7.5	-	142.9	0	41.5	108	140	280.6	59	4.2	-	1.1

Table 1 continued

Name	Location	Date	Type	EC ($\mu\text{S}/\text{cm}$)	pH	T ($^{\circ}\text{C}$)	Na^+ (mg/L)	K^+ (mg/L)	Mg^{2+} (mg/L)	Ca^{2+} (mg/L)	Cl^- (mg/L)	HCO_3^- (mg/L)	SO_4^{2-} (mg/L)	NO_3^- (mg/L)	SiO_2 (mg/L)	σ (%)
41	Ain Saba	Dec-77	S	–	7.5	–	10	0	23	85	14	207.4	134.1	0	–	0.8
43	Rashashbeh	Sep-77	S	–	7.2	–	13	0	26	89	17.4	231.8	135	0	–	0.4
44	Rijmeih	May-83	S	–	8.1	–	9.2	0	18.3	18	12.4	134.2	7	0	–	2.0
45	Ras Alwadi	Jul-78	S	–	7	–	20	0	12	38	25	170.8	10.7	0	–	0.4
46	Tabibieh	Aug-82	S	–	8.2	–	14.7	0	7.2	52	10	150	42	13.2	–	0.0
47	Husenieh	Oct-83	S	–	6.9	–	15.6	0	3.6	32	19.5	109.8	6	3.1	–	1.0
49	Mbaya	Oct-83	S	–	7.6	–	13.3	0	7.3	24	17.8	109.8	2	2.2	–	0.0
51	Artouz Qanat	Aug-84	S	–	7.5	–	26.4	0	4.9	60	46.2	145.2	18	26.4	–	0.7
61	Alfouar spring	Oct-83	S	–	6.9	–	11.7	0	4.9	12	17.8	48.8	2.5	2.7	–	3.9
10276	Mt Hermon	Oct-84	S	–	7.3	–	21.6	2	20.7	42	21.3	183	50	10	–	–0.1
10285	Shabaanet	Oct-84	S	–	7.6	–	73.6	0.5	25.6	66	21.3	256.2	180	5.4	–	–0.1
10291	Mt Hermon	Oct-84	S	–	7.7	–	1.4	0.4	25.5	60	99.4	128.14	4	8.4	–	0.5
10292	Ain Najjem	Oct-84	S	–	7.8	–	4.6	0	19.3	116	61.4	97.6	190	8.8	–	1.3
10297	Almashraa	Oct-84	S	–	8.3	–	23	0	24.3	50	76.5	122	33.4	11.3	–	4.6
10308	Beit Tina1	Oct-84	S	–	7	–	6.7	0.4	34.8	72	31.3	176.9	130	18.1	–	0.2
10309	Beit Tina2	Oct-84	S	–	7.1	–	4.6	3.5	60	104	139.5	30.5	283.4	4.4	–	0.6
10310	Mt Hermon	Oct-84	S	–	7.7	–	0	0	24.3	22	17.8	122	20	2.6	–	2.1
10311	Mt Hermon	Oct-84	S	–	7.3	–	4.6	3.5	18.2	52	32.3	91.5	88.9	8.8	–	–0.3
10322	Mt Hermon	Dec-84	S	–	7.7	–	2.7	0	24.3	84	83.4	122	76.8	21.6	–	0.1
10325	Mt Hermon	Dec-84	S	–	7.7	–	0.5	0	14.6	32	30.9	74.4	31.2	6.2	–	–0.3
10326	Mt Hermon	Dec-84	S	–	8.1	–	0.2	0	12.2	20	21.3	62	10	5.7	–	2.3
10327	Albardeh(Remeh)	Dec-84	S	–	8.3	–	2.3	0.8	23.1	64	81.7	115.9	38.9	21	–	–1.3
10333	Ain Badran	Dec-84	S	–	7.9	–	0.3	0.8	24.3	36	35.5	122	29.7	8	–	1.2

EC electrical conductivity, W well, S spring, σ chemical analyses error

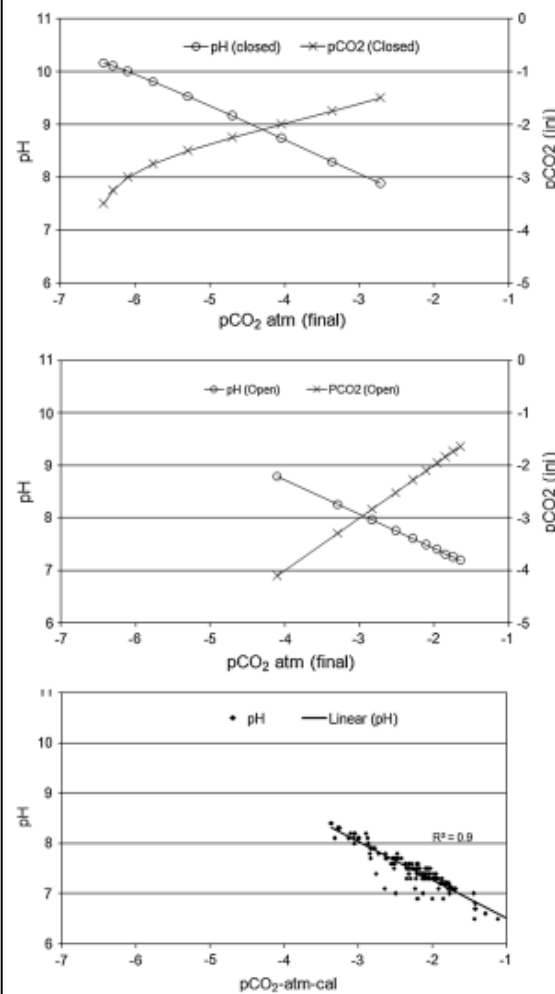


Fig. 3 Open and closed system dissolution of carbonate system determined with PHREEQC and pH values as a function of pCO₂ (atm) calculated values in the water samples

The scatter plot of saturation indices (SI) of calcite and dolomite is shown in Fig. 4b. In this diagram, a central band of 0.4 units wide along each axis, representing errors that may occur in the measurement of pH, Mg²⁺, and Ca²⁺. The four quadrants of the plotting field (I–IV) represent different kinds of equilibrium conditions with respect to calcite and dolomite. The figure shows that some of the water samples are distributed in quadrant I and III, and most of them are situated in the central band of equilibrium. The samples in quadrant I represent supersaturation with respect to both carbonates. The samples plotting in quadrant III represent undersaturation with respect to calcite and dolomite. These samples correspond to water coming from an environment where carbonates are

impoverished, or to water that has a short residence time in the hosting carbonate rocks (Langmuir 1971; Kortatsi 2007).

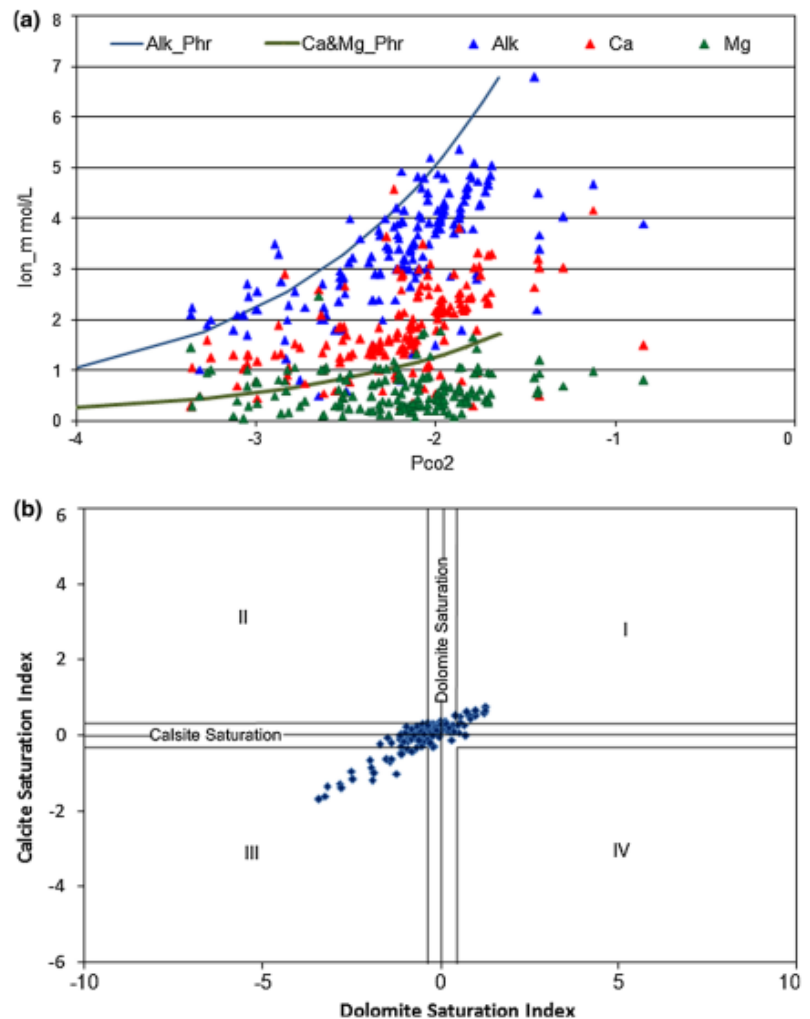
The SI of calcite as a function of calculated pCO₂ are shown in Fig. 5 (chart), and are mainly closed to or exceed zero for most samples and the spatial distribution of SI of calcite is shown in Fig. 5 (map). The highest part of the Jurassic is characterized by low SI of calcite, whereas relatively high values were measured in the lower part levels near the Arneh village. This is mostly due to a short residence time and a lesser amount of CO₂ as a result of vegetation absence in the higher parts characterized by limited soil development. The low SI of calcite near the Arneh village might indicate a quick groundwater circulation from the north part towards the south part through channels and conduits developed along faults and fractures as a preferential flow. The high values encountered in the alluvial and basalt aquifers can indicate a deep groundwater flow from Jurassic aquifers to these aquifers controlled by sub-regional geological structures.

The alternation of limestone and dolomite along the flow path can be characterized by Mg/Ca ratios. Mg/Ca ratios between 0.5 and 0.9 are typical for carbonate aquifers (Hsu 1963; Stadler et al. 2012). For groundwater genetically bound to pure limestones, the Mg/Ca ratio is smaller than 0.1 on the other hand, water from pure dolomite is characterized by Mg/Ca ratios higher than 0.7 (Flakova 1998). However, even very pure limestone can give rise to relatively high Mg/Ca ratios in water with a long residence time (Moral et al. 2008; McMahon et al. 2004; Batiot et al. 2003; López-Chicano et al. 2001; Edmunds and Smedley 2000; Fairchild et al. 2000; Plummer et al. 1978; Plummer 1977; Bicalho et al. 2012). In fresh water, Mg/Ca ratio values greater than 1 can be the result of water interacting with Mg-rich silicate rocks such as volcanic ones, with Mg being derived from olivine (Schoeller 1956; Hem 1985; Vengosh and Rosenthal 1994).

Figure 5 (chart) shows that most of the samples indicate Mg/Ca ratios less than one and many of them less than 0.5. These values imply that the contact time between the infiltration water and hosting rocks was rather short. Few samples show ratios superior to 1 indicating a basaltic rock weathering or precipitation of gypsum resulting from an impoverishment in Ca ions, or sulphate reduction process facilitated by anaerobic conditions.

The dissolution of gypsum leads to increasing sulphate concentration in groundwater and to enhanced solubility of dolomite; consequently it lowers the solubility of calcite. SI of gypsum as a function of SO₄²⁻ concentration are plotted in Fig. 6. The relationship between the two variables shows that the dissolution of gypsum is the main source of sulphate in these waters (correlation coefficient $r = 0.64$). This is associated with an increase in calcium

Fig. 4 **a** Calcium, magnesium, and alkalinity concentration in mmol/L as a function of $p\text{CO}_2$ (atm) calculated values; *solid lines* are the alkalinity, calcium, and magnesium determined with PHREEQC for pure calcite and dolomite dissolution. **b** The saturation indices (SI) of calcite and dolomite determined in the water samples

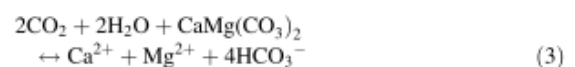
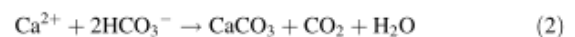


concentration as shown in Fig. 7. This figure shows also that there is no correlation between calcium and sulphate for all the samples only when sulphate concentration becomes greater than 0.5 mmol/L. The trend indicates a positive relationship between the two variables due to gypsum dissolution.

Dedolomitization process

The occurrence of Mesozoic limestones and dolomites associated with gypsiferous layers gives rise to Ca-sulphate-rich water which induces dissolution–precipitation processes in the dolomite–calcite mineral assemblage (Capaccioni et al. 2001). Dedolomitization process means, that the calcite precipitation and dolomite dissolution are driven by anhydrite (gypsum) dissolution (Plummer et al.

1990). The dedolomitization is controlled by the three following reactions:



The increasing concentration of Ca^{2+} during the dissolution of gypsum leads to the precipitation of calcite. A decrease in HCO_3^- concentration causes the dissolution of dolomite and an increase in Mg^{2+} concentrations in water. The increasing in Mg^{2+} concentrations causes an increase in Ca^{2+} concentration, until the equilibrium is reached between water and both minerals. Thus, the gypsum dissolution brings about a substitution of dolomite by calcite.

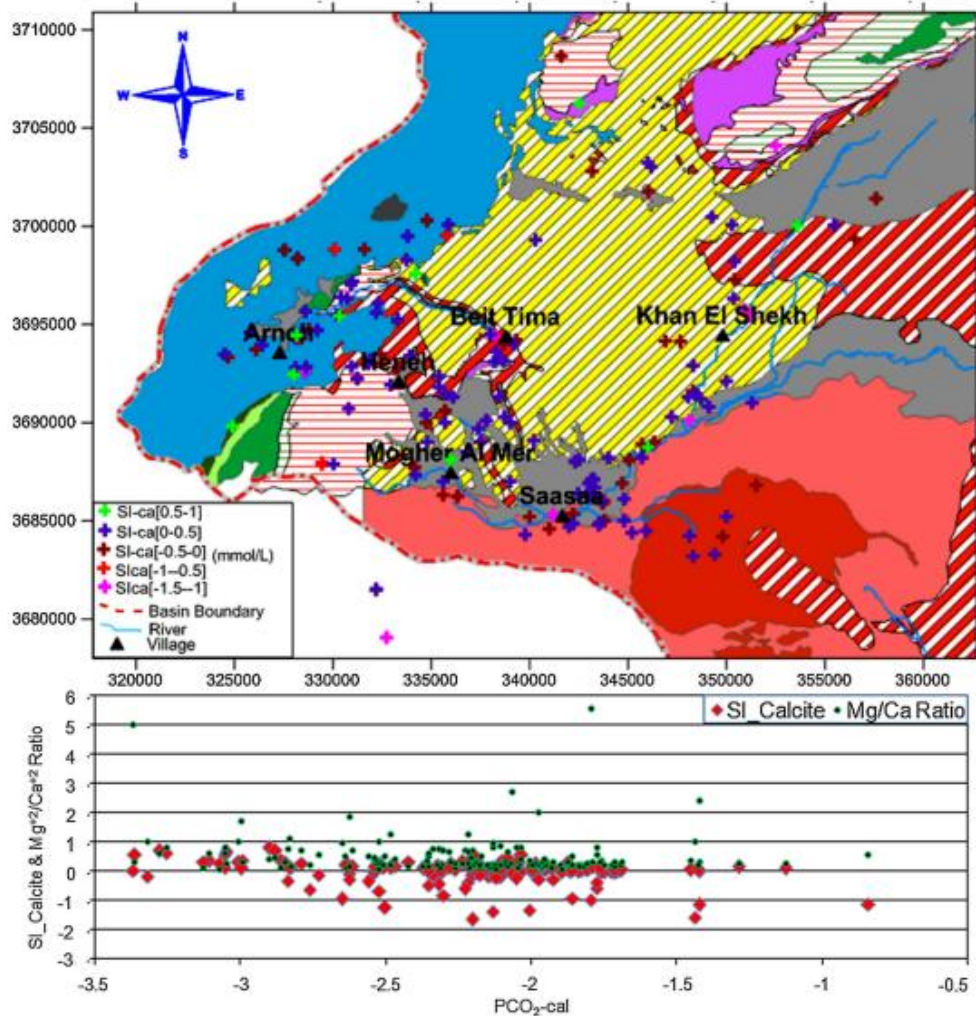


Fig. 5 Classification and spatial distribution of saturation index of calcite in the water samples with chart showing the SI of calcite and Mg^{2+}/Ca^{2+} molar ratio as a function of pCO_2 (atm) calculated values

In the thermodynamic calculation, it is likely that gypsum dissolution is irreversible in most of the system, whereas the water remains at or near saturation with respect to calcite and dolomite. It is appropriate then to choose the dissolved sulphate as a reaction progress variable in examining the trend in the water quality data (Plummer et al. 1990) (Fig. 6). The samples that are characterized by low saturation indices of calcite and by low concentration in sulphate (<1 mmol/L), indicate that little or no gypsum dissolution occurred for these water samples. Some samples show over saturation of dolomite even with less content in sulphate, indicated that the dolomite dissolution was not driven by gypsum dissolution. When the sulphate

concentration increases for some samples, they become near saturation with respect to dolomite if we accept an uncertainty of about ± 0.5 for saturation index determination. The majority of these samples are located in the Jurassic aquifer. SI of gypsum as a function of sulphate concentration evolve from undersaturated to quasi-saturated and sulphate concentration increases with the development of gypsum dissolution. Figure 7 shows that the high values of sulphate (more than 1 mmol/L) which are associated with over saturation with respect to dolomite were measured mainly near the Arneh village. It indicates that the dedolomitization process is occurring there. This phenomenon was observed near Beit Tima and south of

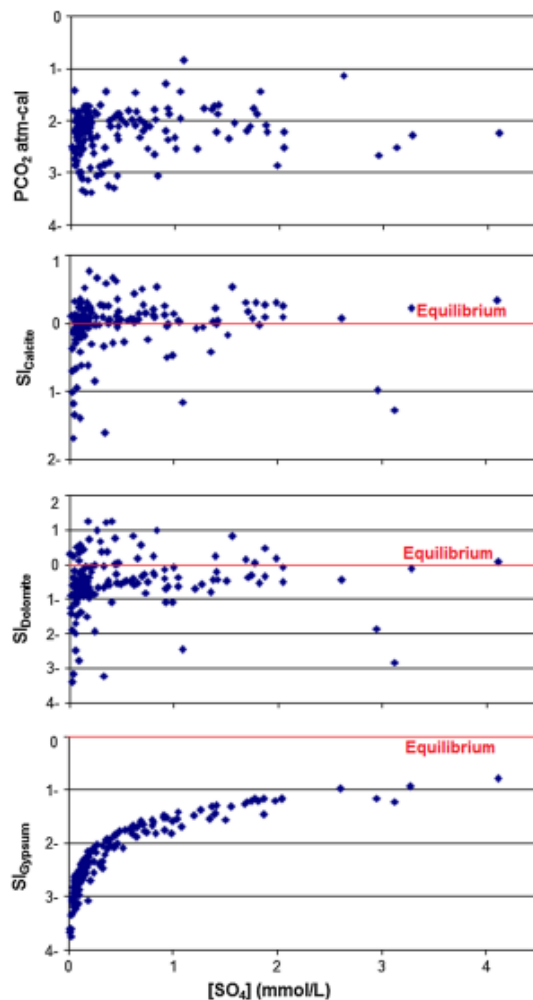


Fig. 6 Saturation indices of calcite, dolomite, and gypsum as well as PCO_2 (atm) calculated values as a function of SO_4^{2-} (mmol/L)

Hench villages (Miocene aquifer). Other high concentrations of sulphate which are not associated with over saturation of dolomite indicate additional sources of sulphate such as anthropogenic influences. As a consequence of dedolomitization reactions, the calcite precipitation in the system causes a decrease of pH values due to H^+ released from HCO_3^- during the incorporation of CO_2 to calcite. In our case, the pH values are hardly going down as shown in Fig. 7. According to Figs. 6 and 7, we can conclude that an approach to dedolomitization processes only occurs in isolated places where the gypsiferous formations are located.

Silicate weathering

The effect of silicate weathering on the water chemistry is primarily the addition of cations and silica, given that high silica in the water samples indicates active hydrolysis of silicate minerals.

The silica values for the samples collected in 2006 are shown in Fig. 8. Clearly, a sharp boundary between three groups is observed. The first one is characterized by low silica concentrations and located in the Jurassic aquifers. The second one is located in the Neogene and Quaternary formations and characterized by higher silica. The highest concentration in silica, (third group), was observed in the basaltic Miocene aquifer which is more weathered compared to the basalt of the Quaternary. High silica content in the Neogene/Quaternary aquifers might indicate a flow pattern from the Miocene basaltic aquifer to the southeast direction toward these aquifers.

The mineral stability diagram is another approach to test the proposed hydrochemical evolution (Drever 1988; Guler and Thyne 2004b). The stability fields for the Na-Plagioclase (albite) and its potential weathering products, paragonite, gibbsite, kaolinite, and pyrophyllite are shown as a function of $\log([\text{Na}^+]/[\text{H}^+])$ and $\log[\text{H}_4\text{SiO}_4]$ in Fig. 8. It shows that the main reaction is the conversion of albite to kaolinite. Meaning that the primary silicate minerals, such as plagioclase and clinopyroxene, can be dissolved and weathered to kaolinite which is most likely to be in equilibrium with groundwater. While noting some samples extending into the albite stability field suggesting equilibrium between clay and primary mineral, it is not likely to be the main process controlling the water chemistry.

Figure 8 also shows the stability fields for the Ca-Plagioclase (anorthite) and its possible weathering products, gibbsite, kaolinite, and Ca-montmorillonite as a function of $\log([\text{Ca}^{2+}]/[\text{H}^+]^2)$ and $\log[\text{H}_4\text{SiO}_4]$. In this case, the kaolinite is more likely to be stable than for example gibbsite, as a result of anorthite weathering products. This may be due to removal of the Ca from the system by the precipitation of Ca salts. Some samples which are located at or close to the stability field of montmorillonite indicated that the typical aquifer of these water samples is basically a basic rock (like basalts) (Appelo and Postma 2005).

The two diagrams show that most of the groundwater samples are not in equilibrium neither with albite nor with anorthite, and they will decompose if they are present in the system.

According to Han and Liu (2004), we can use the variation in the composition of water ($\text{Mg}^{2+}/\text{Ca}^{2+}$ and $\text{Na}^+/\text{Ca}^{2+}$) to distinguish limestone, dolomite, and silicate rock sources of ions. Figure 9a displays the covariation between the two molar ratios. These two ratios are

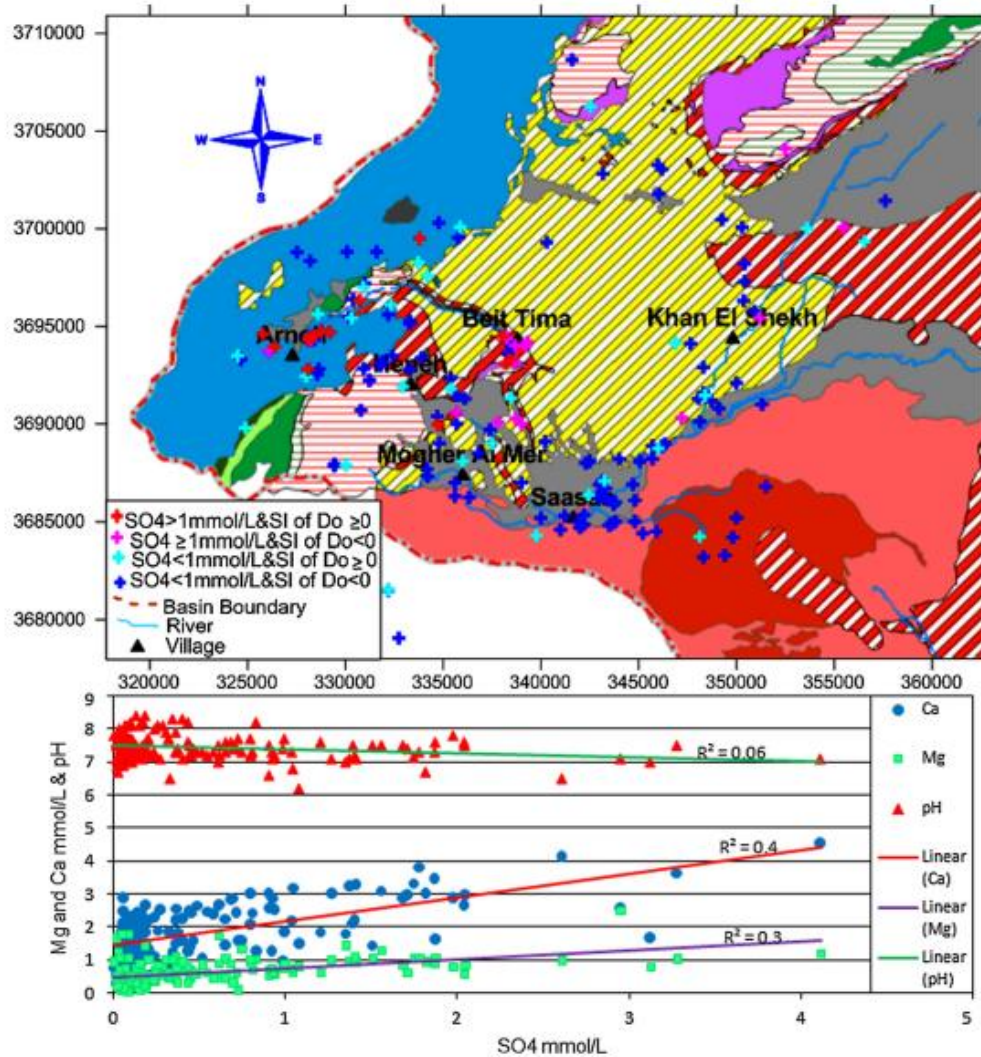


Fig. 7 Classification and spatial distribution of saturation index of dolomite in the water samples, and a scatter charts of Ca²⁺, Mg²⁺ (mmol/L) and pH as a function of SO₄²⁻ (mmol/L)

almost equivalent because both of them vary over three orders of magnitude. Water samples composition seems to be affected by the mixing trend of three types of rock, most likely the carbonate rocks have a higher effect. It is noticeable that the Mg²⁺/Ca²⁺ ratios of most samples are bellowing the Mg²⁺/Ca²⁺ = 0.8 line. This is probably due to equilibration of the water simultaneously with calcite and dolomite. The water equilibrated together with calcite and dolomite gives an ideal molar Mg²⁺/Ca²⁺ ratio of about 0.8 (Appelo and Postma 1993; Han and Liu 2004).

Dissolved solutes and nitrate concentrations

The intensive uses of fertilizers and manure in the agricultural management systems have increased the nitrate pollution of groundwater and have adverse effects on ecosystems and human health (Anastasiadis 2003). Biodegradation of crop residues, agricultural and municipal wastes applied to agricultural fields and waste generated directly by animals are also considered as other sources of nitrate pollution. Figure 10 shows that the low nitrate concentration was mostly measured in

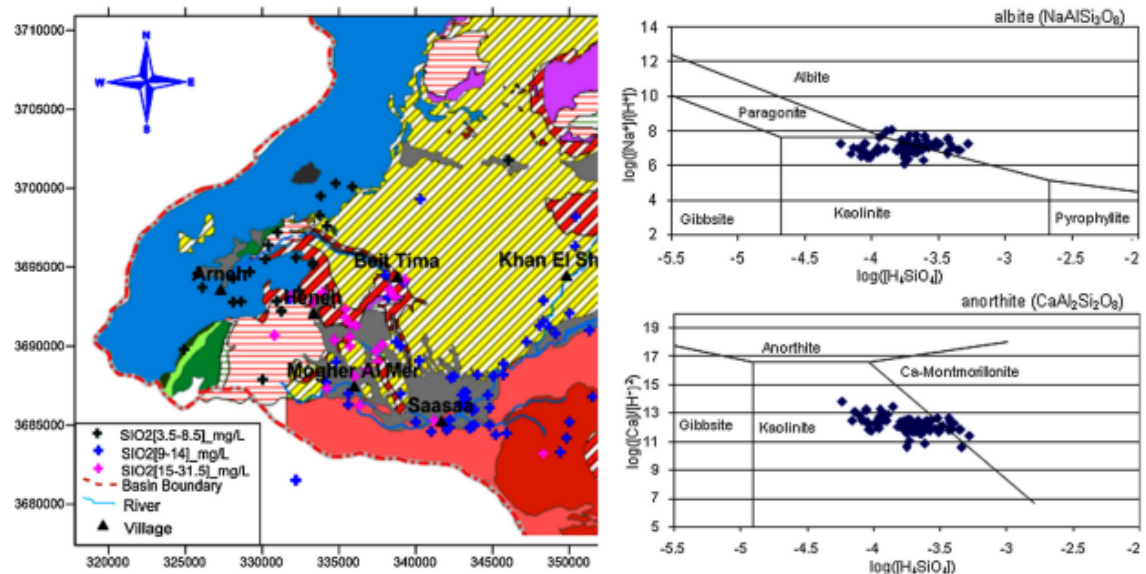


Fig. 8 Classification and spatial distribution of SiO_2 (mg/l) concentration in water samples and stability diagram of both Ca-Plagioclase (anorthite) and Na-Plagioclase (albite) and their possible weathering products

the mountain area (Jurassic and Paleogene aquifers) where there are less agricultural activities. On the other hand, this parameter tends to increase in the plain area (Neogene and Quaternary aquifers). These two aquifers host a considerable number of irrigation wells and intensive agricultural activities using massive input of nitrogenous fertilizers and manures. The effect of irrigated return flow on the groundwater seems to be significant in this area. Inorganic agricultural fertilizers are also thought to be the major sources of chloride in the groundwater. Few water samples are characterized by considerable chloride concentrations associated with relatively high nitrate concentrations as shown in Fig. 10. The high chloride concentration might be attributed to geochemical processes associated with evaporite dissolution. The upward leakage from deeper aquifers, where these formations are located, increases the chloride concentration.

Redox processes

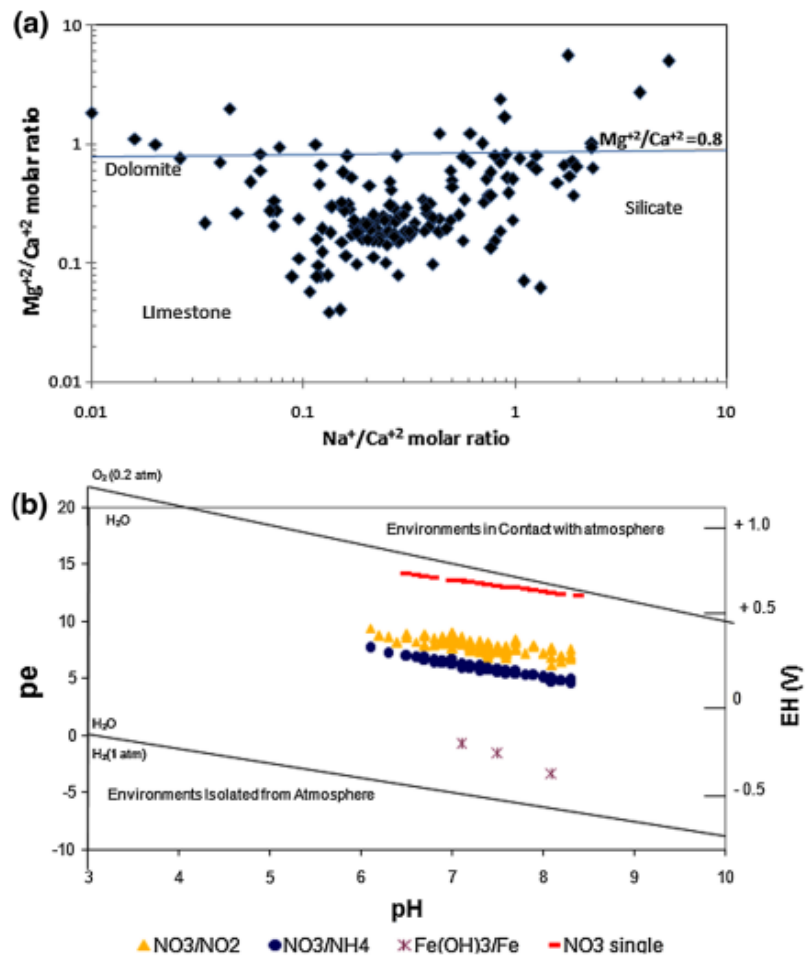
Based on the relationship between pH and Pe, Fig. 9b shows the stability diagram of redox conditions range within the aquifers. It can be stated that the redox conditions in the aquifers vary from aerobics to suboxic conditions, because no redox couple is clearly present in this case.

Stuyfzand classification

In hydrochemical studies, classification serves the purpose of isolating a group of representative clusters (also known as water groups or hydrochemical facies). This can be correlated with location and geology (Suk and Lee 1999; Barbieri et al. 2001; Guler et al. 2002; Guler and Thyne 2004a).

The predominant water types are determined and schemed (Fig. 11) using the Stuyfzand method (Stuyfzand 1989). According to this method, groundwater can be classified as very oligohaline, oligohaline and fresh ($\text{Cl}^- < 150$ mg/L for all sample except one then the code changes between G, g and F). The factor F is mainly dominant in the southern and southeastern parts of the area (plain part) as a result of intensive irrigation activities associated with high evaporation rates and return flow as well as the effect of topographic factor. The upward leakage from deeper aquifers, where evaporites are present, can be another source of chloride. In terms of alkalinity values, the groundwater is classified as moderately low, moderate and moderately high (alkalinity varying between 1 and 8 meq/L then the code changes between 1, 2, and 3). HCO_3^- concentration increases with the general direction of the flow pattern. This indicates the effects of carbonate rocks dissolution by infiltrating CO_2 -rich meteoric water and dissolution of volcanic rocks. The local appearance of

Fig. 9 **a** $\text{Na}^+/\text{Ca}^{2+}$ versus $\text{Mg}^{2+}/\text{Ca}^{2+}$ molar ratios in the water samples, (after Han and Liu 2004). **b** The stability diagram of redox conditions range based on the relationship between pH and pe and the distribution of water samples



Ca- NO_3 water types in the plain area is a result of agricultural pollution. In the western part, mainly in the Jurassic aquifer, the calcium mix water type is present. The “Mix” anions water type refers to all the water in which no anion family makes up more than 50 % of the sum of anions. Generally, the HCO_3^- is the dominating anion and Ca^{2+} is the dominating cation of the hydrochemical types of groundwater in the whole area.

Groundwater flow behaviour

According to water type classification, groundwater discharge (mainly major springs), and geological and structural control, the study area can be divided into four subareas S_1 , S_2 , S_3 , and S_4 (Fig. 12).

The groundwater flows in S_1 from the north and northwest in Mt. Hermon towards the south and southeast

through the karstic channels and conduits. Groundwater in R_1 discharges in many springs located in the valley around the Arneh village; together these springs form one of the two tributaries of the Awaj River (Sebarani). In S_2 , groundwater also flows in karstic channels in the Jurassic aquifer towards the south and east direction afterward discharging in the Upper Beit Jinn spring. In this area, another tributary of the Awaj River (Jinani) is generated. The average annual discharge of upper Beit Jinn spring is very close to the volume of the annual rainfall amount estimated over S_2 (RDAWSA 2006), and since the infiltration coefficient is estimated to 84 % for this area (RDAWSA 2006), the recharge area might not correlate with the size of the geographic surface water catchment. Therefore, the basin boundaries can be extended towards the west (Fig. 12). In S_3 , groundwater flows towards Beit Jinn spring and it is also controlled by faulting and structural blocks. S_4 is the biggest subarea which includes the

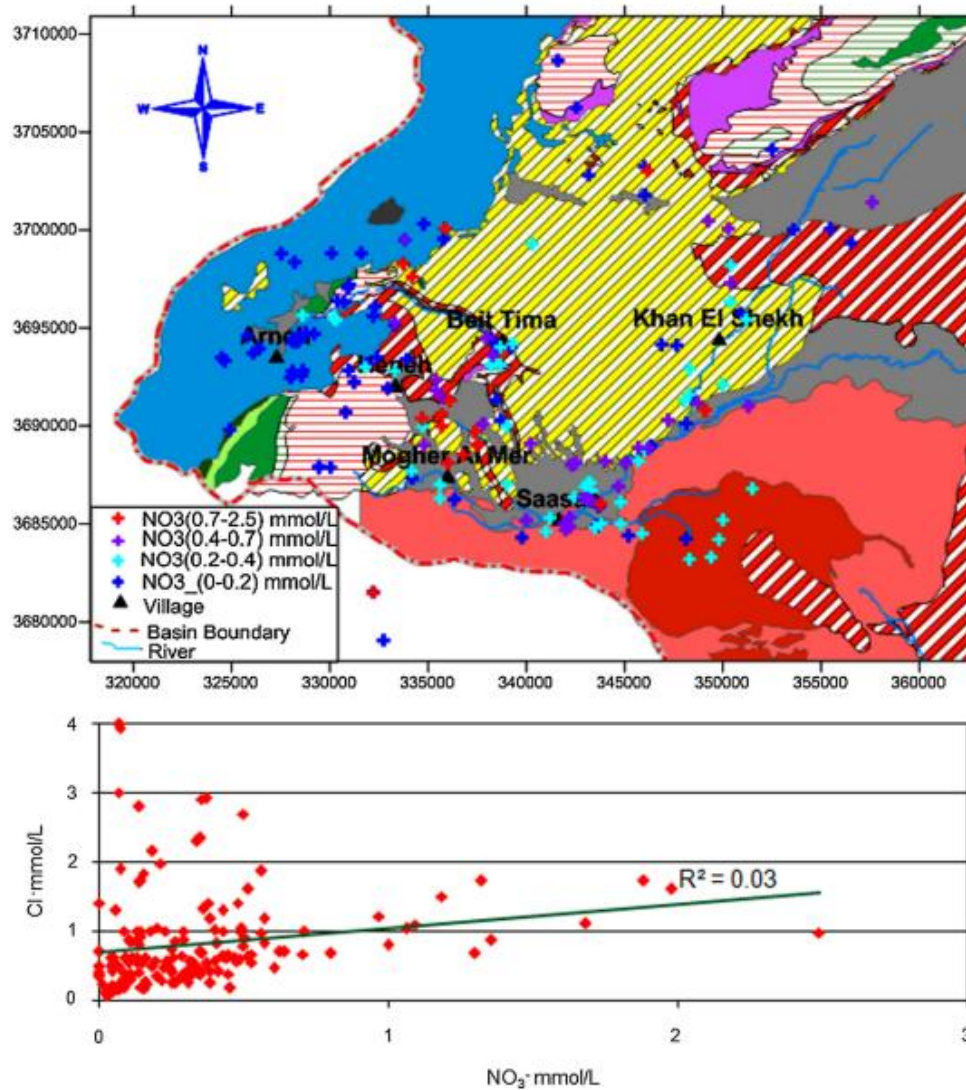


Fig. 10 Classification and spatial distribution of NO_3^- concentrations (mmol/L) and its relationship with Cl^- concentration (mmol/L)

zones with higher groundwater withdrawals for intensive irrigation purposes. The Neogene and Jurassic outcropping formations are the main sources of the water recharge in S_4 but it also receives the input of the upper Paleogene, Quaternary and Miocene basalt aquifers. In this area, water discharges through the major springs, Membeg, Talmassiat, Tell assyouf, and Tabibieh located from west to east. Numerous wells also exist in the Neogene conglomerate aquifer which is recharged from both the direct infiltration and the hydraulic exchange with the deeper Jurassic and

Cretaceous aquifers. At the level of a major northwest-southeast fault cutting through the Neogene Plain, water is thought to converge to Tabibieh Spring. This spring originates in the east-west fault along the Awaj River.

Conclusion

The use of hydrochemistry in this case study has provided useful information about the different mechanisms

a significant role in this part. On the other hand, the situation in the western and northwestern parts seems to be a little different. In this part, the karstic feature is well developed, enhancing the infiltration and dissolution mechanisms. Therefore, the vertical flow seems to be a dominant scheme. Consequently, hydrochemical patterns did not give enough evidences for expecting a huge feeding flow from Jurassic aquifers towards the other aquifers. Important anthropogenic influence through infiltration of irrigation water in the plain area has been also detected.

The results show that the hydrochemical evolution is not clear enough to provide an effective approach to delineate the flow pattern indicating that this area is much more dominated by recharge than discharge processes. Thus, this area could be considered as a part of a main intermediate or regional flow system more than a local one. The flow pattern is clear from the potentiometric map but that does not tell the whole story about the groundwater behaviour.

Nevertheless, an additional survey of the aquifer mineralogy, a new sampling for isotopes analyses and age-dating techniques will be carried out to propose a quantitative model of the hydrosystems. This will serve as a tool to understand the behaviour of the aquifer system and its response in term of water recharge/discharge, residence time, and water quality.

References

- Aghazadeh N, Mogaddam AA (2011) Investigation of hydrochemical characteristics of groundwater in the Harzandat aquifer, Northwest of Iran. *Environ Monit Assess* 176:183–195
- Al-Charideh A (2011) Environmental isotope study of groundwater discharge from the large karst springs in West Syria: a case study of Fiegh and Al-sin springs. *Environ Earth Sci* 63:1–10
- Al-Charideh A (2012a) Geochemical and isotopic characterization of groundwater from shallow and deep limestone aquifers system of Aleppo basin (north Syria). *Environ Earth Sci* 65:1157–1168
- Al-Charideh A (2012b) Recharge rate estimation in the Mountain karst aquifer system of Fiegh spring, Syria. *Environ Earth Sci* 65:1169–1178
- Al-Charideh A, Abou-Zakem B (2009) Geochemical and isotopic characterization of groundwater from the Paleogene limestone aquifer of the Upper Jezireh, Syria. *Environ Earth Sci* 59:1065–1078
- Anastasiadis P (2003) Vulnerability of groundwater to agricultural activities Pollution. In: Proceedings of the 8th international conference on environmental science and technology, Lemnos Island, Greece, 8–10 September Full paper, vol B, pp 24–30
- Angelakis AN (2000) Water resources management in SAR, with emphasis on non-conventional sources. FAO RNE, Egypt
- Appelo CAJ, Postma D (1993) Geochemistry, groundwater and pollution. A.A. Balkema, Rotterdam
- Appelo CAJ, Postma D (2005) Geochemistry, groundwater and pollution, 2nd edn. Taylor & Francis, Amsterdam
- Barbieri P, Adami G, Favretto A, Lutman A, Avoscan W, Reisenhofer E (2001) Robust cluster analysis for detecting physicochemical typologies of freshwater from wells of the plain of Friuli (north-eastern Italy). *Anal Chim Acta* 440:161–170
- Barbieri M, Boschetti T, Petitta M, Tallini M (2005) Stable isotope (^2H , ^{18}O and $^{87}\text{Sr}/^{86}\text{Sr}$) and hydrochemistry monitoring for groundwater hydrodynamics analysis in a karst aquifer (Gran Sasso, Central Italy). *Appl Geochem* 20:2063–2081
- Batiot C, Emblanch C, Blavoux B (2003) Carbone organique total (COT) et magnésium (Mg^{+2}): deux traceurs complémentaires du temps de séjour dans l'aquifère karstique Total Organic Carbon (TOC) and magnesium (Mg^{+2}): two complementary tracers of residence time in karstic systems. *CR Geosci* 335(2):205–214
- Bicalho CC, Batiot-Guilhe C, Seidel JL, Exter SV, Jourde H (2012) Geochemical evidence of water source characterization and hydrodynamic responses in a karst aquifer. *J Hydrol* 450–451:206–218
- Burdon DJ, Safadi C (1964) The karst groundwater of Syria. *J Hydrol* 2:324–347
- Capaccioni B, Didero M, Paletta C, Salvadori P (2001) Hydrochemistry of groundwater from carbonate formation with basal gypsiferous layers. *J Hydrol* 253:14–26
- Deutsch WJ (1997) Groundwater geochemistry: fundamentals and application to contamination. CRC Press, Boca Raton
- Domenico PA, Schwartz FW (1990) Physical and chemical hydrogeology. Wiley, New York, p 824
- Drever JI (1988) The geochemistry of natural waters. Prentice-Hall, Upper Saddle River
- Dubertret L (1932) L'Hydrologie et aperçu sur l'Hydrographie de la Syrie et du Liban dans leurs relations avec la géologie. *Rev Géogr Phys Géol Dynamique*, TVI fas.4
- Edmunds WM, Smedley PL (2000) Residence time indicators in groundwater: the East Midlands Triassic sandstone aquifer. *Appl Geochem* 15(6):737–752
- Edmunds WM, Ma JZ, Aeschbach-Hertig W, Kipfer R, Darbyshire DPF (2006) Groundwater recharge history and hydrogeochemical evolution in the Minqin Basin, North West China. *Appl Geochem* 21:2148–2170
- European Commission (1995) COST Action 65: hydrogeological aspects of groundwater protection in karstic areas. Final report. EUR 16457, Brussels
- Fairchild IJ, Borsato A, Tooth AF, Frisia S, Hawkesworth CJ, Huang Y, McDermott F, Spiro B (2000) Controls on trace element (Sr-Mg) compositions of carbonate cave waters: implications for speleothem climatic records. *Chem Geol* 166(3–4):255–269
- FAO (1993) Integrated rural water management. In: Proceedings of the technical consultation on integrated water management, Rome, Italy
- Flakova R (1998) Formation and changes of groundwater chemical composition of the Western Carpathian carbonate systems. *ACTA Geologica Universitatis Comenianae* Nr. 53. Bratislava, Slovakia, pp 5–25
- Folch A, Mencia A, Puig R, Soler A, Mas-Pla J (2011) Groundwater development effects on different scale hydrogeological systems using head, hydrochemical and isotopic data and implications for water resources management: the Selva basin (NE Spain). *J Hydrol* 403:83–102
- Freeze RA, Cherry JA (1979) Groundwater. Prentice-Hall, Englewood Cliffs
- Guendouz A, Moulla AS, Edmunds WM, Zouari K, Shand P, Mamou A (2003) Hydrogeochemical and isotopic evolution of water in the Complexe Terminal aquifer in the Algerian Sahara. *Hydrogeol J* 11:483–495
- Guler C, Thyne GD (2004a) Delineation of hydrochemical facies distribution in a regional groundwater system by means of fuzzy c-means clustering. *Water Resour Res* 40:1–11

- Guler C, Thyne GD (2004b) Hydrologic and geologic factors controlling surface and groundwater chemistry in Indian Wells-Owens Valley area, southeastern California, USA. *J Hydrol* 285:177–198
- Guler C, Thyne GD, McCray JE, Turner KA (2002) Evaluation of graphical and multivariate statistical methods for classification of water chemistry data. *Hydrogeology* 110:455–474
- Han G, Liu C (2004) Water geochemistry controlled by carbonate dissolution: a study of the river waters draining karst-dominated terrain, Guizhou Province, China. *Chem Geol* 204:1–21
- Hem JD (1985) Study and interpretation of the chemical characteristics of natural water, 3rd edn. U.S. Geological Survey, Water Supply Paper 2254
- Hsu KJ (1963) Solubility of dolomite and the composition of Florida groundwaters. *J Hydrol* 1:288–310
- Huneau F, Dakoure D, Celle-Jeanton H, Vitvar T, Ito M, Compaore NF, Traore S, Jirakova H, Le Coustumer P (2011) Flow pattern and residence time of groundwater within the south-eastern Taoudeni sedimentary basin (Burkina Faso, Mali). *J Hydrol* 409:423–439
- INECO Studies and Integration Consulting (2009) Institutional framework and decision-making practices for water management in Syria. Towards the development of strategy for water pollution prevention and control in the Barada River Basin, Greater Damascus area. Contract No: INCO-CT-2006-517673
- Jianhua S, Qi F, Xiaohu W, Yonghong S, Haiyang X, Zongqiang C (2009) Major ion chemistry of groundwater in the extreme arid region northwest China. *Environ Geol* 57:1079–1087
- JICA (2001) The study of water resources development in the western and central basins in Syrian Arab Republic, phase I, Ministry of Irrigation (MOI) (in Arabic) (unpublished report)
- Kattan Z (1997) Environmental isotope study of the major karst springs in Damascus limestone aquifer systems: case of the Fiegh and Barada springs. *J Hydrol* 193:161–182
- Kattan Z (2006) Characterization of surface water and groundwater in the Damascus Ghotta basin: hydrochemical and environmental isotopes approaches. *Environ Geol* 51:173–201
- Kortatsi BK (2007) Hydrochemical framework of groundwater in the Ankobra Basin, Ghana. *Aquat Geochem* 13:41–74
- La-Moreaux PE, Hughes TH, Memon BA, Lineback N (1989) Hydrogeologic assessment—Fiegh Spring, Damascus, Syria. *Environ Geol Water Sci* 13(2):73–127
- Langmuir D (1971) The geochemistry of some carbonate groundwaters in central Pennsylvania. *Geochim Cosmochim Acta* 35:1023–1045
- Lawrence AR, Gooddy DC, Kanatharana P, Meesilp M, Ramnarong V (2000) Groundwater evolution beneath Hat Yai, a rapidly developing city in Thailand. *Hydrogeol J* 8:564–575
- Li X, Zhang L, Hou X (2008) Use of hydrogeochemistry and environmental isotopes for evaluation of groundwater in Qingshuihe Basin, northwestern China. *Hydrogeol J* 16:335–348
- López-Chicano M, Bouamama M, Vallejos A, Pulido-Bosch A (2001) Factors which determine the hydrogeochemical behaviour of karstic springs. A case study from the Betic Cordilleras, Spain. *Appl Geochem* 16(9–10):1179–1192
- Ma JZ, Edmunds WM (2006) Groundwater and lake evolution in the Badain Jaran desert ecosystem, Inner Mongolia. *Hydrogeol J* 14:1231–1243
- Ma JZ, Wang XS, Edmunds WM (2005) The characteristics of groundwater resources and their changes under the impacts of human activity in the arid Northwest China, a case study of the Shiyang River Basin. *J Arid Environ* 61:277–295
- Mahlknecht J, Gárfias-Solis J, Aravena R, Tesch R (2006) Geochemical and isotopic investigations on groundwater residence time and flow in the Independence Basin, Mexico. *J Hydrol* 324:283–300
- McMahon PB, Böhlke JK, Christenson SC (2004) Geochemistry, radiocarbon ages, and paleorecharge conditions along a transect in the central High Plains aquifer, southwestern Kansas, USA. *Appl Geochem* 19(11):1655–1686
- Meslmani Y, Wardeh M F (2010) Strategy and action plan for adaptation to climate change in Syria, (INC-SY_ Strategy & NAPA-En). Ministry of State for Environment Affairs (MSEA)/United Nations Development Programme (UNDP) Damascus, Syria
- MOI (2005) Annual water resources report of Barada and Awaj Basin, Damascus, Syria (in Arabic) (unpublished report)
- Moral F, Cruz-Sanjulián JJ, Ollás M (2008) Geochemical evolution of groundwater in the carbonate aquifers of Sierra de Segura (Betic Cordillera, southern Spain). *J Hydrol* 360:281–296
- Mourad KA, Berndtsson R (2011) Syrian water resources between the present and the future. *Air Soil Water Res* 4:93–100. doi:10.4137/ASWR.S8076
- Palmer PC, Gannett MW, Stephen R, Hinkle SR (2007) Isotopic characterization of three groundwater recharge sources and inferences for selected aquifers in the upper Klamath Basin of Oregon and California, USA. *J Hydrol* 336:17–29
- Parkhurst DL, Appelo CAJ (1999) PHREEQC for windows version 1.4.07. A hydrogeochemical transport model. U.S. Geological Survey Software
- Plummer LN (1977) Defining reactions and mass transfer in part of the Floridan aquifer. *Water Resour Res* 13(5):801–812
- Plummer LN, Wigley TML, Parkhurst DL (1978) The kinetics of calcite dissolution in CO₂ water systems at 5–60 °C and 0.0–1.0 atm CO₂. *Am J Sci* 278(2):179–216
- Plummer LN, Busby JF, Lee RW, Hanshaw BB (1990) Geochemical modeling of the Madison aquifer in parts of Montana, Wyoming, and south Dakota. *Water Resour Res* 26(9):1981–2014
- Ponikarov VO (1967) The geology of Syria, explanatory notes on the map of Syria, Scale 1:500,000. Part II. Mineral deposits and underground water resources. Technoexport, Moscow
- Rakhmatullaev S, Huneau F, Kazbekov J, Le Coustumer P, Jumanov J, El Oifi B, Motelica-Heino M, Hrkal Z (2010) Groundwater resources and management in the Amu Darya River Basin (Central Asia). *Environ Earth Sci* 59:1183–1193
- Rakhmatullaev S, Huneau F, Kazbekov J, Celle-Jeanton H, Motelica-Heino M, Le Coustumer P, Jumanov J (2012) Groundwater resources of Uzbekistan: an environmental and operational overview. *Cent Eur J Geosci* 4:67–80
- RDAWSA (2006) Interim report—hydrogeological study of Mougher El Mer Area, Damascus Rural water and sanitation project
- Schoeller H (1956) Géochimie des eaux souterraines. Application aux eaux des gisements de pétrole. Soc Ed Technip, Paris
- Selkhozpromexport (1986) Water resources use in Barada and Awaj Basins for irrigation of crops, Syria Arab Republic. USSR, Ministry of Land Reclamation and Water Management, Moscow
- Stadler S, Geyh MA, Ploethner D, Koeniger P (2012) The deep Cretaceous aquifer in the Aleppo and Steppe basins of Syria: assessment of the meteoric origin and geographic source of the groundwater. *Hydrogeol J* 20:1007–1026. doi:10.1007/s10040-012-0862-2
- Stuyfzand PJ (1989) A new hydrochemical classification of water type. *IAHS Red Books* 182:89–98
- Suk H, Lee K-K (1999) Characterization of a ground water hydrochemical system through multivariate analysis: clustering into groundwater zones. *Ground Water* 37:358–366
- Vengosh A, Rosenthal E (1994) Saline groundwater in Israel: its bearing on the water crisis in the country. *J Hydrol* 156:389–430
- Wen X, Wu Y, Zhang Y, Liu F (2005) Hydrochemical characteristics and salinity of groundwater in the Ejina basin, northwestern China. *Environ Geol* 48:665–675
- Wolfart R (1964) Hydrogeology of the Damascus Basin (southwest-Syria). *IAHS Red Books* 64:402–413

Appendices B ***Published Article***

Article published in the journal of Arabian Journal of Geosciences

Origin and recharge mechanisms of groundwater in the upper part of the Awaj River (Syria) based on hydrochemistry and environmental isotope techniques

Origin and recharge mechanisms of groundwater in the upper part of the Awaj River (Syria) based on hydrochemistry and environmental isotope techniques

N. M. Asmael^{1,2} · F. Huneau^{3,4} · E. Garel^{3,4} · H. Celle-Jeanton^{5,6,7} · P. Le Coustumer² · A Dupuy^{2,8} · S. Hamid¹

Received: 2 December 2014 / Accepted: 7 May 2015
© Saudi Society for Geosciences 2015

Abstract The Barada and Awaj basin is the most important and extensively used water basin in Syria. Chemical and isotopic data of groundwater have been used to determine the spatial distribution of hydrogeological features in the upper part of Awaj River catchment area located southwest of this basin. Hydrogeochemical evolution of groundwater reveals the domination of dissolution/precipitation mechanisms in these very complex stratigraphic sequences. The dissolution of carbonate rocks as well as reverse cation exchange processes seem to be the main factors controlling groundwater mineralization. The isotopic composition of precipitation and groundwater indicate that the modern-day atmospheric precipitation is the main source of groundwater recharge before an important evaporation occurred. The isotopic data also imply an existence of hydraulic connection between the different aquifers system. The results obtained allowed us to delineate

two main spatial groundwater zones within the study area with different flow components. The south, central and eastern parts are considered to be one zone which is characterised by a shallow horizontal flow associated with active interaction between groundwater and hosting rocks. The nitrate concentrations in this zone are attributed to anthropogenic sources. The second zone consists in south-western, western and north-western parts where the karstic features are well developed mainly in the Jurassic strata. This zone is characterized by a high vulnerability to pollution confirmed by high values of nitrate coming from sewage water. The deep vertical groundwater flow component seems to be dominant in this zone and is controlled by fractures and geological structures.

Keywords Aquifer · Stable isotopes · Hydrochemical facies · Groundwater pollution · Syria

✉ F. Huneau
huneau@univ-corse.fr

¹ Department of Geology, Faculty of Sciences, Damascus University, P. O. Box 32022, Damascus, Syria

² Université Bordeaux-Montaigne, EA 4592 Géoresources & Environnement, 1 allée F. Daguin, 33607 Pessac, France

³ Faculté des Sciences et Techniques, Laboratoire d'Hydrogéologie, Université de Corse Pascal Paoli, Campus Grimaldi, BP 52, 20250 Corte, France

⁴ CNRS, UMR 6134, SPE, 20250 Corte, France

⁵ Université Blaise Pascal, Laboratoire Magmas et Volcans, Clermont Université, BP 10448, 63038 Clermont-Ferrand, France

⁶ CNRS, UMR 6524, LMV, 63038 Clermont-Ferrand, France

⁷ IRD, R 163, LMV, 63038 Clermont-Ferrand, France

⁸ ENSEIGID-Bordeaux INP, 1 allée F. Daguin, 33607 Pessac, France

Introduction

Over the last few decades, the rapid growth and socio-economic development as well as the effect of climatic changes have severely affected water resources in whole Syria. Abou Zakhem and Hafez (2010) concluded that the average decrease of rainfall in Syria was about 18 % over the last 10 years. In many semi-arid regions, the development of groundwater resources has led to a continuous decline in groundwater levels (Postel 1999; Shah et al. 2000; Luijendijk and Bruggeman 2008). In the case of Syria, reserves have been depleted in some areas, many springs have dried up and rivers discharges are decreasing or have become seasonal, consequently impacting and compromising the sustainability at current and future water use.

Thirty percent of the Syria's population lives in the Barada and Awaj basin where the groundwater is considered as a

major source of water for communities and agricultural purposes. The western part of this basin is occupied by Jurassic and Cretaceous aquifers which are considered as the most important groundwater reservoirs in the whole country and in the major Middle East countries.

The understanding of the hydrochemical evaluation and its relation to both groundwater flow paths and interactions with hosting rocks is important in order to develop management policies that are compatible with the flow system mechanism. Groundwater management in Syria is an issue of great concern to water policy makers, planners and legislators, notably regarding pollution and resources sustainability (FAO 1993; Angelakis 2000).

The stable isotopic composition of groundwater is significantly linked to the air moisture content of precipitation and the altitude at which it falls. Environmental isotope approaches have been used in many studies of groundwater related to recharge environments (Bajjali 2006, 2008; Fritz et al. 1981; Gat 1971).

Groundwater became the main water supply source for small population centres as well as for private use in agriculture and for cattle. The improvement of knowledge on the hydrogeological conditions of the aquifer system in this region is an essential issue in the national water resources management approach.

The main hydrogeological purposes of this study aims at (i) determining the groundwater origin and its geochemical evolution based on rock-water interactions within the framework of its complex geology and morphology, (ii) identifying the main hydro-geochemical processes controlling the water quality in the study area, (iii) understanding the recharge processes and determining the main hydrogeological units in the study area. This study will lead to a better water resources management strategy in the south-west of Barada and Awaj basin which constitute fundamental challenges in this basin.

General setting of the study area

From a hydrological point of view, Syria can be divided into seven hydrogeological basins (Fig. 1b) and the study area is shared between Lebanon, Israel and Syria. The sampling sites and the location of the study area are shown on Fig. 1a, b. Its climate varies largely due to two main geographical features: the Mediterranean Sea and the anti-Lebanon mountains. The climatic conditions range within the study area from semi-humid in the western part of the Mt. Hermon to arid on the plains located in the centre and eastern part. Annual precipitation clearly increases with altitude and varies between about

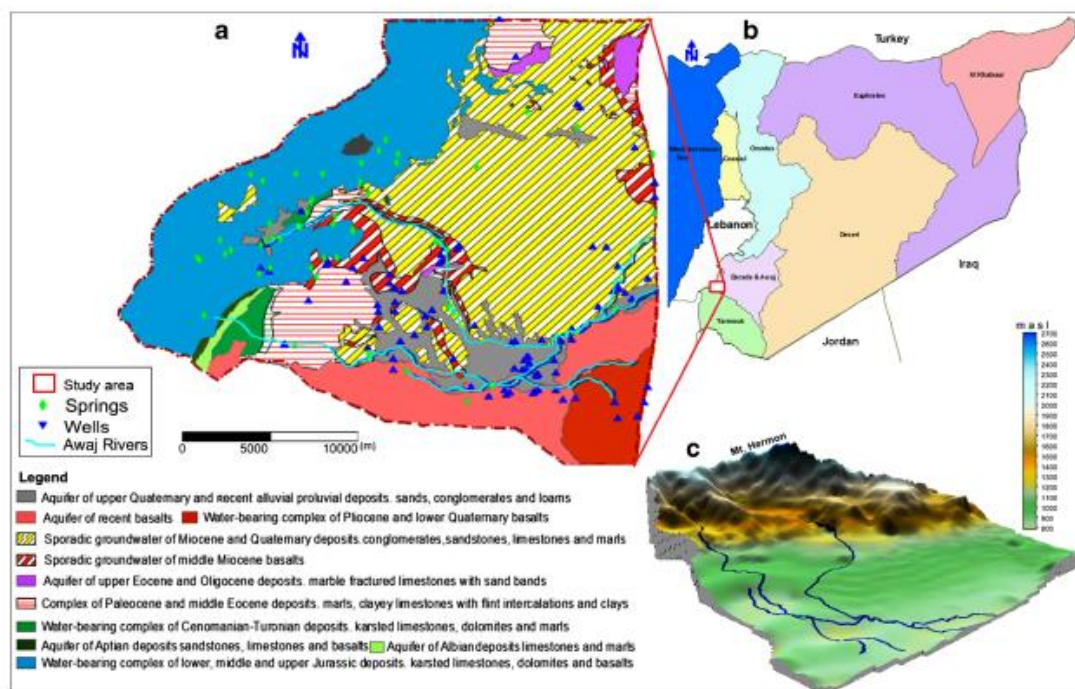


Fig. 1 The location of the study area on the map of Syria which divided into seven hydrogeological basins and the locations of sampling sites as well as the three dimensions view of the study area

Table 1 List of sampling sites and chemical composition of water samples collected during August 2012

Name	Locations	Date	Type	X coord	Y coord	EC μ S/cm	pH	Na ⁺ (mg/L)	K ⁺ (mg/L)	Mg ²⁺ (mg/L)	Ca ²⁺ (mg/L)	Cl ⁻ (mg/L)	HCO ₃ ⁻ (mg/L)	SO ₄ ²⁻ (mg/L)	NO ₃ ⁻ (mg/L)	Ion balance (%)
Beit Jinn	Beit Jinn	16/08/2012	S	330030	3687890	310	7.97	3.4	1.0	8.2	48.7	4.9	176	7.1	2.6	1
Amneh	Amneh	20/08/2012	S	328630	3692830	272	7.90	2.9	0.2	1.7	47.7	9.5	137	3.8	0.7	1
Almashra	Amneh	20/08/2012	S	326100	3693710	352	7.96	3.1	0.5	13.5	44.0	8.3	115	77.7	1.6	-4
Talmasiat	Mogher Al Mer	16/08/2012	S	336330	3686240	384	8.05	11.1	2.6	7.1	59.3	8.7	207	8.3	10.4	1
Jandal	Kalet Jandal	17/08/2012	S	335870	3700080	358	7.99	9.9	1.4	13.4	34.7	19.9	112	18.2	44.2	-3
Marmbej	Mogher Al Mer	16/08/2012	S	334200	3687330	360	8.03	11.9	2.8	6.1	53.2	8.3	194	7.1	10.2	0
Bkassam1	Bkassam	17/08/2012	S	333730	3698280	697	8.04	31.0	5.8	25.8	60.0	49.8	157	39.4	108.6	0
Knaeseh	Remneh	20/08/2012	S	330200	3695500	380	7.82	5.7	2.6	10.3	54.7	8.6	173	24.1	10.4	2
Tamer	Remneh	20/08/2012	S	331000	3697200	330	7.98	4.2	0.4	11.9	45.2	7.7	172	10.7	6.7	1
Tal Assyuf	Mogher Al Mer	16/08/2012	S	339770	3684300	396	7.87	10.4	2.1	9.8	56.7	10.9	201	11.7	15.9	0
Rashashesh	Amneh	20/08/2012	S	328780	3694750	600	7.87	4.1	0.5	18.8	92.2	9.7	167	171.1	2.8	-2
Aljimeh	Remneh	20/08/2012	S	330920	3697020	573	7.89	19.0	4.9	20.0	58.2	32.5	181	26.6	71.6	-1
Ras Alwadi	Kalet Jandal	17/08/2012	S	335790	3699530	323	8.02	4.8	1.1	11.4	42.4	8.3	154	11.6	8.4	2
Njaim Spring	Amneh	20/08/2012	S	326400	3693950	609	7.92	2.9	0.5	15.9	100.8	8.5	150	189.6	1.4	-2
Jandal Drink Well	Kalet Jandal	17/08/2012	W	335180	3700980	278	8.01	2.9	0.3	0.9	52.0	9.2	145	5.3	0.0	1

The coordinates system is special for Syrian Arab Republic
EC electrical conductivity, W well, S spring

90 mm year⁻¹ and about 900 mm year⁻¹ from elevation ranging between 800 and 1,500 m (MOI 2005).

Temperatures can drop down below freezing point at high altitudes (1,500–2,800 m) in winter and can reach 45 °C during summer. The relative humidity is related to temperature oscillation (JICA 2001); thus, low average monthly values are usually about 24–50 % during summer (July and August) and may reach up to 60–70 % during winter (January and February). The annual potential evaporation average varies between 1,500 mm year⁻¹ in the flatlands and 1,100 mm year⁻¹ in the mountainous parts. Evapotranspiration in the mountainous area varies between 300 and 400 mm year⁻¹ and it is similar to precipitation rates in the flatland area (Selkhozpromexport 1986; Kattan 1997b).

The hydrological conditions in the study area are mainly controlled by the diversity of climatic, topographic, geomorphic, geological features and human activities. Awaj River is the main watercourse in this area. Its flow system is strongly governed by seasonal flow regime. This river is formed by the junction of two main tributaries (Jinani and Sebarani), which are recharged by a large number of springs distributed along the slopes of Mt. Hermon (Fig. 1a). The annual average discharge of Awaj River is 4.7 m³ s⁻¹ (MOI 2005). From geomorphological and topographical points of view, the physiography of the area results from Jurassic to recent deposition, tectonics and volcanism. Periodic uplifts along with compressive folding and faulting at shallow depths have resulted in a variety of surface forms and geologic structures. The area is characterized by mountains to the west and northwest with sharp deep valleys in-between, and by a flat area in the east and southeast (Fig. 1c). Major valleys either follow a synclinal structure, occur as strike valleys parallel to hogback or are the result of Pleistocene erosion along normal faults of significant displacement.

Geological and hydrogeological setting

Geology

In the Barada and Awaj basin, pre-Jurassic deposits are not known (Wolfart 1964; United Nations 1982; Selkhozpromexport 1986; Kattan 1997b). The geological formations outcropping in the upper part of Awaj River date from the Jurassic to the Quaternary (Fig. 1a). The Mountainous parts are formed from the exposure of Jurassic deposits at altitudes between 1,500 and 2,800 m. The thickness of these deposits ranges between 2,000 and 2,200 m. On the other hand, the plain areas are characterized by outcroppings of the Neogene and Quaternary deposits. The Cretaceous and Paleogene formations are

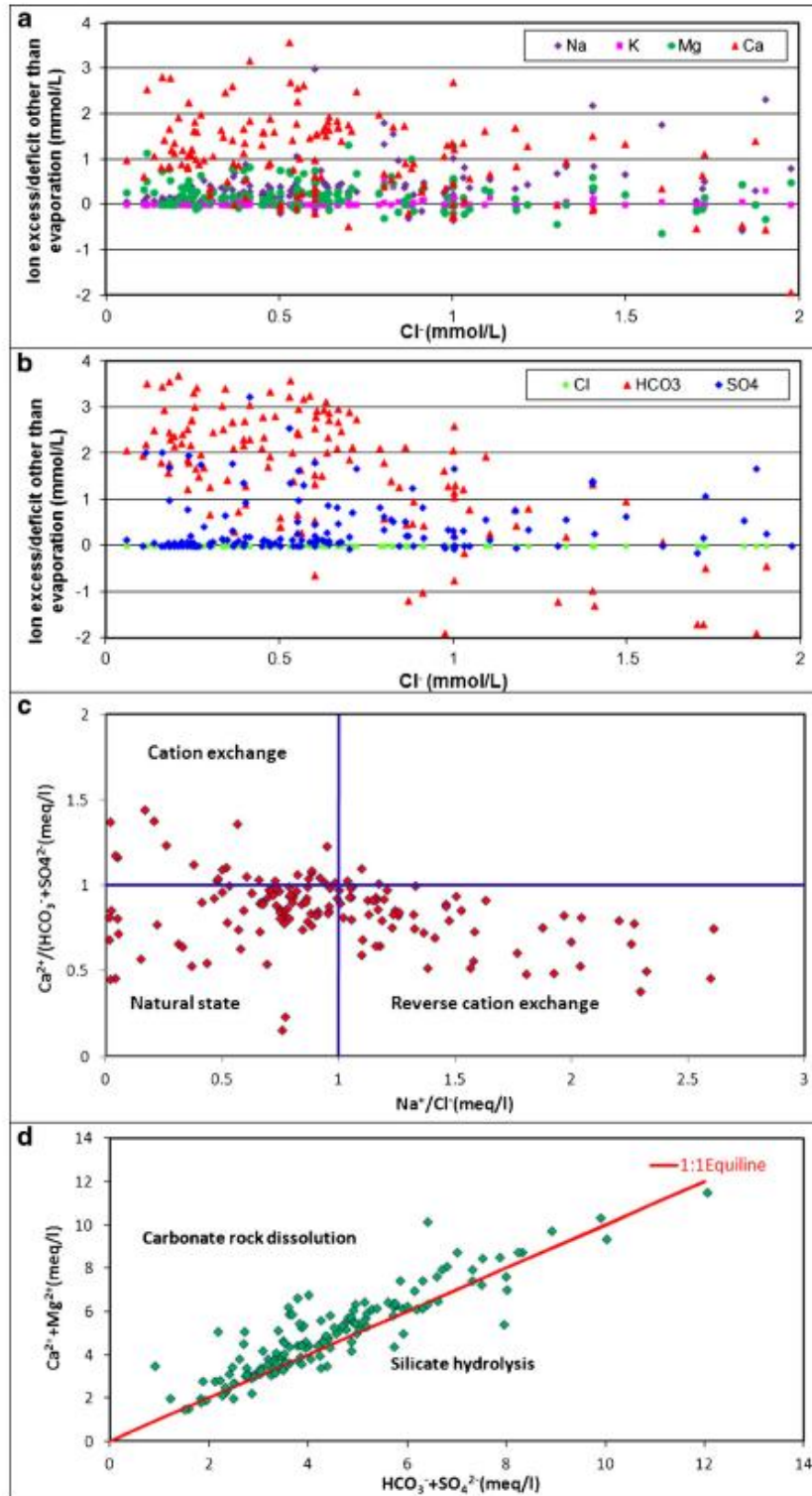
Fig. 2 Ions excess or deficit by mechanisms of other than evaporation (a, b). The scatters plots of Na⁺/Cl⁻ vs Ca²⁺/(HCO₃⁻ + SO₄²⁻) and (Ca²⁺ + mg²⁺) vs (HCO₃⁻ + SO₄²⁻) (c, d), showing the effect of cation exchange, reverse cation exchange, natural state, carbonate rock dissolution and silicate hydrolysis on groundwater composition. (data are including the analysis results of Selkhozpromexport 1986 and fieldwork campaigns of 2006 and 2012)

exposed in the small southwest part of the study area. The thickness of Neogene formation ranges between 100 and 500 m and is characterized by continental rock debris. The dark-coloured Miocene basalt, which is characterized by fractures filled with calcite, is found locally beneath the conglomerates of Pliocene age. The thickness of this formation varies from several meters to about 500 m. The recent basalt is exposed mainly in the south part of the study area. According to Asfahani and Abdul Ghani (2012), four kinds of basalt can be detected in the study area: hard massive basalt, hard basalt, pyroclastic basalt and alternation of basalt products and clay. The Quaternary deposits are mainly found in the plain area in the valleys and around the Awaj River. Its thickness varies from 1 to 10 m.

In terms of geological structural setting, the area is strongly affected by faulting and folding resulting in several folded structures such as Mt. Anti-Lebanon (up to 2,466 m) and Mt. Hermon (2,814 m) (Dubertret 1932; Ponikarov 1967; Selkhozpromexport 1986; La-Moreaux et al. 1989; Kattan 2006). The Hermon ridge is a long and continuous anticline of NE-SW direction and highly deformed. Generally, most strata from Jurassic to Cretaceous age dip in the southeast direction to the east of Mt. Hermon (La-Moreaux et al. 1989). Karst features in the mountainous regions are most common in the outcrop areas and even in the deeper parts of thicker Jurassic limestone and dolomitic limestone whereas the thickness of karstification zone reaches several hundreds of metres. The faults zones, together with karstic features, seem to play a significant role in this area in terms of increasing infiltration coefficient and are controlling groundwater flow behaviour and recharge/discharge mechanisms (Burdon and Safadi 1964).

Hydrogeology

Two main aquifers systems can be distinguished. The first is formed by unconsolidated or semi-consolidated deposits of Neogene and Quaternary, the karstic limestone of Oligocene and Upper Eocene and the fissured basalt of Miocene. The fissured and karstic limestone and dolomitic limestone of Cretaceous (Cenomanian, Turonian) and Jurassic compose the second groundwater aquifer system. Figure 1a shows the major aquifers and water-bearing formation in the study area. The



major hydrogeological units in the study area are classified and described below (Selkhozpromexport 1986):

Jurassic unit

This unit is composed essentially of karstic limestone layers containing gypsum infilling at a considerable depth, interbedded with dolomite, dolomitic limestone and marl layers. The rocks of this unit are outcropping mainly in the Mt. Hermon. Its hydraulic conductivity varies between 2 and 99 m day⁻¹, and its transmissivity is about 3,085 m² day⁻¹ (RDAWSA 2006). The average infiltration coefficient is estimated to be about 70 % for these rocks (Selkhozpromexport 1986). It forms a potential karst groundwater reservoir of very large magnitude. Since its outcrops form major mountains which receive the heaviest precipitation in Syria, its importance as an aquifer cannot be over-emphasized (Burdon and Safadi 1964).

Cretaceous unit

The limestone, dolomitic limestone and crystalline dolomite interbedded with argillaceous limestone, marl and sandstone formations compose the aquifer member of this unit (400–1,000 m). The hydraulic conductivity of this unit goes up to 80 m day⁻¹ and its transmissivity varies between 12 and 7,435 m² day⁻¹ (La-Moreaux et al. 1989). It is outcropping in the small part southwest of the study area. This unit together with Jurassic unit represents the most important water-bearing system in the Barada and Awaj basin and even in Syria in terms of storage capacity and discharge of springs (JICA 2001). The Figei spring, considered to be the third largest spring in the world (La-Moreaux et al. 1989), emerges from this unit. The infiltration coefficient ranges between 56 and 70 % for these rocks exposures (Selkhozpromexport 1986).

Upper Eocene and Oligocene aquifer

This aquifer underlies the Miocene basalt aquifer. Its thickness ranges between 39 and 95 m. It is composed of locally karstic crystalline limestone and marly limestone with interbedded lenses of quartz. Its transmissivity is frequently small and does not exceed 11 m² day⁻¹ (Selkhozpromexport 1986).

Sedimentary Mio-Quaternary aquifer

The rocks of this complex (140–630 m) are widespread on the foothill of Mt. Hermon and in the plain area. They consist of gravels and conglomerates interbedded with marl, clay, sandstone and limestone. As clay content increases and/or aquifer thickness decreases, the transmissivity value can drop down from 756 to 0.05 m² day⁻¹ (Kattan 2006).

Fig. 3 Saturation indices of calcite, dolomite and gypsum as well as the Ca²⁺ (mmol L⁻¹) as a function of SO₄²⁻ (mmol L⁻¹). (data are including the analysis results of Selkhozpromexport 1986 and fieldwork campaigns of 2006 and 2012)

Volcanic Middle Miocene aquifer

The Basaltic aquifer (50–500 m) consists of fissured basalts associated with thin beds and lenses of sand and sandstone. The transmissivity of this aquifer is about 30–60 m² day⁻¹. Almost all of the springs that emerge from the Recent basalt formations are originating from deeper aquifers such as the Neogene conglomerates or other deeper aquifers.

Sampling, analytical methods and data

For major ions (Na⁺, K⁺, Mg²⁺, Ca²⁺, Cl⁻, HCO₃⁻, SO₄²⁻) and field parameters (EC, pH, T) investigations, a total of 151 water samples from springs and wells (Fig. 1a) were used. A total of 109 water samples were collected during two fieldwork campaigns. The first one took place in November and December during 2006 during which 94 samples were collected (Asmael et al. 2014). While in the second one, the result of 15 samples collected during August 2012 was used. The analysed results of 42 water samples were taken from (Selkhozpromexport 1986). For groundwater isotopic composition ($\delta^{18}\text{O}$ and $\delta^2\text{H}$), the results of 18 samples collected during the second field campaign (August 2012) and 3 samples from (Selkhozpromexport 1986) are used. Samples were collected in polyethylene bottles, which were rinsed twice with sample water. Two bottles were collected at each water point. One bottle was filtered (0.45 μm) and acidified with two drops of nitric acid (HNO₃) for cation determination.

Cation concentrations were measured using an absorption spectrophotometer (AAS) whereas the anions were measured with Dionex Ion Chromatograph (DIOEX ICC-1000). Silica (as SiO₂) was measured by using HACH colorimeter. The samples of the second fieldwork campaign were analysed at the Hydrogeology Department of the University of Corsica (UMR 6134 CNRS) for both major ions and environmental isotopes of the water molecule ($\delta^{18}\text{O}$ and $\delta^2\text{H}$). For major ions, we used ionic chromatography in liquid phase (DIONEX ICS-1100) technique, while for isotopes determination, liquid water isotope laser spectrometer (LGR) technique was used.

By using PHREEQC (Parkhurst and Appelo 1999), different calculations were performed in order to determine chemical analyses error, as well as the saturation indices of a selection of minerals and partial pressure of carbon dioxide. Field parameters and major ions of the different sampling points of the second field campaigns are displayed in Table 1.

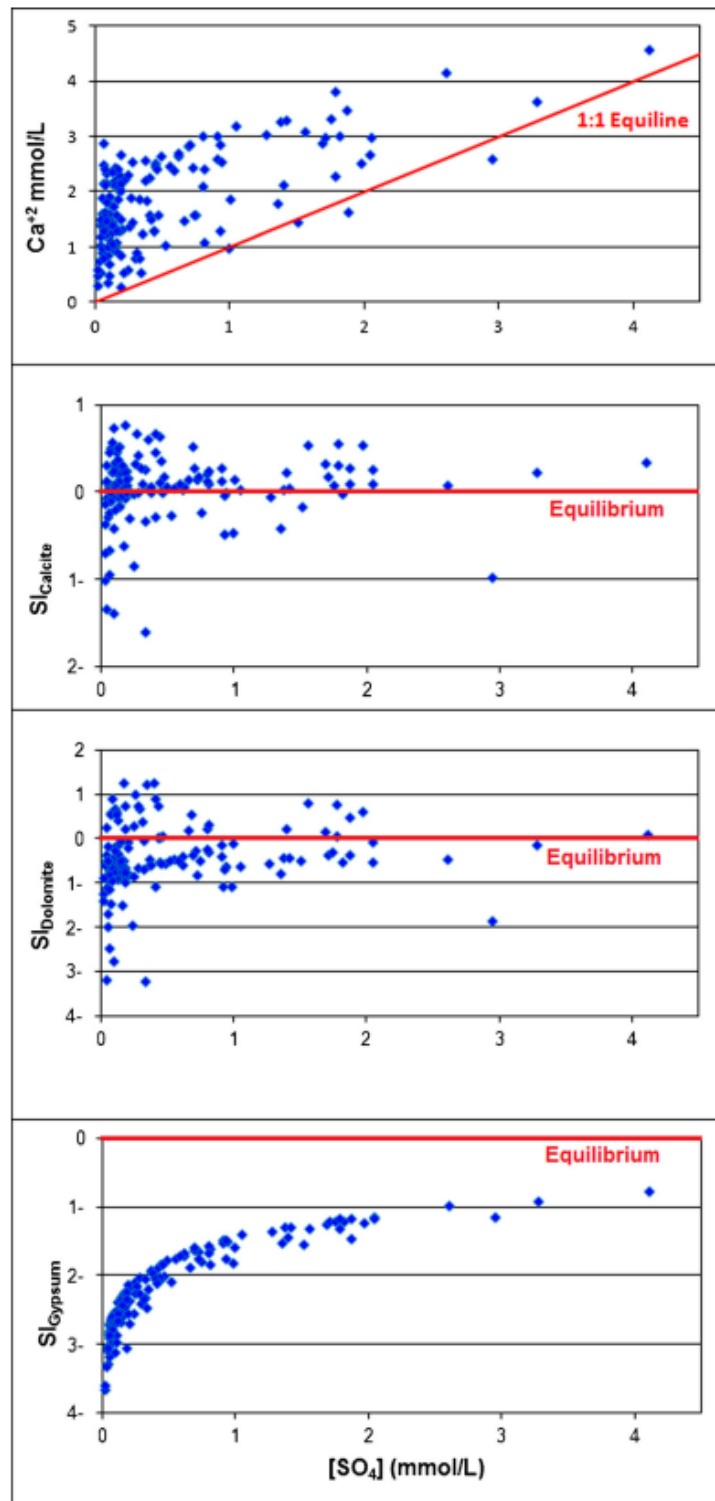
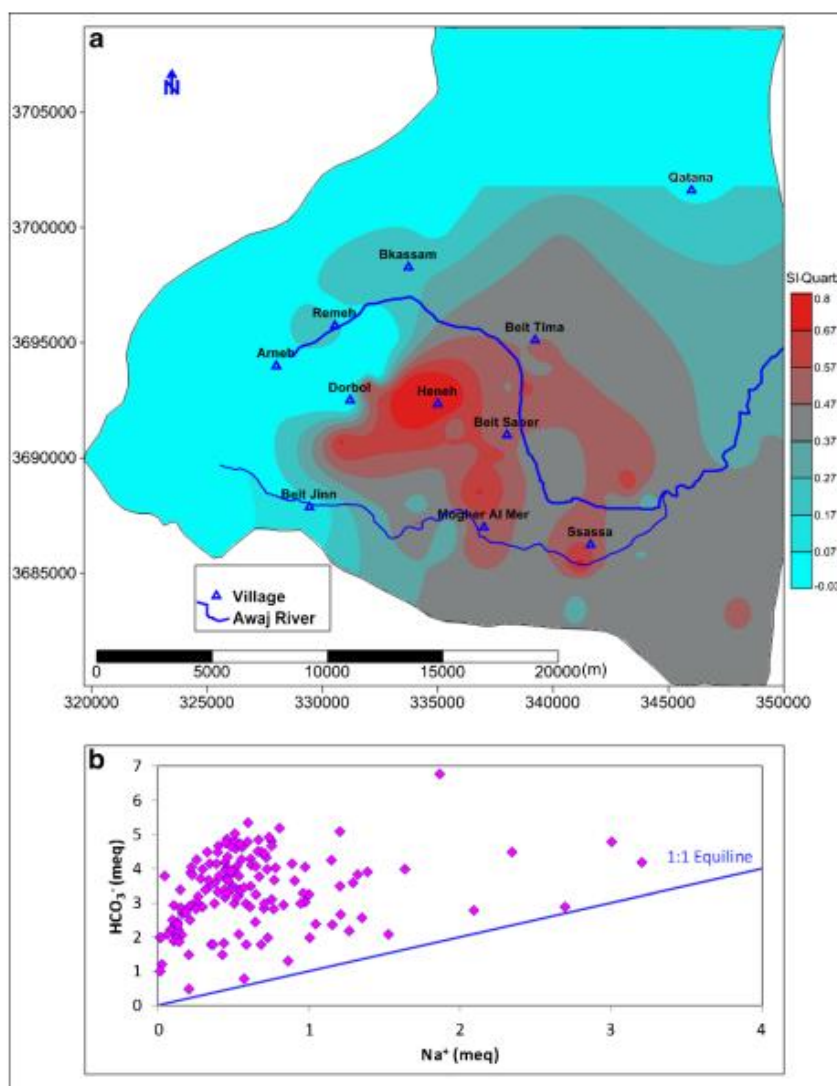


Fig. 4 Spatial distribution of saturation indices of quartz in water samples and scatters plot showing the relationship between Na^+ (meq) vs HCO_3^- (meq). (data are including the analysis results of Selkhazpromexport 1986 and fieldwork campaigns of 2006 and 2012)



Results and discussion

Water-rock interaction and salts dissolution

The major ions measured in the rainwater collected from Ameh station and groundwater samples are used to determine the evaporation factor as well as the effect of evaporation processes on the groundwater chemistry. The spatial distribution of samples in Fig. 2a, b indicates that the major processes controlling groundwater composition are the mechanisms of other than evaporation such as water-rock interaction while

the evaporation process is having a slight effect. Therefore, the concentration of major ions in the groundwater and their spatial distributions and binary relationships has been used in order to determine their sources and their relation with the rock composition and weathering processes.

Figure 2c shows the relationship between Na^+/Cl^- versus $\text{Ca}^{2+}/(\text{HCO}_3^- + \text{SO}_4^{2-})$. The distribution of samples indicates that the natural salt dissolution such as carbonates rock and silicate as well as the effect of reverse cation exchange, enhanced by clay minerals existence, are the main processes controlling groundwater composition in the study area. Few

Fig. 5 **a** Modified piper diagram depicting hydrochemical facies of groundwater in the study area. **b** Spatial distribution and classification of each water facies. (data are including the analysis results of Selkhozpromexport 1986 and fieldwork campaigns of 2006 and 2012)

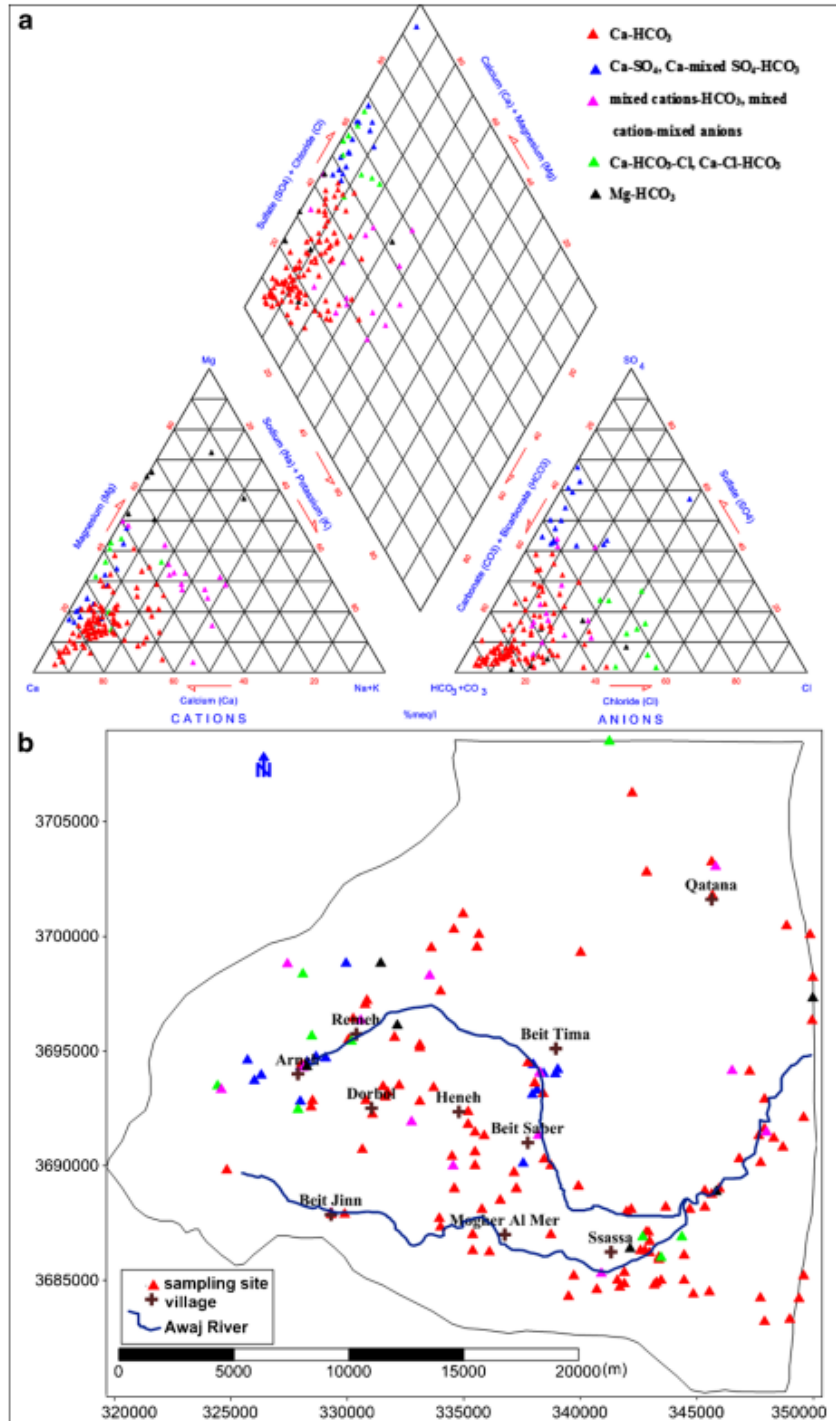
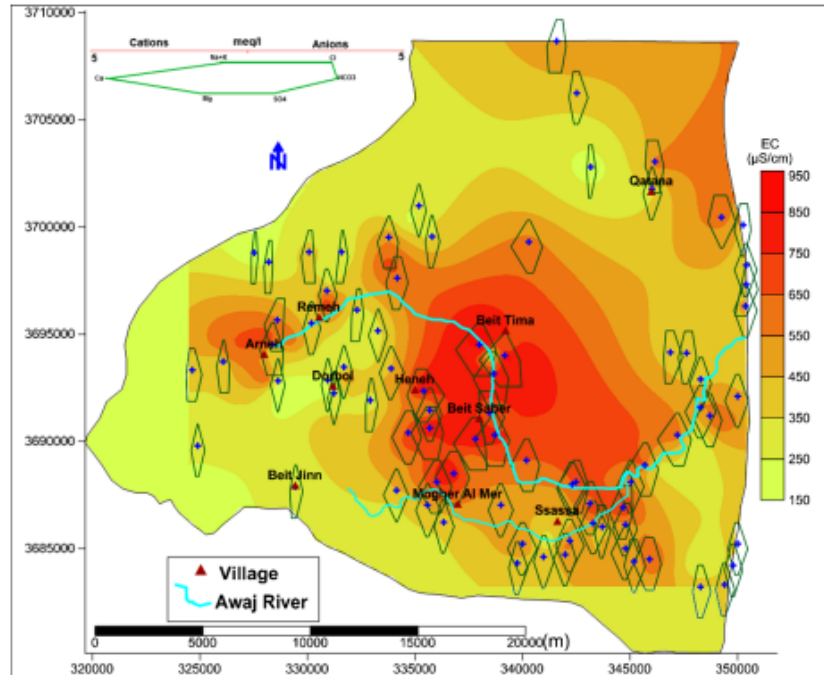


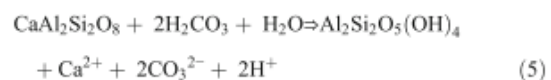
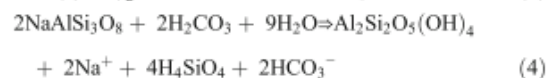
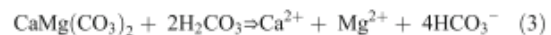
Fig. 6 Stiff diagrams of selected samples showing the variation in mineral composition of groundwater. The spatial distribution of electrical conductivity (EC) is also shown in this figure. (data are including the analysis results of Selkhozpromexport 1986 and fieldwork campaigns of 2006 and 2012)



samples indicated the effect of cation exchange and demonstrate a deficit of Na^+ and an excess of Ca^{2+} . Datta and Tyagi (1996) explained the effect of carbonate and silicate rocks through the scattered plots of $(\text{Ca}^{2+} + \text{mg}^{2+})$ versus $(\text{HCO}_3^- + \text{SO}_4^{2-})$ as shown in Fig. 2d. The majority of water samples are located close and above equiline in the $\text{Ca}^{2+} + \text{Mg}^{2+}$ side, which indicates that, on the one hand, the dissolution of carbonate rocks is the dominant reaction in the system, and on the other hand, the excess calcium and magnesium might derived from other processes such as reverse cation exchange reaction. The locations of few samples below the equiline indicate the effect of silicate hydrolysis.

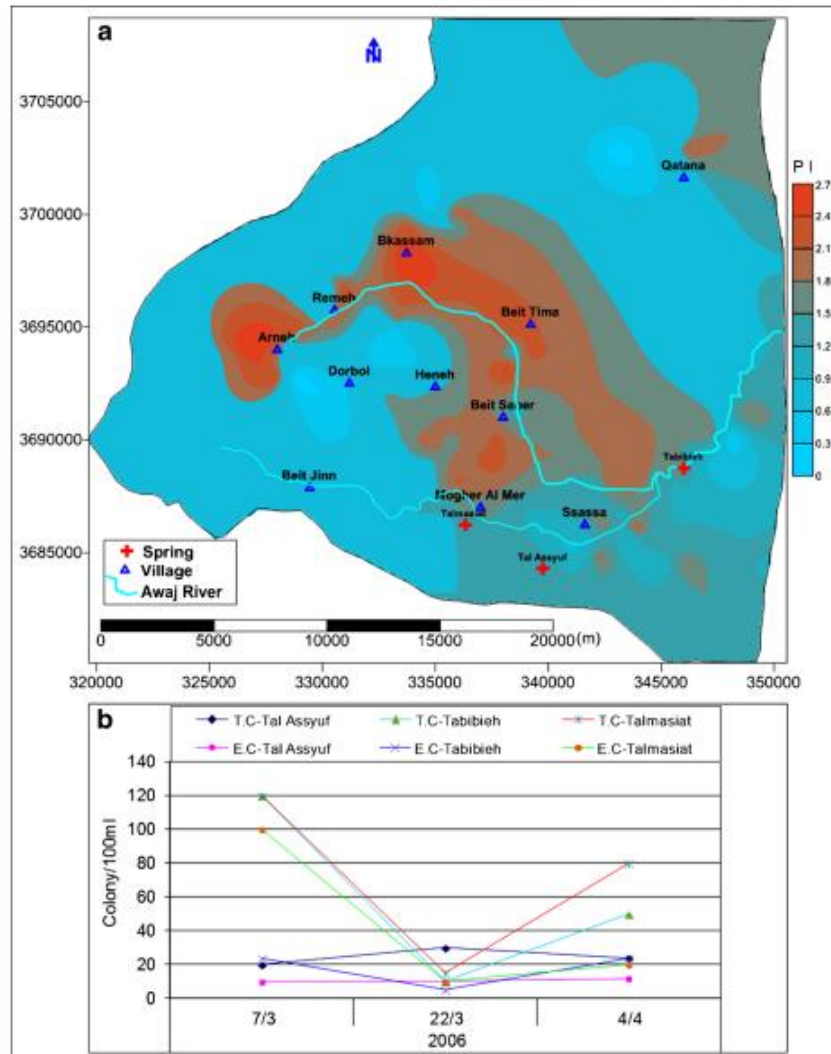
The dissolution of carbonate rock enhanced by CO_2 -rich groundwater is shown in Eqs. 1, 2 and 3. Meteoric water has a great influence on groundwater composition in the active groundwater circulation zone. During infiltration, it saturates with CO_2 as a result of organic matter degradation and becomes aggressive to calcite. When $p\text{CO}_2$ increases from the meteoric average ($10^{-3.5}$) to 10^{-2} atm, the Ca- HCO_3 groundwater type can be formed. In the thermodynamic calculation, it is likely that gypsum dissolution is irreversible in most of the system, whereas the water remains at or near saturation with respect to calcite and dolomite. It is appropriate then to choose the dissolved sulfate as a reaction progress variable in examining the trend in the water quality data (Plummer et al. 1990; Asmael et al. 2014). Figure 3 shows that the saturation index of

calcite is positive for most of samples whereas it remains negative for most samples in terms of dolomite. Meaning that, on the one hand, precipitation of calcite occurs, and on the other hand, precipitation of dolomite continues. With respect to gypsum, all the samples are under saturated. The scarcity of gypsum in the aquifers system might be behind the low values of SI of gypsum. The pronounced relationship between Ca^{+2} and SO_4^{-2} (mmol L^{-1}) in some water samples (Fig. 3) indicates the effect of gypsum dissolution on these water samples composition.



The effect of silicate hydrolysis is by conversion of albite and anorthite to kaolinite according to Eqs. 4 and 5. Hydrolysis of albite and anorthite to kaolinite increases the silicate, sodium and calcium in the groundwater. As shown in Fig. 2d, the effect of carbonate dissolution on

Fig. 7 Spatial distribution of the pollution index (PI) (a). The total coliform and faecal coliform (*E. coli*) measured in three spring water samples during March–April 2006 are also shown (b). (data are including the analysis results of Selkhozpromexport 1986 and fieldwork campaigns of 2006 and 2012)



the groundwater composition is much more in comparison with silicate hydrolysis. This is because of the abundance of carbonate rocks in the study area and its rapid dissolution process compared to silicate. However, silicate hydrolysis increases the concentration of HCO_3^- in groundwater. Figure 4b shows the scatters plot of Na^+ vs HCO_3^- which indicates that the silicate hydrolysis contributes slightly to HCO_3^- increase in the groundwater samples.

All the water samples except one are oversaturated with respect to quartz evidenced by the abundance of crystalline rocks. Figure 4a shows the spatial distribution of SI of quartz which demonstrates that the highest values were measured

surrounding the Miocene basaltic aquifer which is characterized by further hydrolysis.

Hydrochemical facies

Groundwater is classified into hydrochemical facies that are groups of samples whose assigned names indicate the most concentrated cations and anions in the sample. This can be correlated with location and geology (Suk and Lee 1999; Barbieri et al. 2001; Guler et al. 2002; Guler and Thyne 2004).

The mineralogy of the aquifer which water flows through determines which water type or hydrochemical facies will

develop. The vertical and horizontal groundwater flow patterns control the distribution of these facies.

The Piper diagram (Piper 1944) can be used to demonstrate the hydrochemical facies of analysed water samples. This diagram provides a convenient method to display, classify and compare water types based on the ionic composition of different water samples (Hem 1985).

Figure 5 shows that all the water samples demonstrate an excess of Ca^{2+} and Mg^{2+} compared with Na^+ and K^+ . The weak acidic anion (HCO_3^-) of the majority of these samples exceeded the strong acidic anions (Cl^- , SO_4^{2-}). About 70 % of water samples tend to have anion chemistry dominated by HCO_3^- and cation composition dominated by Ca^{2+} (Ca- HCO_3 water type). This indicates the effect of the dissolution/precipitation of carbonate rocks (water-rock interaction) as well as recent recharge of groundwater from atmospheric precipitation. The similarity in water type tends to express the existence of a unique hydrochemical system and that the waters have the same or similar origins and flow paths. Individualised groundwater flow paths are difficult to delineate within the different stratigraphic units. The Ca- SO_4 , Ca- SO_4 - HCO_3 , Ca-mixed SO_4 - HCO_3 and Ca- HCO_3 - SO_4 water types characterise some springs near Arneh and Beit Tima villages (11 % of all water samples). The local presence of this water type suggests the dissolution of evaporite minerals. Kattan (2006) concludes that the water type of major tributary of Awaj River (Sebarani), which is feed by karstic spring located in Arneh region, is calcium-sulfate type. Few samples (6 % of all samples) show a Ca-Cl- HCO_3 and Ca-mixed Cl- HCO_3 water types. The dissolution of evaporite minerals and possible pollution from wastewater, animal manure and chemical fertilizer may have contributed to these samples' chemical composition. The mixed cations-mixed anions as well as the mixed cations- HCO_3 water types characterized about 10 % of the water samples. These water types recognized mainly in the plain area where heavy artificial exploitation is occurring which might enhance mixing between different groundwater flow patterns. The reverse cation exchange as well as the dissolution of silicate mineral appear to play a role in this water type. The remaining samples (about 3 %) show a Mg- HCO_3 and Mg-Ca- HCO_3 water type.

The Stiff diagram map (Stiff 1951) is used to compare the ionic composition of water samples between different locations. Figure 6 shows the spatial distribution of Stiff diagrams constructed for chosen groundwater samples based on their geographical distribution on study area. As discussed earlier, the Stiff diagram reinforces the similarity in the hydrochemical aquifer system based on the correlation in the mineral composition of the groundwater samples. Groundwater is predominantly fresh (electrical conductivity (EC) < 1,000 $\mu\text{S}/\text{Cm}$). In general, Stiff diagrams constructed for well samples demonstrate the largest shapes compared with these of spring samples. This is because the springs are located in

the karstic and well-flushed zones of active water circulation while well water is from zones of less active circulation. In addition to this, the majority of the wells are located in the plain area where the evaporation, the irrigation return flow, the effect of topographic factor and groundwater flow direction increase salt water concentration. The high EC measured near Arneh village in the mountain area is the result of high sulfate concentration.

Pollution index and faecal contamination

There are 14 villages in the study area that discharge their wastewater directly onto land or into the river without any treatment. The uninformed and excessive use of nitrogen fertilizers and untreated waste water in irrigation leads to obvious water quality degradation.

The pollution index (PI) was calculated based on the concentration of nitrate and sulfate anions using the following formula (Stuyfzand 1989):

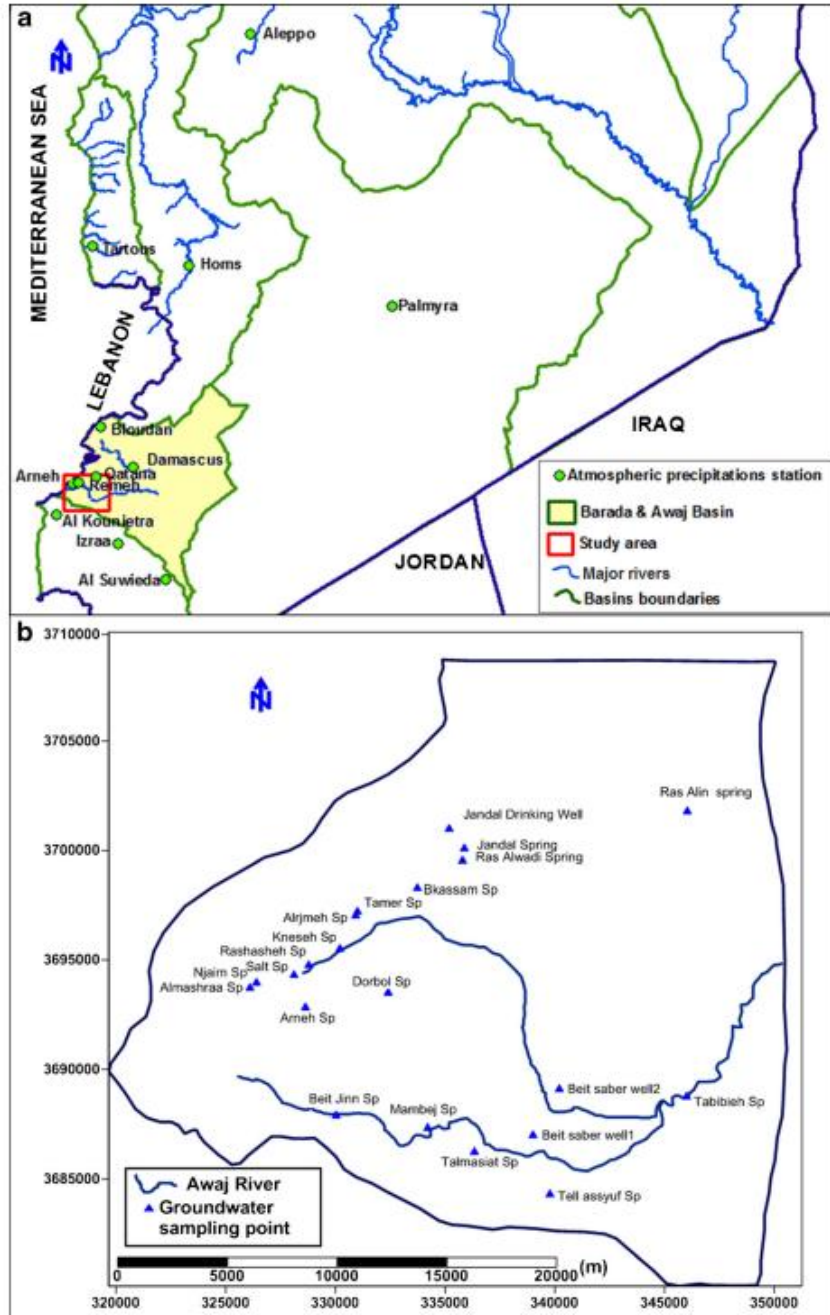
$$\text{PI} = (1.33 \times \text{ABS}(\text{pH}-7) + \text{LN}(10 \times (\text{SO}_4 + \text{NO}_3))) / 1.7 \quad (6)$$

The spatial distribution of this factor, as shown in Fig. 7a, demonstrates that the highest values localized in Arneh and Bkassam villages. The elevated values in Arneh are derived from high concentration of sulfate caused by gypsum dissolution. Whereas the high values in Bkassam are the result of a particular pollution source namely the existence of a septic tank. The high vulnerability of karstic limestone in this region enhances quick infiltration of untreated wastewater and increases the nitrate concentration in the groundwater. On the other hand, the high value of this factor measured in the plain area is caused by high nitrate concentration which results mainly from the use of fertilizers. This area hosts a considerable number of irrigation wells and intensive agricultural activities where nitrogenous fertilizers and manures are massively applied.

The total and faecal coliforms are used as indicators of possible sewage water contamination because they are commonly found in human and animal faeces. Although they are generally not harmful themselves, they indicate the possible presence of pathogenic (disease-causing) bacteria, viruses and protozoa that also live in human and animal digestive systems. Sources of this bacterial contamination are mainly wastewater on-site septic systems as well as domestic and wild animal manure.

Available analysis results of these bacteria in three springs located in the plain area during March–April 2006 (RDAWSA 2006) were used to identify faecal pollution. As shown in Fig. 7b, three springs demonstrate

Fig. 8 The locations of sampling sites of atmospheric precipitation in Barada and Awaj Basin and other basins in Syria (a) as well as the location of groundwater sampling sites for environmental isotopes investigations (b)



pollution with total coliform and faecal coliform (*Escherichia coli*). This indicates that the recently ongoing bacteriological contamination from the untreated sewage or

animals waste due to the relatively short life of both bacteria, consequently the recent recharge of these springs, can be recognized.

Stable isotope composition of atmospheric precipitation and groundwater

Stable isotopes ($\delta^{18}\text{O}$, $\delta^2\text{H}$) have conservative properties and depend only on atmospheric conditions during recharge; consequently, they provide information on the recharge processes of groundwater (Gat 1971; Huneau et al. 2011). The historical data available of the atmospheric precipitation isotopic content from 12 stations (Kattan 1997a, 2006; Selkhozpromexport 1986) were used to interpret the relationship between rainfall and groundwater in the study area. Most of these stations are located in or around this area (Fig. 8a). The values of $\delta^{18}\text{O}$, $\delta^2\text{H}$ and ^3H (T U) as well as the amount of precipitation measured in these atmospheric precipitation stations are shown in Table 2. The values of $\delta^{18}\text{O}$ and $\delta^2\text{H}$ measured in the groundwater samples are reported in Table 3 and the locations of these samples are shown in Fig. 8b.

Figure 9a shows the relationship between $\delta^{18}\text{O}$ and $\delta^2\text{H}$ in both atmospheric precipitation and groundwater samples. All the atmospheric precipitation stations are located between the Mediterranean Meteoric Water Line (MMWL) defined by the equation: $\delta^2\text{H} = 8. \delta^{18}\text{O} + 22$ (Nir 1967) and the Global Meteoric Water Line (GMWL) defined by the equation: $\delta^2\text{H} = 8. \delta^{18}\text{O} + 10$ (Craig 1961). The relationship between $\delta^{18}\text{O}$ and $\delta^2\text{H}$ determined for precipitation stations is given by the following equation:

$$\delta^2\text{H} = 7.9. \delta^{18}\text{O} + 17.9 \tag{7}$$

Kattan (1997a) has found this equation to be:

$$\delta^2\text{H} = 8.26. \delta^{18}\text{O} + 19.3 \tag{8}$$

The d excess in our case is lower than the d excess in the Kattan equation which might indicate a relatively less pronounced evaporation effect as a result of additional stations located in the Mt. Hermon.

The most depleted values of both ^{18}O and ^2H were measured at the Bloudan atmospheric precipitation station which is at higher altitude, while the most enriched values for both these stable isotopes were measured in the Palmyra station which is located in the central desert basin.

The progressive depletion of heavy stable isotopes with increases in altitude is due to the local climate and topography, mainly the air temperature which decreases with altitude. These values were estimated to be -0.23 ‰ per 100 m for ^{18}O and -1.7 ‰ per 100 m for ^2H (Fig. 9c). The deviation of the Damascus, Aleppo and Palmyra stations from the regression line can be caused by global, regional and/or seasonal effects such as the Khamasin rain originating from the north African dessert or due to local and particular climatic conditions affecting weather front in the region.

Fig. 9 a The relationship between $\delta^{18}\text{O}$ and $\delta^2\text{H}$ in atmospheric precipitation (weighted mean) and in groundwater samples. b The relationship between tritium unite and the distance from the Syrian shoreline. c The relationship between both $\delta^{18}\text{O}$ and $\delta^2\text{H}$ and altitude for precipitation and groundwater samples

Based on this gradient, the mean elevation of recharge zones of groundwater in the study area is calculated to be between 900 and 1,600 m.

The relationship between tritium and the distance from the Syrian shoreline (Fig. 9b) shows a positive trend with moving inland as a result of increasing stratospheric influence. The build-up of tritium over land is a result of the cutting off of the supply of low activity oceanic vapour, while influx from aloft continues.

The environmental isotope compositions of groundwater was studied based on 21 samples, 18 springs, 2 shallow wells (Beit Saber well1 and well2, at depths of 40 and 60 m, respectively) and 1 deep well (Jandal drink well, at 150 m depth). All the groundwater samples are located around the local meteoric water line ($\delta^2\text{H}=7.9. \delta^{18}\text{O} + 17.9$) and MMWL (Fig. 9a), which indicates the recent origin of these samples and the domination of the Mediterranean climate. The springs which are located in the plain area and characterized by higher discharge tend to have slightly higher enriched stable isotope compositions compared with other samples. This might be a result of recharge contribution from an area of lower altitude a or from an older component by upward movement of deeper aquifers representing a mixture of several flow paths as a collective flow system (continuous recharge possibility). On the other hand, the small springs in the mountainous area can be attributed to point recharge possibility. The grouping of these springs closer to the meteorological station located in this area indicate that the major source of these springs is the rainfall and snowmelt falling on the uppermost part of the Mt. Hermon. They tend to have slightly depleted stable isotopes signature as a result of the altitude effect.

In general, the distribution of groundwater samples around the precipitation samples implies a significant rapid and important infiltration of atmospheric precipitation through the karstic carbonate rocks before considerable evaporation which takes place earlier than or during the infiltration. Thus, the precipitation provides the major source of recharge to the upper part of Awaj River. The concept behind the grouping of these samples close to each other is that the aquifers are recharging from the same sources and that a hydraulic connection might exist between these aquifers.

Groundwater flow paths

Based on available water level data of 31 groundwater monitoring wells obtained from the Ministry of Irrigation

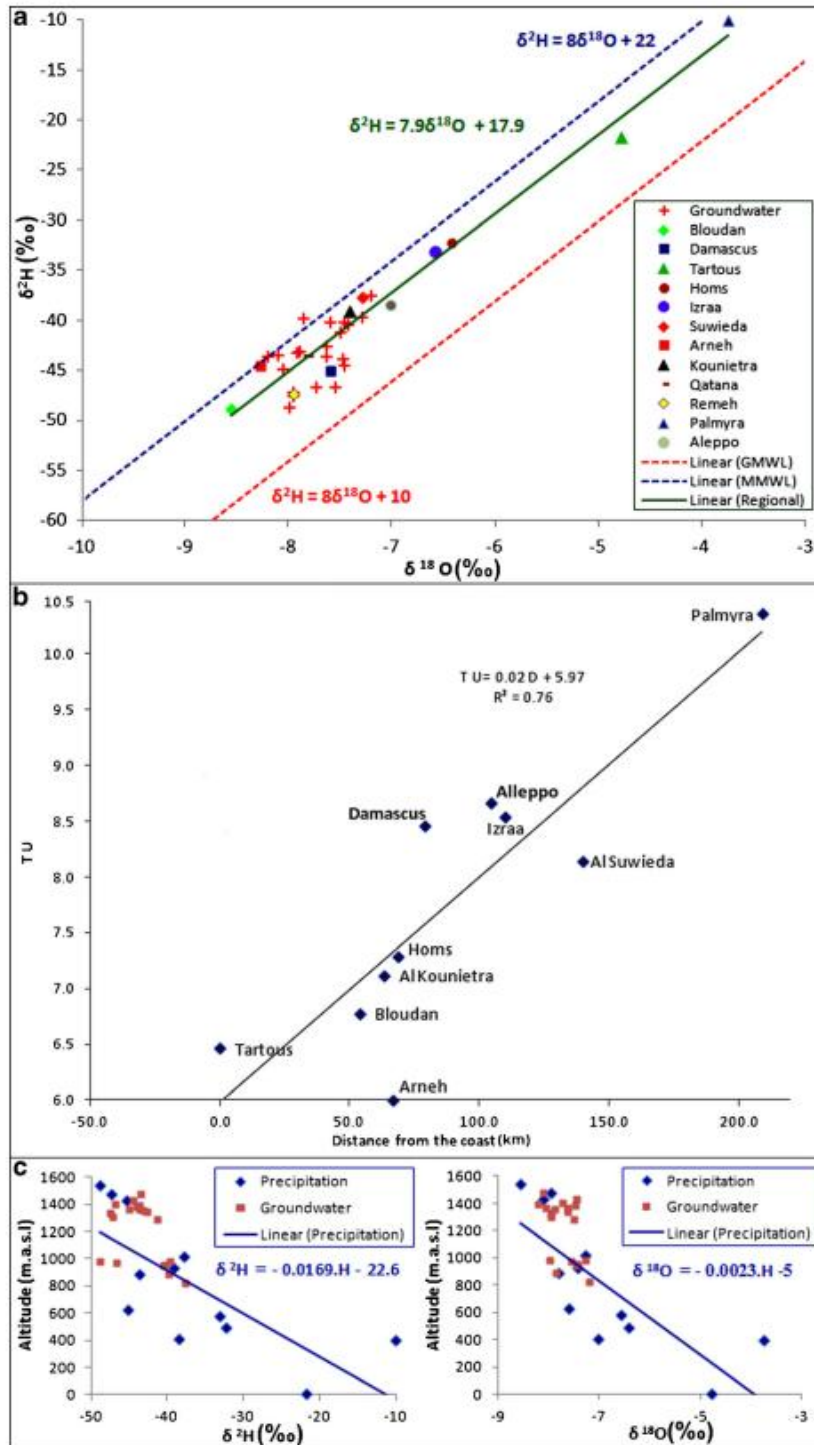


Table 2 Environmental stable isotopic composition and amount of precipitation measured in different meteorological stations in Syria; 1989–1990 data are from Kattan (1997a), 1983–1984 data from Selkhozpromexport (1986) and Arneh data from Kattan (2006)

Station name	Altitude (m)	Distance from the coast (km)	Date	P (mm)	$\delta^{18}\text{O}$	$\delta^2\text{H}$	^3H (T U)	d (%)
Bloudan	1,540	55	Dec 1989	48.1	-8	-44.1	4.3	20.1
			Jan 1990	46.1	-7.8	-40.2	6.9	22
			Feb 1990	101.9	-8.7	-48.7	7.3	20.7
			Mar 1990	51.5	-8.2	-47.8	7	17.9
			Apr 1990	18	-12.2	-87.4	9.5	10.4
Weighted mean					-8.6	-48.8	6.8	19.6
Damascus	625	80	Dec 1989	4.8	-7.3	-47.8	5.5	10.8
			Jan 1990	14.9	-9.6	-62.6	9	14.5
			Feb 1990	30.6	-7.2	-35.5	8.6	21.9
			Mar 1990	28.2	-6.5	-37.9	7	13.8
			Apr 1990	8.4	-9.4	-71.7	13.6	3.8
Weighted mean					-7.6	-45.1	8.5	15.7
Kounietra	930	64	Dec 1989	55.6	-6.4	-30.6	6.5	20.9
			Jan 1990	70.3	-8.5	-48.8	7.5	19.1
			Feb 1990	115.9	-7	-34.6	7.6	21.7
			Mar 1990	86.6	-7.7	-42.3	6.5	19.1
			Apr 1990	7.3	-7.2	-44.5	7.9	13.3
Weighted mean					-7.4	-39.1	7.1	20.2
Tartous	5	0	Dec 1989	96.6	-4.6	-18.5	5.1	18.4
			Jan 1990	72.4	-5.4	-24.9	7.3	18.1
			Feb 1990	132.2	-3.8	-14.2	5.4	16.4
			Mar 1990	95	-4.1	-17.3	5.6	15.3
			Apr 1990	54.8	-7.8	-49	11.8	13.3
Weighted mean					-4.8	-21.7	6.5	16.5
Homs	490	70	Dec 1989	49.6	-6.6	-32.9	5.1	19.8
			Jan 1990	40.8	-6.4	-29.7	7	21.8
			Feb 1990	36.6	-6.5	-30.1	7.9	22.2
			Mar 1990	10.5	-5.1	-30.1	9.2	10.6
			Apr 1990	19.5	-6.4	-41.1	11.3	10.2
Weighted mean					-6.4	-32.2	7.3	19.1
Izraa	580	111	Dec 1989	37	-7.1	-36.9	5.6	20.1
			Jan 1990	65.9	-7.1	-41.6	9.7	14.8
			Feb 1990	60.9	-6.8	-29.6	9.4	24.4
			Mar 1990	55.4	-5.2	-21.5	8	20.3
			Apr 1990	10.1	-7.8	-48.7	9.4	14
Weighted mean					-6.6	-33.1	8.5	19.5
Suwieda	1,020	140	Dec 1989	44.7	-7.8	-40.2	4.6	22.1
			Jan 1990	100	-8.8	-52.5	9.2	17.6
			Feb 1990	65.8	-6.9	-31.7	8.7	23.3
			Mar 1990	76.3	-5	-17.6	7.5	22.3
			Apr 1990	30.6	-8.3	-49	10.3	17.6
Weighted mean					-7.3	-37.7	8.1	20.5
Palmyra	400	211	Dec 1989	11.5	-7	-45.2	7.1	10.5
			Jan 1990	3.8	-6.4	-38.7	12.4	12.2
			Feb 1990	29	-6.3	-22.2	11.4	28
			Mar 1990	24.2	-0.4	16.4	9.8	19.5
			Apr 1990	11.4	-0.3	9.6	11.8	12.1
Weighted mean					-3.7	-10.1	10.4	19.9

Table 2 (continued)

Station name	Altitude (m)	Distance from the coast (km)	Date	P (mm)	$\delta^{18}\text{O}$	$\delta^2\text{H}$	^3H (T U)	d (%)
Aleppo	410	105	Dec 1989	45.1	-7.1	-37.8	6.7	19.2
			Jan 1990	24.9	-10.7	-65	10.8	20.9
			Feb 1990	47.1	-7.1	-38.9	9.1	18.1
			Mar 1990	20.5	-2.8	-10.9	9	11.6
			Apr 1990	3.5	-2	-14	11	2
Weighted mean					-7	-38.5	8.7	17.6
Qatana	890	-	Feb 1983	63	-6.7	-29.6		24
			Mar 1983	43.5	-9.4	-55.2		20
			Jan 1984	56.5	-9.3	-49.4		25
			Mar 1984	64	-6.4	-44.2		7
Weighted mean					-7.8	-43.6		18.7
Remeh	1,480	-	Feb 1983	51	-5.8	-23.4		23
			Mar 1983	64	-11	-71		17
			Mar 1984	100	-7.4	-44.2		15
			Apr 1984	40	-7.2	-47.6		10
Weighted mean					-8	-47.3		16.3
Arneh	1,430	-	1989–1993		-8.3	-44.5	6	21.7

Table 3 Environmental stable isotopic composition measured in groundwater samples collected from 18 sites in the study area during August 2012 as addition to three samples from Selkhozpromexport 1986

Station name	Analysis date	$\delta^2\text{H}$ reportable value (permil)	$\delta^2\text{H}$ standard deviation (permil)	$\delta^{18}\text{O}$ reportable value (permil)	$\delta^{18}\text{O}$ standard deviation (permil)	d (%)	Altitude (m)	Average springs discharge (2004–2005) $\text{m}^3 \text{s}^{-1}$
Beit Saber well1	17/08/2012	-48.76	0.57	-7.99	0.04	15.14	983	-
Beit Saber well2	17/08/2012	-46.65	0.72	-7.54	0.10	13.66	972	-
Jandal Spring	17/08/2012	-47.55	0.60	-7.94	0.09	15.98	1,332	0.05
Ras Alwadi Spring	17/08/2012	-47.22	0.49	-7.94	0.03	16.34	1,304	-
Jandal Drink Well	17/08/2012	-44.98	1.04	-8.04	0.12	19.36	1,368	-
Bkassam Spring	17/08/2012	-46.75	0.29	-7.72	0.05	15.02	1,400	-
Njaim Spring	20/08/2012	-43.30	0.94	-7.91	0.11	19.94		0.01
Almalha Spring	20/08/2012	-43.20	0.67	-7.88	0.11	19.86	1,358	0.01
Arneh Spring	20/08/2012	-43.56	0.32	-8.09	0.10	21.19	1,478	0.03
Almashraa Spring	20/08/2012	-40.24	0.28	-7.60	0.05	20.53		0.03
Rashasbeh Spring	20/08/2012	-42.67	0.85	-7.62	0.10	18.31	1,342	0.03
Knesch Spring	20/08/2012	-43.64	0.94	-7.62	0.09	17.35	1,365	0.09
Aljimeh Spring	20/08/2012	-44.49	0.25	-7.45	0.06	15.15	1,429	0.02
Tamer Spring	20/08/2012	-43.97	0.53	-7.47	0.08	15.82	1,386	-
Mambej Spring	16/08/2012	-39.66	1.04	-7.28	0.12	18.58	980	0.70
Talmasiat Spring	16/08/2012	-40.49	0.68	-7.42	0.08	18.89	950	0.50
Tal Assyuf Spring	16/08/2012	-40.26	0.69	-7.46	0.08	19.40	956	0.50
Beit Jinn Spring	16/08/2012	-41.23	0.51	-7.50	0.05	18.75	1,285	0.80
dorbol spring	1984	-43.6		-8.2		22	1,394	0.02
Tabibieh spring	1984	-37.6		-7.2		20	821	0.4
Ras Alin spring	1984	-39.8		-7.85		23	887	0.28

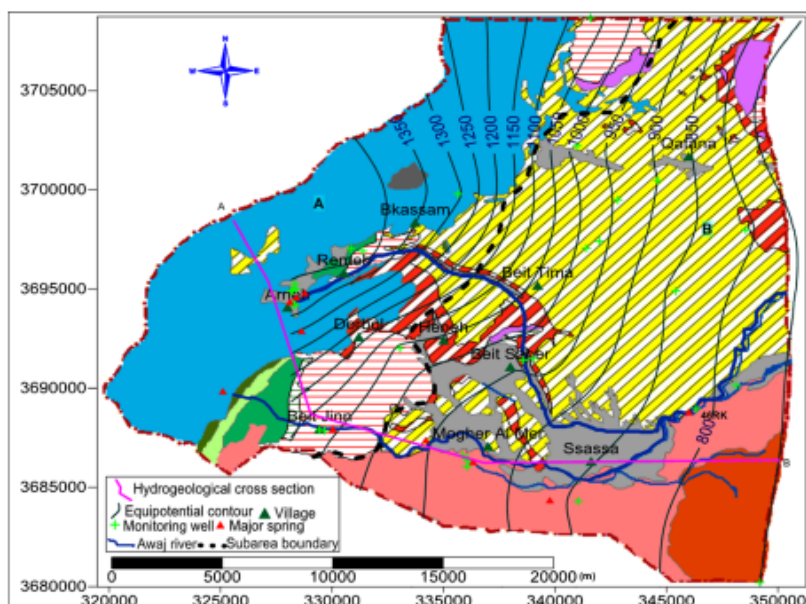
of Syria, a preliminary potentiometric map was constructed for October 2006 as shown on Fig. 10. The interpretation of equipotential contours indicates that the general groundwater flow is organized towards the east direction. Minor flow direction is also recognized from northwest to southeast where several springs characterized by relatively high discharges emerge close to the limit between the basalt formation and other formations in the plain part. A steeper hydraulic gradient is observed in the western and northern mountainous parts, where the karsts and faults are more dominant.

According to water type classification, groundwater discharge (mainly major springs), equipotential contour lines and geological and structural control, the study area can be divided into two main subareas A and B (Fig. 10). The subarea A is characterized by high amount of atmospheric precipitation and infiltration coefficient; the rainfall and snowmelt are the main sources of groundwater recharge. Groundwater movement is primarily along the bed with a significant downward component controlled by developed faults and fractures. However, groundwater discharges in this area occur through many springs located in the foothill of Mt. Hermon in the Jurassic aquifer. The two tributaries of Awaj River are generated in this part. In the subarea B, the Neogene and Quaternary aquifers form the main water supply source for both domestic and agricultural purposes. This area includes the zone with higher

groundwater withdrawals. In this part, there are two main sources of groundwater recharge. The first one is direct infiltration of atmospheric precipitation mainly through Neogene outcropping formation. While the second potential source of groundwater recharge is hydraulic exchange between the deep aquifers (Jurassic and Cretaceous) and the Neogene/Quaternary aquifers. The enormous amount of infiltrated precipitation and snowmelt, mainly in the Jurassic outcropping formations, flows and circulates as deep groundwater through conduits and faults toward the upper aquifers by upward movement. Water discharges in this area through the major springs and numerous wells.

Figure 11a shows the pronounced relationship between the amount of precipitation measured at the Arneh atmospheric precipitation station and the discharge of Beit Jinn spring, both of them located in the mountainous subarea A during various hydrological years. The ranges of spring discharge indicate that the main source of spring recharge is the atmospheric precipitation. The low base flow component during summer period implies the significant effect of rainfall and snowmelt in the winter time on the spring discharge. The spring discharge peaks are almost associated with the peaks of precipitation amounts with respective time lags can be explained by the effect of snowmelt. The fluctuation of monthly groundwater level in the well 46RK located in subarea B (Fig. 10) is also shown on

Fig. 10 Equipotential contour map based on groundwater level measured in 31 monitoring wells during October 2006. The associated hydrogeological sub-areas (A and B) are depicted. A-B cross section, from which the conceptual hydrogeological model was constructed, is also shown



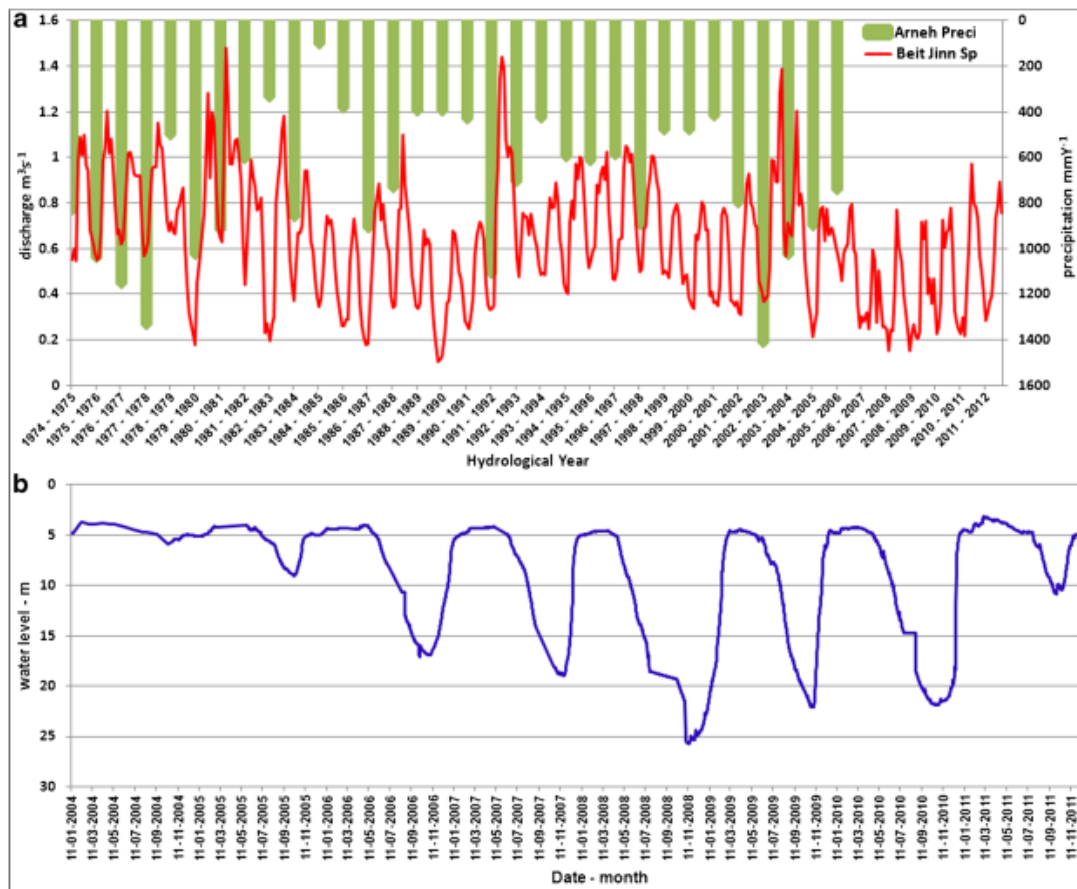


Fig. 11 **a** Monthly discharge of Beit Jinn spring and the amount of annual atmospheric precipitation measured in Arneh station. **b** Monthly level fluctuations of groundwater in the well 46RK from 2004 until 2011

Fig. 11b during the period of 2004–2011. The typical decline during the summer dry period and increase during the rainy winter period depict seasonal trends in the water level as well as the effect of groundwater withdrawal. The decreasing trend in groundwater level during the observation period is caused by groundwater overexploitation.

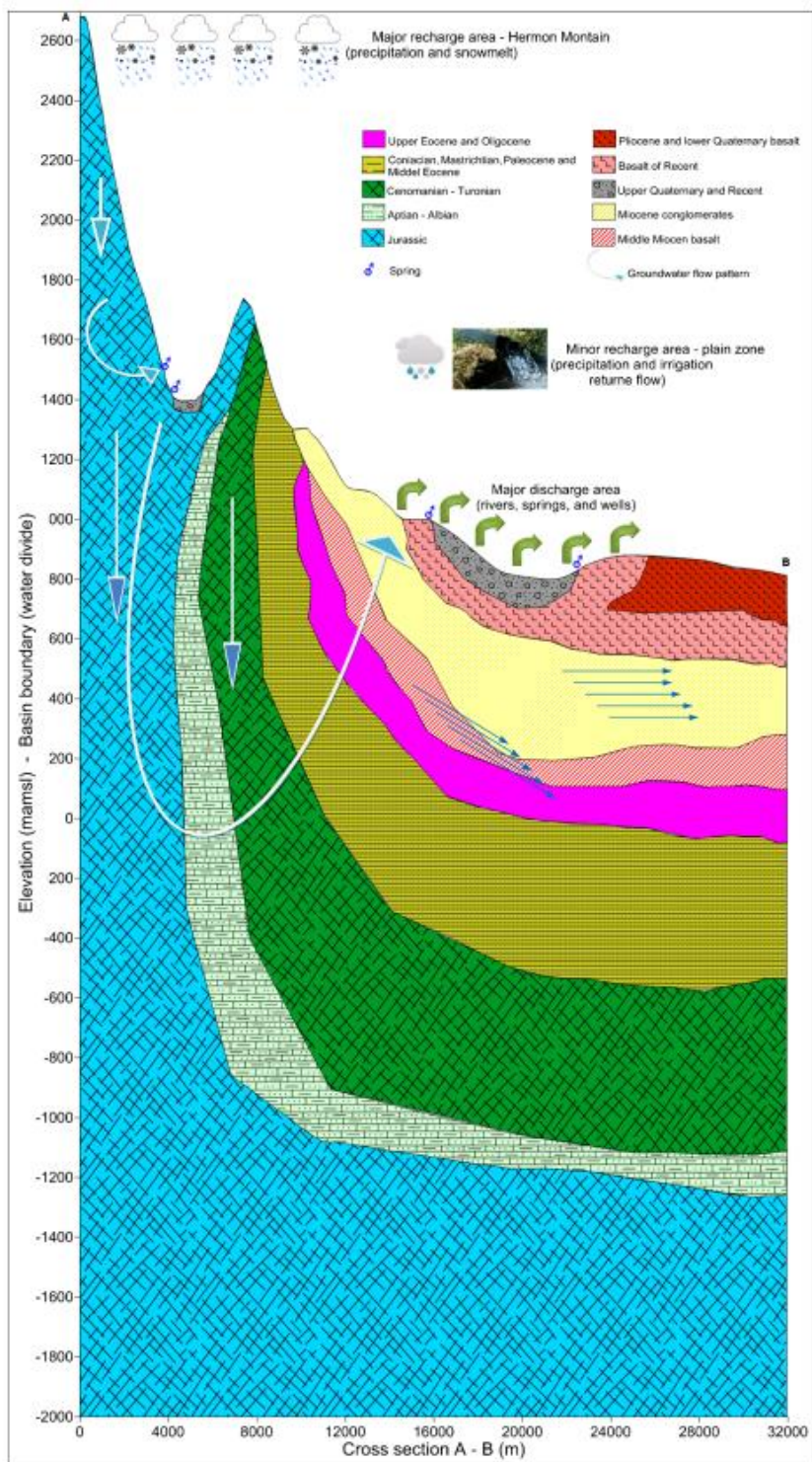
The A-B cross-section view illustrating the conceptual model of groundwater flow system in the study area is shown in Fig. 12. The model describes the recharge and discharge mechanisms in the aquifer systems and the suggested groundwater flow patterns. The flow patterns are controlled by topography, geological structures and the recharge by atmospheric precipitation and underlying aquifers. The distinguishing hydrostratigraphic units are presented.

Conclusion

The obtained results are helpful in identifying the origin and principal mechanisms that control and characterize the main hydrogeological features of the aquifer systems in the study area.

The interpretation of hydrogeochemical data in the upper part of Awaj River reveals a large degree of variability that results from its marked hydrogeological and lithological complexity. The dissolution/precipitation of carbonate minerals is the main process controlling groundwater composition not only in the mountainous

Fig. 12 Schematic hydrostratigraphic units through cross section A-B (Fig. 10) demonstrate conceptual hydrogeological model



part but also in the plain area which is evidenced by the saturation indices of calcite and dolomite. The dissolution of gypsum is recognized in some places in the Jurassic aquifer. The silicate hydrolysis and reverse cation exchange reaction involving clay minerals also play a considerable role in groundwater composition.

Anthropogenic activities have a major impact through the effect of fertilizers on nitrate levels as well as the contamination by sewage water and animal waste. This impact has been detected in some villages in the mountainous part as well as in the plain area through the substantial increases in nitrate and faecal concentrations.

The isotopes data implies an important rapid infiltration of atmospheric precipitation before significant evaporation takes place earlier than or during the infiltration. All the groundwater samples are situated to the left of GMWL suggesting input of local rainfall that derives from weather front originating from the Mediterranean Sea. The infiltrated precipitation provides the main source of recharge to the aquifers system through the karst landscape and fractured rocks in the mountain part (Jurassic aquifer). And, to a lesser extent, through Neogene conglomerate, Quaternary alluvial and basalt formations in the plain part where the mixing of groundwater flow paths might occur.

Nevertheless, the study area can be divided into two sub-areas A and B; the subarea B occupied the south, central and eastern part, namely Neogene conglomerates and Quaternary alluvial aquifers. This part is characterized by a shallow horizontal flow component associated with active interaction between groundwater and hosting rocks, evidenced by water chemistry evolution. The upward movement from deep aquifers seems to play a significant role in this subarea where the discharge occurs mainly through the major springs and groundwater abstraction wells. The subarea A occupies the south-western, western and north-western parts, mainly the Jurassic aquifer where the main groundwater recharge is occurring. In this part, the karstic features are well developed in the upper as well as in the deeper parts facilitated by cracks and fissures. This leads to increase the permeability characteristics and enhance the infiltration and dissolution mechanisms; hence, this part is characterized by a high vulnerability of groundwater to pollution evidenced by high rates of nitrates resulting from sewage water infiltration. The hydrochemical processes are highly irregular in space which is suggestive of an active dissolution phenomena and deep vertical groundwater flow in this part.

Fluctuation of groundwater level is strongly controlled by atmospheric precipitation and anthropogenic influence through the increasing of groundwater abstraction.

In fact, the area can be considered much more dominated by recharge than discharge processes. The main involvement of this study was the delineation of potential recharge area.

The main hydrochemical processes controlling groundwater composition were also inferred. Nevertheless, more samples for isotopes and age-dating will improve the knowledge about the hydrogeological behaviour of the aquifer system. A quantitative hydrogeological model is under construction to assess available groundwater resources in this region under the effects of recent climate changes and overexploitation of groundwater.

References

- Abou Zakhem B, Hafez R (2010) Climatic factors controlling chemical and isotopic characteristics of precipitation in Syria. *Hydrol Process* 24:2641–2654
- Angelakis AN (2000) Water resources management in Syria, with emphasis on non-conventional sources. FAO RNE, Egypt
- Asfahani J, Abdul Ghani B (2012) Automated interpretation of nuclear and electrical well loggings for basalt characterization (case study from southern Syria). *Appl Radiat Isot* 70:2500–2506
- Asmael NM, Huneau F, Garel E, Celle-Jeanton H, Le Coustumer P, Dupuy A (2014) Hydrochemistry to delineate groundwater flow conditions in the mogher Al Mer area (Damascus basin, southwestern Syria). *Environ Earth Sci* 72:3205–3225
- Bajjali W (2006) Recharge mechanism and hydrochemistry evaluation of groundwater in the Nuaimeh Area, Jordan using environmental isotope techniques. *Hydrogeol J* 14:180–191
- Bajjali W (2008) Evaluation of groundwater in a three-aquifer system in Ramtha area, Jordan: recharge mechanisms, hydraulic relationship and geochemical evolution. *Hydrogeol J* 16:1193–1205
- Barbieri P, Adami G, Favretto A, Lutman A, Avoscan W, Reisenhofer E (2001) Robust cluster analysis for detecting physicochemical typologies of freshwater from wells of the plain of Friuli (north-eastern Italy). *Anal Chim Acta* 440:161–170
- Burdon DJ, Safadi C (1964) The karst groundwater of Syria. *J Hyrol* 2: 324–347
- Craig H (1961) Isotopic variations in meteoric waters. *Science* 133:1702–1703
- Datta PS, Tyagi SK (1996) Major ion chemistry of groundwater in Delhi area: chemical weathering processes and groundwater flow regime. *J Geol Soc India* 47:179–188
- Dubertret L (1932) L'Hydrologie et aperçu sur l'Hydrographie de la Syrie et du Liban dans leurs relations avec la géologie. *Rev Géogr Phys Géol Dynamique*, TVI fas.4
- FAO (1993) Integrated Rural Water Management. Proceedings of the Technical Consultation on Integrated Water Management, Rome, Italy
- Fritz P, Suzuki O, Silva C, Salati E (1981) Isotope hydrology of groundwater in the Pampa del Tamarugal, Chile. *J Hydrol* 53:161–184
- Gat JR (1971) Comments on the stable isotope method in regional groundwater investigations. *Water Resour Res* 7:980–993
- Guler C, Thyne GD (2004) Delineation of hydrochemical facies distribution in a regional groundwater system by means of fuzzy c-means clustering. *Water Resour Res* 40:1–11
- Guler C, Thyne GD, McCray JE, Tumer KA (2002) Evaluation of graphical and multivariate statistical methods for classification of water chemistry data. *Hydrogeol J* 10:455–474
- Hem JD (1985) Study and interpretation of the chemical characteristics of natural water, 3rd Edn. U.S. Geol. Surv. Water Supply Paper: 2254
- Huneau F, Dakoure D, Celle-Jeanton H, Vitvar T, Ito M, Compaore NF, Traore S, Jirakova H, Le Coustumer P (2011) Flow pattern and

- residence time of groundwater within the south-eastern Taoudeni sedimentary basin (Burkina Faso, Mali). *J Hydrol* 409:423–439
- JICA (2001) The study of water resources development in the western and central basins in Syrian Arab Republic, phase I, Ministry of Irrigation (MOI). (in Arabic), (Unpublished report)
- Kattan Z (1997a) Chemical and environmental isotopes study of precipitation in Syria. *J Arid Environ* 35:601–615
- Kattan Z (1997b) Environmental isotope study of the major karst springs in Damascus limestone aquifer systems: case of the Figeih and Barada springs. *J Hydrol* 193:161–182
- Kattan Z (2006) Characterization of surface water and groundwater in the Damascus Ghotta basin: hydrochemical and environmental isotopes approaches. *Environ Geol* 51:173–201
- La-Moreaux PE, Hughes TH, Memon BA, Lineback N (1989) Hydrogeologic assessment—Figeih Spring, Damascus, Syria. *Environ Geol Water Sci* 13(2):73–127
- Luijendijk E, Bruggeman A (2008) Groundwater resources in the Jabal Al Hass region, northwest Syria: an assessment of past use and future potential. *Hydrogeol J* 16:511–530. doi:10.1007/s10040-008-0282-5
- MOI (2005) Annual Water Resources Report of Barada and Awaj Basin, Damascus, Syria, (in Arabic), (Unpublished report)
- Nir A (1967) Development of isotope methods applied to groundwater hydrology. Proceedings of a Symposium on Isotope Techniques in the Hydrological Cycle. *Am Geophys Union Monogr Series*, no 11, pp 1–109
- Parkhurst DL, Appelo CAJ (1999) PHREEQC for Windows version 1.4.07. A hydrogeochemical transport model. U.S. Geological Survey Software
- Piper AM (1944) A graphic procedure in the geochemical interpretation of water analyses. *Trans Amer Geophys Union* 25:914–923
- Plummer LN, Busby JF, Lee RW, Hanshaw BB (1990) Geochemical modeling of the Madison aquifer in parts of Montana, Wyoming, and South Dakota. *Water Resour Res* 26(9):1981–2014
- Ponikarov VO (1967) The geology of Syria, explanatory notes on the map of Syria, scale 1:500,000. Part II. Mineral deposits and underground water resources, Technoexport, Moscow
- Postel S (1999) *Pillar of sand: can the irrigation miracle last?* Norton, New York
- RDAWSA (2006) Interim report—hydrogeological study of Mogher Al Mer Area, Damascus Rural water and sanitation project (in Arabic), (Unpublished report)
- Selkhozpromexport (1986) Water resources use in Barada and Awaj Basins for irrigation of crops, Syria Arab Republic. USSR., Ministry of Land Reclamation and Water Management, Moscow
- Shah T, Molden D, Sakthivadivel R, Seckler D (2000) The global groundwater situation: overview of opportunities and challenges. International Water Management Institute, Colombo, Sri Lanka
- Stiff HA (1951) The interpretation of chemical water analysis by means of patterns. *J Petrol Technol* v. 3, no. 10
- Stuyfzand PJ (1989) A new hydrochemical classification of water type. *IAHS Red Books* 182:89–98
- Suk H, Lee K-K (1999) Characterization of a ground water hydrochemical system through multivariate analysis: clustering into groundwater zones. *Ground Water* 37:358–366
- United Nations (1982) *Groundwater in Eastern Mediterranean and Western Asia, Natural Resources*, Water Series no. 9, United Nations, New York
- Wolfart R (1964) Hydrogeology of the Damascus basin (southwest-Syria). *IAHS Red books* 64:402–413

Appendices C *Published Article*

Article published in the journal of Water

**Groundwater Modeling as an Alternative Approach to Limited Data
in the Northeastern Part of Mt. Hermon (Syria), to Develop a
Preliminary Water Budget**

Article

Groundwater Modeling as an Alternative Approach to Limited Data in the Northeastern Part of Mt. Hermon (Syria), to Develop a Preliminary Water Budget

Nazeer M. Asmael ^{1,2,3}, Alain Dupuy ^{2,3}, Frédéric Huneau ^{4,5}, Salim Hamid ¹ and Philippe Le Coustumer ^{2,6,7,*}

¹ Department of Geology, Faculty of Sciences, The University of Damascus, P.O. b 5735 Damascus, Syria; E-Mails: Nazeer_75@hotmail.com (N.M.A.); dr.salim.hamid@hotmail.com (S.H.)

² Université Bordeaux Montaigne, Equipe d'Accueil 4592 Géoressources & Environnement, 1 allée F. Daguin, F-33607 Pessac, France; E-Mail: Alain.Dupuy@ensegid.fr

³ Ecole Nationale Supérieure en Environnement Géologie Imagerie & Développement Institut Polytechnique National de Bordeaux, Equipe d'Accueil 4592 Géoressources & Environnement, 1 allée F. Daguin, F-33607 Pessac, France

⁴ Laboratoire d'Hydrogéologie, Faculté des Sciences et Techniques, Université de Corse Pascal Paoli, Campus Grimaldi, BP 52, F-20250 Corte, France; E-Mail: huneau@univ-corse.fr

⁵ Centre Nationale de la Recherche Scientifique, Unité Mixte de Recherche 6134, Sciences Physiques de l'Environnement, F-20250 Corte, France

⁶ Université de Bordeaux, Equipe d'Accueil 4592 Géoressources & Environnement, 1 allée F. Daguin, F-33607 Pessac, France

⁷ CNRS, UMR 5254, Technopôle Hélioparc Pau Pyrénées.2, avenue du Président Angot, F-64053 Pau Cedex 09, France

* Author to whom correspondence should be addressed; E-Mail: plc@lnet.fr; Tel.: +33-6-203-104-31.

Academic Editor: Markus Disse

Received: 1 April 2015 / Accepted: 14 July 2015 / Published: 21 July 2015

Abstract: In developing countries such as Syria, the lack of hydrological data affects groundwater resource assessment. Groundwater models provide the means to fill the gaps in the available data in order to improve the understanding of groundwater systems. The study area can be considered as the main recharge area of the eastern side of Barada and Awaj basin in the eastern part of Mt. Hermon. The withdrawal for agricultural and domestic purposes removes a considerable amount of water. The steady-state three-dimensional (3D)

groundwater model (FEFLOW which is an advanced finite element groundwater flow and transport modeling tool), was used to quantify groundwater budget components by using all available data of hydrological year 2009–2010. The results obtained may be considered as an essential tool for groundwater management options in the study area. The calibrated model demonstrates a good agreement between the observed and simulated hydraulic head. The result of the sensitivity analysis shows that the model is highly sensitive to hydraulic conductivity changes and sensitive to a lesser extent to water recharge amount. Regarding the upper aquifer horizon, the water budget under steady-state condition indicates that the lateral groundwater inflow from the Jurassic aquifer into this horizon is the most important recharge component. The major discharge component from this aquifer horizon occurs at its eastern boundary toward the outside of the model domain. The model was able to produce a satisfying estimation of the preliminary water budget of the upper aquifer horizon which indicates a positive imbalance of $4.6 \text{ Mm}^3 \cdot \text{y}^{-1}$.

Keywords: groundwater modelling; FEFLOW; water resources management; water budget; aquifer horizon; Mt. Hermon; Syria

1. Introduction

In agricultural countries such as Syria, the availability of water resources is considered to be a key factor for economic development. Syria is classified as a largely arid country, with two thirds of its land being desert and Rocky Mountains [1]. The percentage of the total irrigated areas served by groundwater increased from 49% in 1985 to 60% in 2004 [2,3]. It is well recognized that regional depletion of groundwater resources is a global issue [4,5]. Groundwater extraction facilitates social development and economic growth, but at the same time it may cause a decline in groundwater level and degradation of the ecosystem. Over the last few decades, the rapid growth and socioeconomic development in most of the sectors, particularly agriculture and light industry, where groundwater provides the necessary water supply, have severely affected water resources in the entire country. In most cases, there is no consideration given to the sustainability of the groundwater resources.

From a hydrological point of view, Mt. Hermon is an area shared between Syria, Lebanon and Israel. It is located in the transitional zone of the humid coastal region and dry desert area of southern Syria. Mt. Hermon is important because snowmelt and precipitation in this area serve as a feed for all streams, springs and rivers in that area. The drought in the Middle East that began in 2007 has further strained the limited water resources in the region [6–8]. The decrease in water resources, as a result of climate variability and increasing water demand, is one of the major challenges facing the inhabitants there who mainly depend on agricultural production. Thus, data on groundwater availability are significant for water-users in that area. The irrigated area is either totally dependent on groundwater or combined with Awaj River water (Figure 1c) through several canals branching from this river. The knowledge about the aquifer system of this region is limited. The lack of data is due to the inaccessibility to most parts of this massif region and the difficulties of maintaining meteorological

stations and collecting related data at high altitude. The absence of hydrological data exchange between Israel, Syria and Lebanon is considered to be another obstacle.

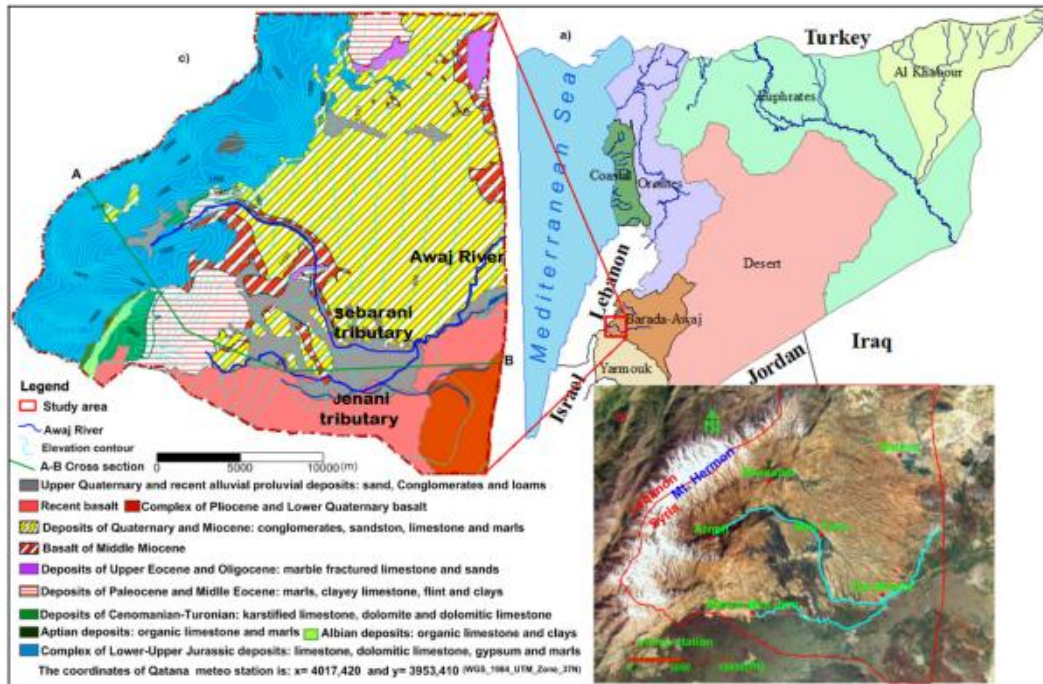


Figure 1. (a): The location of the study area on the map of Syria which is divided into seven hydrogeological basins; (b): The satellite map of the study area shows Mt. Hermon and the locations of meteorological stations; (c): The geological map of the study area showing different geological formations.

Groundwater modeling has been widely used to investigate groundwater system dynamics and understand flow patterns [9,10]. It can also be considered as an alternative approach to overcome the lack of observational data. Groundwater models may provide estimations of the water balance of the system under specified hydrological conditions. The developed model in this case study will be used to calculate the water budget component of the upper aquifer horizon in the model domain, which is considered a vital source for the intensive agricultural activities developed in the study area. Data on water use and pumping are essential in order to develop a water budget or groundwater flow model. The accurate monitoring of agricultural water use is an important factor in reducing the uncertainty of water balance calculation. However, quantifying groundwater abstraction remains a difficult but necessary challenge. Agriculture accounts for 87% of the water withdrawn from Syria's aquifers, rivers and lakes [11,12]. Groundwater abstraction for both agricultural and domestic uses is well developed in the study area. The study aims to (1) develop a groundwater model representing the groundwater flow system in the complex of the northeastern part of Mt. Hermon; (2) improve the hydrogeological understanding of this system and (3) provide a quantitative estimate of the groundwater budget of the upper aquifer horizon of the model domain under steady-state condition.

This horizon is densely inhabited and agricultural activities are well concentrated in it. The outcome of the proposed model could be used as a management tool to improve water use in this semi-arid region in order to achieve sustainable use of groundwater resources.

2. General Settings of the Study Area

The Barada and Awaj basin is one of the seven hydrological basins in Syria and is located in the south-west of the country. The study area occupies the southwestern part of this basin where Mt. Hermon is located (Figure 1a). Mt. Hermon is the highest point of the Anti-Lebanon Mountains. This mountain stretches for a length of 55 km and a width of 25 km of the anticline of mostly karstified limestone [13]. The general slope of the study area is from west to east and south-east. Its gradient reaches a value of about 50% at the slope of Mt. Hermon and less than 2% in the eastern or south-eastern parts. The elevation of this area varies between 800 and 2800 m a.s.l.

In this part of the Mediterranean region, precipitation is restricted to the months of November to April. The annual amount of precipitation is approximately 300 and 1000 mm·y⁻¹ in the flatland and the semi-humid mountain region, respectively. The infiltrated precipitation in the mountainous area either discharges locally as a karstic springs in the upper part of the Arneh valley (Figure 1b) or recharges the aquifers. Climate changes have resulted in a decrease in winter temperatures and total precipitation amount and in an increase in summer temperatures. These factors have led to the domination of a dry continental climate and contributed to the increasing water demand on the unsustainable abstraction of groundwater resources [14].

The model covers the study area of approximately 600 km² (Figure 1b). This area is considered to be a main recharge region of the Awaj River, which is a main water course in that area. This stream is formed by the junction of two main tributaries (Sebarani and Jenani, Figure 1c), which are fed by a large number of karst springs distributed along the slope of Mt. Hermon. The annual median discharge of the Awaj River was 4.7 m³·s⁻¹ between the years 1982 and 2004 but decreased to approximately 2.2 m³·s⁻¹ with a total drought period during summer in more recent years (2004–2014) [1].

The geological structure of the study area is the result of Jurassic to recent deposition, tectonic, and volcanism. Sporadic uplift along with comprehensive folding and faulting at shallow depth have resulted in a variety of surface forms and geologic structures. It can be divided into three parts: mountain ridges, volcanic district and plain area. The major sharp, deep valleys follow synclinal structures, are formed as strike valleys parallel to hogbacks or are the result of Pleistocene erosion along normal faults of significant displacement. The narrow, deep Arneh valley connects the mountainous part to the plain central region.

3. Geological Settings

The main formations outcropping in the study area range from Middle Jurassic up to the Quaternary period (Figure 1c). The complex of thick karstified strata of Jurassic limestone, which interbeds with dolomite, dolomitic limestone gypsiferous limestone and marl is outcropped in the western portion of the study area in Mt. Hermon (Figure 1c). The most important factors controlling karst development in Mt. Hermon are geological features, altitude defining the climatic belts, the local slope gradient and

the paleohydrological evolutionary history of the mountain [15]. The development of karstic features causes a large preferential groundwater flow and relatively little surface runoff [13].

Limited exposure of Cretaceous and Paleogene is found locally in the south-western portion of the study area (Figure 1c). The Cretaceous rock sequence ranges from Aptian to Senonian. The Aptian and Albian formations are mostly composed of organic limestone containing marls and clays. The Cenomanian-Turonian rock strata are composed of limestone, dolomitic limestone layers and crystalline dolomite with interbeds of argillaceous limestone, marl and sandstone. The Paleogene formations consist of intercalation of marly layers, marly limestone, clay and the limestone of Upper Eocene which is characterized by nummulites.

The plain areas are characterized by the exposure of the Neogene and Quaternary deposits. These deposits are mainly made of conglomerates, limestone and marly limestone, and dark colored basalt of Miocene age which is characterized by fractures filled with calcite, soil and clay. The Quaternary basalts resulting from lava overflow from volcanic vents [16] are located in the southern portion of the study area.

The major branches of the Red Sea-Dead Sea-Rift Valley transform faults system form the boundary which links the Arabian plate convergence in southern Turkey with the active seafloor spreading in the Red Sea. This system cuts through the study area which makes it very complex from a tectonic point of view [17]. Mt. Hermon and its northern extension, the Anti-Lebanon Mountains, are part of the Syrian arc fold system, which is a semi-continuous belt extending from western Egypt through the northern Sinai, the Negev desert and the adjacent offshore water of the south-eastern Mediterranean to Syria in the east [18]. As a result of folding and faulting structures, the Jurassic formations are in direct contact with the Paleogene and Neogene formations.

4. Characteristics of Hydrogeology and Aquifers

The majority of water flow in the study area exists as subsurface flow. Highly karstified, tectonically broken rocks and the step-like pattern of the slope create favorable infiltration conditions for precipitation in the elevated Jurassic formations. It is believed that faults, conduits, and fractures have an important role in controlling groundwater flow in this aquifer. The exposed part of the karstified Jurassic aquifers in the mountain area shows unfavorable conditions for exploitation, however, when they underlie at a reasonable depth in the plain area, they form a favorable but relatively deep aquifer. The Neogene and Quaternary deposits in the plain area (Figure 1c) form a porous aquifer. The main aquifers and hydrogeological units are described below.

4.1. Jurassic Aquifer

The thickness of the Jurassic aquifer (third aquifer in Figure 2) in the study area is about 1000 m in average and can reach a thickness of 2000 m in some places within the basin. According to [19], the hydraulic conductivity of this aquifer ranges between 2 and 99.3 $\text{m}\cdot\text{d}^{-1}$ and on average is about 18 $\text{m}\cdot\text{d}^{-1}$ thus the transmissivity could attain a value of around 3085 $\text{m}^2\cdot\text{d}^{-1}$.

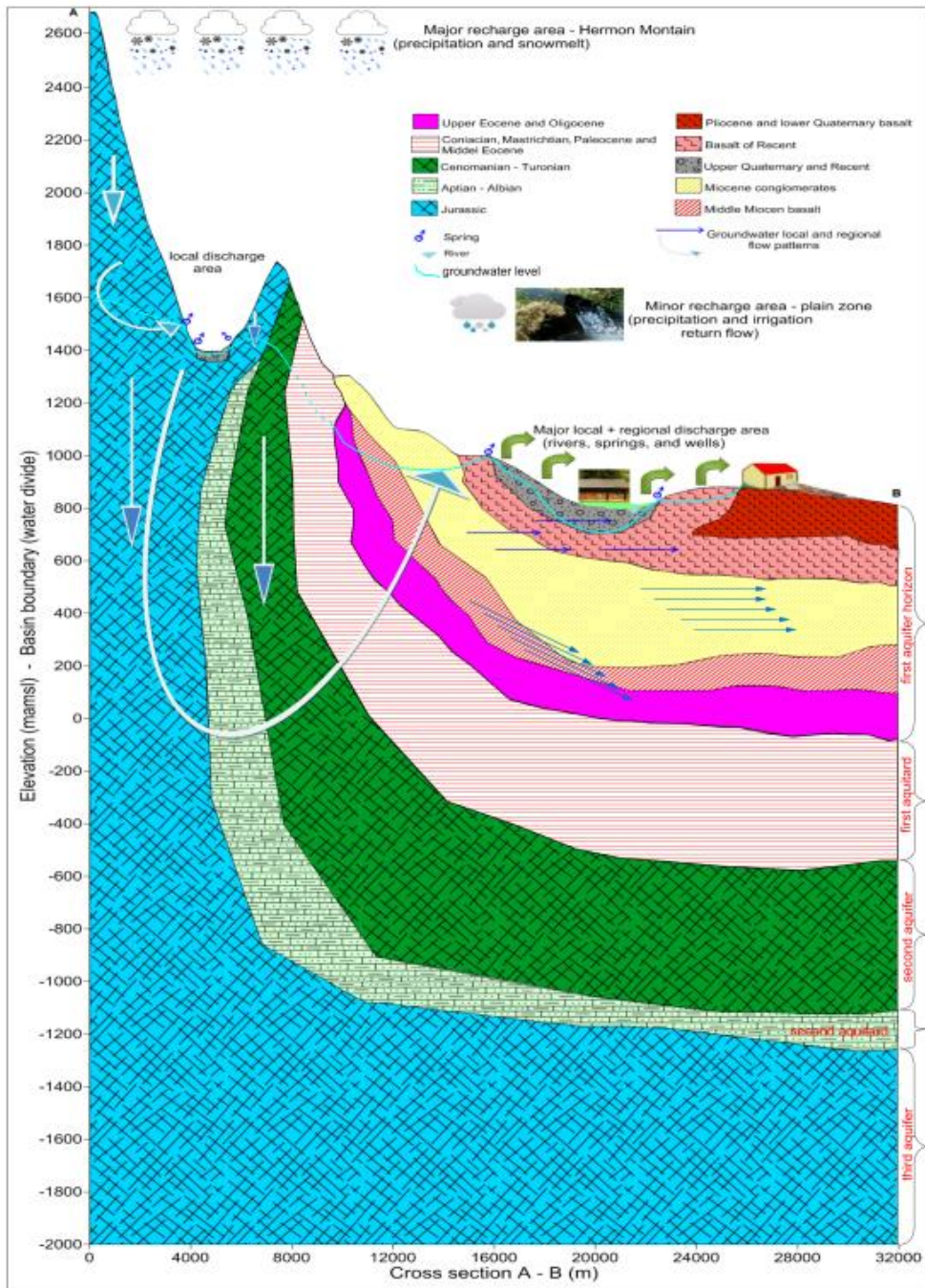


Figure 2. Hydrogeological cross section A–B demonstrates the conceptual hydrogeological model.

4.2. Cretaceous Aquifer

The Cretaceous aquifer is illustrated by Cenomanian-Turonian strata (second aquifer in Figure 2). The thickness of this aquifer varies between 400 and 1000 m. The hydraulic conductivity of this aquifer system can increase to $80 \text{ m}\cdot\text{d}^{-1}$ and its transmissivity ranges from 12 to $7435 \text{ m}^2\cdot\text{d}^{-1}$ [19]. This aquifer unit, together with the Jurassic one, forms the most important water-bearing system in the whole country and even in the Middle East [19–21]. These two units form large fresh groundwater reservoirs with large storage and withdrawal capacity as well as a considerable discharge of issuing springs [22].

4.3. The Sedimentary of Neogene/Quaternary, Volcanic Middle Miocene and Upper Paleogene Limestone Aquifer Horizon

The rock complex of these formations forms the upper aquifer (first aquifer in Figure 2) in the model domain and covers the most part of the study area; they are widespread from the foothill of Mt. Hermon to the eastern boundaries of this area. This horizon consists of: (1) alluvial deposits of Quaternary; (2) the weakly cemented gravels and conglomerates of Neogene which are associated with interbeds of clay, sandstone and limestone; (3) the hydrolyzed basalt of Miocene, which is associated with thin beds and lenses of sand and sandstone and; (4) the fracturing and karstified limestone of Upper Eocene-Oligocene, which is interbedded with lenses of quartz. The similarity in the hydraulic characteristics of these layers [23] as well as their hydraulic connections among hundreds of wells, allowed us to consider them as one aquifer horizon.

There are two intercalated aquitards between these hydrogeological units (Figure 2); the first one consists of deposits of the complex of Coniacian-Mastrichtian and Paleocene- Middle Eocene. Its thickness ranges from 200 to 600 m and is underlaid by Cenomanian-Turonian strata. The second aquitard is illustrated by Aptian-Albian stages and underlying by Jurassic strata. Its average thickness is about 200 m. However, according to [24], all the aquifers in the Barada and Awaj basin are hydraulically connected, although the connection is weak, because there are no beds between these aquifers acting as real aquicludes.

5. Modeling of Groundwater Flow

5.1. Model Construction

In order to simplify the field conditions of the model domain and based on the cross section A–B (Figure 1c) and on the horizontal extent of the aquifers and aquitards in the study area, the design of the conceptual groundwater model (Figure 2) was developed. The vertical and horizontal extent of the subsurface hydrogeological units and their connection are consistent with available information on boreholes [23]. The recharge and discharge areas are delineated. The conceptual model assumed that the preferential groundwater flow occurs mainly in the Jurassic aquifer and discharges as karstic springs into the upper part of the Arneh valley.

The model contains three aquifers and two aquitards in addition to the Quaternary basaltic layer which occupies the southeastern part of the study area and is considered to be a relatively thin aquitard

(Figure 3). The first aquifer extends in the central, eastern and south-eastern parts of the model domain within an area of about 380 km². The thickness of this rock complex varies between 65 and 630 m and reaches its greatest thickness in the east direction. Its top boundary is based on a digital elevation model of the ground surface, excluding the basaltic layer. The second aquifer (Cenomanian-Turonian) extends over an area of about 440 km², while the third aquifer (Jurassic) extends over the whole model area. The first and second aquitards occupied an area of about 420 and 450 km², respectively. The reason behind the different areas of the model layers is that these layers do not extend to the western site where the Jurassic layer is exposed.

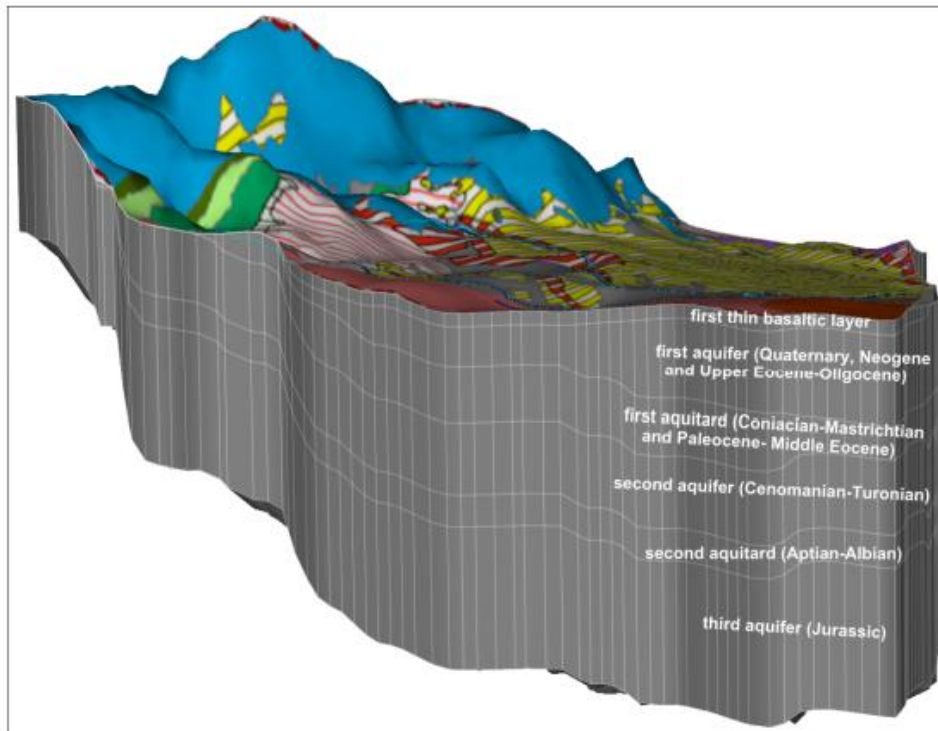


Figure 3. A three-dimensional (3D) representation of the six layers and seven slices constitute the model domain.

By using FEFLOW version 6 packages [25], the framework of super elements was defined and then the two-dimensional (2D) horizontal mesh of finite-element was generated using the automatic triangle option (Figure 4). After this, the three-dimensional (3D) slices elevations, layer properties and boundary conditions were defined. The advanced subsurface flow system was investigated under the steady-state condition. The 3D model grid consists of six layers, which correspond to the aforementioned hydrogeological units, and seven slices (Figure 3). There is a total of 48,702 two-dimensional triangular prismatic mesh elements, with 29,162 nodes which have been generated based on all the basic geometrical information. The finite element method characterized by its flexibility in generating the mesh and its capacity to simulate complex geometric forms and to refine

the nodal grid around points and/or single lines. The finite element grid was generated automatically with reasonable refinement around the points in both the plain and the Arneh valley region which demonstrate the abstraction wells placed in the grid as fixed nodes at their exact positions. The spatial data were prepared by using ArcGIS 10, which can be completely interfaced with FEFLOW.

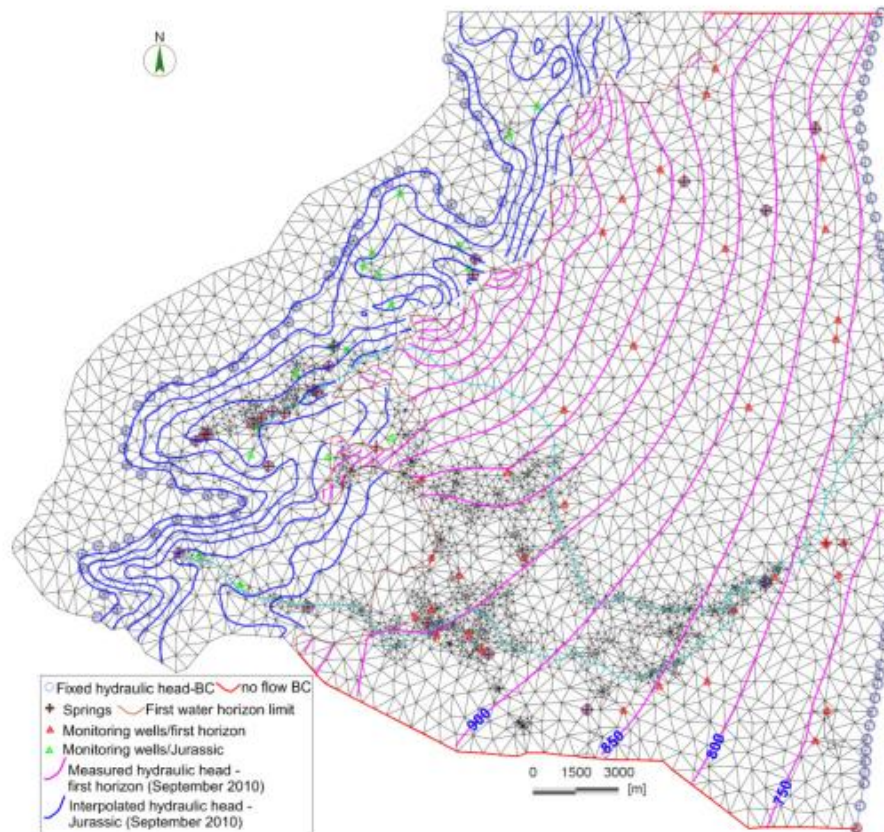


Figure 4. A two-dimensional (2D) FEFLOW representation of the groundwater model mesh and the spatial distribution of boundary conditions, springs and observation wells, as well as the equipotential contours of the measured hydraulic head for September 2010.

5.2. Boundary Conditions

Defining suitable model boundary conditions is an essential step in building numerical groundwater models and is largely responsible for the flow mechanism in the system [26]. The boundary conditions were determined according to topography and hydro-geological conditions. The hinge axis of Mt. Hermon located at the western and north-western boundaries of the study area forms the western boundary of the model. From the south, the basalt of Quaternary layer forms the southern boundary of the model domain at its limit with the Yarmouk basin (Figure 1a). This boundary is implemented as a no flow boundary. The north of Qatana village was used as the northern boundary of the model

(Figure 1b). This boundary was also assigned as a no flow boundary since the equipotential contours intersect with this boundary almost in perpendicular form.

According to the geological and hydrogeological features as well as spring discharges and groundwater level fluctuations in the upper aquifer horizon and Jurassic aquifer, we could distinguish between different hydraulic behaviors that characterize each of these aquifers. We assumed that there was a direct hydraulic connection between these two aquifers where the Neogene conglomerates come into direct contact with Jurassic limestone. This contact occurs in the model domain at the interface between these two aquifers.

The non-saturated zone in the exposed part of the Jurassic aquifer was determined based on available groundwater depths in the boreholes and the altitude of springs located in this part. By using topography and the thickness of this zone, we could interpolate the groundwater equipotential contours in this part. The highest value of these contours (1600 m a.s.l) was used as constant hydraulic head (BCs) in the Jurassic aquifer (Figure 4). The intersection points of these contour lines with the western limit of the upper aquifer, together with the water level measured in the boreholes located in this aquifer during the same period (September 2010), were used to construct the equipotential contour lines for this aquifer. The contour lines were created by using the ordinary kriging algorithm method [27]. The geostatistic analysis of measured groundwater levels resulted in a linear variogram model (Figure 5), which was used to perform the kriging interpolation. The resulting contour lines, as well as the simulated one in the exposed part of Jurassic (Figure 4), were used as reference maps for the steady-state model simulation. The groundwater level interval was taken as 50 m for the upper aquifer horizon and 100 m for the exposed part of Jurassic aquifer. The hydraulic head varies between 700 and 775 m.a.s.l in the outermost nodes on the eastern model boundary and the discrete altitudes of permanent spring discharges were simulated as a constant head (BCs) (Figure 4).

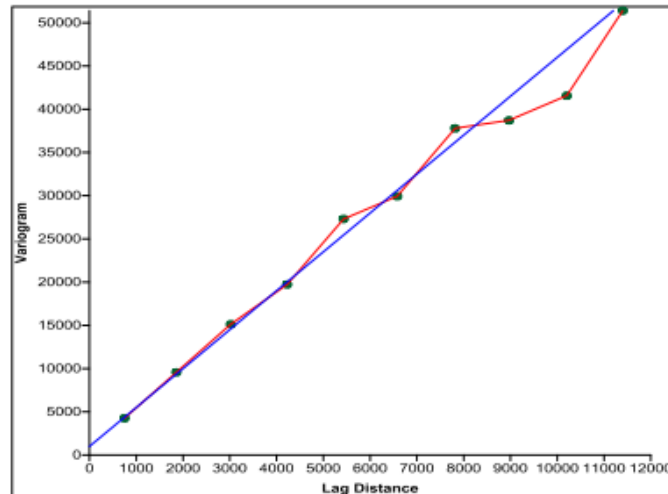


Figure 5. A linear variogram model showing best fit for the measured data.

In order to simulate the lateral flow of groundwater amount from the Jurassic aquifer into the upper aquifer, the Neumann type flux was implemented.

Under natural conditions, we did not observe a significant relationship between Sebarani tributary and groundwater in the plain region. The measured discharges of this tributary in the two gauging stations where it enters the plain region and before its junction with Jenani tributary are almost the same. The Genani tributary flows in the concrete canal which prevents the interaction between surface water and groundwater. Therefore, both tributaries were excluded from the simulation process. The evapotranspiration was also omitted because the water level is situated in general at a depth of more than 5 m, where evaporation and transpiration cannot occur.

5.3. Input Data

The topographic surface of the model domain, the boundaries of the layers, and the dimensions and thickness of each layer were prepared using Arc GIS. The hydraulic head boundaries were based on a potentiometric map of September 2010 and the hydraulic parameters for each layer were obtained from [23,28]. These values were used as initial values for steady-state simulation. The initial and boundary conditions are defined on the mesh nodes, whereas the characteristics of the medium are assigned on an elemental basis.

5.4. Recharge

Groundwater recharge rates vary with climate conditions. The other important factors controlling recharge are surface geology, surface topography, soil type, vegetation, and land use. The recharge amount includes the major input from precipitation and minor input from irrigation return flow. A high amount of groundwater recharge occurs by direct vertical percolation of rainfall and snowmelt through the unsaturated zone of the outcropping part of Jurassic formations. The Neogene/Quaternary aquifer receives a lower recharge portion from rainfall but an important recharge from lateral groundwater inflow from adjacent cavernous limestone in the western side and an additional recharge from irrigation return flow. The groundwater may potentially leak upward from deeper aquifers into this aquifer and form another recharge component which is difficult to quantify.

The amount of recharge into the groundwater during the hydrological year 2009–2010 was calculated by using the isohyetal method to be $173 \text{ Mm}^3 \cdot \text{y}^{-1}$ upon the model area based on available meteorological data in six stations located in the study area (Figure 1b). The total amount of precipitation, which recharged the upper aquifer horizon, was calculated to be $48 \text{ Mm}^3 \cdot \text{y}^{-1}$. The recharge input was entered into the model as a specified flow through the top surface of the first layer. Indirect recharge from conveyance losses of irrigation canals and domestic water, exceeding irrigation water (return flow) and wastewater discharge, were estimated to be $11.8 \text{ Mm}^3 \cdot \text{y}^{-1}$. This estimation was based on certain percentages of water that evaporate or return to the water system according to [29] (Table 1). The simulation was carried out by assuming a constant daily recharge through all three different regions of the model area (mountain, intermediate and central agricultural regions).

5.5. Net Pumping

There are a total of 830 wells used for agricultural purposes, most of them located in the plain region. The 101 wells used for domestic purposes are well distributed in the whole model area

(Figure 6). The annual amount of groundwater abstraction from the upper aquifer horizon was 7 and 8 Mm³·y⁻¹ for agricultural and domestic purposes, respectively. About 85% of the groundwater abstraction wells are screened over the upper aquifer horizon, while 2% and 13% penetrate the Cretaceous and Jurassic aquifer, respectively. For modeling purposes, the annual pumped volume for each well was converted to m³·d⁻¹ and applied as a steady amount throughout the year.

Table 1. Possible amounts of water entering and leaving a groundwater system of the upper aquifer horizon, used to calculate the groundwater budget in this horizon during the hydrological year 2009–2010.

Recharge Components			
Indirect recharge (conveyance losses of domestic and irrigation water, wastewater discharge and irrigation return flow)	Direct recharge from meteoric infiltration	Lateral inflow from Jurassic aquifer- corresponds to FEFLOW simulation	Upward leakage from deeper aquifers corresponds to FEFLOW simulation
(Mm ³ ·y ⁻¹)	(Mm ³ ·y ⁻¹)	(Mm ³ ·y ⁻¹)	(Mm ³ ·y ⁻¹)
11.8	48	52	31
Discharge Components			
Lateral outflow from southern boundary to Yarmouk Basin corresponds to FEFLOW simulation	Spring discharges	Lateral outflow from eastern boundary- corresponds to FEFLOW simulation	Abstraction water for agricultural and domestic use
(Mm ³ ·y ⁻¹)	(Mm ³ ·y ⁻¹)	(Mm ³ ·y ⁻¹)	(Mm ³ ·y ⁻¹)
3.9	37.5	81.8	15

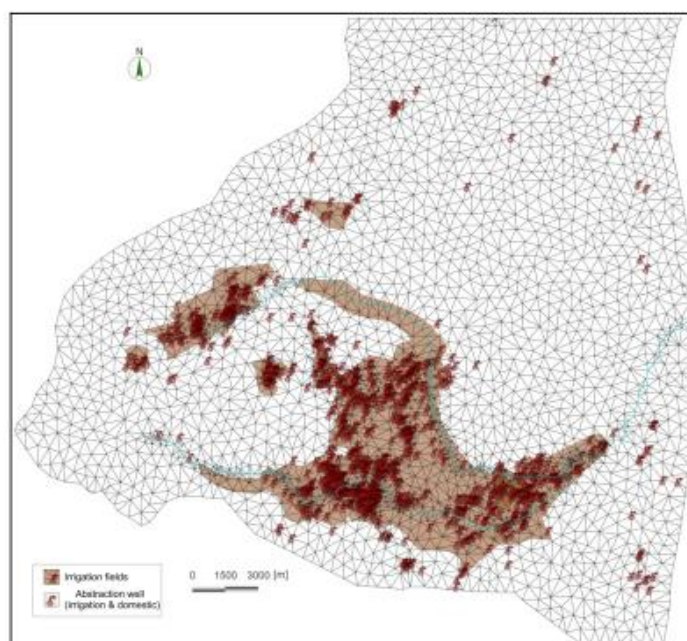


Figure 6. Location sites of irrigation field and spatial distribution of abstraction wells.

The Awaj River is also used for irrigation in the summer period. The amount of surface water used for irrigation is about $35 \text{ Mm}^3 \cdot \text{y}^{-1}$ during the hydrological year 2009–2010. The total area irrigated by both groundwater and surface water is about 75 km^2 of which about 21 km^2 is irrigated by groundwater. The calculated amount of pumped groundwater is less than the amount of water needed for the irrigation if we take into account the amount of $5000 \text{ m}^3 \cdot \text{h}^{-1} \cdot \text{y}^{-1}$ reported by the Ministry of Irrigation (MOI) in Syria [28]. The total discharge of springs located in the upper aquifer was calculated to be $37.5 \text{ m}^3 \cdot \text{y}^{-1}$ for the hydrological year 2009–2010.

6. Results and Discussion

6.1. Steady-State Calibration

Model calibration was performed by trial and error by changing the hydraulic conductivity of the model layers until a reasonable agreement between the simulated and measured groundwater levels was achieved. The calibrated hydraulic conductivity for the upper aquifer horizon varied within a reasonable range based on values between 0.3 and $13 \text{ m} \cdot \text{d}^{-1}$ reported in the literature. For the other aquifers and aquitards, these values were assigned uniformly because there was insufficient data on their spatial distribution across these layers. The uniform hydraulic conductivities for the Cretaceous and Jurassic aquifers were defined as 25 and $18 \text{ m} \cdot \text{d}^{-1}$ respectively, while these values were taken as 0.08 and $0.15 \text{ m} \cdot \text{d}^{-1}$ for the first and second aquitards, respectively.

The measured and simulated groundwater level contours (Figure 7) indicate fairly good agreement in the upper aquifer horizon. In the southern boundaries, where the basaltic layer and the zone which hosts numerous irrigation wells, less agreement was achieved. Furthermore, and due to the definition of no flow boundaries in the north and south part of the model domain, the contours in the model must be perpendicular to these boundaries, while the measured contours are not. This changes the performance of the model near these boundaries. When the upper aquifer horizon comes in contact with the first aquitard, this retards the groundwater flow, and thus the contour lines' behavior changes and they become denser at this interface. This phenomenon can be observed in two places, in the southwest and north of the study area where this aquitard is located and exposed to the surface.

The scatter plot and regression analysis of computed and measured hydraulic heads in the wells located in the upper aquifer horizon are shown in Figure 8. The result indicates that the agreement between simulated and measured hydraulic heads was reasonably good for the measured points.

The sensitivity of the model to input parameters was tested by changing the parameters of interest over the range of values in order to determine the most sensitive parameters responsible for the aquifer behavior. During calibration, it was found that the parameter having the greatest effect on the simulated result was the spatial distribution of the hydraulic conductivity and, to a lesser extent, the recharge amount.

The flow regime in the upper aquifer horizon shows that the flow direction is towards the east with a higher hydraulic gradient in the western part and moderate hydraulic gradient in the plain region. The map also shows that a part of the major valleys' groundwater tends to flow towards the southeast direction. This flow can be considered as part of lateral flow where the conduits of Jurassic aquifer are

laced through the porous medium of Neogene aquifer. Calibration of the groundwater flow in the other aquifers was not possible due to the lack of groundwater level measurement in these aquifers.

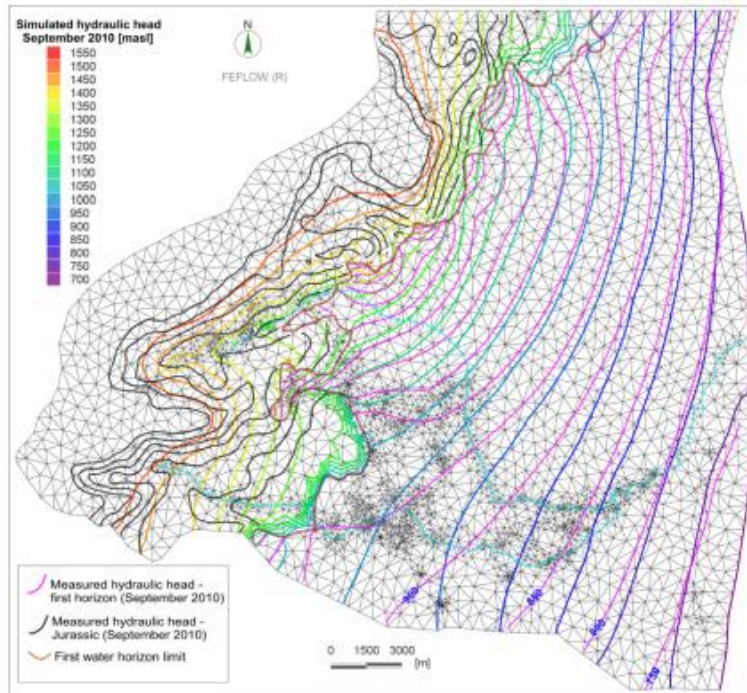


Figure 7. The comparison between the measured and the simulated initial hydraulic head in the upper aquifer horizon and Jurassic aquifer, September 2010.

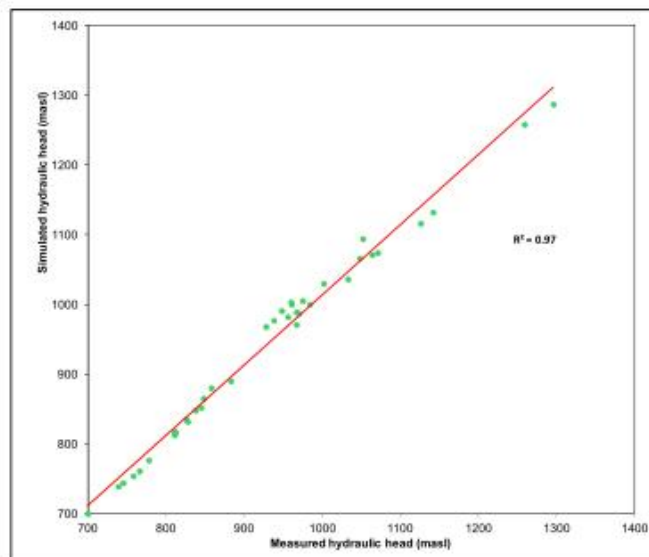


Figure 8. Scatter plot of measured and simulated initial hydraulic heads for September 2010.

The hydraulic connections between the model aquifers depend on the hydraulic gradient differences between them. According to the simulation result, this gradient was high enough to permit hydraulic connections between the deep aquifers and the upper aquifer horizon. The amount of upward movement from the deep aquifers to the upper aquifer was calculated to be $31 \text{ Mm}^3 \cdot \text{y}^{-1}$.

6.2. Preliminary Groundwater Balance for the Upper Aquifer Horizon

The computing of a water budget provides information on whether the aquifer system is being depleted and allows calculation of the amount of water exchanged at the model boundaries. This assists in using the available groundwater resources in a sustainable way. The water budget and flow tools in FEFLOW as well as the FEFLOW classic version can be used to quantify the volume of water across lines (aquifer boundaries), polygons (model layers), and boundary conditions (flow in or out of the model). The steady-state calibration result was used to calculate the preliminary water balance in the upper aquifer horizon. The change in groundwater storage can be estimated based on the quantity of water entering into this aquifer and leaving it during a certain period of time using the following equation:

$$\frac{dV}{dT} = R - (P + Q) \quad (1)$$

where dV/dt is the change in storage ($\text{m}^3 \cdot \text{y}^{-1}$); R is the groundwater recharge by precipitation, lateral inflow, upward leakage and indirect recharge through conveyance loss of irrigation and domestic water, irrigation return flow and wastewater discharge ($\text{m}^3 \cdot \text{y}^{-1}$); P is the total groundwater pumping ($\text{m}^3 \cdot \text{y}^{-1}$); and Q represents the discharges of the springs and cross-boundary groundwater outflow from the model area ($\text{m}^3 \cdot \text{y}^{-1}$). The groundwater budget was calculated based on available recent data of the hydrological year 2009–2010. The precipitation during this year was close to the long-term average [28]. The groundwater used for irrigation is independent of rainfall because there is no rainfall during the summer period.

The water budget of the calibrated model domain is balanced with an internal error estimated at less than 1%. However, the water budget applied on the upper aquifer horizon was calculated based on the difference between the simulated and estimated components of inflow and outflow (Table 1) using Equation (1) as follows: $(11.8 + 48 + 52 + 31) - (3.9 + 37.5 + 81.8 + 15)$. This calculation indicates a positive imbalance equal to $4.6 \text{ Mm}^3 \cdot \text{y}^{-1}$. This imbalance between input and output components is around 3.3% and can be referred to the steady state simulation error which is offset by error in budget estimates in deeper aquifers, so that the overall system gives $dV/dt = 0$. The lateral and upward inflow are the most important input components, providing evidence for the likelihood of large-scale feeding flow from Jurassic aquifers toward the upper aquifer horizon. The atmospheric precipitation is the next most important recharge component. The indirect recharge forms a considerable component in recharging this horizon, which indicates the effect of anthropogenic activities developed in the study area. The largest outflow component is through the eastern boundary. Even given the fact that groundwater flows across the eastern boundary of the model area, the groundwater system in the adjacent eastern region is under great stress compared to the model region. In general, the hydrogeological dynamic characteristics of the study area seem to play a key role in the groundwater flow system despite the development of intensive anthropogenic activities in this area. More data for

longer periods and accurate groundwater pumpage as well as details about hydrodynamic characteristics of deep aquifers are required to determine an accurate water budget.

Based on the FEFLOW numerical model and the other primary information utilized within this study, the different components of the water budget of the upper aquifer horizon are shown in Table 1 and Figure 9.

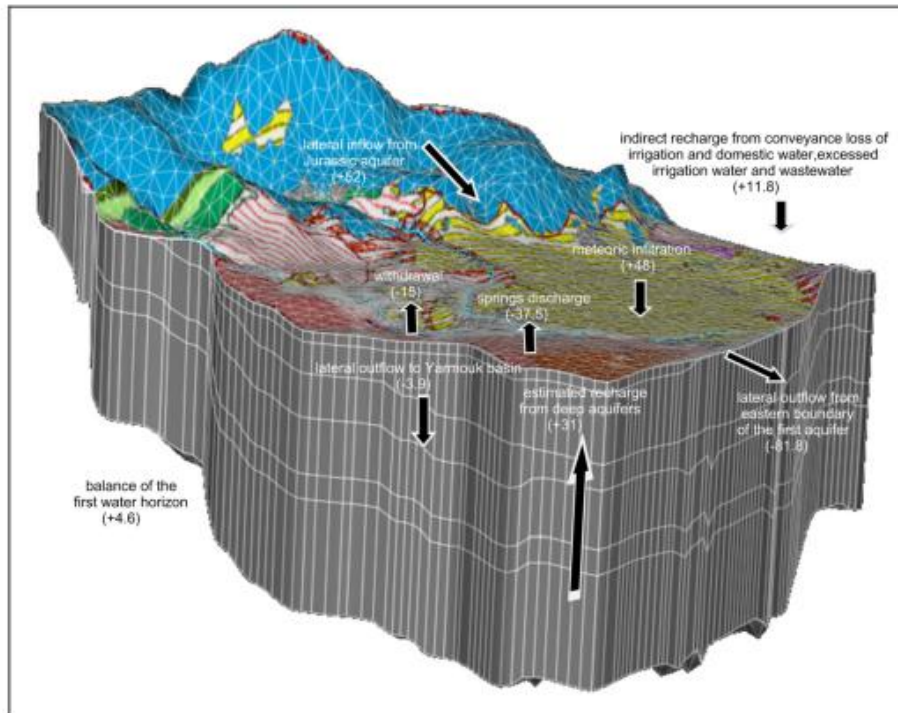


Figure 9. Three dimensional (3D) numerical model showing computed water budget in the upper aquifer horizon applied to steady-state simulation during September 2010. The positive inflow and negative outflow values are expressed in $\text{Mm}^3 \cdot \text{y}^{-1}$.

7. Conclusions

The development of the groundwater model in the eastern part of Mt. Hermon is a useful alternative tool to evaluate groundwater resources in this region. The result of the calibrated model shows reasonable agreement between measured and calculated water levels.

Groundwater flow system in the model domain can be divided into two primary components. The first is shallow aquifer in the unconsolidated Quaternary/Neogene formations in the plain region. Water level in this region is affected by lateral inflow and upward movement of deep groundwater. The second is deep aquifer in the Cretaceous and Jurassic strata, where the preferential flow mechanism potentially contributes to the groundwater flow patterns. The hydraulic connection between the two systems is observed at the foothill of Mt. Hermon where the Neogene formations come into direct contact with the Jurassic formations. Groundwater flow in the first system seems to be

controlled by bedding and lithostratigraphic units with a minor downward component. In the second system, groundwater flow pathways consist of two main components. The first is local and controlled either by conduits and active fault zones, and subsequently discharges as a preferential flow throughout several karstic springs or recharges the upper aquifer horizon as a lateral groundwater flow. The second is recognized as being regional and controlled by the geological structures as deep vertical groundwater flow discharging by springs or upward groundwater leakage to recharge the upper aquifer.

The most important components of the water budget in the upper aquifer horizon were determined. The result indicated that the lateral discharge from the Jurassic karstic aquifer into Neogene conglomerates and the recharge by infiltrated meteoric precipitation are the most important mechanisms in recharging the upper aquifer horizon. The upward movement of groundwater from deeper aquifers plays a considerable role in recharging this aquifer. However, the lateral discharge from the eastern model domain boundary is the largest discharge component, which indicates that the study area can be considered as a main recharge region of the western side of the Barada and Awaj Basin. Nevertheless, the natural characteristics of the hydrogeological dynamism in the study area seem to play a key role in the groundwater flow system despite the development of intensive agricultural/domestic activities in this area.

The result of this study is in agreement with that obtained by the interpretation of the groundwater hydrochemical characteristics of the study area [30]. This result clarifies the recharge/discharge mechanisms between two different, but linked, hydrogeological systems (shallow and deep), and helps to quantify the different components of a water budget in the shallow system.

Increasing groundwater model efficiency requires more information about the hydraulic and dispersive characteristics of deep aquifers and karst setting. However, this model can be considered as a basis for the prediction of future changes in the groundwater system when the model is run in a transient state and with the probable application of different scenarios.

Acknowledgments

The authors are grateful to Abdallah AL-Kattea and Kasem Salih from the General Directorate of the Barada and Awaj Basin (GDBAB)-Syria, and Taghreed Alsaleh from Arab Center for the Studies of Arid Zones and Dry Lands (ACSAD) for their assistance in providing the required data and information for the model construction. Special thanks go also to the French Ministry of Foreign Affairs and Campus France for their financial support (grants Nos. 779091L and 839300A). The authors would like to thank two anonymous reviewers, with special thanks to Alon Rimmer, for their valuable comments which helped to improve the quality of this manuscript.

Author Contributions

All the authors contributed extensively to the work presented in this paper. Nazeer M. Asmael and Alain Dupuy designed and implemented the simulation model. Nazeer M. Asmael wrote the manuscript. All the authors performed the conceptual model based on the result of hydrochemistry and isotopes technique, discussed the results and commented on the manuscript at all stages.

Conflicts of Interest

The authors declare no conflict of interest.

References

1. Melhem, R.; Higano, Y. Policy measures for river water management in Barada Basin, Syria. *Stud. Reg. Sci.* **2001**, *32*, 1–23.
2. Ministry of Agriculture and Agrarian Reform (MAAR). *Syrian Agriculture Database*; MAAR: Damascus, Syria, 2006.
3. Luijendijk, E.; Bruggeman, A. Groundwater resources in the Jabal Al Hass region, northwest Syria: An assessment of past use and future potential. *Hydrogeol. J.* **2008**, *16*, 511–530.
4. Konikow, L.; Kendy, E. Groundwater depletion: A global problem. *Hydrogeol. J.* **2005**, *13*, 317–320.
5. Kløve, B.; Ala-Aho, P.; Bertrand, G.; Gurdak, J.J.; Kupfersberger, H.; Kvaerner, J.; Muotka, T.; Mykrä, H.; Preda, E.; Rossi, P.; *et al.* Climate change impacts on groundwater and dependent ecosystems. *J. Hydrol.* **2013**, *518*, 250–266.
6. U.S. Department of Agriculture (USDA). Foreign Agricultural Service Middle East and Central Asia: Continued Drought in 2009/2010 Threatens Greater Food Grain Shortages, 2008. Available online: http://www.pecad.fas.usda.gov/highlights/2008/09/mideast_cenasia_drought/ (accessed on 16 September 2008).
7. Integrated Regional Information Networks (IRIN). Syria: Drought Pushing Millions into Poverty. Damascus 9 September 2010. Available online: <http://www.irinnews.org/Report/90442/SYRIA-Drought-pushing-millions-into-poverty> (accessed on 12 March 2015).
8. Voss, K.A.; Famiglietti, J.S.; Lo, M.; de Linage, C.; Rodell, M.; Swenson, S.C. Groundwater depletion in the Middle East from GRACE with implications for transboundary water management in the Tigris-Euphrates-Western Iran region. *Water Resour. Res.* **2013**, *49*, 904–914.
9. Anderson, M.P.; Woessner, W.W. *Applied Groundwater Modeling, Simulation of Flow and Advective Transport*; Academic Press: New York, NY, USA, 1992.
10. Chiang, W.H.; Kinzelbach, W.; Rausch, R. *Aquifer Simulation Model for Windows-Groundwater Flow and Transport Modeling, an Integrated Program*; Borntraeger: Berlin, Germany; Stuttgart, Germany, 1998; p. 137.
11. Food and Agriculture Organization of the United Nations (FAO). AQUASTAT. Available online: <http://www.fao.org/nr/water/aquastat/main/index.stm> (accessed on 11 February 2015).
12. Aw-Hassan, A.; Rida, F.; Telleria, R.; Bruggeman, A. The impact of food and agricultural policies on groundwater use in Syria. *J. Hydrol.* **2014**, *513*, 204–215.
13. Rimmer, A.; Salingar, Y. Modelling precipitation-streamflow processes in karst basin: The case of the Jordan River sources, Israel. *J. Hydrol.* **2006**, *331*, 524–542.
14. Alpert, P.; Krichak, D.O.; Sharif, H.; Haim, D.; Osetinsky, I. Climatic trends to extremes employing regional modeling and statistical interpretation over the E. Mediterranean. *Glob. Planet. Chang.* **2008**, *63*, 163–170.
15. Frumkin, A.; Shimrom, A.E.; Miron, Y. Karst morphology across steep climate gradient southern Mt. Hermon. *Z. Geomorphol.* **1998**, *109*, 23–40.

16. Dubertret, L. L'Hydrologie et aperçu sur l'Hydrographie de la Syrie et du Liban dans leurs relations avec la géologie. *Rev. Géogr. Phys. Géol. Dyn.* **1933**, *4*, 347–452. (In French)
17. Mor, D. A time-table for the Levant Volcanic Province, according to K-Ar dating in the Golan Heights, Israel. *J. Afr. Earth Sci.* **1993**, *16*, 223–234.
18. Hartmann, A. Process-Based Modeling of Karst Springs in Mt. Hermon, Israel. Ph.D. Thesis, Albert-Ludwigs-Universität Freiburg im Breisgau, Breisgau, Germany, 2008.
19. Kattan, Z. Characterization of surface water and groundwater in the Damascus Ghotta basin: Hydrochemical and environmental isotopes approaches. *Environ. Geol.* **2006**, *1*, 173–201.
20. United Nations. *Groundwater in Eastern Mediterranean and Western Asia*; Natural Resources Water Series No. 9; United Nations: New York, NY, USA, 1982.
21. Japan International Cooperation Agency (JICA). *The Study of Water Resources Development in the Western and Central Basins in Syrian Arab Republic, Phase I*; JICA: Osaka, Japan, 2001, Unpublished Report. (In Arabic)
22. La-Moreaux, P.E.; Hughes, T.H.; Memon, B.A.; Lineback, N. Hydrogeologic assessment-Figeh Spring, Damascus, Syria. *Environ. Geol. Water Sci.* **1989**, *13*, 73–127.
23. Selkhozpromexport. Water resources use in Barada and Al-Awaj Basins for irrigation of crops. In *USSR, Ministry of Land Reclamation and Water Management*; Selkhozpromexport: Moscow, Russia, 1986.
24. Wolfart, R. Hydrogeology of the Damascus Basin (southwest-Syria). *Int. Assoc. Sci. Hydrol.* **1964**, *64*, 402–413.
25. DHI-WASY GmbH. FEFLOW 6—Finite elements subsurface flow and transport simulation system. In *User's Manual*; DHI-WASY GmbH: Berlin, Germany, 2010.
26. Elango, L. *Numerical Simulation of Groundwater Flow and Solute Transport*, 1st ed.; Allied Publishers Pvt. Ltd.: New Delhi, India, 2005.
27. Krige, D.G. A statistical approach to some basic mine valuation problems on the Witwatersrand. *J. Chem. Metall. Min. Soc. S. Afr.* **1951**, *52*, 119–139.
28. Ministry of Irrigation (MOI). *Annual Water Resources Report of Barada and Awaj Basin, Damascus, Syria*; MOI: Damascus, Syria, 2005; unpublished report. (In Arabic)
29. Water Utility of Damascus Rif (RDAWSA). *Interim Report-Hydrogeological Study of Mogher Al Mer Area, Damascus Rural Water and Sanitation Project*; RDAWSA: Damascus, Syria, 2006; unpublished report. (In Arabic)
30. Asmael, N.M.; Huneau, F.; Garel, E.; Celle-Jeanton, H.; le Coustumer, P.; Dupuy, A. Hydrochemistry to delineate groundwater flow conditions in the Mogher Al Mer area (Damascus Basin, Southwestern Syria). *Environ. Earth Sci.* **2014**, *72*, 3205–3225.

© 2015 by the authors; licensee MDPI, Basel, Switzerland. This article is an open access article distributed under the terms and conditions of the Creative Commons Attribution license (<http://creativecommons.org/licenses/by/4.0/>).

Abstract

Barada and Awaj basin is the most important and extensively used water basin in Syria. The upper part of Awaj River occupies the southwestern part of this basin. In this arid region, groundwater is considered to be as a major source of water supply. In order to assess the main features which characterize the hydrogeological system in this area and calculate the water budget of the upper aquifer horizon, a multi approach methodology using hydrochemistry, environmental stable isotopes and groundwater modeling were used as integrated tools.

The detailed description of hydrogeochemical conditions has underlined the very complex variability of the stratigraphic sequences and hence the numerous hydrogeological units within the study area. Hydrogeochemical evolution reveals the domination of dissolution/precipitation of carbonate rocks as a main mechanism controlling groundwater chemical composition and to less extend, the silicate hydrolysis, dissolution of gypsum and reverse ion exchange. Consequently, hydrochemical patterns did not give enough evidences for the expecting of huge feeding flow from the Jurassic aquifers towards the Neogene/Quaternary aquifer. The similarity in water type tends to express the existence of a unique hydrochemical system where the individualised groundwater flow paths are difficult to delineate.

The isotope compositions imply an important rapid infiltration of atmospheric precipitation before significant evaporation takes place. Hence the infiltrated precipitation provides the main source of groundwater recharge all over the study area and mainly throughout the mountainous parts.

The study area can be dividing into two main sub-regions. The sub-region (A) which characterizes by active dissolution phenomena and deep vertical groundwater flow. And sub-region (B) which characterizes by a shallow horizontal flow component associated with active interaction between groundwater and hosting rocks.

The result of groundwater model indicates a hydraulic connection between the deep aquifers and the overlying upper aquifer through the upward leakage of groundwater. The components of the water budget of the upper aquifer had determined. The lateral discharge from the Jurassic aquifer as well as the meteoric recharge is the most important recharging component of this budget. The upward leakage of groundwater from deeper aquifers also plays an important role. However, the lateral discharge from the eastern boundary is the largest discharge component which indicates that the study area can be considered as a main recharge region of the western side of the Barada and Awaj Basin.

Résumé

Le bassin hydrologique du Barada et de l'Awaj est le plus important et le plus intensément exploité de Syrie. Le sous bassin amont de la rivière Awaj occupe la partie sud-ouest de ce bassin. Dans cette région aride, l'eau souterraine représente la principale réserve et ressource de production d'eau. Dans l'optique de caractériser le fonctionnement du système hydrogéologique multicouche local et de calculer un bilan hydrologique pour l'aquifère superficiel, une méthodologie multi techniques couplant hydrochimie, isotopie et hydrodynamisme a été déployée.

L'analyse détaillée des données hydrochimiques recueillies a mis en évidence la grande variabilité du fond géochimique local, directement fonction de la stratigraphie. Cette complexité stratigraphique induit une vision hydrogéologique complexe de nombreux corps aquifères. L'évolution de la chimie des eaux révèle la prépondérance du phénomène de dissolution/précipitation des roches carbonatées comme principal mécanisme de contrôle de l'hydrochimie, devant l'hydrolyse des silicates, la dissolution du gypse et l'échange ionique. En conséquence il n'a pas été possible de déduire de l'hydrochimie des eaux les preuves d'une recharge par drainance ascendante depuis l'aquifère du jurassique vers les aquifères superficiels, bien que la similarité des faciès hydrochimiques tend à consolider l'hypothèse d'une origine unique des eaux, sans toutefois permettre une identification des chemins d'écoulement.

Les données isotopiques indiquent quant à elles, une infiltration importante et rapide des eaux météoritiques, avant qu'une importante phase d'évaporation n'ait lieu. Ainsi, l'important flux d'infiltration qui se produit essentiellement dans la partie montagneuse de la zone, représente la principale source de recharge du système aquifère multicouche régional.

De ce fait la zone d'étude peut se subdiviser en deux sous régions : la première (A) se caractérise par une dissolution active et des flux de circulation d'eau souterraine fortement orientés verticalement vers la profondeur, alors que la seconde (B) est caractérisée par des écoulements peu profonds associés à des interactions hydrochimiques avec les roches encaissantes.

Les résultats de la modélisation hydrodynamique du système mettent en évidence la connexion hydraulique entre l'aquifère profond du Jurassique et les aquifères surincombants par le biais d'une drainance ascendante. Le bilan hydrologique de l'aquifère se surface a ainsi pu être appréhendé : les principaux flux de recharge proviennent de l'infiltration des eaux météoritiques mais également de l'écoulement latéral du Jurassique dans la partie montagneuse. La drainance ascendante depuis le Jurassique dans la partie aval est également non négligeable. Du point de vue des sorties, le flux d'écoulement le plus important se situe en direction de l'est vers le centre du bassin. Ce constat permet de concevoir que La sous bassin amont de le rivière Awaj est la principale zone de recharge occidentale du bassin de Barada et Awaj.